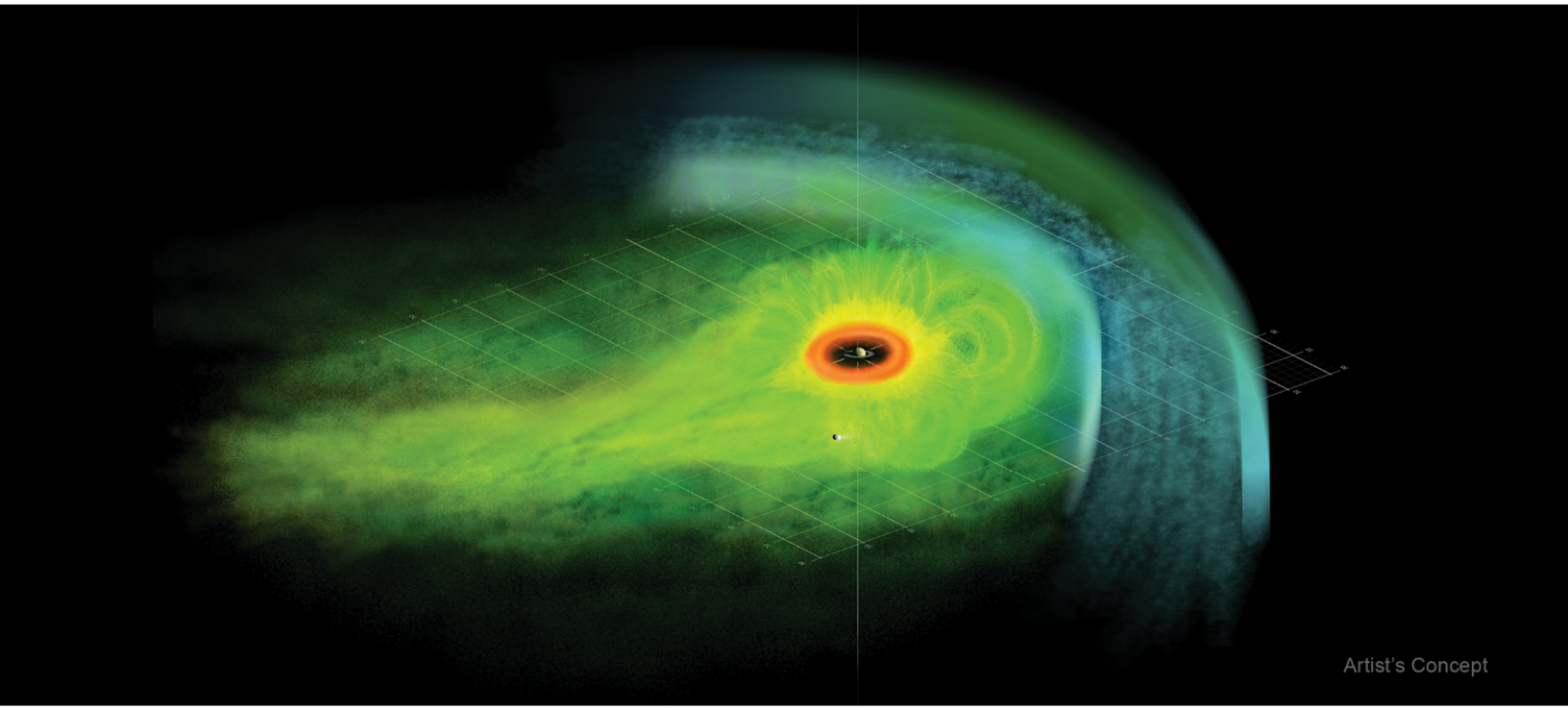

MAPS

Prior to Cassini's arrival, scientists had little information about Saturn's magnetosphere, the giant, invisible magnetic bubble surrounding the planet. Cassini studied Saturn's magnetosphere as never before by mapping the magnetic field, studying the flow of excited plasma within, and observing the influence of the solar wind and how it affects Saturn's auroras. Fields and particles data have provided powerful insights about how Saturn's magnetic field provide linkages between charged particle sources and the rings, moons, and atmospheres, in addition to the inner workings of Saturn's interior.

The **Magnetospheres and Plasma Science (MAPS)** Discipline Working Group (DWG) facilitated and coordinated the data sharing and collective science among the six MAPS instrument teams to ensure that all Cassini's MAPS mission objectives were successfully met. The MAPS DWG has achieved and exceeded in every way the Cassini mission goals and objectives, and has provided a legacy for the outer planets community that will reach far into the future.

CONTENTS

Figures

Tables

EXECUTIVE SUMMARY

…it is clear that the MAPS DWG achieved and exceeded in every way the AO and extended mission goals, and provided a legacy … that will reach far into the future.

The purpose of the Magnetospheres and Plasma Science (MAPS) Discipline Working Group (DWG) was to facilitate and coordinate the data sharing and collective science among the MAPS instruments teams to ensure that all Cassini Announcement of Opportunity (AO) and extended mission objectives were achieved. Without reservation it is clear that the MAPS DWG achieved and exceeded in every way the AO and extended mission goals, and provided a legacy for the outer planets community that will reach far into the future.

Perhaps the most important single contribution to the MAPS science coming from the Interdisciplinary scientist of the MAPS DWG was the creation of the MAPS Rules-of-the-Road. This document outlined a very clear policy that MAPS instruments would share data, that PIs would take responsibility for their teams, and that collaborative work would be the norm for MAPS not the exception. A separate closeout document describes in detail the creation and execution of the Rules-of-the-Road. While the MAPS DWG was not without its conflicts, the legacy of this document was a DWG that shared data that fostered collaborations between instrument teams and created new investigations without significant conflict.

In addition to the MAPS Rules-of-the-Road, another operating principle of the MAPS DWG and the DWG Interdisciplinary Scientists (IDSs) was that the instrument teams should take the lead, and thereby receive the glory, on nearly all investigations. With this guiding principle, the DWG was able to have the most relevant team lead, most investigations, and then have other teams contribute.

KEY SCIENCE RESULTS

Top Science Findings for MAPS

Discovery of the Enceladus plumes and their interaction with Saturn's magnetosphere

One of the most important and surprising discoveries of the entire Cassini mission was the discovery of an atmospheric plume at Enceladus by the magnetometer team [Dougherty et al. 2006] on February 17, 2005. The discovery was confirmed and strengthened by subsequent measurements on later flybys and other instruments. This dynamic atmospheric plume was later shown by the Imaging team to be due to geyser activity on the southern hemisphere of Enceladus. Subsequent modeling based on analytical theory clearly showed that the magnetometer results

required the presence of negatively charged dust particles [Simon et al. 2011]. As a unique feature at Enceladus, dust–plasma interactions play an important role to explain the observations.

The discovery of a large and neutral plasma source at Enceladus led to the potential that the moon's interaction with Saturn would result in currents along the magnetic flux tube that could cause an auroral footprint in Saturn's ionosphere. Although initial Hubble Space Telescope (HST) observations did not detect such an auroral footprint [Wannawichian et al. 2008], a follow-on study discovered an Enceladus-associated aurora in a few percent of the scans of the moon's footprint [Pryor et al. 2011]. The footprint varies in emission magnitude more than can plausibly be explained by changes in magnetospheric parameters, and as such is probably indicative of variable plume activity.

Identifying the highly axisymmetric internal magnetic field of Saturn

Early in the mission the Magnetometer (MAG) team determined that the tilt of Saturn's dipole must be smaller than 0.06 degrees from the spin-axis of Saturn which was further constrained by the Grand Finale measurements to <0.01 degrees [Dougherty et al. 2018]. The time variation of Saturn's intrinsic magnetic field must be an order of magnitude slower than that of Earth's [Cao et al. 2011]. These results are very challenging for dynamo theory, as Cowling's theorem excludes the possibility of a purely axisymmetric magnetic field being maintained by dynamo action. The Cassini Grand Finale gravity measurements indicate that the ~100 m/s zonal flows observed at the cloud deck of Saturn extend almost 10,000 kilometers into the planetary interior. Given that the electrical conductivity at such depth are high enough for significant magnetohydrodynamic (MHD) effects, zonal flow magnetic field interaction in the semi-conducting region of Saturn is now a central issue in understanding the interior dynamics. The amplitude of the wind-induced magnetic perturbations would depend on the amplitude of the deep differential rotation as well as the amplitude of the small-scale deep convective flow. Thus, measuring/constraining wind-induced magnetic perturbations along the Cassini Grand Finale orbits would place important constraints on the properties (profile and amplitude) of deep differential rotation and convective flow in the semi-conducting region of Saturn. This work is still ongoing and we expect additional discoveries.

Discovery of periodicities while the intrinsic rotation rate remains elusive

Many properties of Saturn's magnetosphere exhibit periodicities at approximately the planetary rotation rate, a significant puzzle given the near-alignment of the magnetic and rotational axes. Saturn's kilometric radiation (SKR) is the most intense radio emission component, produced in the auroral regions. The first SKR periodicity measured by Cassini witnessed a value differing by 1% to the SKR period identified from Voyager/Planetary Radio Astronomy (PRA) observations 25 years earlier [Gurnett et al. 2005]. Such a large variation implies that the SKR period does not probe the internal rotation rate. The major discovery was the identification of two SKR periods [Kurth et al. 2008] corresponding to the two Kronian hemispheres, differing by ~1%. Both of those periods were found to vary with time in anti-correlation over yearly timescales and crossed closely after equinox, a trend which was interpreted as a seasonal driving of solar illumination [Gurnett et al. 2011a,

2010a, 2009; Lamy 2011]. These dual periods were also observed in numerous magnetospheric observables including magnetic oscillations, energetic neutral atom (ENA) emissions, and aurorae [Mitchell et al. 2009b; Carbary et al. 2011a, 2010a; Nichols et al. 2010; Andrews et al. 2011, 2010; Provan et al. 2011; Badman et al. 2012a, 2012b]. It is now accepted that these dual rotational modulations all originate from two rotating hemispheric systems of field-aligned currents, whose origin may be atmospheric vortices [Jia et al. 2012].

Discovery of new radiation belts

The Magnetospheric Imaging Instrument (MIMI)/Low Energy Magnetospheric Measurement System (LEMMS) instrument discovered a previously unknown radiation belt collocated with the D-ring and extending up to the dense atmosphere of Saturn. This belt was discovered earlier in the Cassini mission [Kollmann et al. 2015], but its properties were unknown. It was found that the belt is dominated by protons up the GeV range, which is the first time that such high energies were directly observed at any of the giant planets. Their pitch angle distribution is very steep, likely due to a strong interaction with Saturn's atmosphere. The suggested source is Cosmic Ray Albedo Neutron Decay (CRAND). There is no evidence for the presence of energetic electrons or ions heavier than protons [Roussos et al. 2018a; Kollmann et al. 2018].

Identifying the main plasma sources in Saturn's magnetosphere

The dominant ion species seen throughout the magnetosphere are well explained by ionization of material from the water plumes of Enceladus that are estimated to produce ~60–100 kg/s [Fleshman et al. 2013]. Enceladus is also the probable source of most of the N^+ observed in Saturn's inner magnetosphere [Smith et al. 2010]. The finding of very little N^+ in the outer magnetosphere [Smith et al. 2005] indicated that Titan's contribution to the heavy-ion plasma is limited, whereas the fact that H_2^+ becomes comparable to H^+ and W^+ in the outer magnetosphere [Thomsen et al. 2010] indicates that Titan is an important source of lighter ions in that region producing ~0.8 kg/s [Coates et al. 2012]. Observation of probable plasma outflows from Saturn's ionosphere led to an estimate of some 10 s of kg/s lofted from the ionosphere [Felici et al. 2016]. It is, however, not yet clear how often such outflow occurs. During Saturn Orbit Insertion (SOI) a layer of O_2^+ and O^+ was discovered over the A-ring and B-ring [Young et al. 2005]. The ring atmosphere and ionosphere are likely produced by ultraviolet (UV) photo sputtering of the icy rings and subsequent photoionization of O^+. Significant O^+ was also detected outside the main rings, near the F-ring [Tokar et al. 2005], and analysis of the O^+ and W^+ profiles showed seasonal dependence consistent with a ring source that depends on the solar illumination angle [Elrod et al. 2014, 2012]. In contrast, Gurnett et al. [2005] show evidence of deep density depletions over the ring during SOI. These results indicate that the rings are an important source of heavy ions inside the orbit of Mimas.

Global configuration and dynamics of the magnetosphere

Cassini discovered that most of the magnetospheric plasma is produced by Enceladus deep inside the magnetosphere. Combined with very strong centrifugal forces this source controls most of Saturn's magnetospheric dynamics. Cassini has also discovered evidence that, unlike at the Earth, the solar wind plays a relatively small role in magnetospheric dynamics, primarily associated with large dynamic pressure enhancements. Saturn's giant magnetic field is the principal cause of the transport of material between the many bodies in this still evolving system, dumping oxygen into the atmospheres of Titan and Saturn. Cassini detected radially outward plasma flows of ~800 km/s during observation of a plasmoid (magnetically detached plasma bubble) on March 4, 2006.

Understanding the transport of plasma through the magnetosphere and the mechanisms for its eventual loss of plasma has been one of the major points of focus of the MAPS investigation. Plasma transport occurs through convection, plasma interchange, reconnective processes, and plasmoid formation. At the time of Cassini's arrival to Saturn the relative importance of these different processes was poorly understood. Now with 13 years of magnetospheric data we have a much better understanding of these different processes. MAPS studies have addressed the relative importance of Vasyliunas-cycle and Dungey-cycle reconnection, and the formation process and frequency of plasmoids and how they are related to dipolarizations. There have been a whole host of studies on the frequency, distribution, source region, life time, size, and plasma properties of the different interchange events that Cassini has observed.

First in situ measurements of Saturn's topside ionosphere

During the Cassini Grand Finale, Cassini MAPS instruments made an unprecedented series of measurements of Saturn's upper atmosphere, sampling from ~3500–1370 km altitude above the 1 bar pressure level. Prior to these orbits, it was anticipated that Saturn's upper atmosphere consisted primarily of H, H_2, with trace amounts of H_2O and He. The in situ measurements of Saturn's ionosphere allowed the first determination of ion mixing ratios and number densities as well as their temporal variabilities. The measurements of helium provided constraints on possible deep-atmosphere mixing ratios of helium and whether or not Saturn has a solar-like composition or something else. In the equatorial region of Saturn's ionosphere where the ring-ionosphere interaction is important, combined with Radio and Plasma Wave Science (RPWS) and MIMI measurements, Ion and Neutral Mass Spectrometer (INMS) in situ data paint a clear picture of Saturn's equatorial ionosphere being dominated by heavy molecular ions that result from ring-derived material. Near the end of the mission, during the proximal orbits, INMS measured densities of H^+, H_2^+, H_3^+, and He^+ in Saturn's ionosphere.

> All of these unanticipated results have effectively turned our understanding of the high-altitude thermosphere-ionosphere chemistry on its head.

In addition to the primary and expected species, the INMS measurements revealed an atmosphere with an

unexpectedly rich composition, containing significant amounts of organics spanning the entire mass range sampled by INMS and specifically the presence of several species of high mass neutrals, for example, CH_4, CO, CO_2. All of these unanticipated results have effectively turned our understanding of the high-altitude thermosphere-ionosphere chemistry on its head.

Detection of lightning in Saturn's atmosphere and the evolution of a once-per-Saturn-year Great White Spot storm

The first indication of lightning in Saturn's atmosphere was obtained in November 1980 by the radio instrument onboard Voyager 1. Strong impulsive signals in the frequency range of a few MHz were detected and termed SEDs for Saturn Electrostatic Discharges [Warwick et al. 1981]. The Cassini mission has greatly enhanced our knowledge about Saturn lightning, and combined radio and imaging observations, have clearly established the atmospheric origin of the SEDs.

RPWS provided the most complete census of lightning activity from near continuous observations of Saturn electrostatic discharges (SED) and established the frequency of convective storms on Saturn, their duration, and lightning flash rates, see for example, Fischer et al. [2011a, 2011b]. Saturn lightning flashes were first detected optically on the nightside of Saturn around equinox. The Cassini cameras spotted flash-illuminated cloud tops with a diameter of about 200 km, suggesting that the lightning comes from 125–250 km below [Dyudina et al. 2010], and most likely from the water-cloud layer. At Earth the charging of water cloud particles in thunderstorms is most effective in a temperature range of −10° C to −25° C. At Saturn this temperature range is located at a level of 8–10 bars, about 200 km below the cloud tops, i.e., consistent with the altitude range found by Dyudina et al. [2010]. Another indication that the Saturn lightning source is in the water cloud layer comes from Cassini Visual and Infrared Imaging Spectrometer (VIMS) near-infrared spectra of the Great White Spot. They revealed spectroscopic evidence for ammonia and water ices [Sromovsky et al. 2013] brought up to higher altitudes by strong vertical convection. So, it is thought that the same particle charging mechanisms are at work on Saturn and Earth. As most of the sunlight is absorbed above 2 bars, Saturn's weather and thunderstorms at deep pressure levels should be powered by the planet's internal energy [Desch et al. 2006]. It drives the vertical convection which brings up the water cloud to the visible atmospheric level where it is observed as a bright eruption by Cassini Imaging Science Subsystem (ISS) and VIMS. Dyudina et al. [2010] also measured the optical flash energy to be about 10^9 J, which suggests that Saturn lightning is superbolt-like with total energies of about 10^{12} J [Fischer et al. 2011c].

Detailed studies of Saturn's auroras

For the first time, Cassini's presence inside the magnetosphere facilitated the coordinated optical observations of the aurora and in situ measurements of the plasma properties, the magnetic structure, and the field-aligned currents. While there have been various studies of the aurora as reviewed in Grodent [2015], the best way to summarize Cassini work is to highlight one of these coordinated studies. One coordinated auroral observing campaign occurred April 21–22,

2013, involving instruments onboard Cassini and the Hubble Space Telescope. During this campaign both Saturn's northern and southern aurora were observed while Cassini traversed Saturn's high-latitude auroral field lines [Badman et al. 2016]. Signatures of upward field-aligned currents were detected that corresponded to the bright ultraviolet auroral arc seen in the auroral images and various auroral features observed included a bulge that appeared along the pre-dawn auroral oval and an intensification of the auroral field-aligned currents. These observations are interpreted as the response to tail reconnection events instigated by solar wind compression, initially involving Vasyliunas-type reconnection of closed mass-loaded magnetotail field lines, and then proceeding onto open lobe field lines, causing the contraction of the polar cap region on the post-midnight sector. At the same time Kurth et al. [2016] reports on the RPWS monitoring of the Saturn kilometric radiation. This study found that there is a good correlation between the 10 h averages of SKR power flux and the estimated power input to the aurora on the basis of the UV brightness, justifying the SKR as a simple proxy for auroral activity through the campaign. The SKR emissions also give evidence for a recurrent pattern of solar wind interaction with Saturn's magnetosphere, suggesting a two-sector structure and associated corotating interaction regions that influence the level of auroral activity on Saturn. But there are other SKR intensifications that may be due to internal processes. This coordinated campaign is a perfect example of the many coordinated studies that have been performed by the Cassini MAPS teams in working to understand the aurora at Saturn.

Discovery of ring-ionosphere-magnetosphere interaction

Cassini MAPS instruments discovered and characterized a unique ring–ionosphere–magnetosphere interaction. INMS first observed O_2^+, O^+, and H^+ ions over the A-ring in its ion mode during SOI [Waite et al. 2005]. Further Cassini observations revealed that the ring–ionosphere–magnetosphere interaction is driven by photolytic processes, not impact processes [Farrell et al. 2017]. Specifically, the Sun-facing side of the main rings are a source of photo-dissociated neutrals that get ionized to form a relatively low energy exo-ionosphere. This exo-ionosphere cannot directly access the shadowed/unlit side of the rings: the ring particles represent obstacles to their transport. Thus, the plasma density on the unlit side is modulated by ring density, being lowest where the ring obstruction is the highest in the central B-ring. Local maxima are expected where the local ring particle density is low, such as across the Cassini Division. There is little evidence of impact-generated plasma like that which was predicted during the Voyager era. Cassini observation suggested that there is a current system driven by the rings–magnetosphere interaction. While the plasma on field lines over the rings would be corotating, the particles and associated photo-dissociated gas of the rings would be moving in Keplerian motion, creating drag on the plasma. This drag creates an associated change in plasma speed. Beyond the synchronous point, the plasma is slowed by the Keplerian-moving particles and gas, creating a radially outward directed electric field in order to maintain the new sub-corotation speed. This new electric field drives an outward current that then acts to form a magnetohydrodynamic JxB force to balance the plasma-ring drag force. Inward of the synchronous point, the corotating plasma is accelerated by the ring drag force, creating an inward radial electric field and current that forms a JxB force to offset the acceleration. At the edges of the rings, these cross-ring currents become a field-aligned parallel

current that closes down to the ionosphere along connecting magnetic field lines at the outer edge of the A-ring near L = 2.25 and inner edge of the D-ring near L ~1.11. The rings thus behave as an electrical generator in the plasma, driving currents from the ring surfaces along magnetic field lines down to the ionosphere.

Discovery of heavy positive and negative ions in Titan's ionosphere

This is one of the major surprises of the Cassini mission—the high level of chemical complexity observed in Titan's ionosphere. The first in situ ion composition measurements of Titan's ionosphere were made by the INMS in its ion mode and showed a complex composition [Cravens et al. 2006]. From the earliest close encounters Cassini Plasma Spectrometer (CAPS) detected heavy negatively charged ions with mass/charge up to 13,800 amu/q. In addition, heavy positive ions up to ~350 amu/q [Crary et al. 2009] and as high as 1000 amu/q [Coates et al. 2010] were also detected. An unexpected level of chemical complexity was seen in the neutrals as well [Waite et al. 2007]. The existence of negative ions was completely unexpected at the altitudes sampled by Cassini.

Dust–plasma interactions

The discovery of the dense neutral water vapor jets at Enceladus resulted in a continuous, detailed examination of all aspects of the Enceladus plume and the extended effects on the magnetosphere. A major result of this examination is the detection of singly charged nanometer-size water-ice grains [Coates et al. 2009; Jones et al. 2009; Hill et al. 2012; Meier et al. 2014; Dong et al. 2015; Meier et al. 2015]. Such nanograins had been inferred to exist in various cold, tenuous geophysical and astrophysical environments, but the close Enceladus plume encounters by Cassini offered the first (and still the only) opportunity to measure and characterize the nanograins in situ.

This analysis confirms that the nanograins are largely uncharged when they emerge from the surface vents and become increasingly (mostly negatively) charged as they approach Cassini a few tenths of Enceladus radii away. The most plausible charging mechanism is electron attachment from the dense plume plasma. The non-neutrality of the nanograins observed by CAPS, n(−) >> n(+), plausibly cancels the opposite non-neutrality of the plume plasma observed by RPWS Langmuir Probe (LP). Most of the electrons missing from the plume plasma reside on the nanograins.

Discovery of nanodust between the planet and the D-ring

An exciting result of the proximal orbits during the final months of the Cassini mission was the discovery of nanograins between the planet/ionosphere and the D-ring. Understanding the implications of these particles is still a work in progress, and the first in situ measurements by RPWS of the cold ionosphere properties have just been reported [Wahlund et al. 2018]. Several other manuscripts have been submitted by MAPS instrument teams, and they all show a very strong interaction between the D-ring and the ionosphere of Saturn, causing the ionosphere to

become extremely variable with more than two orders of magnitude and trigger a dust-ionosphere layer near the equator.

Discovery of the shape of the heliosphere

Beyond the Saturn system, one of the most important contributions of Cassini to our understanding of the solar heliosphere came from the MIMI/Ion and Neutral Camera (INCA), first ever images of the global heliosphere in > 5.2 keV ENA measurements [Krimigis et al. 2009]. These images identified two striking, previously unexpected, heliospheric signatures: a) the Belt, a broad band of emission in the sky, identified as a high intensity, relatively wide ENA region that wraps around the celestial sphere in ecliptic coordinates, passing through the nose, the anti-nose (tail), and the north and south heliosphere poles; and b) the basins, identified as two extended heliosphere lobes where the ENA minima occur. In addition, INCA measurements could be used to image the shape of our heliosphere with a surprising result that it is now thought to be a sphere rather a structure with a nose and a tail, like a magnetosphere [Dialynas et al. 2018].

MIMI's images came at a time when Voyager 1 and Voyager 2 crossed the termination shock, where the supersonic solar wind presumably terminates at the shock front, at respective distances of ~94 and ~84 AU in 2004 and 2007 at +35° and −26° ecliptic latitudes [Decker et al. 2008, 2005], pinpointing both the size of the local heliosphere and the scale of the heliospheric asymmetry. After this crossing, V1 additionally unexpectedly passed through the heliopause [Krimigis et al. 2013] at a distance of ~122 AU. Due to the powerful synergy between in situ ions from V1 Low Energy Charged Particle (LECP) instrument and ENAs from INCA (in overlapping energy bands), MIMI has made key discoveries, beginning in about 2009, that altered our past notions on the formation and interactions of the heliosphere, and led to a number of surprises concerning the physics that governs this enormous system and also provided insights on the plasma processes at ~100 AU that were substantially at variance with previous theories and models.

Assessment of Overall DWG Science

The Cassini MAPS DWG was successful in carrying out a robust and complete science investigation over the seven-year cruise and more than thirteen years in orbit at Saturn (the nominal mission plus extensions). The Cassini mission addressed each of the nominal and extended mission science objectives. As is typical in scientific investigation, the process of answering questions typically creates new unanticipated questions. This was certainly the case for the Cassini mission and MAPS science, in particular. Cassini was able to make advances in these unanticipated areas due to the capabilities of the Cassini spacecraft and the ability to plan robust and exciting extended mission designs. Although there are certainly questions that are left for future mission to answer (see section entitled Open Questions for Saturn System Science), all of the MAPS science objectives were addressed and advances were made. In the section entitled MAPS DWG Science Assessment, Table MAPS-1 indicates that all MAPS key science objectives were completed except for the determination of Saturn's internal rotation rate. Although tremendous advances have been made to address this determination, as outlined in the Key Open Questions,

the relationship of the SKR to the true rotation period of Saturn is still under investigation. For this reason, this science objective is marked as partially completed.

Key Open Questions

- Internal rotation rate of Saturn.
- Rotational modulation in axisymmetric configuration.
- How are mass and magnetic flux transported in the middle and outer magnetosphere?
- Solar wind control of the Saturnian magnetosphere.
- Why do neutral particles dominate the Saturnian magnetosphere in contrast to Jupiter?
- Very limited plasma measurements in auroral acceleration and source region of related SKR.
- Understanding the Enceladus plume-magnetosphere interaction. Crossing too fast for better time resolution. Limited plasma measurements.
- Composition of the negative ions at Titan and > 100 amu positive ions.

KEY OBJECTIVES FOR MAPS DWG

The scientific goals of the MAPS DWG were, simply stated, to seek to understand as much about Saturn's magnetosphere, ionosphere, moon interaction, and plasma physics as possible. The key science objectives are listed below.

Characterize the vector fields as a function of position and time.

- **MC1b:** Observe Saturn's magnetosphere over a solar cycle, from one solar minimum to the next.
  - Investigate what controls the interplay between the Dungey and Vasyliunas cycles.
  - Study the solar cycle dependence of the magnetospheric dynamics.
  - Investigate magnetospheric structure: variations in force balance.
  - Investigate non-static and other variant radiation belt features.
- **MN1a:** Determine the dynamics of Saturn's magnetotail.
  - Study thoroughly the plasma sheet in Saturn's magnetotail.

- Investigate the relation between solar wind compression events and magnetotail dynamics.
- Investigate the plasma sheet thickness and scale height as functions of radial distance and local time.
- Statistically characterize magnetotail variations, especially those associated with plasmoids, and correlate them with changes in the inner magnetosphere.
- Critically evaluate the Dungey and Vasyliunas cycles in light of the new observations, especially those of flow speeds.

Characterize Saturn's interaction with the magnetosphere.

- **MN1b:** Conduct in situ studies of Saturn's ionosphere and inner radiation belt.
  - Investigate the effects on aurora of solar wind and seasons.
  - Are there UV satellite footprints on Saturn? (like at Jupiter)
  - Is there a seasonal variation in auroral activity?
  - Investigate solar wind–ionosphere–magnetosphere coupling through the auroral regions.
  - Investigate whether there are UV satellite footprints on Saturn and whether there are Region 1 currents connecting the ionosphere and the magnetopause.
  - Investigate the composition of Saturn's ionosphere.
  - Study whether there is a significant polar outflow from Saturn's high latitude ionosphere and whether the outflow exhibits seasonal or solar cycle variation.
  - Determine whether there is a radiation belt between the D-ring inner edge and the atmosphere.
- **MN2a:** Determine the coupling between Saturn's rings and ionosphere.
  - Study how field-aligned currents are coupled to the rings and satellites.
  - Explore the dust dynamics in the proximity region.
  - Investigate the mid-plane of Saturn's D-ring.
  - Determine the grain composition in the proximity region.
  - Investigate the possible interaction of lightning with the inner magnetosphere and the rings.
  - Investigate coupling between E-ring and the Enceladus neutral and plasma tori.

Characterize the absolute energy spectra, composition, and angular distribution of energetic charged particles and plasma, including plasma wave phenomena, as a function of position and time.

- **M_AO2:** Determine current systems, composition, sources, and sinks of magnetosphere-charged particles.
- **M_AO3:** Investigate wave-particle interactions and dynamics of the dayside magnetosphere and the magnetotail of Saturn and their interactions with the solar wind, the satellites, and the rings.

Determine the rotational, seasonal, solar cycle, and secular variations of SKR and its relation to magnetic field oscillations.

- **M_AO1:** Determine the configuration of the nearly axially symmetric magnetic field and its relation to the modulation of SKR.
- **MN1c:** Investigate magnetospheric periodicities, their coupling to the ionosphere, and how the SKR periods are imposed from close to the planet (3–5 R_S) out to the deep tail.
  - Determine what controls the SKR periods and whether there is a solar cycle and/or seasonal variation.
  - Investigate the coupling mechanism between the SKR periods and the internal rotation rate.
  - Study whether the ionosphere and/or thermosphere is differentially rotating.
  - Determine which hemispherical SKR period dominates other periodicities in the magnetosphere and whether this varies with time.

Investigate satellite–magnetosphere interactions.

- **M_AO5:** Investigate interactions of Titan's atmosphere and exosphere with the surrounding plasma.
- **M_AO4:** Study the effect of Titan's interaction with the solar wind and magnetospheric plasma.
- **MC1a:** Determine the temporal variability of Enceladus' plumes.
  - Investigate temporal variations in Enceladus gas production and plume composition, on the scale of seasons and solar cycle.
  - Study plume neutral gas composition.
  - Investigate the physics of the dusty plasma environment.
  - Determine how the magnetosphere reacts to changes in (plume?) gas production rates by studying Enceladus' auroral footprint.
  - Study variability in dust-to-gas mass ratio.

- **MC2a:** Observe seasonal variation of Titan's ionosphere from one solstice to the next.
  - Study how intensity variations of energetic ions and electrons affect the energy deposition in the atmosphere, and the degree of ionization at different depths.
  - Investigate how the energy input from energetic particles varies when Titan resides in the plasma sheet or magnetosheath.

Cruise science and Jupiter objectives.

- **J_AO3:** Explore the dusk side of Jupiter's magnetosphere and intermediate regions of the magnetotail unvisited by previous spacecraft.
- **J_AO4:** Obtain the first high-resolution images of the Io torus.
- **C_AO1:** Extend the sensitivity of composition measurements of interstellar ions by approximately three orders of magnitude.
- **C_AO2:** Investigate the behavior of the solar wind during solar minimum, for comparison with earlier Galileo and Ulysses measurements.
- **C_AO4:** Extend studies of interplanetary dust to the orbit of Saturn.
- **S_AO4:** Study the diurnal variations and magnetic control of the ionosphere of Saturn.

MAPS DWG Science Assessment

Table MAPS-1. MAPS Science Assessment. AO and TM Objectives are paired with MAPS science objectives.

Fully/Mostly Accomplished: **Partially Accomplished:** **Not Accomplished:**

MAPS Science Objectives	AO and TM Science Objectives	MAPS Science Assessment	Comments
Characterize the vector fields			
Seasonal and solar cycle variations	MC1b		
Magnetotail configuration and dynamics	MN1a		
High-order magnetic moments of Saturn	M_AO1, MN1c		
Saturn's interaction with the magnetosphere			
Magnetospheric convection	MN1b		
Aurora and satellite footprints	MN1b		
Plasma loss into the magnetotail	MC1a, MN1a		
Ionospheric convection	MN1b, S_AO4		
Composition of ionosphere/thermosphere	MN1b, MN2a		
Particle distributions			
Plasma sources and sinks	M_AO2		

Table MAPS-1. MAPS Science Assessment. AO and TM Objectives are paired with MAPS science objectives.

Fully/Mostly Accomplished: **Partially Accomplished:** **Not Accomplished:**

MAPS Science Objectives	AO and TM Science Objectives	MAPS Science Assessment	Comments
Plasma kinetics	M_AO3		
Radiation belts	M_AO3, MC1b, MN1b		
Wave-particle interactions	M_AO3		
Periodicities			
Saturn's magnetic field and its relation to the modulation of SKR	M_AO1, MN1c		
Solar cycle/seasonal variation of SKR periods	MN1c		
SKR periods and Saturn's internal rotation rate	MN1c		Rotation rate is still not known
Differential rotation of the ionosphere and/or thermosphere	MN1c		
Satellite/ring magnetosphere interactions			
Titan's interaction with the surrounding plasma	M_AO4, M_AO5, MC2a		
Interaction of the Enceladus plume with the magnetosphere	M_AO2, M_AO3, MC1a, MN2a		
Ring-magnetosphere interaction	M_AO3, MN2a		
Cruise science & other science			
Jupiter's magnetotail, Io Torus	J_AO3, J_AO4		In spite of no-cruise science decision by Project Management
Interstellar particles	C_AO1		
Solar wind from Earth to Saturn	C_AO2		
Interplanetary dust studies of Saturn	C_AO4		

MAPS DWG Magnetosphere Science Results

Titan Science

Instruments on the Cassini Orbiter carried out extensive measurements of the upper atmosphere and ionosphere of Titan as well as its interaction with Saturn's magnetosphere. Over the course of the Cassini mission, the spacecraft performed 127 flybys of Titan. The flybys, varying in trajectory and closest approach altitude, served as gravity assists to change Cassini's trajectory, but also to bring our understanding of the moon's environment to an unprecedented level.

Titan's upper atmosphere and its interaction with the surrounding plasma

- **M_AO5:** Investigate interactions of Titan's atmosphere and exosphere with the surrounding plasma.

- **M_AO4:** Study the effect of Titan's interaction with the solar wind and magnetospheric plasma.
- **MC2a:** Observe seasonal variation of Titan's ionosphere from one solstice to the next.

TITAN'S NEUTRAL ATMOSPHERE

The first neutral measurements made by MAPS instruments were made during the TA pass. These measurements were made in order to characterize the initial ionospheric density and thereby assess safe altitudes for future flybys.

Observations of neutral densities (mainly N_2) have allowed us to make inferences into the thermal structure of Titan's upper atmosphere [cf. Müeller-Wodarg et al. 2008, 2006a; Cui et al. 2009, 2008; Magee et al. 2009; Westlake et al. 2011; Snowden et al. 2013]. The average thermospheric temperature derived from Ion and Neutral Mass Spectrometer (INMS) data is approximately 150 K, which is in good agreement with pre-Cassini estimates [Müeller-Wodarg 2003, 2000; Müeller-Wodarg and Yelle 2002]. However, the temperature of Titan's thermosphere exhibits a high degree of variability that was not predicted prior to Cassini, see for example, Müeller-Wodarg [2003, 2000; Müeller-Wodarg and Yelle 2002]. Pre-Cassini models calculated day–night variations on the order of 10–15 K. Cassini has observed temperature variations much larger than this over the course of a single Titan day, even when observing the same region of atmosphere at a similar local time. The variations in temperature are not correlated with solar input, indicating there are additional heating/cooling mechanisms with magnitudes that are similar to solar insulation. The short-timescales associated with the large variations in temperature has led some to postulate that the magnetosphere may provide sporadic and localized inputs [Westlake et al. 2011] or internal gravity waves may be depositing significant energy into the upper atmosphere [Müeller-Wodarg et al. 2006b; Snowden et al. 2013]. Atmospheric escape may also significantly alter the temperature of the upper thermosphere [Tucker et al. 2013] as can spatial and temporal variation of minor species that are strong sources of radiative cooling such as hydrogen cyanide (HCN) and CH_4.

Prior to the arrival of Cassini at Saturn, modeling of the production of energetic neutral atoms (ENAs) began as a preparation for the first observations.

The INCA instrument had the capability of remotely measuring the exosphere of Titan, an ambient neutral population too tenuous to be measured by in situ mass spectrometers. Prior to the arrival of Cassini at Saturn, modeling of the production of energetic neutral atoms (ENAs) began as a preparation for the first observations. Amsif et al. [1997] developed a model that included the inner and outer exosphere, as well as the five major species contained in Titan's atmosphere, namely, H, H_2, N, N_2, and CH_4. The ENA production was modeled using a proton spectrum from the Voyager flyby. Taking into account the production from both the inner and outer exosphere (estimated using a Chamberlain model), they predicted that Cassini would be able to image the

exosphere out to at least five Titan radii. Dandouras and Amsif [1999] analyzed the production of synthetic ENA images while taking into account the same exospheric model from Amsif et al. [1997], but included the geometry of the interaction region and the expected ENA trajectories. They concluded that the INCA instrument would be able to provide information regarding the ion fluxes and spectra, as well as the magnetic field environment in the vicinity of Titan, based on a shadowing effect produced by the presence of the moon itself.

Combining data from the INCA and the INMS instruments, Dandouras et al. [2008] calculated profiles of the main exospheric species that revealed the non-thermal nature of their distributions. They also found that the ENA emissions from the interaction region get absorbed below an altitude of about 1000 km, where energetic ions deposit their energy. In terms of the extension of the atmosphere, they were able to measure it up to an altitude of 40,000 km.

Using data from SOI to 2007, Brandt et al. [2012] studied the exospheric composition of Titan. For this, 36-minute accumulation time hydrogen data from the INCA detector when observing Titan without the magnetosphere behind it were analyzed. Combining these observations with a model for the production of ENAs, they found that the molecular hydrogen exosphere of Titan extends to a distance of about 50,000 km (almost 20 Titan radii) confirming the lower limit of 5 Titan radii obtained by Amsif et al. [1997]. Taking into account the profiles obtained and the fact that ENAs have direct access to Titan's atmosphere, they estimated a precipitating energy flux from ENAs of 5×10^6 keV/(cm^2 s), a number comparable to previous estimates of precipitating energetic ions [Sittler et al. 2009a] and solar extreme ultraviolet (EUV) [Tobiska 2004].

TITAN'S IONOSPHERE

Voyager measurements, both in situ of the magnetotail and radio occultation of the main ionosphere, showed the existence of an ionosphere at Titan [Neubauer et al. 1984; Bird et al. 1997]. Subsequent theoretical modeling suggested that the ionospheric composition could be quite complex, largely due to the presence of hydrocarbons associated with dissociation and ionization of methane [Nagy and Cravens 1998; Keller et al. 1998, 1992; Fox and Yelle 1997]. But the series of Cassini measurements by the MAPS instruments quantified the ionospheric densities and the extent of the ionosphere.

The main structure of Titan's ionosphere emerged after a few flybys [Ågren et al. 2009, 2007; Robertson et al. 2009] and it became clear that solar EUV radiation dominated the ionization of Titan's upper atmosphere, and varied with the long-term EUV output from the Sun [Edberg et al. 2013a; Madanian et al. 2016; Shebanits et al. 2017] (Figure MAPS-1). Energetic particle precipitation from the magnetosphere is important on the nightside of Titan, but only occasionally makes a significant difference on the dayside [Edberg et al. 2013b]. A most surprising find was the importance of the ionosphere for the production of complex organic chemistry and aerosol particles (dust) below about 1100-km altitude, see for example, Coates et al. [2011, 2007]; Wahlund et al. [2009]; Vuitton et al. [2009]; Ågren et al. [2012]; Lavvas et al. [2013]; Shebanits et al. [2016; 2013], where the Langmuir probe provided a measure of the detailed amounts of organic ions and charged

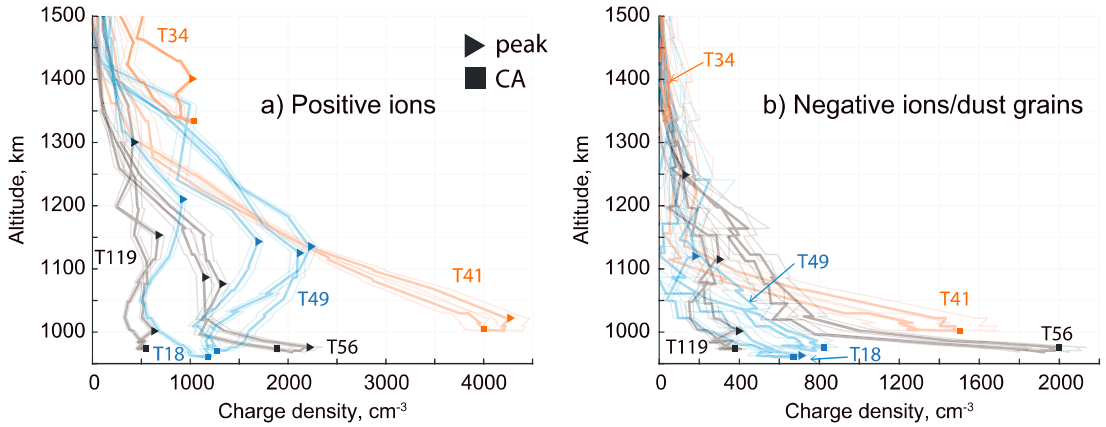

Figure MAPS-1. Examples from six flybys of Titan of altitude profiles of the positive ion and negative ion/aerosol number densities as derived from the RPWS Langmuir probe measurements [Shebanits et al. 2017]. Note the dominance of charged aerosol particles below 1100 km. Dayside flybys are colored in orange, terminator in blue, and nightside in black; the triangles mark the peaks and the squares mark the closest-approach (CA) maxima.

aerosol particles. The mechanism starts with EUV producing an N_2^+ ion that then reacts primarily with methane, with subsequently more complex C-H-N chemistry and aerosol formation [Lavvas et al. 2013].

The major ion species produced in the ionosphere is N_2^+, since N_2 is the major neutral species. However, chemical considerations told us that the main ion species at mass 28 is not N_2^+ but $HCNH^+$, so another ion species, CH_3^+, was used to almost directly deduce ion production rates [Richard et al. 2015a, 2015b; Vigren et al. 2015; Sagnières et al. 2015]. The rapid chemical reaction of N_2^+ with CH_4 produces CH_3^+ (mass 15). The ionization rate of CH_4 can be deduced by the measured CH_4^+ ions at mass 16 [Richard et al. 2015a, 2015b].

Sources of ionization deep on the nightside were also studied by Cassini. Globally, solar radiation accounts for 90% of total ionization, but precipitation of energetic electrons and ions leading to ionization is obviously locally important on the nightside [Ågren et al. 2007; Cravens et al. 2009a, 2008a, 2008b; Vigren et al. 2015; Snowden and Yelle 2014a, 2014b; Edberg et al. 2013a, 2013b; Robertson et al. 2009; Galand et al. 2014]. As on Venus and Mars, the two possible sources of the nightside ionosphere are local/direct ionization from precipitation (i.e., a diffuse aurora) and transport of plasma from the dayside. Evidence for the precipitation source is provided by INMS measurements of primary or almost primary ion species (CH_3^+, CH_4^+, CH_5^+, …), which have short chemical lifetimes and could only be produced locally and also by MIMI data which provided in situ data to understand the upstream conditions at Titan's orbit as well as the energy deposition by energetic ions in the atmosphere. Cassini data from the T5 and T18 flybys has been used to study the energy deposition by energetic ions as well as the energetic protons [Cravens et al. 2008a, 2008b; Cui et al. 2009; Smith et al. 2009].

Modeling combined with Cassini data determined that the precipitation ionization source depends on magnetic topology and on the location of Titan in Saturn's magnetosphere. Incident

magnetospheric electron fluxes and the associated nightside ionosphere were more robust when Titan was located in the plasma sheet region as opposed to the magnetic lobes of Saturn's magnetosphere [Richard et al. 2015a; Rymer et al. 2009a] and that ionization rates can vary by up to 80% from one location to another due to finite gyro radius effects [Regoli et al. 2016].

The chemistry of Titan's upper atmosphere and ionosphere is complex due to the presence of a large number of organic species extending up to high mass numbers. The neutral and ion chemistry is linked together [Waite et al. 2007]. The INMS has played a key role in improving our understanding of this chemistry. Photodissociation and photoionization of N_2 and CH_4 form ion and neutral species that are very reactive and that initiate a series of reactions that produce increasing larger species, up to aerosol-sized particles [Waite et al. 2007]. Primary N_2^+ ions react with CH_4 to produce CH_3^+, which again reacts with CH_4 to produce $C_2H_5^+$. $C_2H_5^+$ reacts with HCN to produce the very abundant species $HCNH^+$. Reactions of $C_2H_5^+$ and $HCNH^+$ with C_2H_2, C_2H_4, and C_4H_2 drive a chain of reactions leading to families of $C_nH_m^+$ species, including protonated benzene ($C_6H_7^+$), and up to masses exceeding 99 Da [Anicich and McEwan 1997; Cravens et al. 2006; Vuitton et al. 2009, 2007, 2006; Westlake et al. 2014; Cui et al. 2009; Mandt et al. 2012]. See Figure MAPS-2.

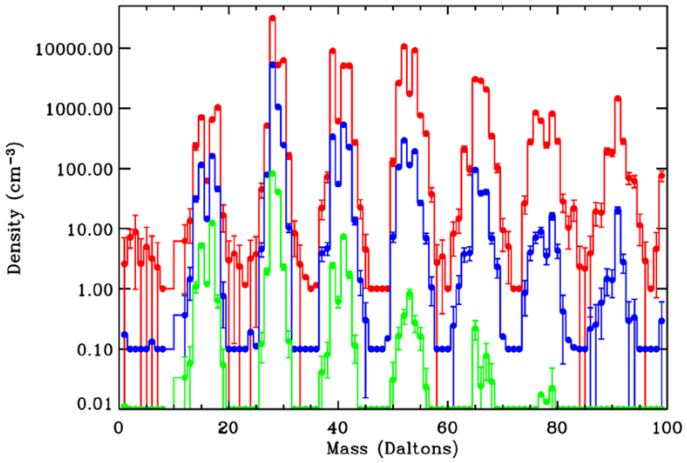

Figure MAPS-2. Shown are the first INMS measurements of ion densities versus Mass number at three different altitudes for the T5 nightside ionosphere [Cravens et al. 2006]. *Red*: 1027–1200 km. *Blue*: 1200–1400 km. *Green*: 1400–1600 km. Chemical complexity increases with decreasing altitude.

Titan's ionosphere consists of positive and negative ions, some of which have masses of up to and possibly beyond thousands of Da [Waite et al. 2007; Coates et al. 2007; Crary et al. 2009]. The study of Vuitton et al. [2007] identified over 100 ions in the INMS spectrum including several N-bearing species such as protonated ammonia (NH_4^+), $CH_2NH_2^+$, and CH_3CNH^+. Titan's atmosphere is a reducing atmosphere (little or no oxygen species are present) and as such the ionization will flow from species whose parent neutral molecules have low proton affinities (PAs) to those whose parent neutral molecules have greater PAs.

Measurements made by CAPS and INMS between altitudes of 950 to 1400 km were responsible for one of the major surprises of the Cassini mission, the high level of chemical

complexity observed in Titan's ionosphere. From the earliest close encounters electron spectrometer (ELS) detected heavy negatively charged ions with mass/charge up to 13,800 amu/q. In addition, heavy positive ions up to ~350 amu/q [Crary et al. 2009] and as high as 1000 amu/q [Coates et al. 2010] were detected by Ion Beam Spectrometer (IBS) (Figure MAPS-3). An unexpected level of chemical complexity was seen in the neutrals as well [Waite et al. 2007]. Before Cassini, models of Titan's chemistry had shown some complexity in the interaction of the neutral atmosphere with positive ions [Wilson and Atreya 2004]. The observations from Cassini necessitated more sophisticated modelling of the positive ion composition [Cravens et al. 2009b]. The negative ion observations by ELS were completely unexpected at the altitudes sampled by Cassini, opening up a whole new field for modeling and understanding the complex chemistry of Titan's atmosphere.

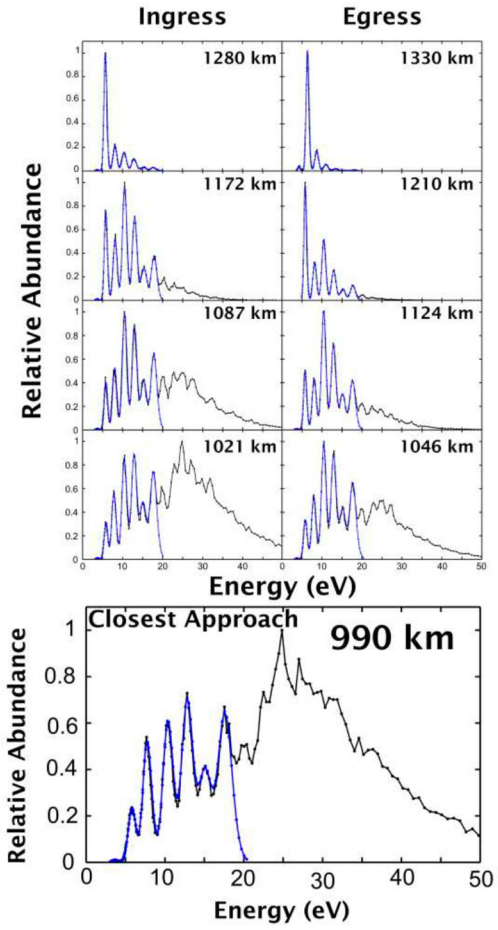

Figure MAPS-3. Shown are nine ion mass spectra obtained by the CAPS-IBS instrument at various altitudes during the T26 flyby. The blue lines show the INMS data converted using the CAPS-IBS instrument response model.

Westlake et al. [2014] analyzed the T57 flyby in detail between the CAPS and INMS observations to determine the characteristics of the processes responsible for the production and

loss of the large hydrocarbons observed at Titan. The work suggested that an ion-molecule reaction pathway could be responsible for the production of the heavy ions, namely reactions that utilize abundant building blocks such as C_2H_2 and C_2H_4, which have been shown to be energetically favorable and that have already been identified as ion growth patterns for the lighter ions detected by the INMS.

An additional discovery made by the Cassini MAPS instruments is the presence of large negative ions in Titan's ionosphere. After initial discovery by CAPS, further studies have been made of the spatial distribution and density of these ions on parameters including altitude and solar zenith angle [Wellbrock et al. 2013; Desai et al. 2017]. Wellbrock et al. [2013] have shown that the highest densities of negative ions are found at lower altitudes. Moreover, the average altitudes where peak ion densities occur decrease with increasing ion mass. In addition, the maximum altitudes at which ions from a specific mass group are observed (the reference altitude) decrease with increasing mass group. The highest mass negative ions were observed during the T16 encounter. A recent analysis of this data shows that polar winter is where the heaviest negative ions are seen [Wellbrock et al. 2019]. This helps to constrain the chemical processes at work to produce these large ions. The relativity low-mass negative ions were identified as CN^-, C_3N^-, and C_5N^- in the first chemical models used to describe the negative ions seen at these altitudes [Vuitton et al. 2009].

While some progress has been made on formation of higher mass ions, this topic is still under study. The geometric configuration of heavy ions is relatively unconstrained, and chains, rings or even fullerenes may be possible. Sittler et al. [2009a, 2009b] have suggested that the latter may trap and transport oxygen to the surface although there are as yet no observations that confirm this hypothesis. Agglomeration of large molecules caused by charging [Michael et al. 2011] or chemical processes [Lavvas et al. 2013] have been suggested as potential mechanisms to produce the large negative ions. However recent work by Desai et al. [2017] shows that chains of negative ions at intermediate masses may provide another pathway for heavy ion formation. Heavy negative and positive ions may also link up to form embryo aerosols of both negative and positive charge [Coates et al. 2007; Crary et al. 2009].

Desai et al. [2017] used observations of negative ions by CAPS/ELS to show mass peaks where unsaturated carbon-chain negative ions such as CN^-/C_2H^-, C_3N^-/C_4H^-, C_5N^-/C_6H^-, etc., might exist. Higher mass ions ~117 ± 3 amu/q and 154 ± 8 amu/q could be longer negative carbon chains with 10 or 12 or more carbon atoms in saturated aromatic versions. Thus, negative ions exist at masses where INMS cannot measure positive ions, which makes the two instruments not only complementary in their measurements but make them highly dependent on each other if we are going to have deeper insight into the composition of Titan's ionosphere. A second example of INMS/CAPS interdependence are IBS observations of heavy positive ions above 1000 amu/q [Crary et al. 2009] which complements INMS measurements that are limited to $m/q \leq 100$ amu/q.

TITAN'S MAGNETOSPHERIC INTERACTION

All the Cassini MAPS instruments have provided data, that with associated modeling, has increased our understanding of Titan's plasma interaction with Saturn's magnetosphere and, rarely, with the solar wind plasma. Titan's interaction with the magnetosphere of Saturn results in the formation of an induced magnetosphere around Titan. The virtual absence of an intrinsic field at Titan makes this interaction mainly atmospheric as fields and charged particles from Saturn or the Sun impinge on the moon's chemically complex atmosphere, exosphere and ionosphere. Atmospheric interactions are common elsewhere in the solar system with Mars and Venus as their most typical examples. In these cases, as well as in Titan's, charged particles from its atmosphere (originating from photoionization, charge exchange and electron impact) become electromagnetically coupled to those carried by the plasma winds that flow past it [Bertucci et al. 2011].

The Cassini/RPWS sensors have mapped the interaction region—for example, Modolo et al. [2007a, 2007b]—proved the existence of cold ionospheric flows from Titan—for example, Edberg et al. [2011, 2010]—as well as more energetic ion pick-up [Modolo et al. 2007b] (Figure MAPS-4), and studied how these processes change when Titan enters the magnetosheath [Bertucci et al. 2008; Garnier et al. 2009]. Titan's ionosphere also acts as a conductive medium where electric currents generated in the induced magnetosphere close [Rosenqvist et al. 2009; Ågren et al. 2011]. The escape rate through the cold plasma was determined to be a few kg/s (10^{25} ions/s), which is considered small compared to the exosphere escape rates.

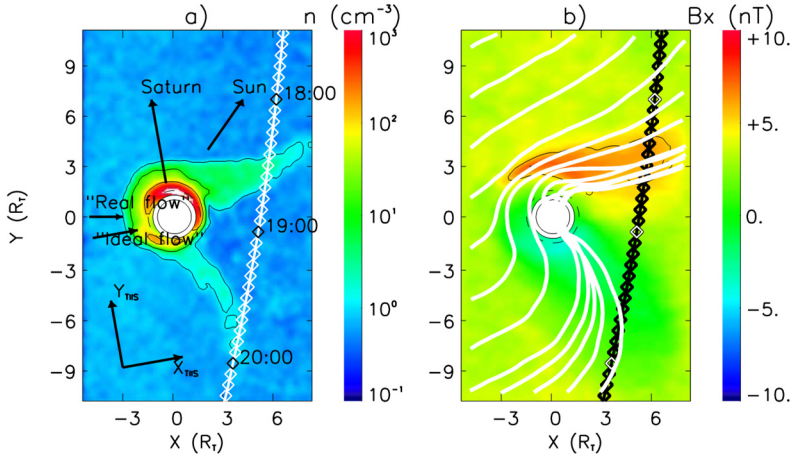

Figure MAPS-4. The induced magnetosphere of Titan as measured and modelled during the T9 flyby through the tail [Modolo et al. 2007b].

Many of the individual encounters with Titan have been studied. In joint studies of the TA flyby a comparison between MAG and RPWS-data was done by Wahlund et al. [2005] and a comparison between Cassini and Voyager data using both plasma spectrometer (PLS) and magnetic field data by Hartle et al. [2006a, 2006b]. Magnetic field and PLS electron data from flybys TA, TB, and T3 [Neubauer et al. 2006] showed a draping boundary as the outer boundary of strong magnetic field draping. In addition, the shape of the tail was found to be similar to a delta wing in aerodynamics.

It was shown that the long travel time of frozen-in magnetic field lines into the lower ionosphere of Titan led to the observation of old or fossil field lines compared with their times of arrival in front of Titan. This concept was later called memory effect by Bertucci et al. [2008] in a paper discussing Titan encounter T32 which occurred for the first time in the Saturnian magnetosheath but also contained old Saturnian magnetospheric field as a memory effect, see also Ma et al. [2009]. A special study of the magnetotails has investigated the tails by wake flybys with closest approach (CA) distances > 2.5 R_T in the whole set of flybys TA-T84 [Simon et al. 2014]. The resulting eight flybys confirmed the delta wing structure found in Neubauer et al. [2006] leading to a thickness of the wing of ±3 R_T.

The interaction between Titan and the corotating Saturnian plasma forms an induced magnetosphere with an elongated Alfven-wing-style magnetotail. During the first mid-tail flyby T9, Cassini plasma and magnetic field instruments detected in one tail lobe a magnetic flux tube connected with ionosphere and filled with cold ionospheric plasma. This magnetic structure indicates that Titan's ionosphere appears to be escaping along field lines down the tail, leading to particle loss from the atmosphere [Wei et al. 2007].

The first opportunity to study the induced tail at medium distances occurred at T9 [Bertucci et al. 2007]. This data analysis led to a number of modelling papers which helped to disentangle the detailed plasma and magnetic field characteristics [Kallio et al. 2007; Wei et al. 2007; Ma et al. 2007] of the complex magnetotail. All the early papers also led to the conclusion that an internal magnetic field of Titan was at most very small. Using the magnetic field observations on flyby orbits very close to Titan, Wei et al. [2010] found an upper limit on the moment of 0.78 nT × R_{Ti}^3 improving the Voyager 1 upper limit by a factor of five.

One most remarkable features revealed by Cassini MAG instrument was that Titan's induced magnetosphere is formed by layers of different polarity of the external magnetic field that allow to reconstruct the history of the moon's magnetic environment. Indeed, in the same way as older sediments lay beneath more recent deposits in geology, the magnetic fields fossilized in the deep layers of Titan's induced magnetosphere provide information about the orientation of the field Titan was exposed up to three hours before the encounter with Cassini [Bertucci et al. 2008]. This magnetic memory of Titan is significantly longer than at Venus and Mars and is a result of the capacity of Titan plasma to remove momentum form the external plasma. A further study of the ionosphere of Titan with its embedded magnetic field on the nightside ionosphere was published by Cravens et al. [2009a]. During the interaction between Titan's ionosphere and its ambient plasma, Cassini observations find that the lower ionosphere of Titan is often magnetized, with large scale magnetic fields and some structures resemble magnetic flux ropes. These flux ropes are either starting to form or maturely formed, with their axial orientations in agreement with the formation mechanism [Wei et al. 2010].

This magnetic memory of Titan is significantly longer than at Venus and Mars and is a result of the capacity of Titan plasma to remove momentum form the external plasma.

Titan's orbit is typically located inside Saturn's magnetosphere, but could occasionally move outside it into the magnetosheath or even into the solar wind. T96 was the first encounter presumably occurring in the supersonic solar wind and the observed structures at Titan's unique example of interaction with the supersonic solar wind were similar to structures found at Mars and Venus (an induced magnetospheric boundary and a collisional bow shock) [Bertucci et al. 2015]. Omidi et al. [2017] made simulations which showed that a deformed bow shock could form that would encompass both Titan and Saturn's magnetosphere.

To understand the internal magnetic moments of Titan, we use the radial component of Cassini magnetometer observations near Titan surface (from 950 km to 1100 km) is used to calculate the permanent dipole moment. The upper limit to Titan's permanent dipole moment is 1.25 nT × R_{Ti}^3, using the observations during the southern summer season of Saturn (April 2005 to March 2009). This weak internal field indicates the interior of Titan may not contain a liquid core sufficiently electrically conductive for a magnetic dynamo to be generated inside Titan or even for the simple amplification of the external magnetic field [Wei et al. 2010]. For the signs of the calculated internal field components, the g11 and h11 component, corresponding with the Titan-to-Saturn direction and the corotation direction, respectively, are in agreement with the signs of the averaged ambient field around Titan during the observation period. This indicates that these estimated internal moments may be due to the penetration of the ambient field into the interior of Titan, generating induced fields. After Saturn's equinox, August 2009, the ambient of field of Titan changes sign in the Titan-to-Saturn direction and the corotation direction, as Titan moved from below Saturn's current sheet to above it. Thus, we compare the calculated internal moments using the observations before and after Saturn's equinox, and find that the g11 and h11 moment change sign in agreement with the sign of Titan's ambient field.

The Cassini/CAPS instrument measured pick-up ions in the form of beams of CH_4^+ and N_2^+ that can be explained theoretically as the result of kinetic interactions between Titan and the magnetosphere [Hartle and Killen 2006; Hartle and Sittler 2007; Hartle et al. 2011]. It is no surprise that beam composition is consistent with the composition Titan's exosphere and atmosphere which is dominated by N_2 (98.4%) and CH_4 (1.4%) [cf. Waite et al. 2005].

Sittler et al. [2010] observed nearly field aligned outflows from the topside ionosphere during the T9 flyby and estimated the loss of methane ions due to pick-up from the exosphere at ~5 × 10^{22} mol/s [Sittler et al. 2009a]. The outflows serve ultimately as a sink from Titan's atmosphere of roughly ~5 × 10^{24} mol/s. Later, Coates et al. [2012] observed similar amounts of ionospheric outflows during the T9, T63, and T75 flybys. The theoretical cause of these outflows was originally discussed in Hartle et al. [2008]. It is produced by a field-aligned polarization electric field E_{pol} ~−$1/n_e e \nabla_{||} P_e$ so that above the ionospheric density peak the outward acceleration is > 10 times the force of gravity for m/q ~28 amu/q ions. (Note: the ionospheric electron temperature T_e ~1000° K is much greater than the ionospheric ion temperature T_{ION} < 180° K, which gives rise to charge separation and hence the dipolar electric field.) Sittler et al. [2010] found that the resulting ion outflow speeds were ~7 km/s with T_{ION} ~50,000° K. Therefore both significant accelerations and heating must have occurred at altitudes above 5000 km. Later, using electron observations, Coates et al. [2015] measured the total potential

drop of this electric field to be ~0.2 μV/m to heights ~15,000 km, which is sufficient to accelerate methane ions to the observed speeds ~5–6 km/s. Future 3-D hybrid simulations similar to that done by Lipatov et al. [2014, 2012, 2011] will be required to understand the heating, for example, due to wave-particle interactions, of ions to the observed high temperatures. In addition to the outflows, Sittler et al. [2010] also found evidence of Alfven waves during the T9 flyby with transverse velocity and magnetic field fluctuations that were anti-correlated with time and thus consistent with field-aligned propagation of these waves.

One other surprising observation that affects Titan atmospheric chemistry was CAPS' discovery of kilovolt oxygen ions with inflows ranging up to ~1023 O^+/s [Hartle et al. 2006a, 2006b] arriving from the magnetosphere at the exobase of Titan's atmosphere. Its likely origins are Enceladus and the rings, see Johnson et al. [2005]; Cassidy and Johnson [2010]. Oxygen combined with the complex chemical makeup of the ionosphere is most likely the source of CO in the atmosphere [Hörst et al. 2008; Krasnopolsky 2012]. The influx of O^+ into the atmosphere, where it undoubtedly affects Titan's already complex chemistry, is one more unusual and interesting aspect of Saturn's magnetosphere in which it acts as a conduit for the chemistry of one moon (Enceladus plumes) to affect the chemistry of another.

The peak ionospheric density at Titan was found to be dependent on solar cycle variations by Edberg et al. [2013a]. RPWS measurements of the electron density in the ionospheric peak region made during 2012 (T83–T88) showed significant increases compared to previous averages. These measurements suggest that a solar cycle variation caused by the rise of EUV fluxes during solar maximum. The study uses a power law to estimate the peak electron density at the subsolar point of Titan during solar maximum conditions and find it to be about 6500 cm^{-3}, i.e., 85–160% more than had been previously measured during the entire Cassini mission.

TITAN'S ATMOSPHERIC LOSS

Both CAPS and the INMS have provided crucial data for estimating processes that contribute to atmospheric loss. The review article by Johnson et al. [2009] highlights mechanisms and estimates of loss. They are primarily H_2 thermal (or Jeans) escape, CH_4 destruction/precipitation, N_2/CH_4 sputtering, ion pick-up causing ionospheric outflows, CH_4 hydrodynamic outflow [Yelle et al. 2008], and CH_4 plus H_2 hydrodynamic outflow [Strobel 2008].

Waite et al. [2005] presented the first observations of H_2, CH_4 and N_2 altitude profiles extending above the exobase to ~1400 km. There is a break in the altitude profiles above the exobase that is consistent with atmospheric escape. Cui et al. [2008] and Bell et al. [2009] estimated H_2 escape to be ~10^{10} amu/q/cm^2/s locally, and ~1.6 × 10^{28} amu/q/s globally (integrated over the entire surface area of the atmosphere). Sittler et al. [2010] reported that during the T9 and T18 flybys H^+ and H_2^+ ions were present in the flow of plasma moving towards Titan. The ions also happened to be moving perpendicular to the local magnetic field, leading Sittler et al. [2010] to conclude that they were seeing pick-up ions from Titan's hydrogen corona which can extend to ~20 Titan radii (i.e., out to the Hill sphere).

The primary chemical losses occur when methane is dissociated and ionized by photochemical reactions initiated by solar UV and particle impact. Further reactions with neutrals and ions then make heavier hydrocarbons and nitriles, which can eventually grow into aerosols that precipitate to Titan's surface. Sittler et al. [2009a], using an analogy to molecular clouds and planetary nebulas, suggested that negative chains of carbon atoms form and eventually fold into fullerenes, implying that the same might be going on at Titan. They then estimated precipitation to the surface to be ~2.7 × 10^{-14} kg/m^2/s at 950 km altitude and a global rate of ~4 × 10^{27} amu/q/s. This mass loss rate appears to dominate all other present day atmospheric loss mechanisms [e.g., Johnson et al. 2009] and, because it is large, in order to maintain a steady state methane concentration would require upward diffusion of methane, presumably from a source of methane from Titan's surface.

Sittler et al. [2009a] estimated the loss rate due to pick-up ions to be between ~5 × 10^{22} ions/s and ~10^{24} amu/q/s, which is much smaller than the lower bound given by Johnson et al. [2009] of ~10^{26} amu/q/s possibly due to the inclusion of scavenging down Titan's ion tail, see for example, Sillanpää et al. [2006]; Hartle et al. [2006b]. Escape caused by ionospheric outflows are ~5 × 10^{24} mol/s or ~10^{26} amu/q/s [Sittler et al. 2010; Coates et al. 2012] which may be included in the Johnson et al. [2009] estimate. The escape fluxes caused by sputtering, hot atomic recoils and charge transfer by ENAs also cause heating of the thermosphere and corona [De LaHaye et al. 2007a, 2007b]. Adding all these terms Johnson et al. [2009] find a total escape rate of ~0.32 to ~3.8 × 10^{28} amu/q/s.

Recent work highlights the need to reanalyze INMS data using detailed models of sputtering and energy deposition in the upper atmosphere in order to understand the energy distribution of neutral molecules in the exosphere region. Snowden and Yelle [2014a, 2014b] used Fourier's Law to extract energy deposition rates in the upper atmosphere from INMS data. They determined that precipitation of magnetospheric ions observed by CAPS is too small to explain the observed temperature variations and escape rates. They suggest that gravity waves produced in the lower atmosphere could produce the variability, but a source for the waves has not been identified.

Tucker et al. [2016] showed that using the Louisville Theorem approach, with a non-thermal energy distribution at the exobase, can lead to incorrect estimations of the upper atmospheric thermal structure and, consequently, escape rates due to collisions in the transitional region. Furthermore, such corona fits obtain different exobase energy distributions for N_2 and CH_4 density distributions, which is suggestive of different heating mechanisms occurring between species. Therefore, ion/pick-up fluxes and spectra extracted from CAPS data and model development of gas-kinetic models are needed for detailed simulations of the ion-neutral interaction. Such models can consider the ion - neutral interaction at the microscopic level, and include the production of hot recoil molecules.

The final topic is hydrodynamic loss proposed by Yelle et al. [2008] and Strobel [2008]. By using CH_4 and N_2 ingress altitude profiles with methane diffusing through atmospheric N_2, and then using the ^{40}Ar density profiles, they were able to separate the molecular and eddy diffusivities, which then required an upward methane flux ~4–5 × 10^{10} amu/q/cm^2/s and globally

~4.5 × 10^{28} amu/q/s. This estimate is close to the chemical destruction/precipitation of methane to heavier molecules and aerosols. The model by Strobel [2008] called slow wind argues that solar UV penetrates below the ionosphere where it is deposited. This excess heat is then conducted upward to higher altitudes to drive the hydrodynamic slow wind. But, in order to meet the upward flux required by Yelle et al. [2008] this heat must be transported above the exobase where there are no collisions to conduct the heat, which is its major weakness. Direct Simulation Monte Carlo (DSMC) simulations by Tucker and Johnson [2009] did not show any enhancement of the methane escape rate significantly greater than the Jeans escape rate ~3 × 10^{22} amu/q/s. Therefore, it is highly unlikely that Titan is currently undergoing hydrodynamic escape of CH_4. Tucker et al. [2013] showed that H_2 escape cools the background gas resulting in non-isothermal density profiles without requiring a significant escape rate. Volkov et al. [2011a, 2011b] examined the hydrodynamic escape problem in detail using DSMC simulations. They found that above a Jeans parameter of 6 at the exobase the thermal escape rate is enhanced towards the analytical Jeans rate only by a factor of 1.4–1.7. This is in contrast to Strobel [2008] which predicts a CH_4 escape rate orders of magnitude larger than the Jeans rates, due to an overestimation of heat conduction in the transitional region.

Icy Satellite Science

Interaction of the Enceladus plume with the magnetosphere

- **M_AO2:** Determine current systems, composition, sources, and sinks of magnetosphere charged particles.
- **M_AO3:** Investigate wave-particle interactions and dynamics of the dayside magnetosphere and the magnetotail of Saturn and their interactions with the solar wind, the satellites, and the rings.
- **MC1a:** Determine the temporal variability of Enceladus' plumes.
  - Investigate temporal variations in Enceladus gas production and plume composition, on the scale of seasons and solar cycle.
  - Study plume neutral gas composition.
  - Investigate the physics of the dusty plasma environment.
  - Determine how the magnetosphere reacts to changes in (plume?) gas production rates by studying Enceladus' auroral footprint.
  - Study variability in dust-to-gas mass ratio.
- **MN2a:** Determine the coupling between Saturn's rings and ionosphere.
  - Study how field aligned currents are coupled to the rings and satellites.
  - Explore the dust dynamics in the proximity region.
  - Investigate the mid-plane of Saturn's D-ring.

- Determine the grain composition in the proximity region.
- Investigate the possible interaction of lightning with the inner magnetosphere and the rings.
- Investigate Coupling Between E-ring and the Enceladus neutral and plasma tori.

The initial Cassini MAPS teams began planning for Enceladus encounters as if Enceladus was just another small icy satellite albeit of some additional interest due to the fact that it was embedded in the E-ring. All this changed with discovery of an atmospheric plume at Enceladus by the magnetometer team [Dougherty et al. 2006] on February 17, 2005. With later confirmation by subsequent measurements by many Cassini instruments on later flybys Enceladus quickly became one of the most important objects in the Saturnian system. The main question to answer, "Does Enceladus have liquid water beneath the surface?", because the answer could be the major determining factor if life could exist there.

With the discovery of a thin neutral atmosphere by the magnetic signature of an electrodynamic interaction, all the other Cassini MAPS teams began to reexamine their previous data and to also plan new observing strategies for future encounters.

In 2005, and far from Enceladus, CAPS/Ion Mass Spectrometer (IMS) measured pick-up water group ions (O^+, OH^+, H_2O^+ and H_3O^+ or, collectively, W^+) throughout Saturn's inner magnetosphere [Young et al. 2005; Sittler et al. 2006a, 2006b, 2005; Tokar et al. 2008]. The source of these ions is charge exchange collisions that scatter water group neutrals, replacing a fraction of the co-rotating core distribution with a new and slower-moving ion population without changing the total ion content. The newly-created ions are moving near the local Keplerian speed, which is slower than the co-rotation speed, and hence are picked-up by Saturn's magnetic field. IMS detected these water-group ions within their source region, the Enceladus torus, thus providing the first measurements of W^+ ions throughout their toroidal source region and far from Enceladus. High ion count rates in IMS were observed at the ion pick-up energies, with largest signals near the Enceladus and Dione orbits.

Although encounters with Enceladus later in the mission would be at much closer distances, CAPS was still able to detect indications of a strong interaction between Enceladus and magnetospheric plasma … .

Striking observations were also obtained with IMS during the close encounters of Cassini with Enceladus. On the same encounter where MAG made its discovery, the spacecraft flew within 175 km of Enceladus, and passed through its surrounding cloud of neutrals and plasma. Although encounters with Enceladus later in the mission would be at much closer distances, CAPS was still able to detect indications of a strong interaction between Enceladus and magnetospheric plasma [Tokar et al. 2006]. Originally detected by the Hubble space telescope, Enceladus was known to sit in a cloud of neutral OH forming a torus around Saturn. The cloud detected by CAPS extends from about 3 to 8 R_S with maximum concentration of ~10^3 cm^{-3} inferred to exist near the orbit of

Enceladus (3.95 R_S). The OH cloud is produced by dissociation of H_2O, and although the peak concentration suggested that the largest source of water molecules was in the region near the orbit of Enceladus, the nature of this source was unknown. IMS measurements during the 2005 encounter established a strong perturbation of the plasma flow caused by Enceladus, and perhaps most importantly, the presence of W^+ ions. This population had been detected earlier during SOI [Young et al. 2005].

Later in the mission, during closer encounters with Enceladus, CAPS obtained in situ measurements of W^+ ions freshly produced in the dense Enceladus plume. The dominant species there are light ions (H^+, H_2^+), W^+ ions, and single water cluster ions, ($H_2O \times H_2O^+$). All were observed close to, and nearly due south, of Enceladus. The ions have kinetic energies in the IMS frame roughly equal to ions that are at rest with respect to Enceladus and rammed into the CAPS sensors at the spacecraft speed. This is the signature of freshly produced ions in the plume due, e.g., to charge exchange interactions of incoming magnetospheric ions with neutral plume gas. Figure MAPS-5 shows an example of these ions detected by IMS during the E3 encounter only 52 km from Enceladus. The high count rates close to the ion ram energies in CAPS (denoted by vertical arrows) are clearly visible. Further details of these data are discussed in Tokar et al. [2009].

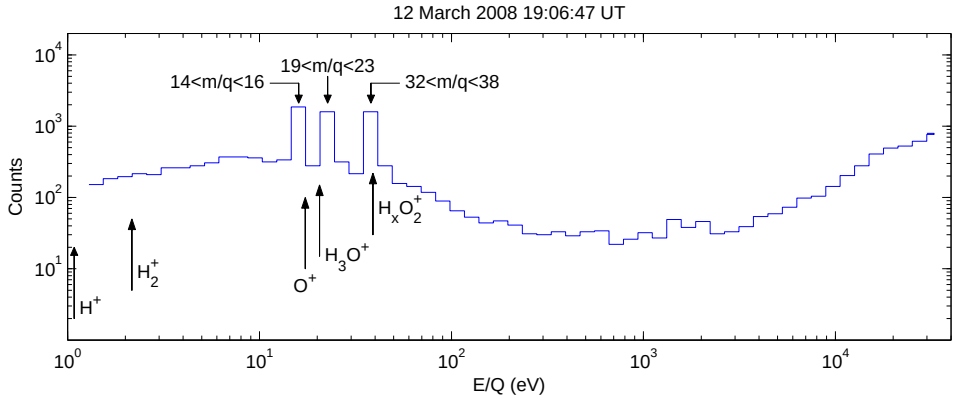

Figure MAPS-5. Individual ion counting rates versus energy per charge measured by IMS anode 5 within the plume during the March 12, 2008 (E3) flyby of Enceladus. Figure from Tokar et al. [2009].

The E7 encounter on November 2, 2009 provided additional observations of the plume stagnation region as Cassini passed directly through the Enceladus plume. The IMS detector sensitive to rammed ions observed stagnation and fresh ions at the ion ram energies. The strong interaction region within the plume is clearly visible in the CAPS IMS data as are the water group ions near 10 eV that are at rest in the Enceladus frame.

The E7 encounter also exhibited the close correspondence between IMS observations of ion slowing and the observed entry into the dense water vapor plume measured by INMS. The data suggest that magnetospheric plasma enters the dense plume leading to charge exchange with plume water vapor followed by subsequent pick-up into the corotating flow. The signature of this process is very sharp on the Saturn-ward side of the plume as the new ions are picked-up and gyrate away from Saturn. The transition out of the plume opposite Saturn for E7 is more extended

due to a number of factors—for example, ion drift velocity and variable ion gyro radii for the various masses created. Note that the IMS observed ion flow speed from the count distributions in the ram direction imply speeds as low as a few km/s in the Enceladus frame.

RPWS results from the E8 flyby reported observations of whistler mode auroral hiss emissions produced by magnetic field-aligned electron beams [Gurnett et al. 2011b]. A ray path analysis of the funnel emission shows the hiss source region within a few moon radii of the Enceladus surface. Figure MAPS-6 is adapted from Gurnett et al. [2011b] Figure 2, and shows the auroral hiss funnel from the E8 flyby in the top panel and the nearly field-aligned electron beams from the CAPS ELS instrument in the second panel. The magnetometer observations of the field-aligned currents which accelerate the electron beams are shown in the bottom panel. The ramp-like signature of the southward current is associated with a shear-mode Alfven wave excited by the moon-plasma interaction. Parallel electric fields, often associated with the Alfven wave, are believed to be accelerated by these waves along magnetic field lines that map to the Enceladus footprint in Saturn's aurora [Gurnett and Pryor 2012]. Sulaiman et al. [2018] showed evidence of currents

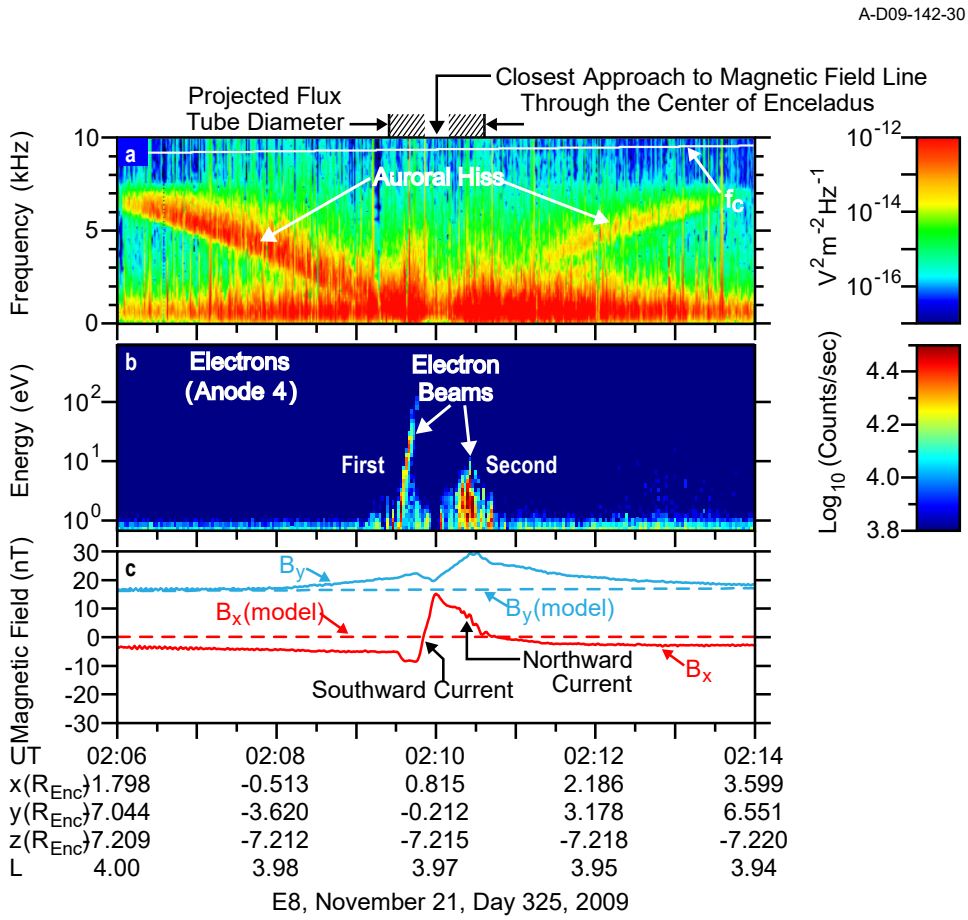

Figure MAPS-6. The auroral hiss funnel from the E8 flyby in the top panel and the nearly field-aligned electron beams from the CAPS ELS instrument in the second panel. Figure from Gurnett et al. [2011a].

between Enceladus and Saturn in the form of very low frequency (VLF) saucers generated by electron beams from Saturn's ionosphere on the Enceladus flux tube.

In addition to the dense neutral water vapor measured by INMS and the resulting cold plasma measured by CAPS and RPWS-LP, the south-polar plume of Enceladus was also found by CAPS and INMS to carry singly charged nanometer-size water-ice grains [Coates et al. 2009; Farrell et al. 2009; Jones et al. 2009; Hill et al. 2012; Morooka et al. 2011; Meier et al. 2015, 2014; Dong et al. 2015]. Such nanograins had been inferred to exist in various cold, tenuous geophysical and astrophysical environments, but the close Enceladus plume encounters by Cassini offered the first (and still the only) opportunity to measure and characterize the nanograins in situ. Before the CAPS shutdown in June 2012 there were three close Enceladus encounters that provided the CAPS ram pointing required to measure these high mass-per-charge particles—E3 on March 12, 2008, E5 on October 9, 2008, and E7 on November 2, 2009. The detailed analysis was reported by Hill et al. [2012]. RPWS data was used by Farrell et al. [2009] to present high-time resolution spectral evidence from the E3 flyby of small water-ice grain impacts on the electric antennas in the vicinity of Enceladus and a sudden, large drop in the electron density in the same region, a density depletion that they attribute to the absorption of electrons by sub-millimeter-sized icy particles. Morooka et al. [2011] presented Langmuir Probe observations to provide evidence for the presence of dusty plasma in the Enceladus plume region. The data show large increases in the ion and electron densities just south of the equatorial plane in the plume region for four Enceladus flybys in 2008, but there is a two order of magnitude difference in these plasma densities with $n_e/n_i < 0.01$. This plasma signature is attributed to electron absorption by dust grains in the plume, which subsequently become negatively charged. Data shows the strong drop in the ne/ni density ratio in this same region where the presence of dust grains had been previously determined [Farrell et al. 2009]. The density profiles of these micron size dust grains was measured by the CDA and RPWS instruments [Ye et al. 2014a]. Additionally, RPWS measurements show almost Keplerian ion speeds measured by the Langmuir Probe which are well below the plasma corotation speed, reaching a minimum below Keplerian speeds in the plume region. The interaction between the cold plasma and the negatively charged small dust grains is believed to cause this slowing of the plasma that moves with Enceladus, explaining the lack of a plasma wake behind the moon.

The presence of dust grains inferred by the ion-electron density difference led to a number of research results. Ye et al. [2014b] discovered that, after a dust grain impacted the RPWS electric antennas, a dust ringing effect was observed by the RPWS wideband receiver, characterized as periodic plasma oscillations. The frequency of these oscillations was shown to be consistent with the local electron plasma frequency, providing a measurement of the electron density. Densities derived from this method in the Enceladus plume region were found to be consistent with electron densities derived by the Langmuir Probe for four consecutive Enceladus flybys in 2008. Shafiq et al. [2011] presented Langmuir Probe observations of the E3 flyby to derive estimates of the dusty plasma parameters and found that the dust density would vary depending on the grain size. The submicron-sized dust grains dominate in the plume region with densities of 10^2 cm^{-3}. The micrometer-sized and larger sized grains are estimated to have densities of only 6.3×10^{-5} cm^{-3}.

Analysis by the CAPS team confirms that the nanograins are largely uncharged when they emerge from the surface vents, and become increasingly (mostly negatively) charged as they approach Cassini a few tenths of Enceladus radii away. The charged nanograin density versus distance from the surface source is shown in Figure MAPS-7, from Hill et al. [2012]. The dashed line shows the r^{-2} dependence that would be expected if the grains were already charged when they emerged from the source. The most plausible charging mechanism is electron attachment from the dense plume plasma. The non-neutrality of the nanograins observed by CAPS, n(−) >> n(+), plausibly cancels the opposite non-neutrality of the plume plasma observed by RPWS-LP. Most of the electrons missing from the plume plasma reside on the nanograins.

This dynamic atmospheric plume was shown by the Imaging team to be due to geyser activity on the southern hemisphere of Enceladus. The electrodynamic interaction involves southern and northern Alfvén wings such that the atmospheric influence not only shows up in the southern, but also the northern wing, hemispheric coupling [Saur et al. 2007]. Using these concepts and magnetic field observations of flybys E0, E1, E2, and neutral density measurements at E2 the time variability of the plumes was investigated [Saur et al. 2008]. Subsequent modelling based on analytical theory clearly showed that the magnetometer results required the presence of negatively charged dust particles [Simon et al. 2011]. The paper also proves the presence of the hemispheric coupling currents required by Saur et al. [2007]. The interaction was later modelled numerically in detail using a hybrid (fluid electron) kinetic code including charged dust particles [Kriegel et al. 2011]. As a unique feature at Enceladus dust–plasma interactions play an important role to explain the observations.

Further modeling has been applied to a spherical obstacle in a plasma flow to show the effect of the moon and local pick-up separately [Jia et al. 2010a]. With this model, we have refined the plume geometry with E2 data [Jia et al. 2010b] and constrained the outgassing rate of the Enceladus plume with data from the nine early flybys [Jia et al. 2010c, 2010d].

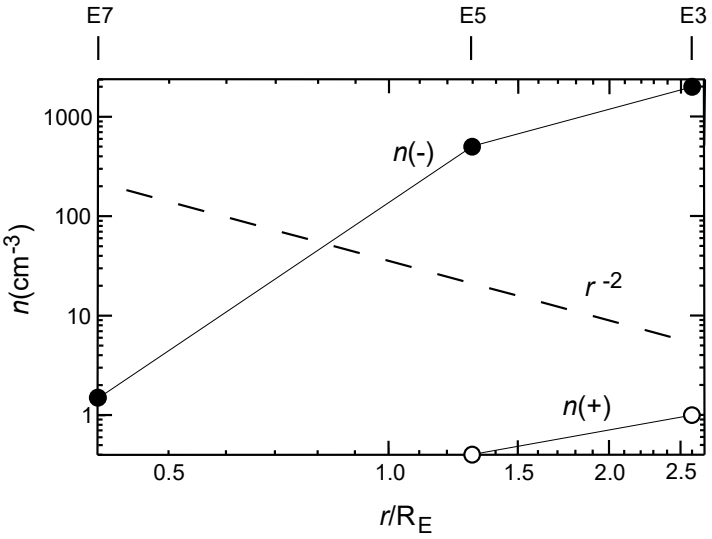

Figure MAPS-7. Total charged nanograin number density within the CAPS E/q range versus distance from the south-pole source vent.

Plume brightness is found to be varying by a factor of a few around the apocenter of Enceladus orbit, using visual images. In contrast, when we plot our deduced outgassing rate against time, we have found 50% variation in gas production rate during the first nine passes E0–E8. The magnetometer could not confirm this postulation with local interaction data. Then, the field perturbation perpendicular to both the direction of magnetospheric flow, and to the magnetic field has been studied with our multi-fluid code, to illustrate the effect of charged dust in creating such a field perturbation [Jia et al. 2011].

Beyond the plasma interaction physics that has been explored by the Cassini/MAPS team, extensive measurements by the INMS team has contributed to characterization of the neutral species in the plume, the plume distribution and to questions about the internal ocean.

The first close flyby of Enceladus with a ram pointing orientation for INMS occurred during the E2 encounter on the July 14, 2005 when Cassini passed with 168.2 km of the flank of Enceladus. The presence of water vapor emanating from the south polar cap was noted over 4000 km before the encounter. A day later on July 15, 2005, the first INMS measurements of the plume's composition were made in the plume's outer edge, and revealed that the plume consists predominantly of water vapor, with small amounts of carbon dioxide, methane, a species of mass 28 (carbon dioxide and molecular nitrogen were suggested), and trace quantities of acetylene and propane.

The next major milestone for INMS occurred during the E5 flyby that occurred at a much higher relative velocity of ~18 km/s, approached from the Northern hemisphere and fly out along the south polar axis. This produced the highest signal to noise mass spectra of Enceladus of the entire mission due to the long outbound duration in the plume. The integrated mass spectra, reproduced from Waite et al. [2009] Figure 1, shows a much more complex spectrum extending out to the limits of the INMS mass range (99 u) (Figure MAPS-8).

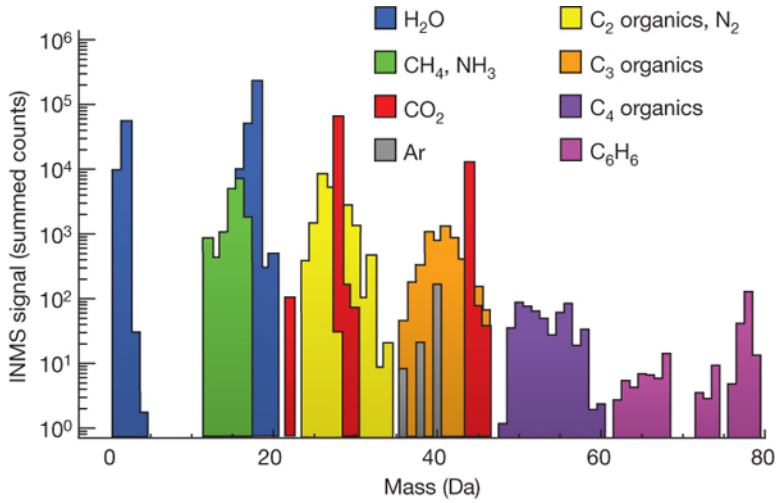

Figure MAPS-8. A complex spectrum extending out to the limits of the INMS mass range (99 u). Figure from Waite et al. [2009] Figure 1.

A mass deconvolution of the E5 integrated mass spectra indicates a host of complex organic compounds, as well as, the compounds previously cited on flyby E2: water, carbon dioxide, methane, mass 28, ammonia, acetylene, and propane. Of particular note was that water seems to be converted into molecular hydrogen and some other compounds abundance altered due to the high flyby speed. This conversion was interpreted and later verified [Walker et al. 2015] as due to raw titanium vapor from ice grain impacts reacting with water to form TiO and TiO_2 and leaving behind the H_2. The serendipitous side effect of this reaction allowed the INMS team to determine the D/H ratio in water from Enceladus, which was found to be similar to comet Halley ($2.9\ (+1.5/-0.7) \times 10^{-4}$) suggesting that Enceladus had never come into chemical equilibrium with the protoplanetary nebula of Saturn otherwise the ratio would have been much closer to the protoplanetary value of 2×10^{-5}.

The INMS data obtained during the E14, E17, and E18 flybys, all at relative flyby speeds of 7–8 km/s and all along or in parallel tracks near the Baghdad tiger stripe, provide a consistent and repeatable depiction of the mass spectra at relative speeds low enough that fragmentation effects are minimized. The spectra above 50 u (not shown) were near the noise level and further reinforce the point that the relative speeds above 8 km/s can lead to significant fragmentation of heavy organics buried in ice grains that complicate the interpretation of the mass spectra from E3 (~14 km/s) and E5 (~18 km/s). One can mass deconvolve the combined spectra from the slower flybys (E14, E17, and E18) (see Figure MAPS-9). The detailed analysis of this data set is the subject of a paper in preparation by Magee et al. [2018].

During six encounters between 2008 and 2013, the Cassini INMS made in situ measurements deep within the Enceladus plumes. Throughout each encounter, those measurements showed density variations that reflected the nature of the source, particularly of the high-velocity jets. Since

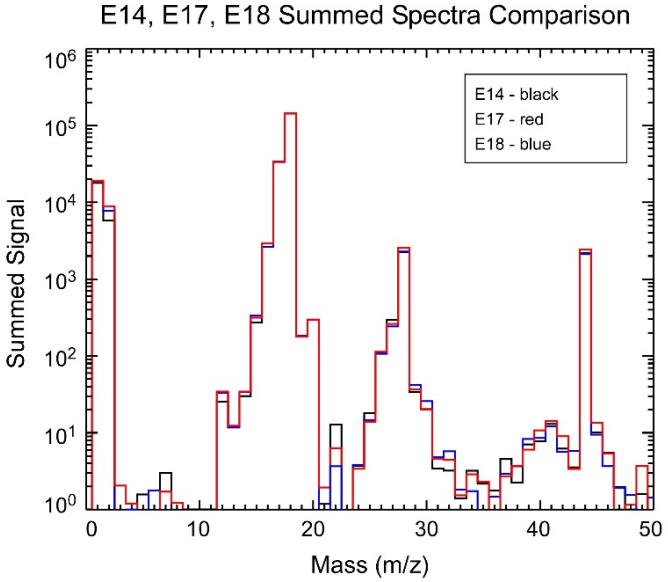

Figure MAPS-9. Overlaid mass spectra for flybys E14, E17, and E18. Note the consistency of the spectra.

the dominant constituent of the vapor, H_2O, interacted with the walls of the INMS inlet, changes in the external vapor density are tracked by using more-volatile species that responded promptly to those changes. To understand the plumes requires examination of each of the three components of Enceladus ejecta, fast and dense jets, slower diffuse gas, and ice grains.

The vapor plumes show variability that was first reported by Hedman et al. [2013]. A comparison of data from the last three encounters, E14, E17, and E18, are consistent with the VIMS observation of variability in jet production and a slower, more diffuse gas flux from the four sulci or tiger stripes. Teolis et al. [2017] used data from all INMS and Ultraviolet Imaging Spectrograph (UVIS) encounters to constrain a time-dependent and high-resolution model of the plumes.

During the final low-altitude flybys of Enceladus, the most abundant, non-sticky species in the plume, CO_2 at 44 u, was sampled at a higher rate, to enable higher-resolution measurements of local density variations along Cassini's trajectory, achieving resolution of 0.25 s temporal and 1.9 km spatial. As shown in Figure MAPS-10, CO_2 data from E17 clearly resolved density variations, indicative of gas jets, along Cassini's trajectory. Hurley et al. [2015] suggested on the basis of Monte Carlo models that the plume source may be continuously distributed, albeit variable, along the tiger stripes. These models included one lower-velocity component for the tiger stripes and a second, higher-velocity component for the jets. The complete plume three-dimensional structure is difficult to uniquely constrain solely on the basis of the few INMS flybys as multiple combinations of jet pointing directions and intensities can fit the data, and temporal variability further increases the potential solutions.

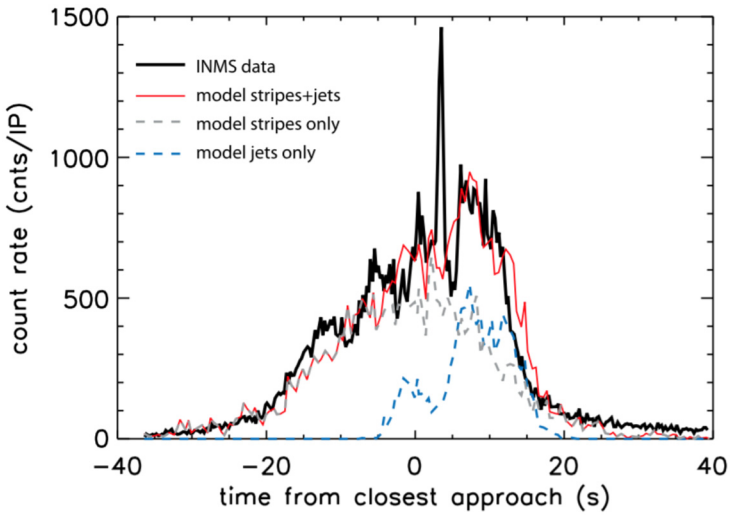

Figure MAPS-10. INMS measurements of mass 44 u species during the E17 flyby are shown in black. Model [Hurley et al. 2015] predictions using constant emission along the tiger stripes at 500 m/s and 270 K (gray dashed line) are selected to match the rise and fall on the outskirts of the plume. The jet model using Mach 4 (1500 m/s and 270 K) are included (blue dashed line) to reproduce the overall enhancement near closest approach. The sum of the two models, shown in red, reproduces the overall structure of the plume, but misses some of the fine structure.

During Cassini's close (99, 74, 74 km) E14, E17, and E18 flybys through the Enceladus gas/dust plume on October 1, 2011, March 27, 2012, and April 14, 2012, the INMS measured in situ the detailed spatial structure of the neutral gas along the trajectories. These encounters were the first to fly close enough to the plume sources with the required pointing and sufficient data acquisition rate, to enable resolution of individual gas jets within the broad plume by INMS. During these flybys two INMS objectives were to: 1) constrain the locations, magnitudes and gas velocity from the plume surface sources; and 2) extrapolate the three-dimensional structure of the plume, including the diffuse plume and individual major jets. Since these flybys, the INMS team have carried out detailed plume modeling, combining the along-track densities measured at different times/dates by INMS, with and occultation, surface temperature, and imaging data from UVIS, Composite Infrared Spectrometer (CIRS) and ISS. The goals were to constrain the physics of the jet sources, that is, the nozzle dimension and gas thermodynamic properties including temperature, density, flow and expansion rate, and provide necessary inputs for future modeling of the plume interaction with the Saturn system, that is, the E-ring and magnetospheric sources and mass loading.

The results of our studies are now published in the papers by Perry et al. [2015] and Teolis et al. [2017]. Teolis et al. [2017] describes a detailed comparison of several plume source scenarios. The findings indicate that a time variable source, consisting of: 1) a source continuously (but non-uniformly) distributed along the tiger stripes; and 2) sharp gas jets as inferred from ISS data [Porco et al. 2014], provide the best fit to the INMS and UVIS data.

In the curtain and jet cases, the model suggests that a gas source with a Mach number distribution, containing a slow (with thermal velocity, Mach 0) isotropic emission, and a super-sonic (high velocity) component, was required to fit the broad distribution, and the fine structure, respectively, observed in the UVIS/INMS data. The fits use a 4-point Mach number distribution ranging from zero (gas at rest) to 16 (the fast component), as necessary to best fit the shapes of the features in the INMS and UVIS data. The curtain model considered three cases: 1) a uniform emission along the tiger stripes; 2) emission correlated to the tiger stripe temperature from CIRS data (Figure MAPS-11); and 3) emission optimized to fit the INMS and UVIS data. For jets, the model considered two cases: 1) jets with equal intensities; and 2) jet intensity optimized to fit the data. The optimized models typically give multiple solutions, corresponding to reductions/ enhancements in different combinations of jets, or different vapor source distributions along the tiger stripes. Figures MAPS-26–MAPS-30 show the averages over these solution 'families' to compare and contrast the quality of the fits in the cases of continuous distributed emission and of discrete gas jets. It is clear on the basis of the plots, that neither the thermal plume cases, nor the cases of uniform curtains or jets, provide very good fits to the data. Both optimized curtains and jets yield rough agreement with the data but, as shown in the plots, some features of the data are better matched by the jets. The models could not fit all of the INMS and UVIS data simultaneously with a unique model solution. Therefore, given the curtain and [Porco et al. 2014], jets as a modeling constraint, an assumption of time variability of plume source distribution and/or individual jets between the Cassini flybys, is required to fit the data. The changes over time of the individual jets appears to be chaotic, exhibiting no obvious correlation to the Enceladus mean anomaly, as seen (for the plume as a whole) in VIMS data [Hedman et al. 2013].

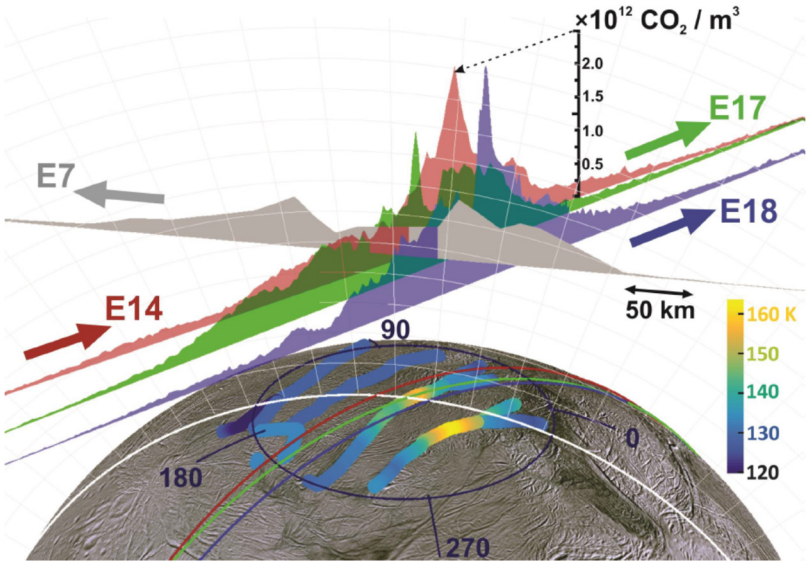

Figure MAPS-11. To scale 3-D representation of the E14, E17, E18 and also (lower resolution) E7 INMS data, with vertical areas representing (in linear scale) the density, and the flat base of the areas corresponding to the Cassini trajectories. Lines across the surface are the ground tracks. The Tiger stripes are colored according to the temperature estimated by CIRS. Figure from Teolis et al. [2017].

Table MAPS-2 shows the major species composition of Enceladus' plume gas and the volume mixing ratios reproduced from Waite et al. [2017] Table 1.

Table MAPS-2. The major species composition of Enceladus' plume gas. Volume mixing ratios are derived from Cassini INMS measurements [Waite et al. 2017].

Constituent	Mixing Ratio (%)
H_2O	96 to 99
CO_2	0.3 to 0.8
CH_4	0.1 to 0.3
NH_3	0.4 to 1.3
H_2	0.4 to 1.4

Ring Science

Ring-magnetosphere-ionosphere interaction

- **MN2a:** Determine the coupling between Saturn's rings and ionosphere.
  - Study how field aligned currents are coupled to the rings and satellites.
  - Explore the dust dynamics in the proximity region.
  - Investigate the mid-plane of Saturn's D-ring.
  - Determine the grain composition in the proximity region.

  - Investigate the possible interaction of lightning with the inner magnetosphere and the rings.
  - Investigate Coupling Between E-ring and the Enceladus neutral and plasma tori.
- **M_AO2:** Determine current systems, composition, sources, and sinks of magnetosphere charged particles.
- **M_AO3:** Investigate wave-particle interactions and dynamics of the dayside magnetosphere and the magnetotail of Saturn and their interactions with the solar wind, the satellites, and the rings.

The Cassini mission brought about a profound new view the interaction of the amazing Saturnian main ring system with the magnetospheric space environment. During the Voyager era, it was presumed that meteors continually bombarded the rings. The spokes were thought to represent a stunning visual manifestation of these intense impacts. The associated impact-ionized vapor plume then delivered ring water and oxygen ions along connecting magnetic field lines to the ionosphere. These water ions were thought to chemically disrupt the ionosphere hydrogen cycle and deplete the ionosphere locally of electrons. It was also thought that these ring-generated ions possibly modify the color of the cloud tops. In this view, the rings were considered a source of quasi-energetic plasma delivering heavy ions to the exobase above the cloud-tops. Figure MAPS-12 shows the predicted impact-generated plasma flux from the rings, with peak densities over the dense portion of the central B-ring [Wilson and Waite 1989]. Voyager, unfortunately, did not actually fly over the rings and thus confirmation of this impact-driven ring plasma source could only be inferred.

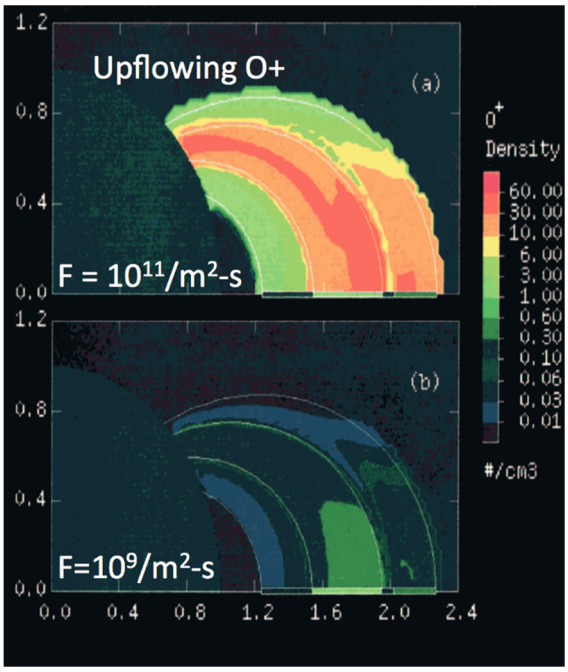

Figure MAPS-12. Wilson and Waite Impact-Driven Ring Plasma Model [Wilson and Waite 1989].

Cassini's orbit provided several important periods during which measurements were made of the rings and their interaction with the magnetosphere and ionosphere. First measurements of this important system began with Cassini's very first passage through the magnetosphere during SOI. During this period, Cassini crossed the ring plane in a gap between the F-ring and G-ring and also flew directly across magnetic field lines that connect back down to the main rings. The RPWS instrument thus obtained unique direct measurements of the plasma environment across the main A-ring, B-ring, and C-ring [Gurnett et al. 2005; Wang et al. 2006]. Near the very end of the mission, Cassini again was able to make measurements while crossing these flux tubes, this time by many instruments. After SOI, during the first few years of the mission, Cassini made a number of inclined and equatorial crossings of the E-ring, particularly near the orbit of Enceladus. Later, Cassini shifted to high inclination orbits and crossed the E-ring multiple times in 2016, providing opportunities to compare the vertical dust density profiles to those measured before equinox [Kurth et al. 2006; Ye et al. 2016a].

During Cassini's SOI on July 1, 2004, the spacecraft passed over the B-ring, A-ring, F-ring, and the Cassini division before descending (inside the G-ring) through the ring plane. The trajectory provided the first in situ plasma measurements over Saturn's main rings, complementing data obtained by the Voyager 2 plasma science instrument outside the main rings. During SOI, data form the MAPS instruments presented a new view of the plasma environment over the main rings. Data from RPWS [Gurnett et al. 2005] shows the plasma density as derived from the narrow-banded upper hybrid waves, electron plasma oscillations, and high frequency edge of the auroral hiss (see Figure MAPS-13). From the same RPWS measurements, Wang et al. [2006] were able

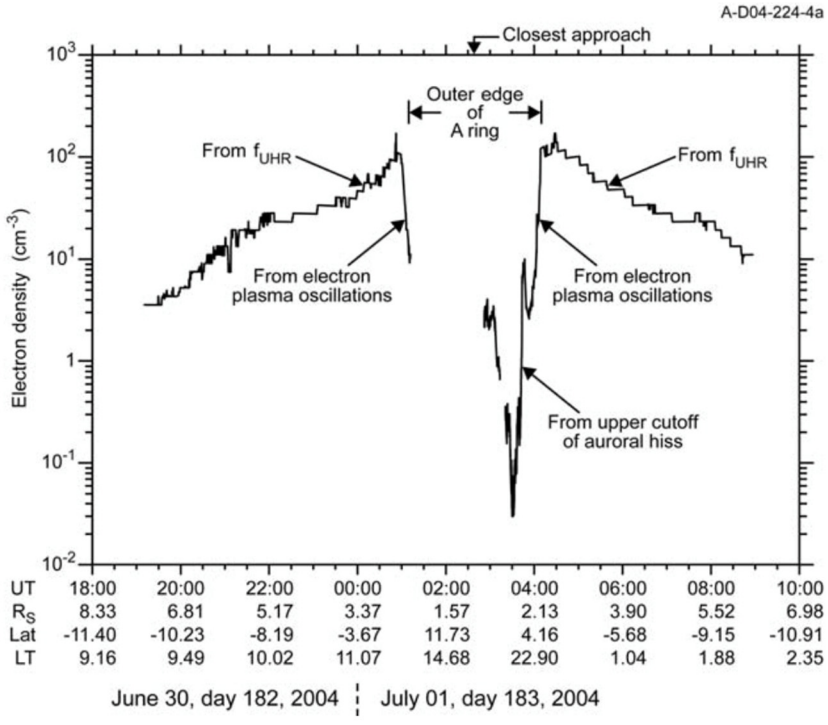

Figure MAPS-13. The electron density over the main rings as derived by the plasma waves detected by RPWS. See Gurnett et al. [2005] for more details.

to provide information on the micron sized dust at the inbound and outbound ring plane crossings before and after SOI.

This RPWS electron density profile was unexpected and almost diametrically opposite to what would have been predicted from an impact-driven ring plasma system, where the maximum in plasma density is expected in the central B-ring. There are two stunning features to this profile. First, immediately adjacent to the dense A-ring, there is an electron density maximum at over 100 electrons/cm^3 , with the high density region (>10/cm^3) extending out to beyond L = 5. It would later be found [Persoon et al. 2015, 2009] that this high density region is a plasma torus created by ionization and pick-up of new ions born in the Enceladus plume and a seasonal contribution from photo-ionized neutrals originating from the rings themselves. Second, the region over the main rings is devoid of plasma, with an electron density drop of near 10000 from the outer edge of the A-ring to values of 0.04 electrons/cm^3 at 1.76 R_S over the central portion of the B-ring [Xin et al. 2006; Farrell et al. 2017]. This void region has been identified as a ring plasma cavity (RPC) with its lowest density near the synchronous location. The profile of electron density over the main rings varied inversely with ring optical depth, with the lowest plasma densities observed over the central dense B-ring and a local maxima sense when passing over field lines connected to the Cassini Division. (In Figure MAPS-13, this Cassini Division plasma maxima is seen near 03:45 spacecraft event time (SCET) with the local peak near 10/cm^3.)

During the same period (SOI) CAPS IMS observed an enhanced ion flux (compared to background outside the rings) outside of the main rings and in the vicinity of the F-ring and G-ring as Cassini crossed the ring plane during orbit insertion on July 1, 2004. Near the edge of the main rings the IMS ion flux as a function of energy per charge provided strong evidence for the presence of O_2^+. Analysis led to the conclusion that the enhanced ion flux between the F-ring and G-ring consisted of the water group ions O^+, OH^+, and H_2O^+ (the other water group ion H_3O^+ could not be identified) coming from Enceladus with an admixture of O_2^+, predominantly from the extended ring O_2 atmosphere. The O_2^+ component appeared to be dominant at SOI and was later found to vary with season [Elrod et al. 2014, 2012] due to the changing orientation of the ring plane relative to the solar UV flux (Figure MAPS-14).

Near the edge of the main rings the IMS ion flux as a function of energy per charge provided strong evidence for the presence of O_2^+.

RPWS observations confirm the model of Tseng et al. [2013a] that the ring-ionosphere-magnetosphere interaction is driven by photolytic processes, not impact processes [Farrell et al. 2017]. Specifically, the Sun-facing side of the main rings are a source of photo-dissociated neutrals that then get ionized to form a relatively low energy exo-ionosphere. This exo-ionosphere cannot directly access the shadowed/unlit side of the rings: the ring particles represent obstacles to their transport. Thus, the plasma density on the unlit side is modulated by ring density, being lowest where the ring obstruction is the highest, (in the central B-ring). Local maxima are expected where the local ring particle density is low, like across the Cassini Division. There is little evidence of impact-generated plasma like that predicted during the Voyager era.

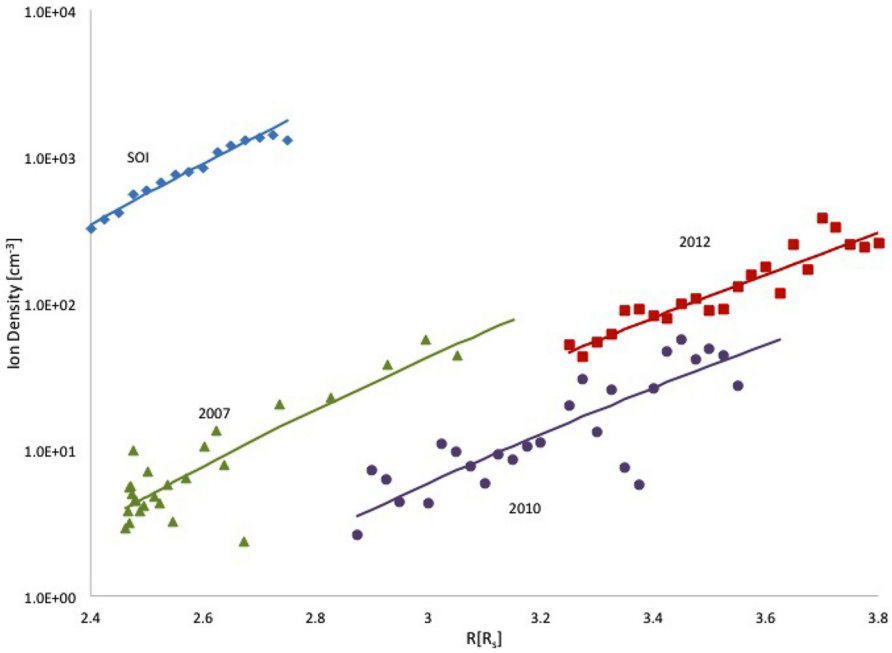

Figure MAPS-14. Ion densities extracted from CAPS IMS data at SOI in 2004, and inferred for subsequent years by modelling. The modeling indicates the seasonal dependence of ring plasma. This region contains ions formed from neutrals scattered out of the ring atmosphere as well as ions formed from neutrals in the Enceladus torus. SOI was dominated by O_2^+ and the later years by water group ions. Figure from Elrod et al. [2014].

The seasonal dependence observed and modeled using CAPS data confirmed that the O_2^+ ionization source was indeed solar UV acting on oxygen in the ring atmosphere as predicted by Tseng et al. [2010]. Seasonally varying oxygen was subsequently observed at much larger radii by the MIMI instrument, confirming that oxygen originating in the rings can be scattered throughout the inner magnetosphere and, consequently, also into Saturn's atmosphere. This likely accounts for oxygen observed in Saturn's thermosphere. Subsequent modeling [Tseng et al. 2013a] shows that model calculations based on the CAPS data were in reasonable agreement with that data.

Laboratory data showed that radiation decomposition of ice would lead to the production of roughly twice as much H_2 as O_2, thereby maintaining the near stoichiometry of irradiated ice grains —for example, Brown et al. [1982]. Indeed CAPS measurements have shown that the Saturnian magnetosphere is permeated with H_2^+ and H^+ from a variety of sources (Titan, the Enceladus torus, and Saturn's atmosphere), including the ring atmosphere [Tseng et al. 2013b, 2011]. Since H_2 is much lighter than O_2 it has a proportionately larger neutral scale height, and can also be easily scattered throughout the magnetosphere by the heavier molecules. Ionization of the H_2 component of the extended ring atmosphere, and the pick-up of H_2^+ formed by this process, was shown by Tseng et al. [2011] to be an important component of magnetospheric H_2^+ detected by CAPS [Thomsen et al. 2010].

Surprisingly, the IMS ion densities observed between the outer edge of the main rings and Mimas and populated by ionization of neutrals from the ring atmosphere and the Enceladus torus,

exhibited an unexpected radial dependence [Elrod et al. 2014, 2012]. Not only did the plasma detected by CAPS in this region exhibit a seasonal dependence, with the O_2^+ component dominated by the water products from the Enceladus torus at Equinox, but the observed radial dependence suggested that an ion loss process other that electron-ion recombination, charge exchange or diffusion was acting [Elrod et al. 2014; Tseng et al. 2013a]. Since the CAPS ion densities and the RPWS electron densities differed, particularly at SOI, the observed radial dependence of the CAPS ion data was subsequently determined to be due quenching of the ions on nano-grains. These grains, a fraction of which were negatively charged, were presumed to be emitted from the edge of the main rings and present in the tenuous F-ring and G-ring, acted as ion sinks [Johnson et al. 2017]. That this process was occurring in this region of the magnetosphere was subsequently confirmed by the RPWS instrument during the F-ring orbits when, unfortunately, the CAPS instrument was turned off.

IMS observed ion fluxes over the main rings consistent with the presence of atomic and molecular oxygen ions [Young et al. 2005]. CAPS IMS observations over the main rings detected both O^+ and O_2^+ at densities of a few per cm^3 using the IMS time-of-flight (TOF) sensor (Figure MAPS-15) [Tokar et al. 2005; Elrod et al. 2012]. Further analysis by Elrod et al. [2012] shows much higher densities of O^+ when CAPS was over the outer edge of the B-ring and again when CAPS was over the inner edge of the A-ring.

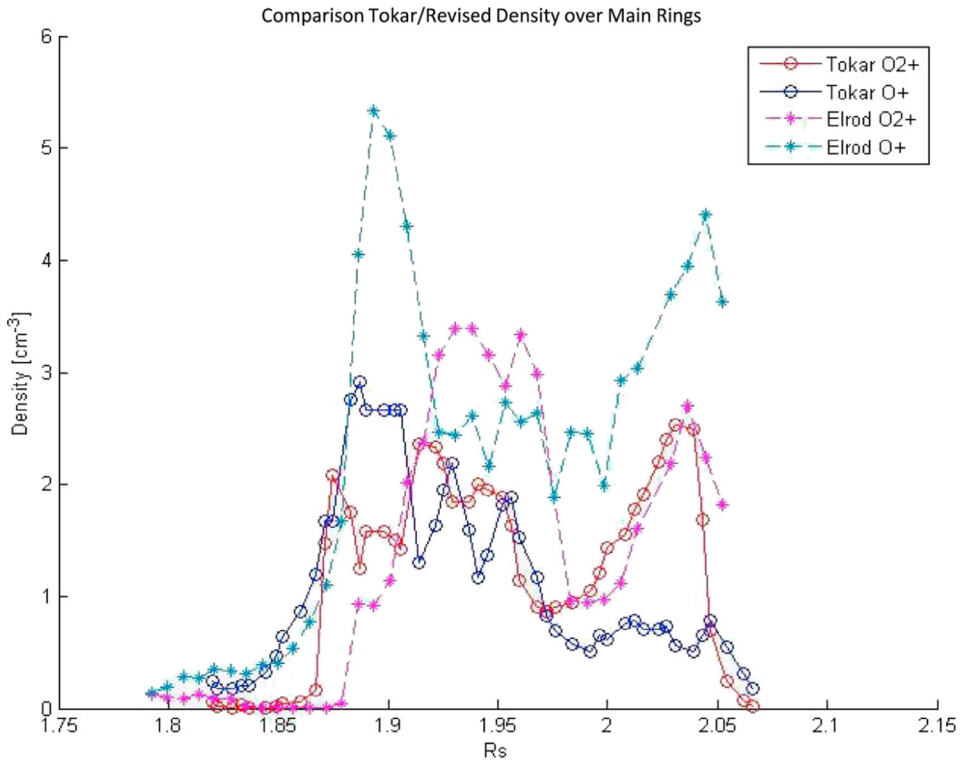

Figure MAPS-15. Densities of O^+ and O_2^+ obtained from IMS data over the main rings as a function of radial distance from Saturn in R_S. Data from Tokar et al. [2005] and re-analyzed by Elrod et al. [2012].

The IMS data suggested the presence of a ring atmosphere that was predominantly O_2 rather than H_2O and much more robust than predicted. Since the energetic ion density in this region is highly depleted due to absorption by ring particles, for example, Cooper et al. [2017], the CAPS team proposed that the atmosphere was produced by UV-induced decomposition of ice on the ring particles [Johnson et al. 2006]. Such a neutral atmosphere would have a scale height confining it close to the ring plane. Because ions were detected well above the ring plane, this also led to the prediction that ion-neutral scattering would produce both a ring ionosphere with a much larger scale height, and a neutral oxygen cloud that permeated Saturn's magnetosphere [Johnson et al. 2006; Luhman et al. 2006; Bouhram et al. 2006]. Following ionization, pick-up and scattering of the neutrals from this atmosphere was shown to populate the magnetosphere with oxygen atoms and molecules which are eventually ionized far from the main rings [Johnson et al. 2006]. Molecular oxygen ions in were eventually discovered in the inner magnetosphere as well [Martens et al. 2008]. This has been subsequently confirmed by additional data and modeling.

Interestingly, the INMS instrument also observed only water-group ions in the F-ring. Unlike the neutrals, the ion densities were not symmetrical with respect to the equatorial plane, varying in both total density and the relative fractions within the water group. The predominance of O^+ versus the other water-group ions indicates that there may be a source of O^+ other than as a byproduct of water. One possibility is that CH_4^+ contributes a fraction of the 16 u ions. The lack of O_2^+, which INMS observed during Cassini's insertion into orbit about Saturn, is likely due to the INMS energy limit: at the F-ring speeds, O_2^+ exceeds the INMS limit for ions. The lack of H_2^+ is surprising and not yet explained. As with neutrals, noise prevents INMS measurement of H^+ at 1 u.

In addition to the ion and electron plasma population detected in the vicinity of the ring, the INMS instruments was able to detect the neutral parent molecules. INMS found two neutrals with remarkable consistency during the F-ring passes: H_2 and a species at 28 u (Figure MAPS-16). The scale height, or the half-width-half-max of the INMS counts, for both of these species was approximately 3,000 km, or 0.05 Saturn radii (R_S). This parameter and the total counts were nearly identical in each pass.

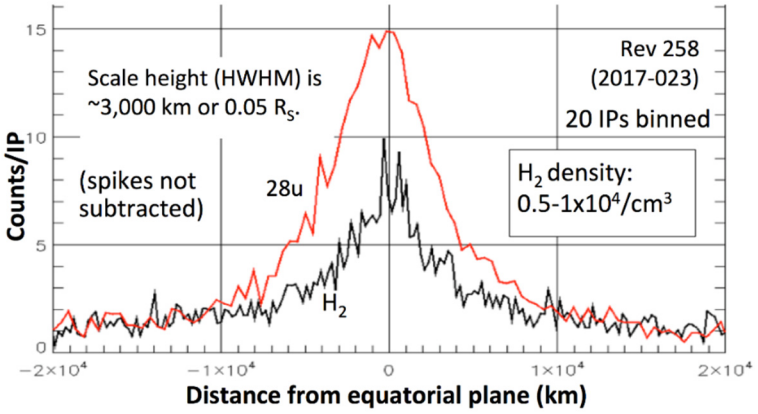

Figure MAPS-16. The major neutrals measured by INMS in the F-ring. Twenty measurements (integration periods or IPs) were binned for this plot.

Although H_2 was expected in this area of the rings, models and Earth-based observations predicted a larger scale height for H_2 from Saturn's atmosphere, and the narrow distribution of the observed H_2 suggests that it is more liked to originate in the rings. The lack of variability indicates a stable ring atmosphere. Atomic hydrogen is not measured by INMS due to instrumental noise at 1 u.

CH_4 (16 u) and CO_2 (44 u) are the only other measured species. They both have a count rate that is approximately 20% of the H_2 rate. CH_4 is confirmed by the presence of 15 u counts at the correct electron impact dissociative ionization ratio, the amount produced from CH_4 in the INMS ionization chamber. CO_2 is not a common dissociation product and may be a native species. It exists on the surface of several icy moons. Count rates for both CH_4 and CO_2 are depressed due to dissociation and they may be more abundant than indicated by the measurements. There are small amounts of 26 u and 27 u, which are expected products from ionization of C_2H_4, one possibility for the 28 u measurements. However, the count rates for these two cracking products are lower than expected if the entire 28 u signal was produced by C_2H_4. This deficiency implies that another species such as CO may contribute to the 28 u signal.

Several expected neutrals are missing, most notably H_2O and O_2. Since water is temporarily adsorbed onto the walls of the INMS inlet, H_2O counts are suppressed and delayed. Combined with the radiation background, which increases after passing through the equatorial plane, INMS would not detect low densities of H_2O, particularly after some loss due to high-velocity dissociation. Models show that O_2 could be abundant, but that densities decrease a factor of 1,000 approaching the location of Cassini's trajectory; moreover, much of the O_2 would be lost due to dissociation.

The observation suggested that there is a current system driven by the rings-magnetosphere interaction, with the electron beams and currents near the synchronous point … possibly being part of the current closure system.

In addition to the surprising neutral and plasma composition and the existence of a unique ring ionosphere, Cassini instruments were also able to the study the current systems that connects the rings, the ring ionosphere, Saturn's magnetosphere, and Saturn's own ionosphere. Xin et al. [2006] reported a strong auroral hiss signal detected at the deepest depletion of the electrons within the RPC near 1.76 R_S. The whistler-mode auroral hiss emission is a classic signature of the presence of energetic field aligned electron beams, in this case flowing outward from the rings along field lines connecting to the ionosphere. They reported that the RPC environment had a stunning similarity to plasma cavities found in polar auroral regions, usually associated with field aligned currents that drive the aurora. The observation suggested that there is a current system driven by the rings-magnetosphere interaction, with the electron beams and currents near the synchronous point at 1.76 R_S possibly being part of the current closure system.

Figure MAPS-17 illustrates the concept of this new ring current system presented in Xin et al. [2006]. While the plasma on field lines over the rings would be corotating, the particles and associated photo-dissociated gas of the rings would be moving in Keplerian motion, creating drag

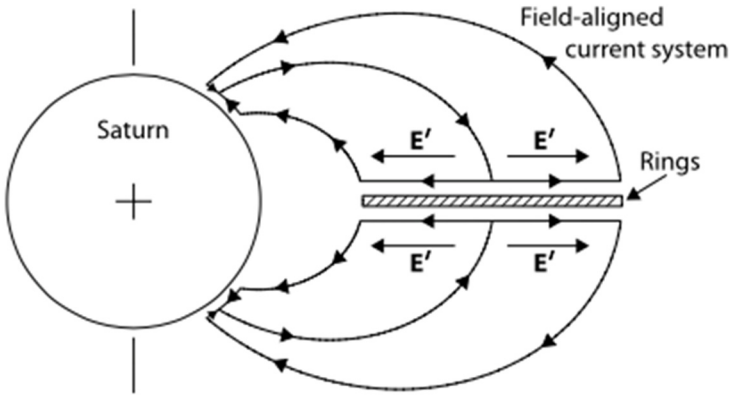

Figure MAPS-17. The proposed large-scale current system that would be induced in Saturn's magnetosphere by the interaction of the rings (including any associated gas) with the corotating magnetospheric plasma. Figure from Xin et al. [2006].

on the plasma. This drag creates an associated change in plasma speed, ΔV. Beyond the synchronous point, the plasma is slowed by the Keplerian-moving particles and gas, creating an outward radially-directed E-field in order to maintain the new sub-corotation speed E′ = ΔV × B. This new E-field drives an outward current, J, which acts to then form a magnetohydrodynamic J × B force to balance the plasma-ring drag force. Inward of the synchronous point, the corotating plasma is accelerated by the ring drag force, creating an inward radial E-field and current that forms a J × B force to offset the acceleration. At the edges of the rings, these cross-ring currents become field-aligned parallel current that close down to the ionosphere along connecting magnetic field lines at the outer edge of the A-ring near L = 2.25 and inner edge of the D-ring near L ~1.11. The rings thus behave as an electrical generator in the plasma, driving currents from the ring surfaces along magnetic field lines down to the ionosphere.

While detailed analysis of the proximal orbits is still ongoing, Wahlund et al. [2018] reported on a very strong Saturnian ionosphere D-ring electrical connection, which would represent the current closure of the Xin et al. [2006] model at the inner radial edge of the main rings. Using the RPWS Langmuir Probe, they found that Cassini passed through a cold, dense electron region during proximal perigee, which has been interpreted to be entry into the Saturnian ionosphere.

At higher altitude proximal perigee passes, like orbit 277, Cassini passed through the inner edge of the D-ring (also immersed in the outer edge of the ionosphere). In these cases, the electron density had a distinct bite-out or decrease near the equator which is believed to be due to the presence of D-ring particulates that have absorbed the local ionospheric plasma. The RPWS instrument also detected micron-sized dust grain impacts revealing the presence of these D-ring particulates. The complex dusty plasma interactions remain a subject of considerable study even after the end of the mission [Ye et al. 2018].

An additional surprise during the proximal orbits was that the MIMI/INCA and Charge-Energy-Mass Spectrometer (CHEMS) instruments, that were designed to measure energetic particles, were detecting signatures of D-ring dust falling into Saturn's equatorial atmosphere. These particles

are of 1–3 nm size, much smaller than what is detected by the CDA instrument designed to measure dust. The dust is reaching the atmosphere within 4 h and provides a continuous influx of about 5 kg/s from the rings into the atmosphere [Hsu et al. 2018; Mitchell et al. 2018].

The ionosphere of Saturn and its connection to the ring ionosphere system is still a work in progress. First in situ measurements by RPWS of the cold ionosphere properties have just been reported [Wahlund et al. 2018]. Several other manuscripts have been submitted, and they all show a very strong interaction between the D-ring and the ionosphere of Saturn, causing the ionosphere to become extremely variable with more than two orders of magnitude and trigger a dust-ionosphere layer near the equator.

Magnetosphere Science

Seasonal and solar cycle variations

- **MC1b:** Observe Saturn's magnetosphere over a solar cycle, from one solar minimum to the next.
  - Investigate what controls the interplay between the Dungey and Vasyliunas cycles?
  - Study the solar cycle dependence of the magnetospheric dynamics.
  - Investigate magnetospheric structure: variations in force balance.
  - Investigate non-static and other variant radiation belt features.

Cassini spent 13 years in Saturn's magnetosphere. This allowed the MAPS instruments aboard the spacecraft to make measurements of Saturn's magnetosphere and of the important moons such as Enceladus and Titan over more than a solar cycle and over nearly half of a Saturnian year. This allowed MAPS scientists to study the effects of both the solar cycle and the Kronian season on the magnetosphere. Many of the results of the seasonal and solar cycle variation are detailed in the section of this summary where their underlying processes are addressed. For example, see sections entitled:

- Titan's upper atmosphere and its interaction with the surrounding plasma
- Magnetotail configuration and dynamics
- Magnetospheric structure and convection
- Plasma loss into the magnetotail; Radiation belts
- Time varying modulation of SKR and associated planetary period oscillation (PPO) signals

In this section we will highlight just a few of the results related to solar cycle and seasonal effects produced by the MAPS instruments teams.

One of the most important discoveries of the Cassini mission was the identification the ring ionosphere, the ring sources of plasma and the activity of Enceladus. Many of these interesting new phenomena exhibited seasonal dependence due to the inclination of the rings relative to the activating solar UV. Amount these effects was the discovery of a seasonally-dependent source of plasma between the A-ring and Enceladus. Additionally, a seasonal dependence was observed and modeled using CAPS data that confirmed that the O_2^+ ionization source was indeed solar UV acting on oxygen in the ring atmosphere as predicted by Tseng et al. [2010]. Seasonally varying oxygen was subsequently observed at much larger radii by the MIMI instrument, confirming that oxygen originating in the rings can be scattered throughout the inner magnetosphere and, consequently, also into Saturn's atmosphere. Surprisingly, the IMS ion densities observed between the outer edge of the main rings and Mimas, and populated by ionization of neutrals from the ring atmosphere and the Enceladus torus, exhibited an unexpected radial dependence [Elrod et al. 2014, 2012]. Not only did the plasma detected by CAPS in this region exhibit a seasonal dependence, with the O_2^+ component dominated by the water products from the Enceladus torus at Equinox, but the observed radial dependence suggested that an ion loss process other that electron-ion recombination, charge exchange or diffusion was acting [Elrod et al. 2014; Tseng et al. 2013a].

As outlined in the section entitled Time varying modulation of SKR and associated PPO signals, many aspects of Saturn's magnetosphere are modulated at the assumed rotation period as approximated by the SKR signal. Extensive studies of the SKR period as well as associated auroral activity have shown a mark dependence on the Saturnian season. The SKR spectrum was studied statistically with RPWS observations from a wide variety of Cassini's positions. Southern SKR was predominant during Saturn's southern summer up to 2010–mid 2011 (slightly after the equinox of 2009), while the northern SKR was predominant after, consistent with a seasonal control of field-aligned currents driving auroral emissions by solar illumination of Saturn's ionosphere.

The major discovery brought by RPWS was then the identification of 2 SKR periods [Kurth et al. 2008] corresponding to the 2 Kronian hemispheres, differing by ~1%. These periods were found to both vary with time in anti-correlation over yearly timescales and crossed closely after equinox, a trend which was interpreted as a seasonal driving of solar illumination [Gurnett et al. 2011a, 2010b, 2009; Lamy 2011]. These dual periods were later noticed in narrowband (NB) emissions and auroral hiss as well [Gurnett et al. 2010b; Ye et al. 2017, 2010] and more generally observed in numerous magnetospheric observables including magnetic oscillations, ENA emissions, aurorae [Mitchell et al. 2009b; Carbary et al. 2011a, 2010a; Nichols et al. 2010; Andrews et al. 2011, 2010a; Provan et al. 2011; Badman et al. 2012a, 2012b]. It is now accepted that these dual rotational modulations all originate from two rotating hemispheric systems of field-aligned currents, whose origin may be atmospheric vortices [Jia et al. 2012].

Clearly related to the variation in aurora and the SKR signal, the PPO current were found to have similar seasonal dependence. MAG data comparing high-latitude data sets from 2006/2007 and 2008 in Saturn's late southern summer to a third interval of high-latitude data was obtained in 2012/2013 during northern spring [Bradley et al. 2018]. The PPO currents were found to be of similar form but somewhat weaker than in 2008, while the sub-corotation currents exhibited strong

opposite seasonal asymmetries in the north and south polar regions, indicative of weak polar ionospheric conductivity in the winter polar cap. Investigation of the current signatures observed on the F-ring and proximal orbits spanning northern summer solstice at the end of the Cassini mission are currently ongoing [Hunt et al. 2018a].

Thus far we have outlined several seasonal variations at Saturn. Most of these have been related to either the ring plane inclination or to current system. The CAPS instrument measurements of the in situ plasma do not show such a strong variation. In fact, on the time scale of months to years, most of Saturn's magnetospheric plasma does not exhibit strong variability, less than a factor of three [Wilson et al. 2017], in spite of the fact that the Enceladus plume source does appear to vary on the scale of several months [Smith et al. 2010]. In the very inner magnetosphere, just outside the main rings, heavy ion densities (O_2^+ and W^+) show a seasonal dependence, as could be expected for a ring source that depends on the solar illumination angle [Elrod et al. 2014, 2012]. Utilizing many measurements by the RPWS instrument in the inner magnetosphere, Persoon et al. [2013, 2009] were able to develop an empirical plasma density model for the Saturnian system.

Beyond the seasonal dependence, there was an expectation that the solar cycle would have effects on Saturn's magnetosphere. The strength of this dependence would depend on the overall capability of the solar wind to feed energy into and drive the magnetosphere. Sections entitled Magnetotail configuration and dynamics, Magnetospheric structure and convection, Plasma loss into the magnetotail, and Time varying modulation of SKR and associated PPO signals address how efficient the solar wind is at influencing the global magnetosphere and therefore many results related to solar cycle can be found in studies highlighted in those sections.

Above in the previous paragraphs, we outline the dependence of the SKR on seasonal effects. The SKR also exhibit solar cycle effects. [Kimura et al. 2013] investigated the very long-term (six years of measurements) variations of northern and southern SKR spectra, separated by polarization. This study confirms the prominent role of solar wind pressure over one solar cycle, and additionally identified a seasonal dependence of the SKR activity, with a maximum in summer.

Saturn is often placed in between Earth (solar wind driven) and Jupiter (internally driven) in terms of its magnetospheric dynamics, but this is an overly-simplistic picture. Much work has been done to characterize the structure of the solar wind upstream of the planet. Jackman et al. [2004] analyzed several solar rotations worth of upstream interplanetary magnetic field (IMF) data while Cassini was approaching Saturn, and Jackman et al. [2005a] followed up with an analysis of the solar wind excursion on Cassini's long first capture orbit. Overall it was found that during the declining phase of the solar cycle, the IMF is structured into a very clear pattern of two compressions per solar rotation separated by rarefactions. This structuring is very useful because it helps to predict

Saturn is often placed in between Earth (solar wind driven) and Jupiter (internally driven) in terms of its magnetospheric dynamics, but this is an overly-simplistic picture.

the phasing of intermittent driving of the magnetosphere by the solar wind. Jackman et al. [2004] developed an empirical formula to calculate how much open flux is generated through dayside reconnection, dependent on the IMF direction, the solar wind velocity, and assuming a certain length of a predicted reconnection x-line at the dayside magnetopause. This formula has since been widely used by many other authors, in particular to compare to auroral images which seem to indicate addition and removal of flux, for example, Badman et al. [2012a, 2005]. The solar wind conditions at Saturn (and Jupiter) spanning all stages of the solar cycle were summarized in Jackman and Arridge [2011a]. Reconnection voltages were predicted to be slightly lower at solar minimum than solar maximum, while increased photoionization of the Enceladus torus at solar maximum can lead to a more plasma dominated system at this stage of the solar cycle.

In addition to the MAG results, MIMI also discovered that energetic particles with oscillations at the solar wind period (~26 d) likely display solar cycle variations. This solar wind periodicity was discerned during solar minimum (i.e., 2008–2010) when the solar wind structure was not disrupted by solar activity. The solar wind periodicity was first recognized in the energetic electrons [Carbary et al. 2009a], but was perhaps even stronger in the energetic ions [Carbary et al. 2013]. Because solar activity varied with the ~22-year solar cycle, the appearance of this 26-day periodicity itself should vary with the solar cycle.

The solar cycle is also evident in MIMI/LEMMS measurements of Saturn's radiation belts. The very energetic protons (E > 1 MeV) that form Saturn's ionic radiation belts were found to be modulated with the solar cycle, which provided clues that they might derive from CRAND from Saturn's atmosphere [Roussos et al. 2011]. As at Earth, the cosmic rays causing CRAND at Saturn are themselves modulated by the solar cycle, and LEMMS detected this for the first time using observations over many years. The ring current boundary, deduced from LEMMS observations, also appears to fluctuate in response to solar energetic particle (SEP) events, which are themselves conditioned according to the solar cycle [Roussos et al. 2014].

The section entitled Radiation belts outlines the MAPS contribution to our understanding of the radiation environment at Saturn. The MIMI measurements achieved a comprehensive description of the radiation belts of Saturn during approximately 200 orbits which crossed into the radiation belts, allowing us to understand and quantify their average structure, but also to monitor time variations, despite the single point measurements. Studies by Christon et al. [2014a, 2014b, 2013] provide the most detailed characterization of trace energetic ions and their charge states at an outer planet, showing how their origin may be connected to the planet's rings, the activity of Enceladus and seasonal or solar cycle effects.

Finally, a recent study by Roussos et al. [2018c] uses a novel technique to overcome the lack of an upstream solar wind monitor at Saturn. Cassini MIMI/LEMMS observations of SEP and Galactic Cosmic Ray (GCR) transients, that are both linked to energetic processes in the heliosphere such as Interplanetary Coronal Mass Ejections (ICMEs) and Corotating Interaction Regions (CIRs), are used to trace enhanced solar wind conditions at Saturn's distance. A survey of the MIMI/LEMMS dataset between 2004 and 2016 resulted in the identification of 46 SEP events. Most events last more than two weeks and have their lowest occurrence rate around the extended

solar minimum between 2008 and 2010, suggesting that they are associated to ICMEs rather than CIRs, which are the main source of activity during the declining phase and the minimum of the solar cycle. Also, 17 time periods (> 50 days each) are identified where GCRs show a clear solar periodicity (~13 or 26 days). The 13-day period that derives from two CIRs per solar rotation dominates over the 26-day period in only one of the 17 cases catalogued. This interval belongs to the second half of 2008 when expansions of Saturn's electron radiation belts were previously reported to show a similar periodicity. That observation not only links the variability of Saturn's electron belts to solar wind processes, but also indicates that the source of the observed periodicity in GCRs may be local. In this case, GCR measurements can be used to provide the phase of CIRs at Saturn. The survey results also suggest that magnetospheric convection induced by solar wind disturbances associated with SEPs is a necessary driver for the formation of transient radiation belts that were observed throughout Saturn's magnetosphere on several occasions during 2005 and on day 105 of 2012. Also, an enhanced solar wind perturbation period that is connected to an SEP of day 332/2013 was the definite source of a strong magnetospheric compression (enhanced SKR and low frequency extension (LFE) were also detected at this time) which led to open flux loading in the magnetotail. This event lists can a guide to better constrain or identify the arrival times of interplanetary shocks or solar wind compressions for single case studies or statistical investigations on how Saturn and its moons (particularly Titan) respond to extreme solar wind conditions or on the transport of SEPs and GCRs in the heliosphere.

Magnetotail configuration and dynamics

- **MN1a:** Determine the dynamics of Saturn's magnetotail.
  - Study thoroughly the plasma sheet in Saturn's magnetotail.
  - Investigate the relation between solar wind compression events and magnetotail dynamics.
  - Investigate the plasma sheet thickness and scale height as functions of radial distance and local time.
  - Statistically characterize magnetotail variations, especially those associated with plasmoids, and correlate them with changes in the inner magnetosphere.
  - Critically evaluate the Dungey and Vasyliunas cycles in light of the new observations, especially those of flow speeds.

Measurements made by Cassini in the magnetotail, have allowed MAPS team members to study the dynamic nature of this region of the magnetosphere. Studies include characterizing reconnection, the observation and characterization of plasmoid-like structures, observation of dipolarization events, describing the warping of Saturn's current sheet and studying the response of the magnetosphere to the solar wind.

Since the outer magnetosphere is very dynamic, it is very challenging to describe its average properties. Still, the continuous in situ measurements by CHEMS and LEMMS and the remote

monitoring by INCA have provided unique insights into that region. A detailed study of the outer magnetosphere's average structure is given by Krimigis et al. [2007]; Sergis et al. [2009], which highlight the distinct day-night asymmetry in the vertical extent of the ring current (or plasma sheet). INCA images have been used to determine the most active sites for dipolarization (or large-scale injection events) in the outer magnetosphere being in the post-midnight sector of the magnetosphere [Mitchell et al. 2009b, 2005; Carbary et al. 2008a]. They have revealed the wavy structure of the magnetodisk [Carbary et al. 2016, 2015, 2008b; Carbary 2013] and links to auroral emissions. Energetic electrons have been used to identify an unexpected source of high energy electrons, seen as quasi-periodic pulsations with a period of about 65 minutes. These events are seen globally, they can accelerate electrons to the MeV range instantly and have been linked to reconnection, auroral transients, and similar periodic observations in magnetic field and plasma wave data [Roussos et al. 2016b; Palmaerts et al. 2016a, 2016b; Carbary et al. 2016]. The magnetospheric topology (e.g., open versus closed field lines or the cusp) has been discussed in the context of MIMI observations—for example, Gurnett et al. [2010b]; Arridge et al. [2016a], while MIMI data have been central in the study and interpretation of reconnection/dipolarization events, in combination with other datasets—for example, Badman et al. [2016, 2013]; Jackman et al. [2015, 2008]; Masters et al. [2010]. CHEMS observations also revealed outer magnetosphere asymmetries in the fractional abundance of solar wind-originating ions penetrating into the magnetosphere of Saturn [Allen et al. 2018]. These asymmetries indicate that solar wind He^{++} particles may be entering the magnetosphere due to a combination of Dungey-type reconnection as well as Kelvin-Helmholtz (K-H) instabilities [Allen et al. 2018].

Cassini MAG measurements (often in concert with plasma measurements) have been used to characterize the tail in terms of distinguishing the lobe and plasma sheet regions and exploring how they change with distance from the planet. The current sheet is found to be warped out of the equatorial plane [Arridge et al. 2008a], with a characteristic hinging distance of ~25 R_S. This warping made a significant impact in Saturn's southern hemisphere summer in 2006 when Cassini executed its deepest tail orbits, first in the equatorial plane (below the hinged current sheet) and later at higher latitudes (close to the hinged current sheet). The current sheet has also been found to flap, or oscillate vertically with a period close to the ~10 hours linked to the mysterious planetary periodicities. Jackman and Arridge [2011b] performed a statistical study of Saturn's lobes and plasma sheet during 2006, developing numerical definitions for these regions, and deriving the falloff of the field strength in the lobes with radial distance. They found that the near magnetotail of Saturn is similar to that of Jupiter and Earth (when scaled to a common distance). Unlike at Earth, we do not have spacecraft coverage of the asymptotic tail region, but rather have likely only covered the part of the tail where the magnetopause boundary is still flaring outward and where the lobe field strength is falling off before reaching a steady asymptotic level. We do not know the exact length of Saturn's tail, but can consider arguments first made by Dungey [1965] for the Earth where length was estimated by time for open field lines to be dragged over the poles before ultimately sinking in toward the center of the tail before reconnection (giving ~1000 R_E). Milan et al. [2005] examined the case at Saturn where the polar cap refresh time (i.e., the time for magnetic flux to be cycled through dayside to nightside reconnection) is expected to be many days—for example, Jackman et al. [2004], compared to a much shorter (~10–11 hours) planetary rotation period. This may be expected to twist the lobes of the tail

and Milan argued each turn of a twisted lobe could be ~900 R_S long. They theorized that Saturn is a last-in-first-out system in which recently opened field lines are the first to be closed by reconnection in the tail, due to this twist. This implies that Saturn's tail lobes contain a core of old open field lines that can be stretched to incredible lengths (>15000 R_S).

Saturn's magnetosphere is observed to undergo dramatic, explosive energy release events. The first indication of such behavior was on the outbound pass of SOI where Bunce et al. [2005] reported an episode of solar wind compression-induced tail reconnection, with dipolarizing field and injection of hot plasma. The products of reconnection tailward of the x-line (plasmoids and travelling compression regions, TCRs), were first observed with the Cassini magnetometer by Jackman et al. [2007]. They are identified primarily by a bipolar deflection in the north-south component of the field, with northward turnings implying reconnection products tailward of the x-line and southward turnings implying dipolarizations planetward of the x-line. Multi-instrument views of reconnection events reveal changes in the flow pattern from azimuthal to tailward and local heating of the plasma, for example, Jackman et al. [2008]. It is sometimes observed that northward turnings are not purely bipolar but instead have an extended interval where the field remains northward. This has been interpreted as the Kronian equivalent of the post-plasmoid plasma sheet [Jackman et al. 2011], which represents an interval where previously open flux is being closed by reconnection.

Over the years, catalogues of reconnection events were built up from by-eye surveys and basic automation involving simple background thresholding of the magnetic field and searching for significant deflections above or below these thresholds. Surveys covering the deepest tail orbits of 2006 revealed a significant imbalance between the rate of mass loss inferred from plasmoid release and the rate of mass loading from the moon Enceladus, which has been termed the mass budget problem [Jackman et al. 2014]. More sophisticated automated event searches have returned surveys of > 2000 events from tail orbits during 2006, 2009, and 2010, and Smith et al. [2016] revealed that the rate of observed reconnection events peaked post-midnight, with a highly variable radial location of the reconnection x-line, with an average ranging from 20–30 R_S from the planet. To date only one study has identified the x-line region itself [Arridge et al. 2016b], while more recently Smith et al. [2018a] presented a series of very short duration reconnection-related inward and outward flows in quick succession on the dusk flank. Their interpretation was that over a 7-hour interval investigated, reconnection sites had formed both tailward and planetward of the spacecraft, showing that reconnection can operate on small spatial/temporal scales. A second case study showed an event during which the reconnection site was inferred to retreat tailward, resulting in progressively hotter, dipolarizing material reaching Cassini.

The properties of dipolarizations planetward of the x-line give us another view of the impact of reconnection on the magnetosphere. Jackman et al. [2013] published a case study which showed rapid acceleration of newly-reconnected field lines back toward the planet. The transition from a radially stretched to dipolar field configuration can cause a current which usually flows across the tail to divert into the ionosphere, potentially leading to bright, distinct spots of auroral emission. Jackman et al. [2015] further showed that dipolarization of the field can be accompanied by ion flows at speeds of up to 1500 km/s toward the planet following tail reconnection, representing a significant departure

from the slower, sub-corotational flow typically seen in the tail. A reconnection event that starts at a small x-line can have a big impact on the magnetosphere as a whole.

Dipolarizations themselves have also been shown to have a dramatic effect on the local plasma: Smith et al. [2018b] investigated dipolarizations as identified from southward deflections of the magnetic field and found they were clustered preferentially post-midnight. The analysis of the accompanying CAPS data showed that the dipolarizing material was systematically hotter and less dense than the ambient plasma sheet. This density depletion and heating was found to be much more variable post-midnight, suggesting a more variable reconnection site.

By analyzing Cassini's MAG and CAPS data, Yao et al. [2017a] revealed that there are two fundamentally different drivers of dipolarization (i.e., magnetic reconnection and electrical current re-distribution) at Saturn, similarly to what is found in the terrestrial magnetotail.

Beyond reconnection and dipolarizations, several studies have been done of larger scale reconfigurations of the magnetotail. Some of this work is reported in a series of papers by Jackman and coauthors. Jackman et al. [2009a] revealed evidence of plasmoid-like magnetic structures and other phenomena indicative of the Saturnian equivalent of terrestrial substorms. In general, there was a good correlation between the timing of reconnection events and enhancements in the auroral SKR emission. Eight of nine reconnection events studied occur at SKR phases where the SKR power would be expected to be rising with time. Thus, while the recurrence rate of substorm-like events at Saturn is likely much longer than the planetary rotation timescale, the events are favored to occur at a particular phase of the rotation. Three examples were found in which the SKR spectrum extended to lower frequencies than usual. These low frequency extension SKR events were labeled LFEs and were interpreted as an expansion of the auroral particle acceleration region to higher altitudes (lower radio frequency) along magnetic field lines as a direct consequence of an increase in the magnetosphere-ionosphere current density driven by substorm-like events. Saturnian substorms are likely a much more prevalent phenomenon than this small number of observations suggests, but the statistics in this study were hampered by viewing geometries, primary the small amount of time that Cassini spent in the deep magnetotail near the nominal current sheet location. Many examples of LFEs are observed by Cassini from a wide set of vantage points, but the spacecraft is only in the right position to observe the corresponding magnetic signature (if any) a fraction of the time.

In general, there was a good correlation between the timing of reconnection events and enhancements in the auroral SKR emission.

Jackman et al. [2010] also explored the dynamic response of Saturn's magnetotail to an episode of solar wind compression that took place while Cassini was sampling Saturn's nightside equatorial magnetosphere in 2006. Following an initial increase in solar wind dynamic pressure, the magnetosphere was compressed and became more streamlined, with an elevated lobe field strength as external pressure compressed the tail. Then, assuming a favorable IMF direction (for

at least part of the interval, as seems entirely plausible), dayside reconnection may have been ongoing, leading to an increase in the amount of open flux inside the magnetosphere, flaring of the magnetotail, and continued elevated lobe field strength. Because of the longer time scales involved at Saturn for loading of the tail with open flux, it can take several days for the tail to be inflated to a point where reconnection is likely to occur, and this study suggested that the time scale observed in this case was of order ~6–7 days. No strong evidence for magnetotail reconnection events during this loading phase were detected, however, toward the end of this period a sharp decrease in lobe field strength and what appears to be significant current sheet deflection toward the equator from its previously hinged position was observed. Several days later the current sheet was displaced southward from its previously hinged position, and magnetic signatures consistent with the passage of a plasmoid were observed. These field signatures are closely correlated with intense radio emission, evidenced by low-frequency extensions (LFEs) of radio emission, corresponding to radio sources detected at higher altitudes. All of the above features are believed to be a common consequence of the impact of a solar wind compression on Saturn's magnetosphere.

Additional evidence for significant dynamical effects attributable to solar wind variability has been reported by the CAPS team. CAPS observations from SOI outbound, in the pre-dawn tail, showed sudden energization of plasma associated with a field dipolarization, which was interpreted as evidence of a solar wind compression-related tail collapse via magnetic reconnection. Under conditions of high solar wind dynamic pressure, the magnetotail appears to enter a state of sustained lobe reconnection, resulting in a more Dungey-like configuration [Thomsen et al. 2015a]. In the inner magnetosphere, there is no apparent relation between the depth of electron penetration and solar wind properties [Thomsen et al. 2016], although the energization of ions in a large-scale standing wave might be caused by a solar wind pressure impulse [Thomsen et al. 2017a].

Jackman et al. [2015] presented a rare observation of strong planetward flow following a reconnection episode in Saturn's tail from August of 2006, when the Cassini spacecraft was sampling the region near 32 R_S and 22 h local time (LT). Cassini observed a strong northward-to-southward turning of the magnetic field, which is interpreted as the signature of dipolarization of the field as seen by the spacecraft planetward of the reconnection X-line. This event was accompanied by very rapid (up to ~1500 km s^{-1}) thermal plasma flow toward the planet. At energies above 28 keV, energetic hydrogen and oxygen ion flow bursts were observed to stream planetward from a reconnection site downtail of the spacecraft. Meanwhile, a strong field-aligned beam of energetic hydrogen was also observed to stream tailward, likely from an ionospheric source. SKR radio emissions enhancements similar to ones previously associated with plasmoid formation and release were detected slightly more than an hour after the observation of the dipolarization. The reconnection episode as inferred from the planetward directional flow duration lasts on the order of ~1.5 h, a significant fraction of a planetary rotation. The continuing presence of energetic O^+ ions throughout the event demonstrates that this must be a case of long-lasting Vasyliunas-type reconnection occurring beyond 32 R_S in the premidnight region, perhaps indicating quasi-steady reconnection of the type. Because of the persistent presence of O^+, we find little evidence for lobe involvement in the reconnection.

Kimura et al. [2013] investigated the very long-term (six years of measurements) variations of northern and southern SKR spectra, separated by polarization. This study confirms the prominent role of solar wind pressure over one solar cycle, and additionally identified a seasonal dependence of the SKR activity, with a maximum in summer.

Felici et al. [2016] presented a case study of data from Saturn's magnetotail, when Cassini was located at ~22 hour Local Time at 36 R_S from Saturn that suggests for the first time that a low-energy ionospheric outflow event has been detected at planets other than Earth. During several entries into the magnetotail lobe, tailward flowing cold electrons and a cold ion beam were observed directly adjacent to the plasma sheet and extending deeper into the lobe. The electrons and ions appear to be dispersed, dropping to lower energies with time. The composition of both the plasma sheet and lobe ions show very low fluxes (sometimes zero within measurement error) of water group ions. The magnetic field has a swept-forward configuration which is atypical for this region, and the total magnetic field strength is larger than expected at this distance from the planet. Ultraviolet auroral observations show a dawn brightening, SKR is enhanced and extends down to lower frequencies, and upstream heliospheric models suggest that the magnetosphere is being compressed by a region of high solar wind ram pressure. This event is interpreted as the observation of ionospheric outflow in Saturn's magnetotail, with the active atmospheric regions most likely the main auroral oval.

The majority of the previously discussed studies involved periods where Saturn's magnetosphere encountered a high density solar wind. The study by Kinrade et al. [2017] discusses observations during a period that Saturn's magnetosphere was in a rarified solar wind region. During this period on June 14, 2014 (day 165), the Hubble Space Telescope observed an unusual auroral morphology, where for 2 h, the Saturn's far ultraviolet (FUV) aurora faded almost entirely, with the exception of a distinct emission spot at high latitude. The spot remained fixed in local time between 10 and 15 LT and moved poleward to a minimum colatitude of ~4°. Interestingly, the spot constituted the entirety of the northern auroral emission, with no emissions present at any other local time, including Saturn's characteristic dawn arc, the complete absence of which is rarely observed. Solar wind parameters from propagation models, together with a Cassini magnetopause bow shock crossing, indicate that Saturn's magnetosphere in an expanded magnetosphere configuration during the interval, suggesting it was likely embedded in a rarefaction region. The spot was possibly sustained by reconnection either poleward of the cusp or at low latitudes under a strong component of interplanetary magnetic field transverse to the solar wind flow. The subsequent poleward motion could then arise from either reconfiguration of successive open field lines across the polar cap or convection of newly opened field lines. The spot's fixed LT position may be attributed to the negative IMF BY conditions incident at the time, combined with increased subcorotation of open flux toward higher latitudes. The emission intensity was also possibly enhanced by a sector of upward PPO current rotating through the region. These observations show conclusively that the mechanisms producing noon auroral spots and the main oval auroras (i.e., the dawn arc) are distinct, since in this case the cusp spot occurred without the arc. These observations also suggest that reconnection can occur in an expanded magnetosphere, in agreement with the cusp observations of Arridge et al. [2016a], who found evidence of reconnection under a range of upstream solar wind conditions.

Magnetospheric structure and convection

- **MN1b:** Conduct in situ studies of Saturn's ionosphere and inner radiation belt.
  - Investigate the effects on aurora of solar wind and seasons.
  - Are there UV satellite footprints on Saturn? (like at Jupiter)
  - Is there a seasonal variation in auroral activity?
  - Investigate solar wind - ionosphere - magnetosphere coupling through the auroral regions.
  - Investigate whether there are UV satellite footprints on Saturn and whether there are Region 1 currents connecting the ionosphere and the magnetopause.
  - Investigate the composition of Saturn's ionosphere.
  - Study whether there is a significant polar outflow from Saturn's high latitude ionosphere and whether the outflow exhibits seasonal or solar cycle variation.
  - Determine whether there is a radiation belt between the D-ring inner edge and the atmosphere.

Understanding the structure of the magnetosphere and the convection systems within the magnetosphere are clearly two of the most important goals of the MAPS investigation. Each MAPS instrument team and the IDS teams have contributed extensively to the study of this aspect of Saturn and have published extensive literature. In this summary document it is only possible to summarize a small fraction of the work done by the MAPS instruments. We refer the interested read to the individual MAPS instrument team reports and the published literature for a more complete coverage of the extensive contribution of Cassini to understanding Saturn's magnetospheric structure.

The Cassini spacecraft crossed the bow shock of Saturn for the first time at 09:45 UT on June 27, 2004, at a radial distance of 49.2 R_S from Saturn. After the initial crossing, the large apoapsis orbits by the Cassini spacecraft around Saturn over many years enabled hundreds of bow shock crossings. This allowed for thorough analyses of the three-dimensional shape, a capability to predict the location of the boundary and to investigating the microphysics of high Mach number shocks. Studying the global shape, location, and dynamics of the bow shock offers important insights into the physics governing its formation and the magnetosphere's response to solar wind dynamics.

Studying the global shape, location, and dynamics of the bow shock offers important insights into the physics governing its formation and the magnetosphere's response to solar wind dynamics.

A number of authors have used the Cassini data to develop models of the average shape of Saturn's bow shock as well as the response of this surface to changes in the dynamic pressure of the upstream solar wind. Masters et al. [2008] and Went et al. [2011] developed an exhaustive semi-empirical model of Saturn's dayside bow shock. The average three-dimensional shape of the boundary was constructed and equations relating the response of the subsolar point to variations in solar wind dynamic pressure derived. Achilleos et al. [2006] presented magnetic field signatures of some of the earliest crossings in the mission. Their results showed clearly defined overshoot and foot signatures that are typical of quasi-perpendicular shocks. This is by virtue of the Parker spiral structure of the IMF at 10 AU, where the magnetic fields met the bow shock with very large azimuthal components.

In addition, a number of studies have investigated the properties of the bow shocks themselves at Saturn [Masters et al. 2017, 2013a, 2013b; Sulaiman et al. 2015; Sundberg et al. 2017], and the particles and regions associated with the bow shock, including hot flow anomalies [Masters et al. 2009], superthermal electrons [Masters et al. 2016], and upstream whistler mode waves [Sulaiman et al. 2017] occurred during a period of high solar wind pressure that caused Saturn's bow shock to be pushed inside Titan's orbit, exposing the moon and its ionosphere to the solar wind. Omidi et al. [2017] using electromagnetic hybrid (kinetic ions and fluid electrons) simulations and Cassini observations, showed a formation of a single deformed bow shock for the Titan-Saturn system. Sulaiman et al. [2016] characterized Saturn's bow shock using the largest sample of crossings to date. They showed Saturn's dayside bow shock was in the quasi-perpendicular configuration for a large majority of the time. The bow shock was found to exhibit characteristics akin to both terrestrial and astrophysical regimes. Clarke et al. [2010a] investigated 35 Cassini orbits on which the spacecraft crossed Saturn's magnetopause and bow shock during 2004–2007, and concluded that the bow shock and magnetopause oscillate approximately in phase, within a phase uncertainty of about ±25°. The typical amplitude is 1–2 R_S and the period is significantly organized by the phase of the interior magnetic field oscillations, with a period near that of planetary rotation. Saturn's (dayside) bow shocks are predominantly quasi-perpendicular by virtue of the Parker spiral at 10 AU.

The Cassini spacecraft has shown that Saturn's bow shock can occasionally reach a high-Mach number typical of astrophysical shocks. In this regime Cassini has provided the first in situ evidence for suprathermal electron acceleration under quasi-parallel upstream magnetic conditions [Masters et al. 2016]. Masters et al. [2013b, 2011a] explore several different aspects of Saturn's shock structure. They investigated the Mach number dependence of electron heating across a bow shock. Their work presented a positive correlation between the electron temperature increase across the shock and kinetic energy of an incident proton, where electron heating accounts for ~3%–~7% [Masters et al. 2011a]. In addition, they compared observations of overshoots between Mercury's and Saturn's bow shocks, both of which represent drastically different Mach numbers in parameter space. They showed, on average, the overshoots at Saturn's bow shock were much higher than those observed at Mercury's. This supported the larger role of particle dynamics at higher Mach numbers [Masters et al. 2013b]. In addition, Sulaiman et al. [2015] showed evidence for cyclic reformation controlled by specular ion reflection occurring at the predicted time scale of

~0.3 τ c, where τ c is the ion gyroperiod. In addition, they experimentally revealed the relationship between reformation and alfvenic Mach number (Figure MAPS-18).

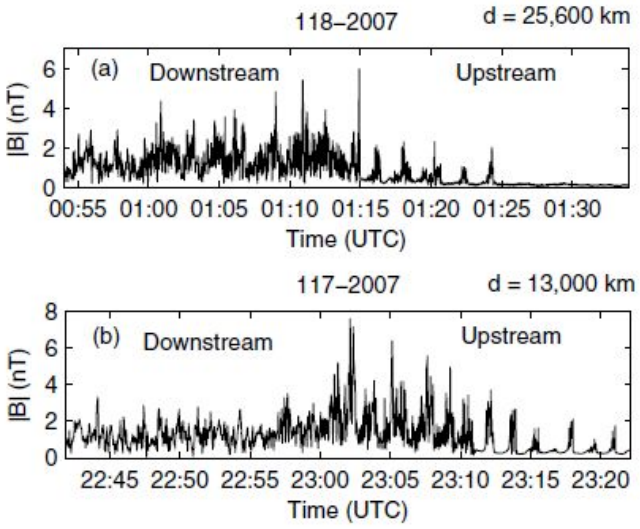

Figure MAPS-18. The panels are two examples of magnetic field plots showing quasi-perpendicular bow shock crossings with re-formation cycles occurring upstream of the shock. Figure adapted from Sulaiman et al. [2015] Figure 2.

Collisionless shock waves are also known to be efficient particle accelerators. It is widely believed that a large proportion of cosmic rays originate from energetic charged particles accelerated at collisionless shocks associated with supernova explosions in our galaxy. Masters et al. [2013a] confirmed, for the first time, electron acceleration up to relativistic energies at an unusually strong Saturn bow shock under a quasi-perpendicular configuration. This contradicted previous knowledge purporting a magnetic dependence on this phenomenon. Further works by Masters et al. [2016] and Masters et al. [2017] provided the full picture of suprathermal electrons at Saturn's bow shock. They showed results that are consistent with the theory in which the "injection" of thermal electrons into an acceleration process is possible for all magnetic field configurations at high Mach numbers.

Long-term sampling of Saturn's magnetosheath by Cassini afforded the most complete coverage of this intermediary region between the unshocked solar wind and Saturn's magnetosphere. A relatively high Alfvén Mach number solar wind and a polar-flattened magnetosphere make Saturn's magnetosheath both physically and geometrically distinct from the Earth's. Fast rotating gas giants, such as Saturn, are bulged along the equator and flattened along the poles owing to their embedded plasma disks and for this reason, Sulaiman et al. [2014] showed that the magnetic structure of Saturn's magnetosheath significantly deviated from axisymmetry. Their results showed large northward/southward components in the magnetic field despite the prevailing Parker spiral configuration being largely in the equatorial plane.

Using CAPS and other MAPS data, Sergis et al. [2013] investigated the properties of the magnetosheath. At energies of a few keV the magnetosheath is comprised of shocked solar wind plasma, while at energies above a few keV there is a strong presence of water group ions forming localized structures that are being convected downstream in the plasma flow. Under average magnetic field conditions in the magnetosheath, the kinetic properties of these hot water group ions can enable escape upstream from the bow shock. To help future scientists access the CAPS data to study the magnetosheath, Thomsen et al. [2017a] provides a comprehensive survey of intervals in which the observed magnetosheath flow was encompassed within the plasma analyzer field of view, and for which the computed numerical moments are accurate. The data extend over eight years from 2004 day 299 to 2012 day 151. The magnetosheath population is characterized by ion energies between ~100 eV and ~2 keV and electrons up to about 100 eV. The solar wind is best identified in the electrons, which have energies generally below 10 eV.

Saturn's magnetopause marks the boundary between the impinging solar wind and the region of space dominated by Saturn's intrinsic magnetic field. The magnetopause presents an obstacle to the solar wind. Cassini MAPS instruments have made extensive measurements of crossing of the magnetopause and have allowed us to examine the ways in which energy can be transferred in to and out of near-Saturn space. Understanding this is crucial for revealing the dynamics of the coupled planetary system of magnetosphere, moons, rings, and atmosphere.

A good understanding of the geometry of the magnetopause, and how its position changes with the pressure of the solar wind, is important for characterizing the distant dayside magnetosphere and in developing a three-dimensional global model of the magnetospheric magnetic field. Arridge et al. [2006] used early measurements of the magnetopause from Cassini/MAG, combined with measurements from Voyager 1/2 and Pioneer 11, to develop a new model of Saturn's magnetopause. This new model revealed that Saturn's magnetosphere was more compressible than previously thought: more compressible than Earth's magnetosphere, but less than Jupiter. This was confirmed and enhanced in further studies using larger datasets from Cassini/MAG [Kanani et al. 2010; Pilkington et al. 2015]. In a study by Achilleos et al. [2008], the MAG team analyzed some of the early orbits and the points along those orbits where the spacecraft crossed the magnetopause. By analyzing the distribution of the magnetopause crossings, it was concluded that the size of the magnetosphere was certainly being controlled by the dynamic pressure of the solar wind upstream of the planet, but that there was also evidence for an additional influence, probably due to a process internal to the magnetosphere. The system preferentially spent most of the time in one of two states, characterized by subsolar magnetopause distances near ~22 and ~27 Saturn radii.

A study some years later [Pilkington et al. 2015] built upon this work by constructing an up-to-date empirical model of Saturn's magnetopause. The work found that one could not satisfactorily fit these crossings in their entirety by assuming a system whose size responded only to solar wind pressure. By separating the crossings into subsets based on additional plasma data from the MIMI instrument, the study demonstrated that Saturn's magnetosphere plausibly made transitions between states which were plasma-light and plasma-loaded.

Magnetic reconnection is a fundamental process that can operate at a current sheet. It results in the release of energy stored in the local magnetic field, leading to acceleration of charged particles and allowing the direct transfer of mass and energy across an otherwise closed boundary. While evidence for the known operation of reconnection at Saturn's magnetopause has been sparse, MAG observations have formed the basis of important assessments that have broad implications. The first such assessment demonstrated that conditions at the magnetopause boundary of Saturn's magnetosphere are dramatically unlike those at Earth's magnetopause. As a result, reconnection at Saturn's magnetopause should be more restricted to regions where magnetic field lines adjacent to the boundary are locally anti-parallel to each other [Masters et al. 2012a]. This Cassini result began a shift in how we think about the solar wind-magnetosphere interaction at Saturn, with implications for other magnetized planets.

MAG data has also shown that when reconnection operates at Saturn's magnetopause it likely does so at a speed that is far slower than that associated with reconnection in environments closer to the Sun, for example, the solar corona, the solar wind, Earth's magnetopause, Earth's magnetotail [Masters et al. 2014]. The reason for this is the way that solar wind properties change as the plasma moves away from the Sun. The Alfvén speed, which dictates the speed of reconnection, drops with heliocentric distance, producing a relatively slow reconnection process at Saturn's magnetopause and consistent with the lack of evidence for rapid boundary later response discussed above. This result directly contributed to further work that showed that driving of Saturn's magnetosphere by global magnetopause reconnection is rarely strong enough to compete with the internal driving of the system that results from the combination of fast planetary rotation and plasma production due to the plumes of Enceladus [Masters 2015].

Magnetic reconnection at Earth has been proposed to occur only at the magnetopause and in the nightside magnetotail. At Saturn and Jupiter, internal sources are additional drivers for magnetospheric dynamics, and it is usually believed that internal sources could drive magnetic reconnection in the nightside inner magnetosphere. However, Guo et al. [2018] report in situ evidence of active magnetic reconnection process in the dayside of Saturn's magnetodisc at ~2 R_S away from Saturn's magnetopause. This study would directly support drizzle magnetic reconnection picture proposed by Delamere et al. [2015], and is also consistent with the rotating reconnection site picture proposed by Yao et al. [2017b].

The other important mechanism by which solar wind energy can enter a planetary magnetosphere is via a viscous-like interaction. This is underpinned by another fundamental process: Growth of the K-H instability. Where there are large plasma flow shears across a magnetopause this instability can lead to the evolution of small boundary perturbations in to gentle waves and eventually in to large, rolled-up vortices. The first evidence for magnetopause surface waves from Cassini came in the form of normal to the boundary determined from magnetic field observations that exhibited an oscillation in a preferred direction from one magnetopause crossing to the next [Masters et al. 2009]. The direction of wave propagation (direction of boundary normal oscillation) was controlled by the local direction of the magnetic field inside the boundary, consistent with K-H-driven waves. After this first observation, extensive continued studies of the K-H waves at magnetopause crossings has shown that such waves are ubiquitous [Masters et al. 2012b].

In addition to understanding reconnection and the K-H interaction at lower latitudes, it is important to understand how the magnetic cusps play a role in energy and particle transfer between the solar wind and the magnetosphere. At Earth, the solar wind is the primary energy source which can drive dynamical processes, and it is also a primary source of plasma. Before Cassini's arrival it was not clear what role the solar wind played in driving the magnetosphere, and so understanding the coupling between the solar wind and the magnetosphere, characterizing the phenomena of the distant dayside/flank planetary environment, was an important goal. This included studying viscous and magnetic reconnection processes at the magnetopause. Flux transfer events are a signature of dayside magnetic reconnection at Earth, Mercury and Jupiter, and consist of a rope of magnetic flux and plasma peeling away from the magnetopause. Jasinksi et al. [2016] presented an example of a flux transfer event at Saturn (the only one) and showed that this single event made a fairly small contribution (< 10%) to the magnetic flux transport budget, although it was not clear how typical this event was, and if they are more prevalent at locations on the magnetopause not sampled by Cassini.

… it is important to understand how the magnetic cusps play a role in energy and particle transfer between the solar wind and the magnetosphere.

At higher latitudes, a region known as the cusp maps to a very wide region of the magnetopause and so is ideal for remote monitoring of the magnetopause for reconnection signatures, revealing coupling between the solar wind and the magnetosphere. Cassini's inclined orbits during 2007/2008 and 2013/2014 were ideal to study this coupling process in plasma (CAPS) and the magnetic field (MAG). Some of the early inclined orbits in early 2007 showed evidence of solar wind plasma gaining entry into the magnetosphere [Arridge et al. 2016a]. This work showed evidence for movement of the cusp region in phase with magnetospheric (so-called planetary-period) oscillations, indicating the presence of current systems in the magnetosphere. It was also found that magnetopause reconnection was possible under both compressed and expanded magnetospheric conditions [Jasinski et al. 2016; Arridge et al. 2016a] and that the reconnection process could proceed in an unsteady fashion and at various locations on the magnetopause [Jasinski et al. 2016, 2014; Arridge et al. 2016a]. During SOI, the CAPS instrument showed that at latitudes above the extended plasma sheet/ring current there is a region that is largely devoid of plasma, known as the magnetospheric lobe [Young et al. 2005]. The lobe is commonly seen in the magnetotail, for example, Thomsen et al. [2015a], as the plasma sheet rocks and flaps up and down. Lobe field lines are thought to be connected by magnetopause reconnection into the solar wind and have thus lost their magnetospheric contents. At low altitudes, the lobe maps into the polar cap. The polar cap boundary is identified based on a sharp drop in ELS electron fluxes and corresponding signatures in other data sets (Figure MAPS-19), for example, Jinks et al. [2014]. A survey of polar cap boundary crossings showed that the main upward field-aligned currents associated with the aurorae reside equatorward of the open-closed boundary [Jinks et al. 2014].

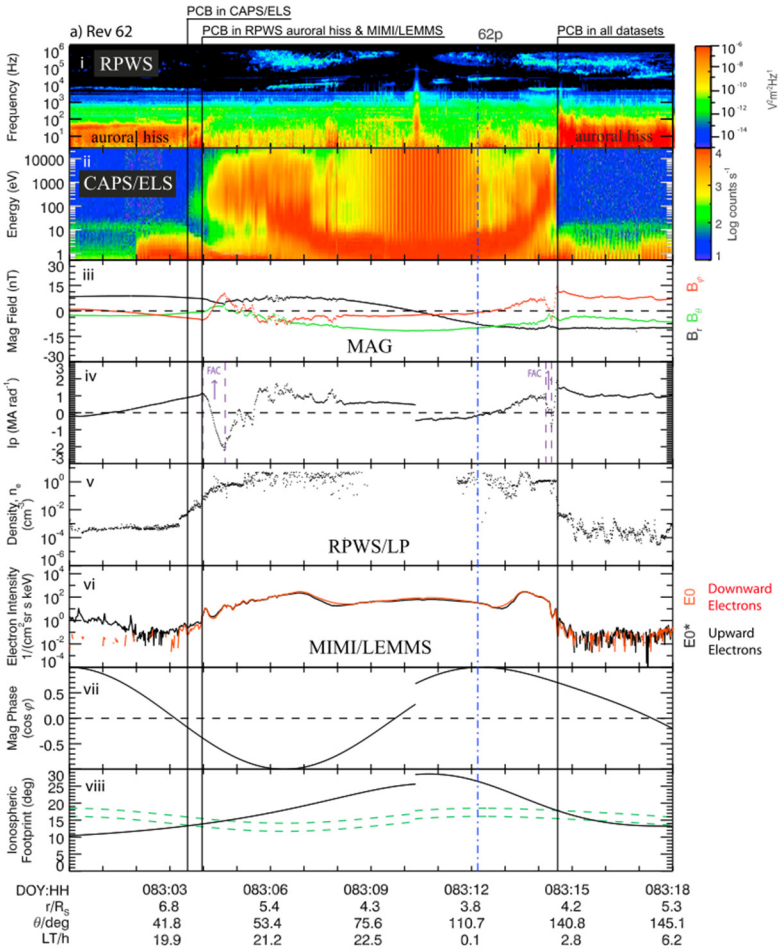

Figure MAPS-19. Polar cap boundary as seen in several different Cassini data sets. The sharp change in the ELS electron spectrum is the most definitive signature. The polar cap is largely devoid of electrons (counts below ~20 eV are due to spacecraft photoelectrons). Figure from Jinks et al. [2014].

Near noon, open magnetic field lines (which will ultimately become the lobe/polar cap) are filled with incoming magnetosheath plasma, which penetrates down to low altitudes. CAPS observations of this region, known as the cusp, demonstrate that the process of reconnection occurs at Saturn's magnetopause, with indications that the reconnection is pulsed [Jasinski et al. 2014]. The first reported cusp observation was associated with the arrival of a solar wind shock front, which compressed the magnetosphere and probably provided more favorable conditions for magnetopause reconnection [Jasinski et al. 2014]. Evidence for both bursty and more continuous reconnection is observed at different cusp events, and the locations of the reconnection site vary along the subsolar magnetopause. Magnetic reconnection and plasma injection into the cusp can occur for a variety of upstream conditions [Jasinski et al. 2017, 2016; Arridge et al. 2016a].

Saturn's magnetosphere is an example of a rapidly rotating system dominated over much of its extent by a large magnetodisk of rotating plasma, this material falling further behind corotation with the planet as we go to larger distances from the planet. Because the system is so large,

centrifugal force becomes very effective at keeping the cold plasma confined as this near-equatorial disk. In order to develop a first-principles model of Saturn's magnetodisk region, Achilleos et al. [2010a] adapted a model of field and plasma developed for the Jovian system by Caudal [1986], using plasma data available at that time to constrain the model's boundary conditions. This model was successfully used to explain the observed response of the planet's magnetospheric field to changes in system size. We were also able to compare the model contributions to the total magnetodisk current associated with the various forces on the plasma (centrifugal force and pressure gradient force) for both the Kronian and Jovian magnetodisk systems. A follow-up study by Achilleos et al. [2010b] explored particularly the influence of global changes in the energetic particle population on Saturn's magnetodisk structure. This model was also used in a study by Sorba et al. [2017], who developed theoretical compressibility curves showing how the magnetodisk size responds to changes in solar wind pressure and internal plasma content (energetic particles). These theoretical results were in good agreement with the observational analysis of Pilkington et al. [2015] and we were also able to use the model to explain why one would expect the compressibility of the system to vary with system size. We have also had some success in using this magnetodisc model, combined with the current sheet elevation model of Arridge et al. [2011a], in order to model global, near-planetary-period oscillations in the magnetic field and plasma properties [Achilleos et al. 2014].

It has been shown that periodic variations of the plasma density peak at different rotation phases depending on radial distance in the magnetosphere. We showed that this variation arises as a consequence of the interaction between simple rotation and the expansion and contraction of the magnetosphere associated with propagating compressional disturbances [Ramer et al. 2017]. Propagating compressional disturbances also cause the magnetopause to move in and out non-sinusoidally and somewhat asymmetrically [Kivelson and Jia 2014]. The simulation also explains the dawn-dusk asymmetry of field configuration and plasma flows in Saturn's magnetosphere [Jia and Kivelson 2016].

The rotation period of Saturn's magnetosphere was found to vary with time, and changing periodicities were identified in magnetic fields, radio emissions, and charged particles [Andrews et al. 2012, 2011, 2008; Provan et al. 2014, 2013, 2011, 2009]. The plasma motion of the magnetodisk is very much affected by the oscillating magnetic field of Saturn, which is different in the two hemispheres. These planetary period oscillations strongly influence the magnetic and plasma properties of the outer magnetosphere [Andrews et al. 2010a; Provan et al. 2012] as well as the density of thermal ions [Nemeth et al. 2011; Szego et al. 2011]. The thermal plasma sheet properties are different for the different ion species. The proton sheet is smoothly modulated by the flapping of the magnetodisk while heavy ions form a narrow sheet surrounding the magnetic equator. The periodicity of the observed heavy-ion rich events was found to be close to the SKR period of the southern hemisphere.

Szego et al. [2012] observed that the ion density moments derived by Thomsen et al. [2010] from Cassini CAPS measurements exhibit peaks around zero-crossings of the magnetic field. The proton peaks are broader while the heavy ion peaks are sharper. They found that the positions of these peaks can be explained by the simple structural model of Arridge et al. [2011a]. Szego et al.

[2013] modified this simple structural model to include the dual periodicity of the magnetic field, and found an even better agreement for the positions of the ion peaks.

Using numerical ion moments, Nemeth et al. [2015] investigated the azimuthal flow velocities measured by CAPS along with their periodicities. They observed a significant positive correlation between the azimuthal plasma speed and the plasma density, both anti-correlating with the magnitude of the radial component of the magnetic field. They found that the dense plasma near the magnetic equator rotates around the planet at high speed, but the dilute plasma of higher latitudes is rotating significantly slower.

Nemeth et al. [2016] analyzed the quasi-periodic variation of several plasma parameters. The variation of the magnetic field was used to recover the position of the magnetodisk, and the position information was further used to model the variation of the density and azimuthal velocity moments of the thermal ions. This simple technique provides very good fits for all three parameters simultaneously.

Saturn's disk-like magnetosphere produces a unique and interesting current system. The magnetodisk current flows in the equatorial magnetosphere eastward around the planet extending the field lines radially outward, carried by the differential drift of ions and electrons in the plasma trapped on Saturn's magnetic field lines, which grades into the cross-tail plasma sheet current separating the lobes of the magnetic tail on the nightside. Although the existence of the ring current was first established from magnetic data acquired during the Pioneer-11 and Voyager flybys, little was known of the variability of the current, and its physical nature remained a matter of controversy, whether due to centrifugal action of the plasma mass or to the effect of plasma pressure. Data from the initial sequence of near-equatorial Cassini orbits was first used to determine the strength and radial extent of the current, showing that this varies strongly with the size of the magnetosphere dependent on the dynamic pressure of the impinging solar wind [Bunce et al. 2007]. While the inner edge of the current lies nearly unvaryingly at an equatorial radial distance of ~7 R_S, the radius of the outer edge varies between ~15 R_S when the magnetosphere is strongly compressed to ~22 R_S when it is significantly expanded, these distances typically lying a only few R_S inside the dayside magnetopause. Correspondingly, the total eastward current varies from ~9 to ~15 MA, with a magnetic dipole moment that varies between ~0.2 and ~0.6 that of the internal field of the planet. A consequence is that while the dayside and comparably-near nightside field is quasi-dipolar in form when the system is compressed, the field lines extend into an equatorial magnetodisk when it is expanded [Bunce et al. 2008]. Later, when data from the first highly inclined Cassini orbits became available, the first direct measurements of the north-south thickness of the current sheet were also made, with values being typically ~3 R_S on the dayside, while varying between ~1 and ~5 R_S on the nightside [Kellett et al. 2009].

Cassini/MAG data revealed the magnetodisc [Arridge et al. 2008b; Bunce et al. 2008] was particularly sensitive to the solar wind pressure, essentially disappearing on the dayside when the magnetosphere was compressed by the solar wind and explaining why it was not detected by Pioneer 11 or Voyagers 1/2 [Arridge et al. 2008b].

The current sheet was also found to be warped out of the equatorial plane, as expected by analogy with Earth and Jupiter, but it was also found to be deformed at noon. Effectively the current sheet had the geometry of a shallow bowl, or upturned umbrella [Arridge et al. 2008a]. Subsequently, a detailed study of data from Earth's magnetosphere has revealed a similar effect at Earth [Tsyganenko and Andreeva 2014], inspired by Cassini/MAG measurements at Saturn. Superimposed upon this global warping was a flapping motion that occurred in phased with other periodicities in Saturn's magnetosphere [Arridge et al. 2011a, 2008c] and which had a lag or delay that propagated into the outer magnetosphere. However, latitudinal effects were also shown to play an important role, connected with differing periods in the northern and southern hemispheres [Provan et al. 2012].

Small ripples were also found superimposed on this bowl-shape [Arridge et al. 2007] that are largely propagating away from Saturn, indicating a source closer to the planet, possibly produced by plasma transport in the inner/middle magnetosphere [Martin and Arridge 2017].

The presence of the current sheet, and its deformation into a bowl-shape, has important consequences for Titan's magnetic and plasma environment, and so the structure of its induced magnetosphere [Backes et al. 2005; Arridge et al. 2011b; Simon et al. 2013], as not only is the magnetic field (oriented in a different location to that found by Voyager 1), but also the bowl-shaped current sheet means that the Titan is not continuously immersed in Saturn's magnetospheric plasma.

Detailed collaborative work of the MAPS teams also examined the physical nature of the current [Kellett et al. 2011, 2010; Sergis et al. 2018]. It was shown that inside ~10–12 R_S the current is carried principally by the relatively unvarying population of warm (~100 eV) water plasma picked-up from the Enceladus torus, comprising principally of inertia and pressure anisotropy currents. Beyond these distances it is carried mainly by the more variable hot tenuous plasma. While, by analogy with Earth, the term ring current particles is often taken to be synonymous with hot injected plasma, this usage has thus proven to be inappropriate at Saturn, since the outwardly-transported warm water plasma is at least as significant in carrying the current.

The middle magnetosphere is the region where the so-called ring current of Saturn resides. This current likely has important components below the energy range of MIMI. But it has been found to contain energetic ions and electron below 1 MeV, with relatively high fluxes. It is populated by large scale injections in the nightside magnetosphere of Saturn, which populate the ring current with a series of rotating, energetic ion and electron bundles, called sometimes blobs due to their appearance as such in remote sensing images by MIMI/INCA. The energy density of the energetic ion population is high enough to increase the plasma beta (the ratio of total particle pressure divided by magnetic pressure) above one, therefore causing a significant stretching of the magnetic field lines. Depending on the abundance of oxygen in the energetic ion distributions, the dynamics of the current

Depending on the abundance of oxygen in the energetic ion distributions, the dynamics of the current sheet may be dominated by the presence of energetic particles.

sheet may be dominated by the presence of energetic particles. All these results are summarized in a series of studies by Sergis et al. [2017, 2013, 2011, 2010, 2009, 2007]; Krimigis et al. [2007]; Dialynas et al. [2013, 2009]; Carbary et al. [2014, 2012, 2010b, 2008b]; Kollmann et al. [2011]. All these measurements provided a most comprehensive, average description of Saturn's ring current, which can inform numerous empirical and physical models of Saturn's magnetosphere, for example, Achilleos et al. [2010a]. The time variations in the ring current have been linked to changes in the radiation belts [Roussos et al. 2018b, 2014; Kollmann et al. 2017], injections [Mitchell et al. 2016, 2015, 2009a], revealing the coupling of the system with different regions of the magnetosphere and the interplanetary space and the aurora, for example, Mitchell et al. [2009b]. The average properties of the ring current, as monitored by ENAs, have been inverted in order to probe the characteristics of Saturn's neutral gas cloud [Dialynas et al. 2013]. Meanwhile, the average distribution of the middle magnetosphere energetic particles has been studies using observations from CHEMS [Allen et al. 2018].

Many of the studies focusing of the inner magnetosphere extended into the region of the ring current, meaning that energy spectra, angular and L-shell distributions, composition, as well as asymmetries are equally well quantified for $9 < L < 15$.

In the inner and middle magnetospheres, significant work has been done to characterize not only the current systems, but also the plasma properties. In these regions the primary spatial dependence of magnetospheric properties is in the radial direction. From the first SOI pass through the magnetosphere [Young et al. 2005], several distinct magnetospheric regions could be identified: an outer region (inside the magnetopause) with extremely low density, later understood as magnetospheric lobe; then a significantly denser region with variable density and dominantly H^+, later understood as the higher-latitude manifestation of the plasma sheet/ring current; and finally, a much denser inner plasmasphere with W^+. Subsequent analyses of the SOI data [Sittler et al. 2008, 2006a, 2006b, 2005] provided quantitative estimates of the H^+, W^+, and electron plasma parameters in the inner magnetosphere and demonstrated that the plasma flow velocity is near corotation throughout the region (corotation is the azimuthal flow that results from essentially rigid rotation with the planet; it is enforced by currents flowing along the magnetic field lines between the upper atmosphere and the magnetospheric plasma). The proton and water-group temperatures were consistent with local ionization and pick-up into the corotating flow. The electrons in the inner magnetosphere consist of two populations: a cool component whose temperature tracks the proton temperature and a hotter population that increases in energy with decreasing radial distance [Young et al. 2005; Sittler et al. 2006a, 2006b; Schippers et al. 2008]. Later work [Rymer et al. 2007; Rymer 2010] showed that the cold electron component was consistent with a local pick-up source and subsequent heating via Coulomb collisions with the protons. The hot component was consistent with adiabatic transport inwards from a source in the plasma sheet/ring current region.

Calculation of the ion plasma moments (density, temperature, flow velocity) from CAPS data is complicated by incomplete and variable viewing. Nonetheless, application of a numerical computational scheme to the full data set through March 2009 enabled a survey of the properties of H^+, W^+, and H_2^+ (the third most common ion species in the magnetosphere, as revealed by CAPS time-of-flight measurements) throughout the magnetosphere [Thomsen et al. 2010]. The survey

confirmed that densities decrease and temperatures increase with radial distance inside ~20 R_S, and the W^+ density declines more rapidly than light ions. The flow velocity remains primarily in the corotational direction essentially all the way to the magnetopause, but the speed is lower than full corotation. Combined with the higher-energy measurements of MIMI, the CAPS data enabled a comprehensive survey of the total plasma pressure throughout the magnetosphere and thus an understanding of the currents that distort the dipole field within the plasma sheet and ring current region [Sergis et al. 2017, 2010]. A more recent survey of plasma moments calculated with a forward modeling approach that includes anisotropic temperatures explores both the radial and local time variations of the plasma (Figure MAPS-20), [Wilson et al. 2017].

Due to strong centrifugal forces on corotating plasma, Saturn's magnetosphere is flattened into a disk shape, especially on the night side and during times of relatively low solar wind dynamic pressure, for example, Arridge et al. [2008b, 2007]. CAPS data allow determination of the latitudinal scale heights of H^+, W^+, and H_2^+ and show that the heavy ions are more strongly confined to the equatorial plane, for example, Thomsen et al. [2010]. In the magnetotail, the magnetodisk structure is particularly prominent, with the current flowing in a relatively thin region of dense plasma separating the lobes of oppositely-directed magnetic field. The magnetodisk consists of a structured plasma sheet: a low-latitude heavy ion layer displaying narrow substructures, and a higher-latitude, smooth, broad ion layer composed dominantly of light ions (Figure MAPS-20), [Szego et al. 2011]. The density and azimuthal flow speed decline with increasing latitude [Nemeth et al. 2015] as a direct consequence of the sub-corotation of the plasma in the outer magnetosphere, for example, McAndrews et al. [2009]; Thomsen et al. [2014a, 2013]; Wilson et al. [2017]. Highest speeds occur on field lines at lowest latitudes mapping to the rapidly rotating inner regions of the plasma sheet, and the speed falls as one moves to higher latitudes, where the field lines are connected to strongly sub-corotating plasma at large radial distances.

An extremely important aspect of understanding the magnetosphere of Saturn is understanding the convection patterns and transport of plasma through and out of the magnetosphere. Saturn's magnetosphere is dominated throughout the equatorial magnetosphere by (partial) corotation with the planet. This was widely expected before the Cassini encounter, and although the expectation was not universally held, the basic result was no big surprise.

It is now clear that the dominant source of plasma for Saturn's entire equatorial magnetosphere is the inner icy satellites, in particular, the south-polar geyser plumes of Enceladus orbiting Saturn at L = 3.95, where L is the planet-centered distance normalized to Saturn's equatorial radius, $R_S \approx 60{,}300$ km [Young et al. 2005]. If tiny Enceladus is to dominate the source of Saturn's magnetospheric plasma, and hence its magnetospheric dynamics, there must be a mechanism for transporting this plasma radially from its inner-magnetospheric source to a sink in the outer magnetosphere and ultimately to the downstream solar wind. This transport mechanism is now known to be the centrifugal interchange instability.

In Saturn's magnetosphere, the centrifugal acceleration $\Omega 2/r$ is outward, and exceeds Saturn's inward gravitational acceleration beyond L ~ 2. Outward moving flux tubes release centrifugal potential energy from the system at a rate $\Omega 2/r$ per unit mass, and inward moving flux

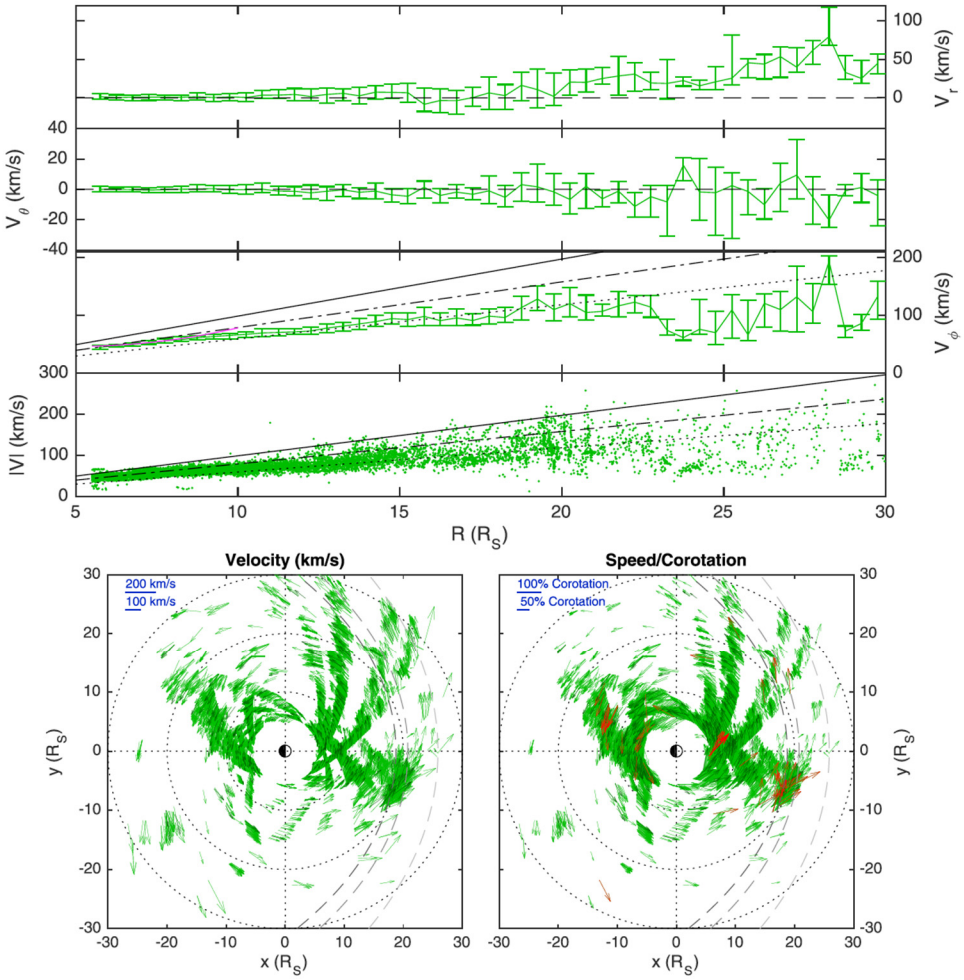

Figure MAPS-20. A recent survey of plasma moments calculated with a forward modeling approach that includes anisotropic temperatures explores both the radial and local time variations of the plasma. *Top three panels*: Radial profiles of plasma velocity components, in 0.5-Rs bins. *Fourth panel from the top*: All measured flow speeds. *Bottom left panel*: Equatorial plane projections of flow vectors with length proportional to flow speed. *Bottom right panel*: Same as the panel to the left, but with length proportional to the fraction of corotation. All data points are shown in green, while dark green shows every thirtieth data point. Figure from Wilson et al. [2017].

tubes add centrifugal potential energy to the system at the same rate per unit mass. Because of the inward density gradient of the combined plasma distribution (per unit magnetic flux), the combined flux-tube interchange process releases potential energy from the system and is therefore gravitationally unstable. The reverse would be true if the background density gradient (per unit magnetic flux) were reversed. In this sense the interchange motion is centrifugally driven. (Flux-tube interchange motions, by definition, involve no net radial transport of magnetic flux.)

It is also important to note that the azimuthal gradient and curvature drifts of the hot tenuous plasma result in plasma being injected inward by the interchange process, relative to a corotating frame of reference. This drift is prograde (eastward) for positive ions and retrograde (westward) for

negative ions and electrons. Its speed at a given distance is proportional to particle thermal energy. The injection process thus gives rise to an energy-longitude dispersion signature of the injected plasma, which has been called the smoking gun of interchange convection. This signature was repeatedly observed by CAPS on every Cassini pass through the inner magnetosphere, (L between ~5 and ~12), where the magnetic configuration is well described by an aligned dipole model [Burch et al. 2005; Hill et al. 2005; Young et al. 2005; Chen and Hill 2008; Chen et al. 2010; Rymer et al. 2009b, 2008]. An early example of this injection-dispersion signature, appropriate to this off-equatorial orbit, is shown in Figure MAPS-21 from Hill et al. [2005].

One unexpected feature of these CAPS observations was that Saturn's inflow channels (containing hot tenuous plasma) were always narrower in longitude than the neighboring outflow channels (containing cooler denser plasma), by a factor ~10 [Chen and Hill 2008; Chen et al. 2010]. All previous theoretical models of interchange convection had inflow and outflow channels of equal width, because of assumptions made for analytical convenience. Recent numerical simulations using the more flexible Rice Convection Model (RCM), driven by CAPS observational inputs [Liu et al. 2010; Liu and Hill 2012; Hill 2017, 2016; Hill et al. 2018], have clarified the reason for this apparent discrepancy between observation and theory. At Saturn (unlike at Jupiter) the source region for newly injected plasma, both from new ionization and from charge-exchange reactions with ambient neutral molecules, is broadly distributed throughout the radial range in which the resultant interchange radial transport occurs (L between ~5 and ~12).

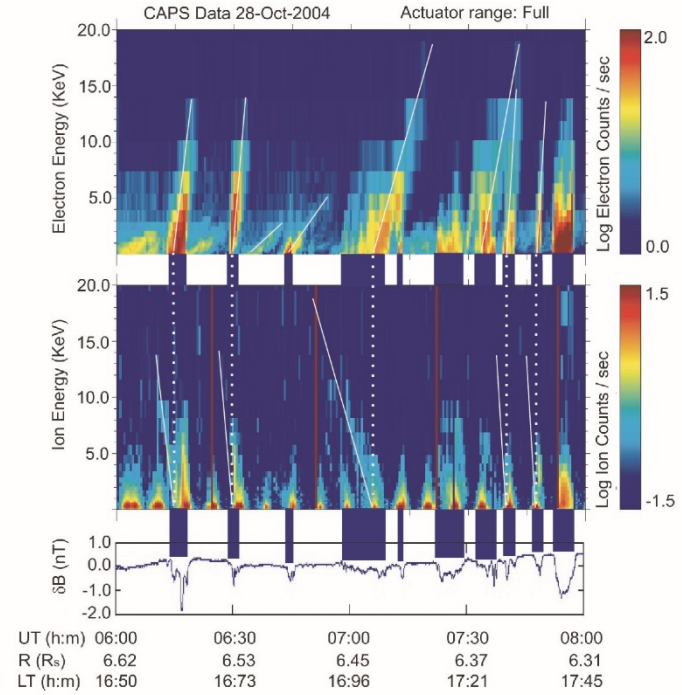

Figure MAPS-21. Early example of injection-dispersion signature, appropriate to off equatorial orbit. Linear energy-time spectrograms for electrons (*Top panel*) and positive ions (*Middle panel*) from the CAPS detectors during the second Cassini orbit of Saturn. *Bottom panel* shows simultaneous magnetic-field magnitude perturbations.

Injections at Saturn have been coarsely characterized as small and large scale. The latter would likely be accompanied by reconfigurations of the planetary magnetic field. Small-scale injections are probably confined to a small range of planetary longitudes and physically can be flux tube bundles, flow channels, or more elaborate structures. This group of injections also perturbs the magnetic field locally, for example, Andre et al. [2007, 2005], but probably at the level of a few percent of the planetary field. Andre et al. [2007] and Rymer et al. [2009b] present multi-instrument displays of interchange events in the magnetosphere of Saturn. This group of injections have been characterized as particle distributions with phase space densities that are very different from the surrounding medium in which they are observed [Mauk et al. 1998; Paranicas et al. 2016]. Mitchell et al. [2015] summarized the observational differences between small- and large-scale injections at Saturn. They found that small scale injections tended to be found inward of about 12–15 R_S, although they also found large-scale injections that could be inward of that distance. It is probably the case that small-scale injections (which are found very frequently in the data) extend in energy up to the tens of keV or so. Rymer et al. [2007] used phase space density profiles derived from CAPS data to approximate a starting radial distance of interchange injections that are observed by Cassini. Paranicas et al. [2016] approximated the inward flow speed of injections and found values comparable to the theoretical computations of Hill [2016] for $5 < L < 10$. It is believed that the radial speed of injections decreases as they approach Saturn.

Large-scale injections at Saturn have received much less attention in the literature than small scale ones. Thomsen et al. [2013] has provided a good summary of the situation. Large scale injections have been characterized by the MIMI data set. Mitchell et al. [2009b] linked some of these injections to UV data from HST and Cassini. Paranicas et al. [2010, 2007] looked at the radial range of injection remnants. Because these extend into the hundreds of keV, it is likely Paranicas was studying large-scale injections. The effects of tail collapse, plasmoid production, and related processes have been documented with the help of magnetometer data, for example, Jackman et al. [2015, 2011].

Because of their ubiquity, injections at Saturn have been used to characterize other features of the magnetosphere. Mauk et al. [2005] and Müeller et al. [2010] created azimuthal plasma flow speeds as a function of Saturn distance using MIMI injection data. Plasma flow speeds were later found using the plasma data, for example, Thomsen et al. [2010].

There are useful and well-established relationships between the local rate of plasma mass or momentum loading (through new ionization, charge exchange, or outward mass transport), on one hand, and the radial variation of the rotational lag behind rigid corotation with the planet, on the other hand. Rates of ionization, charge exchange, and net outward mass transport are difficult if not impossible to measure directly. But the corotation lag is straightforward to measure directly if one has access to reliable in situ plasma measurements. Tokar et al. [2006] reported surprisingly strong and asymmetric plasma flow perturbations during the distant and highly inclined July 2005 Cassini encounter with Enceladus. This study also concluded that plasma mass is added to Saturn's magnetosphere at a rate > ~100 kg/s in the near vicinity of Enceladus, a conclusion that was controversial at the time but was subsequently verified by many independent analyses, for example, Chen et al. [2010]. Pontius and Hill [2009] applied a similar analysis, not to the localized plasma

loading in the immediate vicinity of Enceladus, but to the much broader region 3 < ~L < ~10 where significant corotation lag was reported by Wilson et al. [2009, 2008] from their analysis of CAPS data. The study showed that the corotation lag as a fraction of the local rigid corotation speed. The data-model comparison of Pontius and Hill [2009] concludes that the plasma loading rate in this much larger volume is also > ~100 kg/s, comparable to that in the near vicinity of Enceladus.

Plasma loss into the magnetotail

- **MC1a:** Determine the temporal variability of Enceladus' plumes.
  - Investigate temporal variations in Enceladus gas production and plume composition, on the scale of seasons and solar cycle.
  - Study plume neutral gas composition.
  - Investigate the physics of the dusty plasma environment
  - Determine how the magnetosphere reacts to changes in (plume?) gas production rates by studying Enceladus' auroral footprint.
  - Study variability in dust-to-gas mass ratio.
- **MN1a:** Determine the dynamics of Saturn's magnetotail.
  - Study thoroughly the plasma sheet in Saturn's magnetotail.
  - Investigate the relation between solar wind compression events and magnetotail dynamics.
  - Investigate the plasma sheet thickness and scale height as functions of radial distance and local time.
  - Statistically characterize magnetotail variations, especially those associated with plasmoids, and correlate them with changes in the inner magnetosphere.
  - Critically evaluate the Dungey and Vasyliunas cycles in light of the new observations, especially those of flow speeds.

Enceladus, the rings, and Titan are all sources of plasma in Saturn's magnetosphere. The roughly 100 kg/s of mass being added must eventually find its way out of the inner and middle magnetosphere and into the magnetotail where it can be lost. Large-scale reconnection events that may produce plasmoids provides one potential escape route for the cool W^+ plasma that has accumulated from the interior source region. There remains some controversy as to whether this escape route is adequate to balance the interior source rate, estimated to be roughly 100 kg/s or more as noted above. It is plausible, but not yet demonstrated, that an unseen spectrum of smaller but more frequent plasmoids could contribute importantly to the escape rate.

Magnetic reconnection in the magnetotail current sheet can produce plasmoids, magnetic flux ropes (or closed magnetic loops) that are disconnected from the planet at one (or both) ends. These structures have been routinely observed in the magnetotails of Earth and Jupiter. Their detection

at Saturn by Cassini was limited by orbital geometry because the 2006 deep magnetotail passes by Cassini occurred near Saturn's northern winter solstice, when the warped magnetotail current sheet was presumably displaced well northward of Cassini's orbital plane (see Figure MAPS-22). Despite this problem, three plasmoid-like magnetic signatures were identified in the Cassini magnetometer data [Jackman et al. 2007]. Two of these events actually crossed the current sheet, where ion fluxes were sufficient to permit composition and velocity-moment information to be extracted from CAPS data. These two events were analyzed in detail by Hill et al. [2008]. The most dramatic event occurred on March 4, 2006, at a planet-centered distance of 44 R_S and at 0300 LT. Results are shown in Figure MAPS-23 and Figure MAPS-24.

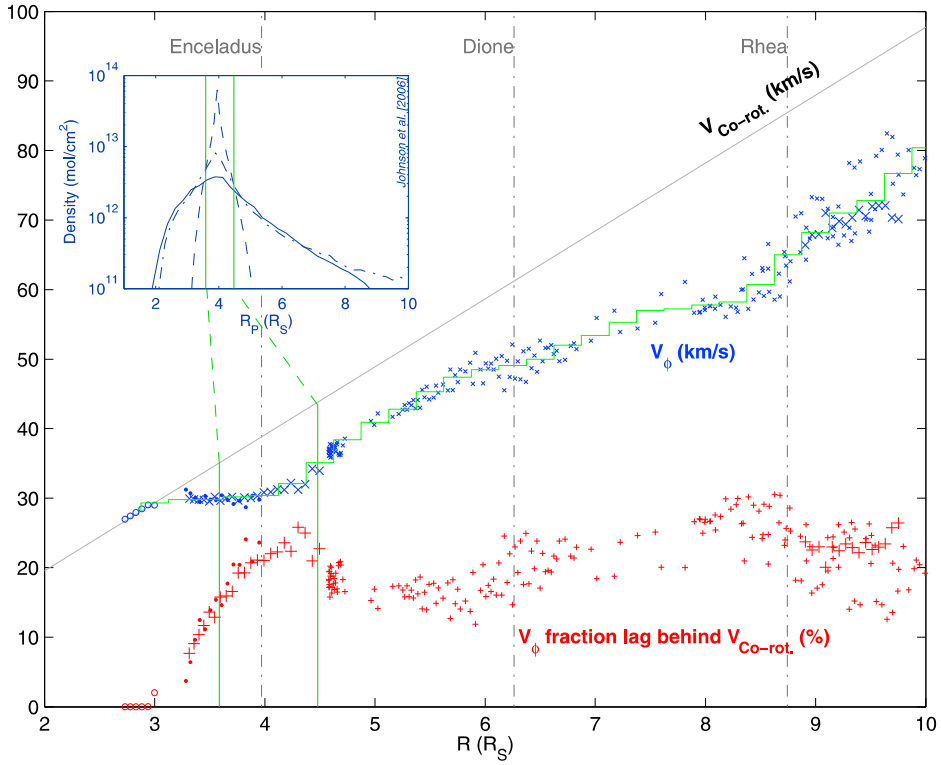

Figure MAPS-22. CAPS plasma flow measurements. Data for L > 5.5 are from forward modeling of thermalized ion velocity moments [Wilson et al. 2008]. Data for L < 5.5 are obtained from analysis of freshly picked-up charge-exchange products under the assumption of gyrotropy. Red symbols at the bottom show azimuthal speeds as a fraction of the local corotation speed. Figure from Wilson et al. [2009] Figure 4.

Early in this event, before the sharp B_θ reversal near 2300 UT, water-group ions (W^+) dominated the plasma composition, indicating a pinching off of a formerly closed flux tube containing plasma from the interior source, as in Vasyliunas-cycle reconnection. At about 23:10 UT the W^+ peak went off-scale above the energy-per-charge range of the CAPS IMS (50 V), so W^+ velocity moments became unavailable though their flux remained high. The velocity moments (based on H^+ after 23:10) indicate sub-corotational azimuthal flow throughout the event and a dramatic tailward acceleration (with Vr increasing up to ~800 km/s) late in the event. Rigid corotation at this distance would be 430 km/s in the V_Φ direction.

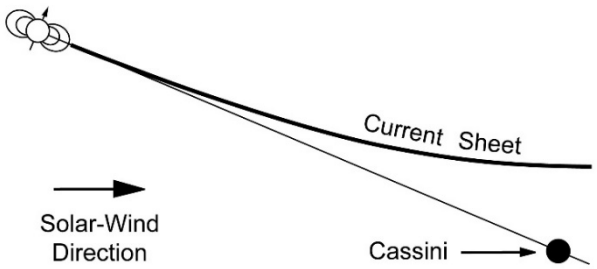

Figure MAPS-23. Orbital geometry during the deep-tail passes of Cassini. Figure from Hill et al. [2008] Figure 1.

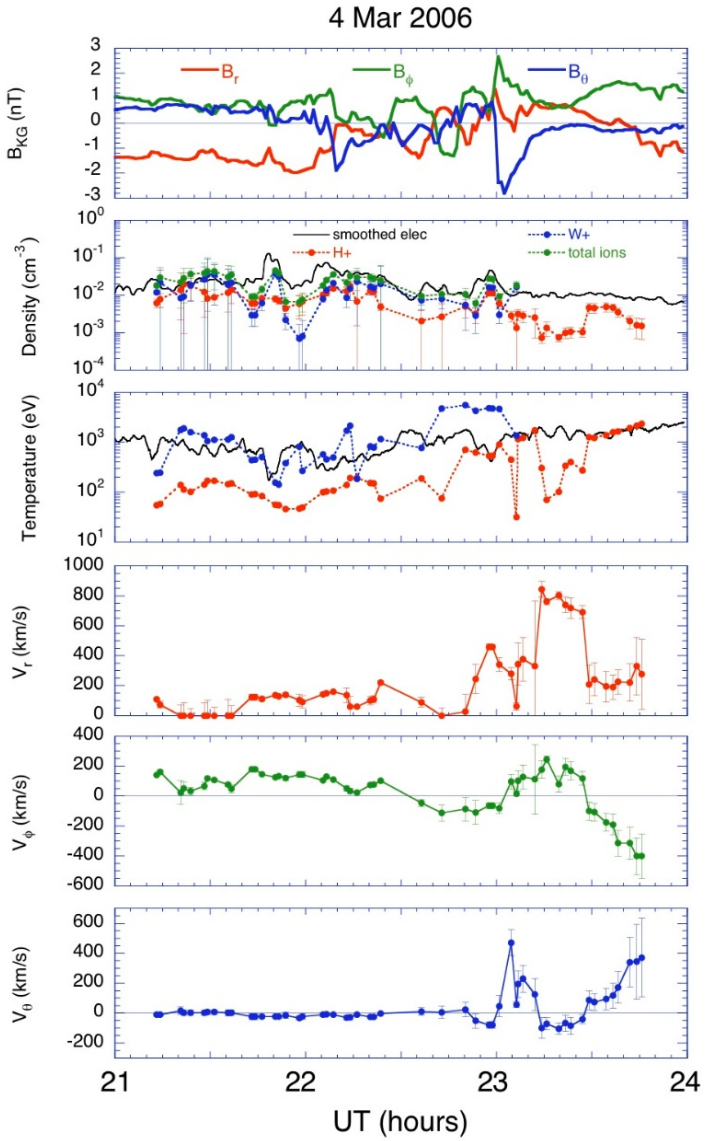

Figure MAPS-24. Magnetic field components and particle velocity moments for the plasmoid encountered by Cassini at 44 R_S near 0300 LT. Figure from Hill et al. [2008] Figure 3.

A particularly interesting feature of this event is that Cassini was in a position to see not only the plasmoid properties observed in situ by CAPS and MAG, but also the plasmoids earlier initiation closer to Saturn as observed by MIMI in ENA bursts. The viewing geometry is shown in Figure MAPS-25. The ENAs were hydrogen and oxygen atoms having speeds consistent with covering the distance from source to Cassini (~26.5 R_S) in the allotted time (~25 min). The plasmoid structure itself could also have covered the same distance in the same time interval [Hill et al. 2008].

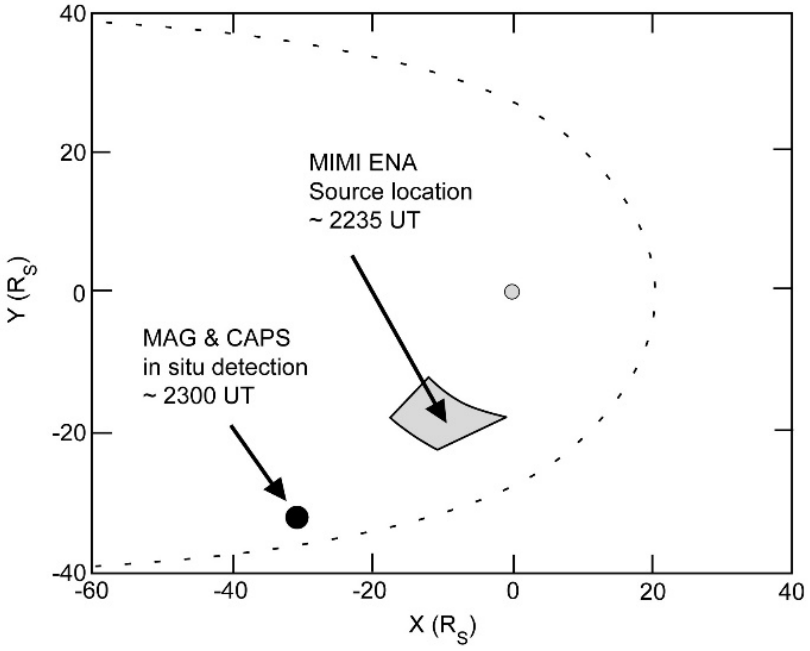

Figure MAPS-25. During the in situ CAPS and MAG plasmoid observations on March 4, 2006, Cassini was within the large dot indicated, and the ENA bursts observed from the same location ~25 min earlier were deduced to have a source within the quasi-rectangular shaded box. The dashed contour is a cartoon depiction of the typical shape and location of Saturn's magnetopause.

Magnetotail reconnection also provides a fresh source of hot, tenuous plasma to the region planetward of the reconnection site, where it produces a dipolarization signature in the magnetic field. It can also provide seed particles both for the inflow channels of the interchange cells in the inner magnetosphere, as described earlier, and for the intermittent ENA bursts observed by MIMI from the middle and outer magnetosphere, and the associated SKR bursts observed by RPWS from the footprints of the same field lines.

Theoretically, there is a clear distinction between Vasyliunas-cycle reconnection involving the pinching off of formerly closed flux tubes, containing cool dense plasma from the inner-magnetosphere source, and the more Earth-like Dungey-cycle reconnection involving the closure of formerly open flux tubes of the magnetotail lobes, containing hotter and more tenuous plasma of magnetosheath origin. The large plasmoid described above is readily explained by the Vasyliunas cycle alone. But two detailed multi-instrument event studies [Thomsen et al. 2015a, 2015b] have also found evidence of both Vasyliunas and Dungey cycles occurring either

simultaneously or sequentially. In addition, Cowley et al. [2015] estimate that based on the duration of observed plasmoid field perturbations the mass loss due to plasmoids is at least an order of magnitude smaller than necessary. Given the typically several-hour interval between plasmoid releases it has been suggested that the overall plasma structure released by such events may be at least an order of magnitude longer than the few tens of R_S lengths inferred from the magnetic data direct.

Thomsen et al. [2015b] examined a high-latitude dawnside Cassini pass from the low-density lobe region into the higher-density closed field-line region. They inferred a stripping of plasma from the outer region of closed magnetic flux tubes as those tubes cross the night side magnetosphere from dusk to dawn, attributable to Vasyliunas-cycle reconnection, together with an interval (or region) of Dungey-cycle reconnection at the high-latitude boundary between open and closed field lines.

On the other hand, Thomsen et al. [2015a] examined a deep-tail near-equatorial Cassini pass near 37 R_S near midnight LT. They found a prolonged period (~5 hours) of planet-ward plasma-sheet flow attributable to an even more prolonged period of magnetotail compression due to the passage of a recurrent solar-wind structure containing enhanced dynamic pressure. They conclude that Dungey-cycle reconnection takes precedence over Vasyliunas-cycle reconnection when the solar-wind pressure is high.

In addition, numerous reconnection-related events during the main Cassini tail exploration interval in 2006, namely planetward-travelling dipolarizations and tailward-travelling plasmoid structures, which were found to be related in timing to both the pulsing of the SKR emissions and the magnetic PPO phase [Jackman et al. 2016, 2009a]. Specifically, the events were found to be preferentially initiated during intervals when the PPO perturbations stretch the field lines radially outward from the planet and thin the plasma sheet leading to instability (see entitled Time varying modulation of SKR and associated PPO signals), especially when the two PPO systems act in this manner in concert, i.e., when they are near antiphase. Ongoing work is presently investigating dipolarization events and auroral storms during the sequence of proximal orbits observed just prior to end of mission.

Plasma composition, distribution, sources, and sinks

- **M_AO2:** Determine current systems, composition, sources, and sinks of magnetosphere charged particles.

Understanding the plasma composition, distribution, sources and sink in Saturn's magnetosphere begins with understanding the neutral gas sources. Prior to the arrival of Cassini in the Saturn system, Voyager measurements seemed to indicate that Titan was the main sources of the neutral gas in the system and therefore the main sources of plasma. However, with the discovery of the activity of Enceladus and better mass resolved measurements of the neutral and the plasma composition it became clear that Enceladus, the other icy satellites and the rings are the major source of distributed mass in the Saturn system.

Our understanding of the neutral gas distribution comes from measurements made by the INMS instrument. In 2008, the INMS investigation made in situ measurements of neutral species near Saturn's equatorial plane within 0.5 R_S of the orbit of Enceladus. After removing the large background and modeling to interpret instrumental effects, the data provide constraints on the neutral distribution and composition. These data show an azimuthal asymmetry in the neutral densities and provide measurements used to compare to simulations of neutral H_2O emitted from Enceladus (Figure MAPS-26). Far from Enceladus, the neutral water densities, at a few times 10^3 molecules/cm^3, are near the detection limit of INMS. Near Enceladus, but outside of the plumes and north of the equatorial plane, the INMS detects particles within 5,000 km of Enceladus, with the density increasing to approximately 10^5 molecules/cm^3 at the equatorial plane.

INMS observes inner-magnetosphere neutrals with a mass of 28 u that have unexpectedly high densities, no apparent source, and no clear molecular identification. With densities as high as 30% of the neutral-water density, the candidate molecules, N_2 and CO, should be abundant in the Enceladus emissions, but multiple observational approaches show that neither molecule comprises more than 3% of the H_2O density.

Although RPWS cannot distinguish the species of ions in the magnetosphere, measurements of the electron density in the inner magnetosphere show that adjacent to the dense A-ring there is an electron density maximum at over 100 electrons/cm^3, with the high density region (> 10/cm^3)

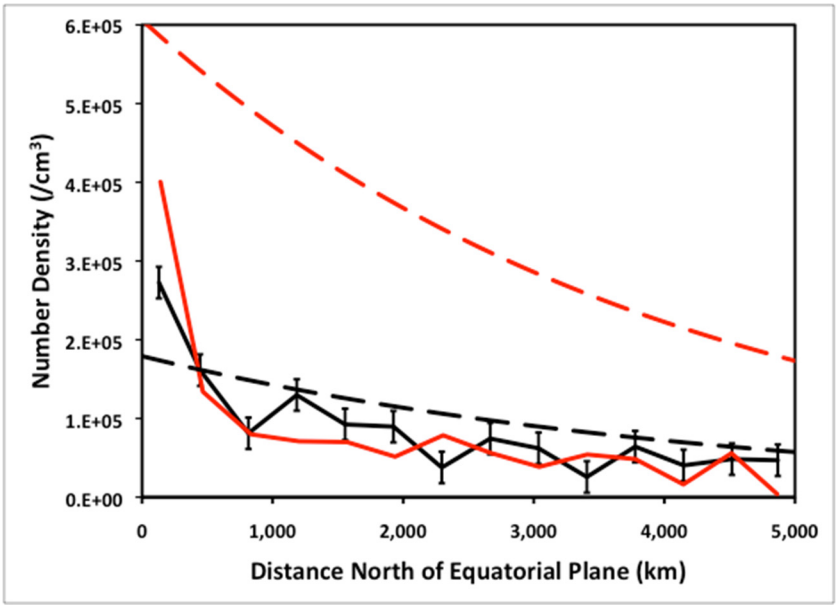

Figure MAPS-26. Neutral cloud density north of Enceladus, before close approach and outside of proximal influence of the south-pole plumes. The solid lines are the INMS data. The dashed lines are simulations using the charge-exchange model of the neutral cloud [Smith 2010]. The E5 simulation is based on the source rate derived from modeling the E5 plumes, and the E3 simulation is based on the source rate derived from modeling the E3 plumes. The E3 and E5 INMS densities are similar to each other and to the E3 simulation. E5 error bars (not shown to reduce clutter) are the same size as E3 error bars.

extending out to beyond L = 5. Persoon et al. [2015, 2009] found that this high density region is a plasma torus created by ionization and pick-up of new ions born in the Enceladus plume and a seasonal contribution from photo-ionized neutrals originating from the rings themselves. Thus, at equinox, the maximum in plasma density in this torus shifts radially outward to 4 R_S, but at solstice, the sun-facing rings become a neutral and plasma source shifting the torus plasma maximum closer to the A-ring—see Persoon et al. [2015] Figures 6 and 7. The peak density in the torus is about 10% of the Io torus at Jupiter and represents a dominant controlling element in the inner magnetosphere of Saturn [Gurnett et al. 2007]. These RPWS measurements in the inner magnetosphere have allowed Persoon et al. [2013, 2009] to develop an empirical plasma density model for the Saturnian system.

In addition to the direct measurements of the neutral distribution by the INMS instrument, one of the best pointers to the source of plasma in the magnetosphere is the composition. CAPS finds that the dominant magnetospheric ions are W^+, H^+, and H_2^+ [Young et al. 2005; Thomsen et al. 2010] were well explained by the later discovery of the prodigious output of water from the south-polar plumes of Enceladus. It was noted by Young et al. [2005] that the presence of H_3O^+ within the W^+ ion group indicated ion-molecule reactions occurring in a water-rich atmosphere, attributed to the E-ring and inner icy satellites, which ultimately was determined to be Enceladus. A careful separation of the individual components of the water-group species and determination of the radial distance dependence of their relative proportions [Wilson et al. 2015] provided vital constraints on models of the physics and chemistry of Enceladus-originating material.

INMS has extracted the water-group ion fractions from open source ion (OSI) measurements in Saturn's inner magnetosphere. These fractions are sensitive probes of the source, transport, and loss mechanisms that govern Saturn's magnetosphere. INMS samples only a small portion of velocity space at a time, which enables investigation of the distributions within velocity space but also limits sensitivity and complicates the separation of various factors that affect the relative ion fractions. Densities and count rates can be low, sometimes requiring the sum of 10,000 IPs for a two-sigma result. Figure MAPS-27 shows that ion fractions depend on distance from the orbit of Enceladus. Models show that the water-group fractions depend most strongly on the local fraction of neutrals. In contrast to CAPS results, INMS data show H_3O^+ fractions less than 0.1 except for measurements taken directly in the plumes. These fractions are now being used to calibration ion and neutral models of Saturn's magnetosphere.

Another example of source determination through composition is N^+ [Smith et al. 2008, 2007, 2005] (see Figure MAPS-28). Originally expected from Titan, the radial dependence of the N^+ phase space density and the energy of this population suggested instead an inner magnetosphere source, probably Enceladus, with both molecular nitrogen and ammonia emitted there. Surprisingly little N^+ has been found in the outer magnetosphere, indicating that nitrogen ions coming from Titan do not accumulate to significant densities.

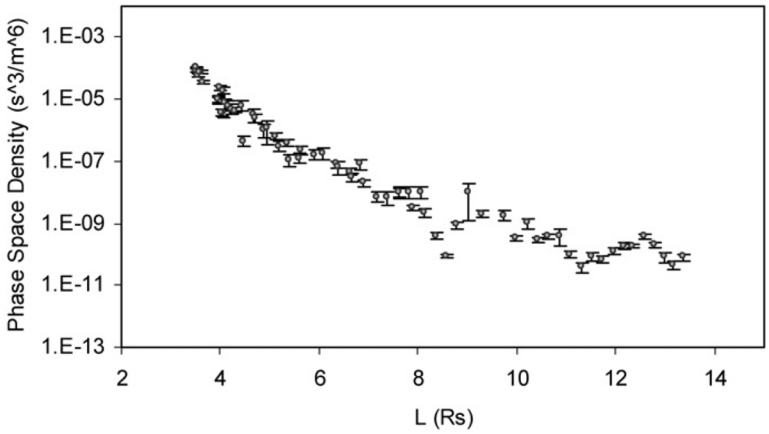

Figure MAPS-27. Nitrogen ion phase space density averaged over energy and angle, as a function of distance from Saturn. Clear decline with distance indicates a source in the inner region, inconsistent with a Titan source in the outer magnetosphere (L ~20). Figure from Smith et al. [2007].

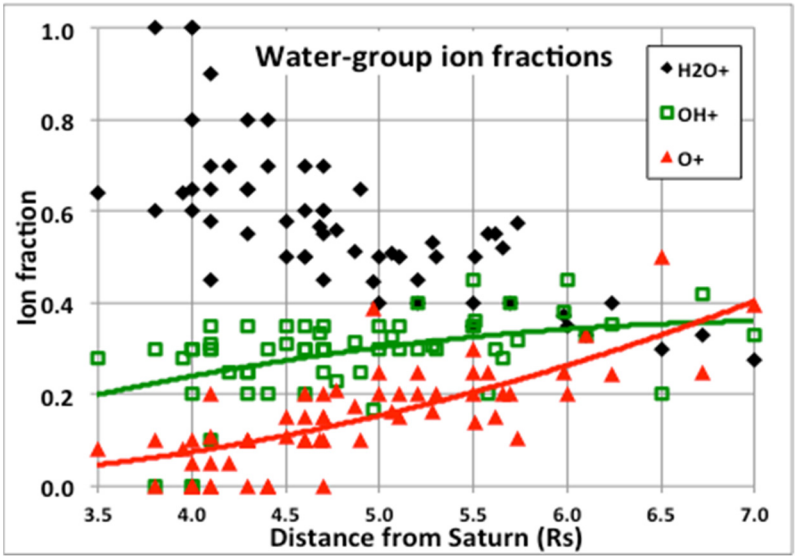

Figure MAPS-28. The fraction of water-group ions plotted as a function of distance from Saturn. INMS finds that the highest fraction of H_3O^+ is near 4 R_S, as expected, as that is the orbit of Enceladus, the source of the neutral water that becomes the plasma.

As indicated above, the dominant ion species seen throughout the magnetosphere are well explained by ionization of material from the water plumes of Enceladus. Cassini MAPS instruments observations of the plumes themselves are detailed in the section entitled Interaction of the Enceladus plume with the magnetosphere. In addition, MAPS instruments and CAPS in particular showed Enceladus to be the probable source of most of the N^+ observed in Saturn's inner magnetosphere, and CAPS measurements further helped reveal the existence of temporal variability in the plume source [Smith et al. 2010].

Before the arrival of Cassini in the Saturn system, Titan was regarded as the major source of neutrals and hence ions to the Saturn magnetosphere. The primary tracers of Titan's contributions to magnetospheric plasma have been N^+ and H_2^+. The finding of very little N^+ in the outer magnetosphere [Smith et al. 2005] indicated that Titan's contribution to the heavy-ion plasma is limited, whereas the fact that H_2^+ becomes comparable to H^+ and W^+ in the outer magnetosphere [Thomsen et al. 2010] indicates that Titan is an important source of lighter ions in that region. From observations during passage through Titan's wake region, the total mass loss rate from Titan is estimated to be a few × 10^{25} amu/q/sec (~0.8 kg/s) [Coates et al. 2012], compared to estimates of ~60–100 kg/s from Enceladus [Fleshman et al. 2013].

CAPS was turned off before the F-Ring and proximal orbits, so the only direct exploration of ring-associated plasma occurred during SOI, where a layer of O^+ and O_2^+ was discovered over the A-ring and B-ring [Young et al. 2005]. Subsequent analysis of the SOI data [Tokar et al. 2005] produced densities and temperatures of these two species (Figure MAPS-29). The ring atmosphere and ionosphere are likely produced by UV photo sputtering of the icy rings and subsequent photoionization of O_2^+. Significant O_2^+ was also detected outside the main rings, near the F-ring [Tokar et al. 2005], and analysis of the O_2^+ and W^+ profiles showed the seasonal dependence mentioned above, consistent with a ring source that depends on the solar illumination angle [Elrod et al. 2014, 2012]. The result indicates that the rings are an important source of O_2^+ and O^+ ions inside the orbit of Mimas.

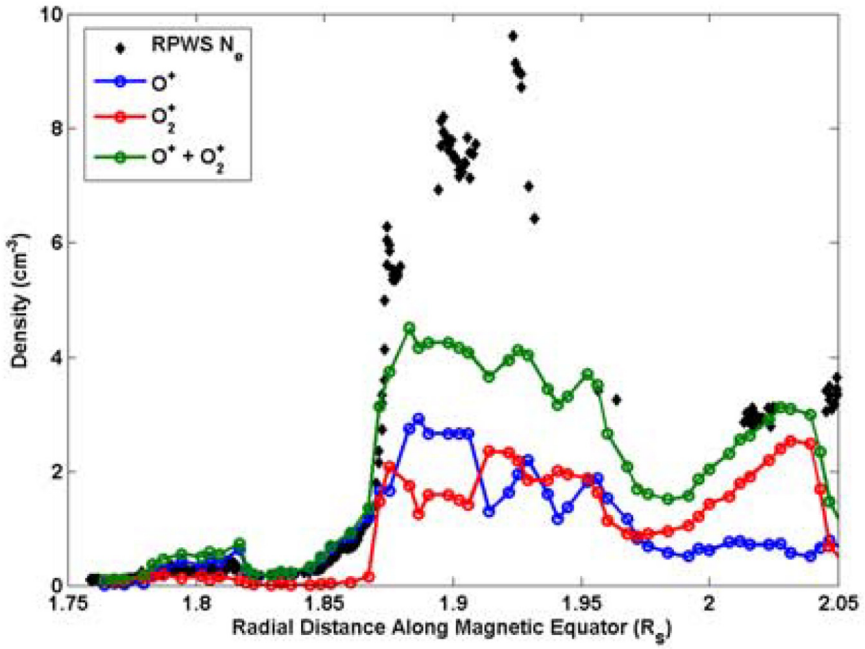

Figure MAPS-29. Radial dependence of O^+ and O_2^+ densities from CAPS observations over the main rings during SOI. Figure from Tokar et al. [2005].

CAPS has also detected O_2^+ in the vicinity of Dione [Tokar et al. 2012], and the observed radial dependence of the ratio O_2^+/W^+ suggested that there is a neutral O_2 source in the vicinity of Rhea [Martens et al. 2008]. Although the evidence for oxygen from Rhea is somewhat skimpy, CAPS has clearly detected non-gyrotropic outflowing CO_2^+ there, as well as another negatively-charged species, previously thought to be O^- but now found to be closer to mass 23 [Desai et al. 2018]. The latter is perhaps a carbon-based ion deriving from implanted exogenic compounds. Examination of the plasma conditions on flybys of Rhea [Wilson et al. 2010] revealed that the plasma flowing near it had no radial component on the Saturn-side of the moon, but had a radially outward component on the anti-Saturn-side. This is potentially due to an electric field enhancement near the moon, as observed in hybrid simulations.

Observation of probable plasma outflows from the ionosphere at the outer edge of the night side plasma sheet and extending into the lobes led to an estimate of some 10 s of kg/s lofted from the ionosphere (Figure MAPS-30) [Felici et al. 2016]. The observations occurred during a probable solar wind dynamic pressure enhancement, which may be important for producing significant outflow. It is not yet clear how often such outflow occurs, nor whether the outflow is actually captured into the closed region of the magnetosphere, rather than just escaping into the solar wind. Additionally, the field-aligned angular distributions of the suprathermal electrons within the plasma sheet/ring current region may indicate an ionospheric origin [Schippers et al. 2008], but no supporting evidence from the ion data has been reported.

With regard to dayside entry of solar wind plasma via reconnection or the K-H instability, there is considerable evidence that both processes take place. Magnetopause encounters frequently exhibit a low-latitude boundary layer (LLBL), in which magnetosheath plasma can be found just inside the magnetopause. From a survey of 354 crossings of the LLBL [Masters et al. 2011b, 2011c], the estimated thickness of the LLBL is only of the order of 1 Saturn radius, with no clear dawn-dusk asymmetry. Thus, while solar wind plasma can and does enter the magnetosphere on the dayside, it does not get very far in. This is supported by the fact that the ratio of m/q = 2 to H^+ ions in the outer magnetosphere is almost always significantly greater than the values of 1 to 10% typically seen within the solar wind [Thomsen et al. 2010], indicating that the plasma in the outer magnetosphere is dominantly of inner magnetospheric and/or Titan origin, with very little contribution from solar wind plasma there.

On the night side, plasma with solar wind-like composition has been observed at 37 R_S near local midnight [Thomsen et al. 2015a]. In that event, it appeared that prolonged high solar wind dynamic pressure may have caused erosion of the tail plasma sheet through ongoing Vasyliunas-type reconnection that then involved open lobe field lines and created a more Earth-like, Dungey-style outer plasma sheet dominantly of solar wind origin. Other evidence for Dungey-style reconnection following a Vasyliunas-style reconnection event is the post-plasmoid plasma sheet, for example, Jackman et al. [2011]. One other event that showed the possibility of a Dungey region, in which field lines were probably closed but the densities were quite low and there was very little O^+, was seen in a rapid high-latitude pass near dawn with clear evidence of Vasyliunas-type reconnection at latitudes just equatorward of the Dungey region [Thomsen et al. 2015b].

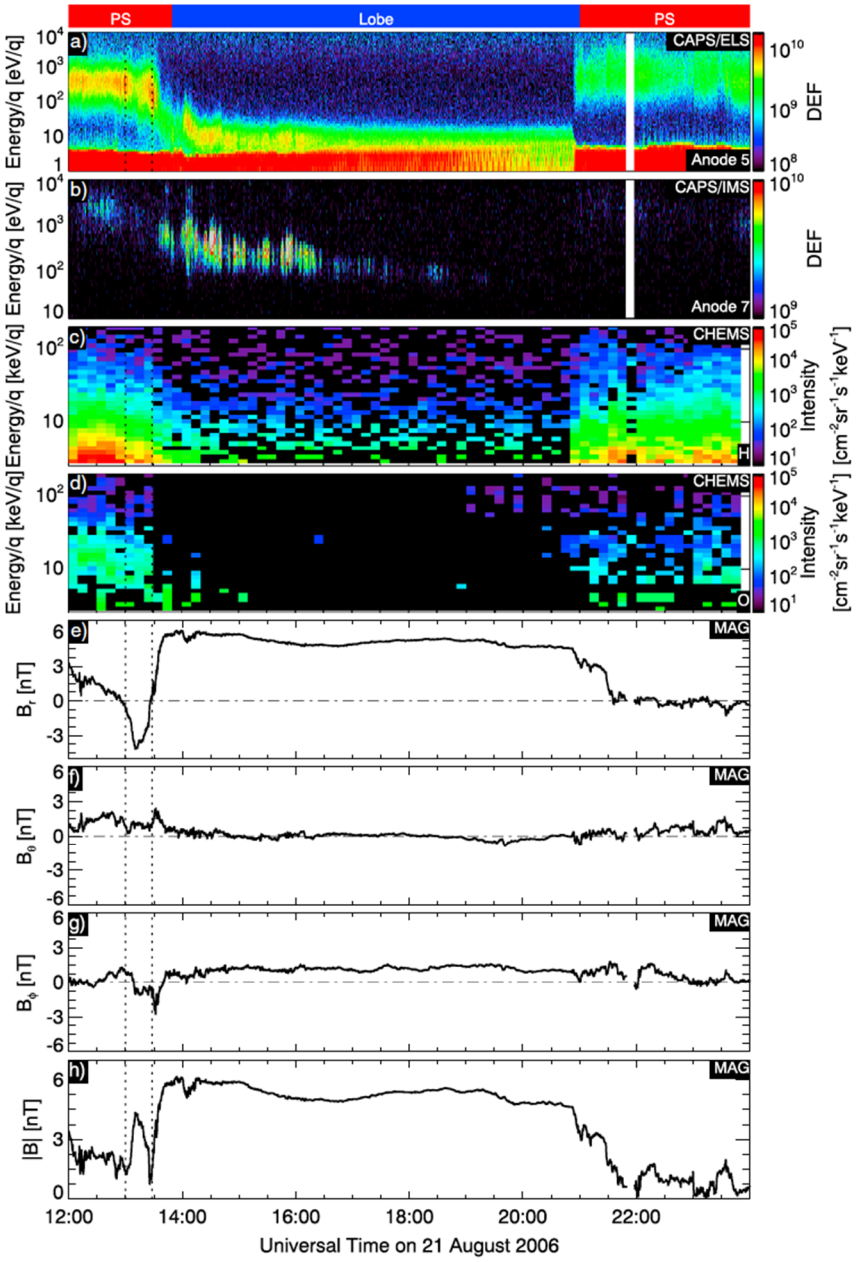

Figure MAPS-30. CAPS observations of an outflowing H^+ population from Saturn's ionosphere, seen in the lobe near the plasma sheet boundary at 36 RJ down tail. Figure from Felici et al. [2016].

CAPS measurements consistently show that plasma flow in the inner magnetosphere is dominantly in the corotation direction, with a magnitude near full corotation at low radial distances but tending toward a fraction (~60%) of full corotation by 10 R_S, see Sittler et al. [2005]; Wilson et al. [2017, 2009, 2008]; Thomsen et al. [2010]; Livi et al. [2014]. Radial velocities are much smaller and difficult to measure [Wilson et al. 2008].

There is widespread agreement that the primary mechanism for radial transport within the inner magnetosphere, which is needed to remove the continuously-produced plasma from Enceladus, is the process of centrifugally-driven flux-tube interchange. This process is described in detail in the section entitled Magnetospheric Structure and Convection, but CAPS data have been instrumental in the discovery [Young et al. 2005; Hill et al. 2005; Burch et al. 2005] and diagnosis [Andre et al. 2007; Chen and Hill 2008; Menietti et al. 2008; Rymer et al. 2009b; Chen et al. 2010; DeJong et al. 2010; Thomsen et al. 2014b; Paranicas et al. 2016] of the hot-plasma injection events that are the inward-moving half of the flux-tube interchange. There has been only one reported observation of the outward-moving cold plasma fingers that should form the other half of the process [Thomsen et al. 2015b]. Estimates of the inflow speeds within the injection channels range from a few km/s to ~260 km/s [Burch et al. 2005; Rymer et al. 2009b; Chen et al. 2010; Paranicas et al. 2016]. Composition suggests that the plasma inside the injection channels comes from the outer magnetosphere [Thomsen et al. 2014b].

One unanticipated discovery of the Cassini mission is the existence of an inner magnetospheric convection pattern superimposed on the dominant corotation pattern [Andriopoulou et al. 2014, 2012; Thomsen et al. 2012; Wilson et al. 2013]. The pattern consists of a general dusk-to-dawn drift, such that particles drift inward while they corotate from noon to midnight and outward as they return from midnight to noon (Figure MAPS-31). The result is an inward displacement at midnight compared to noon. A number of hypotheses regarding this convection have been advanced, but it remains an unsolved puzzle.

Beyond 10 R_S, CAPS measurements show consistently that the plasma flow overwhelmingly remains in the corotational direction at essentially all local times, indicating continued influence of connection to the corotating ionosphere, but the speed of the flow is well below full corotation, for example, McAndrews et al. [2009]; Thomsen et al. [2014a, 2013, 2010]; Wilson et al. [2017]. Beyond about 15–20 R_S, there is little evidence for inflowing plasma on the night side, where, particularly near the flanks, flows tend to have more of an outward component. From the lack of inward flow in the pre-dawn sector, it appears that dense plasma is not often able to make the turn and return sunward to the dayside magnetosphere at distances beyond ~15 R_S.

One of the principal ways in which plasma produced in the inner magnetosphere can be shed to the solar wind is through the process of magnetic reconnection in the tail. This is covered in greater detail in the section entitled Plasma loss into the magnetotail and Magnetotail configuration and dynamics flux tubes loaded with inner magnetospheric plasma are transported via interchange to the outer magnetosphere. Strong centrifugal forces distend them radially, especially near the equatorial plane. On the dayside, the pressure of the solar wind helps confine the distended flux tubes, but when they rotate into the night side, that confinement goes away, and centrifugal force can overwhelm the magnetic tension. The result is that the flux tubes pinch off (or reconnect), shedding a plasmoid that is no longer connected to the planet and which carries away the load of plasma the flux tube bore before reconnection occurred. This is the so-called Vasyliunas cycle. CAPS data have been instrumental in identifying the resulting down tail flows of the disconnected plasmoids [Hill et al. 2008; McAndrews et al. 2009; Jackman et al. 2015, 2014; Arridge et al. 2015;

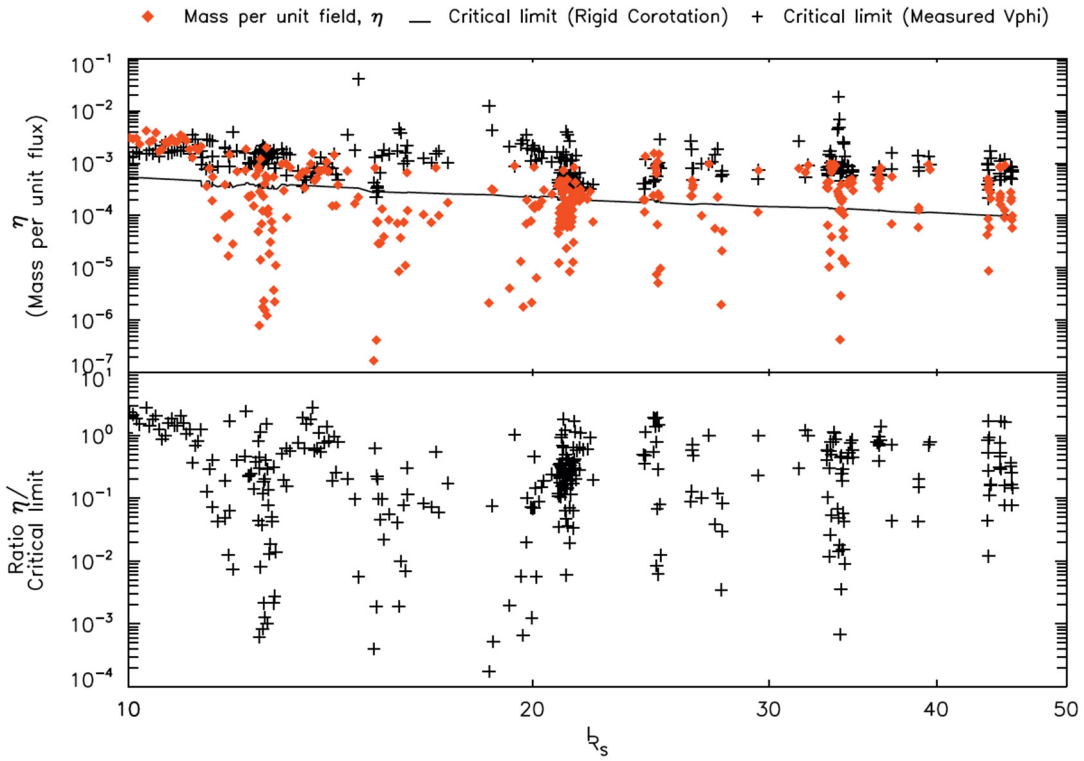

Figure MAPS-31. Comparison of nightside flux-tube content (red diamonds), estimated from CAPS/IMS data, with the theoretical critical limit above which the flux tube will pinch off and release a plasmoid downtail (black +). The observed flux-tube content is roughly bounded by the critical limit, suggesting that nightside reconnection and plasmoid formation keep the tail near marginal stability. Figure from McAndrews et al. [2009].

Smith et al. 2018a, 2018b, 2016]. There is ongoing debate as to whether plasmoids can carry away enough plasma to balance the new production in the inner magnetosphere.

Magnetic reconnection and nonlinear K-H waves at the magnetopause could both potentially allow magnetospheric mass loss. Evidence for the operation of both processes has been seen, for example, McAndrews et al. [2008]; Masters et al. [2012b, 2010, 2009]; Wilson et al. [2012]; Delamere et al. [2013]; Fuselier et al. [2014]; Jasinski et al. [2016]. However, to date the contribution of neither process to the overall mass balance problem has been quantitatively assessed. While energetic W^+ ions are commonly seen in the dayside magnetosheath, there is no evidence for thermal W^+ there [Sergis et al. 2013] or in the upstream region [Thomsen et al. 2007].

As mentioned in the section entitled Magnetotail configuration and dynamics, plasma flows along the night-side flanks of the magnetosphere tend to have an outward component, suggesting the likelihood that plasma is lost as a planetary wind down the flanks. An estimate of total mass loss from the tail (excluding plasmoids) [Thomsen et al. 2014a] is within the range of previous estimates of the total mass-loading rate from ionization of water gas from Enceladus.

Plasma kinetics and wave-particle interactions

- **M_AO3:** Investigate wave-particle interactions and dynamics of the dayside magnetosphere and the magnetotail of Saturn and their interactions with the solar wind, the satellites, and the rings.

Similar to the section entitled Seasonal and solar cycle variations, many of the kinetic and wave-particle interaction results of the MAPS instruments is outlined in other sections of this document. Specifically, effects related to the magnetospheric interaction with Titan are outlined in the section entitled Titan's upper atmosphere and its interaction with the surrounding plasma, results related to the magnetosphere can be found in the sections entitled Magnetotail configuration and dynamics, Magnetospheric structure and convection, and Plasma loss into the magnetotail, and many results can be additionally found in the section entitled Time varying modulation of SKR and associated PPO signals. In this section, we reiterate just a few of those results.

Several MAPS instruments found that Titan's interaction with the magnetosphere of Saturn features important plasma kinetic physics. The CAPS instruments, for example, discovered pick-up ions in the form of beams of CH_4^+ and N_2^+ that can be explained theoretically as the result of kinetic interactions between Titan and the magnetosphere [Hartle and Killen 2006; Hartle and Sittler 2007; Hartle et al. 2011]. It is no surprise that beam composition is consistent with the composition Titan's exosphere and atmosphere which is dominated by N_2 (98.4%) and CH_4 (1.4%) [cf. Waite et al. 2005].

Sittler et al. [2010] observed nearly field aligned outflows from the topside ionosphere during the T9 flyby and estimated the loss of methane ions due to pick-up from the exosphere at ~5×10^{22} mol/s [Sittler et al. 2009a]. The outflows serve ultimately as a sink from Titan's atmosphere of roughly ~5×10^{24} mol/s. Later, Coates et al. [2012] observed similar amounts of ionospheric outflows during the T9, T63, and T75 flybys. The theoretical cause of these outflows was originally discussed in Hartle et al. [2008]. It is produced by a field-aligned polarization electric field Epol ~$-1/n_e e \nabla_{||} P_e$ so that above the ionospheric density peak the outward acceleration is > 10 times the force of gravity for m/q ~28 amu/q ions. Sittler et al. [2010] found that the resulting ion outflow speeds were ~7 km/s with T_{ION} ~50,000° K. Therefore, both significant accelerations and heating must have occurred at altitudes above 5000 km. Later, using electron observations, Coates et al. [2015] measured the total potential drop of this electric field to be ~0.2 μV/m to heights ~15,000 km, which is sufficient to accelerate methane ions to the observed speeds ~5–6 km/s. Future 3-D hybrid simulations similar to that done by Lipatov et al. [2014, 2012, 2011] will be required to understand the heating, for example, due to wave-particle interactions, of ions to the observed high temperatures. In addition to the outflows, Sittler et al. [2010] also found evidence of Alfven waves during the T9 flyby with transverse velocity and magnetic field fluctuations that were anti-correlated with time and thus consistent with field-aligned propagation of these waves.

The T9 flyby was further studied by magnetometer team, which considered the ionosphere of Titan with its embedded magnetic field a study of Titan's nightside ionosphere was published by Cravens et al. [2009a]. T96, the first encounter presumably occurring in the supersonic solar wind, was also modelled using a hybrid kinetic code [Feyerabend et al. 2016]. An important kinetic process

in the interaction between a streaming magnetized plasma and Titan's atmosphere is the pick-up process, which has been observed to lead to the generation of often strong ion cyclotron waves in the cases of atmospheric interactions (Venus, Mars, Galilean satellites of Jupiter, Saturnian satellites, comets). In the case of Titan only two flybys T63 and T98 were associated with ion cyclotron waves are of relatively high amplitude, as a study of the MAG team shows [Russell et al. 2016].

The T9 flyby was modeled by Ma et al. [2007]. The wake region of Titan is an important component of Titan's interaction with its surrounding plasma. The Cassini spacecraft passed through the distant downstream region of Titan on December 26, 2005 (T9 flyby). In this study, we compared the observational data with numerical results using a 7-species Hall MHD Titan model. There is a good agreement between the observed and modeled parameters, given the uncertainties in plasma measurements and the approximations inherent in the Hall MHD model. Our simulation results also show that Hall MHD model results fit the observations better than the non-Hall MHD model for the flyby, consistent with the importance of kinetic effects in the Titan interaction. Based on the model results, we also identified the controlling physical processes in different plasma regions based on ion gyradius.

Beyond Titan, kinetic effects also play a role at other satellite interactions. The current system, detected by MAG in Rhea's plasma wake, results from the combination of: i) ion kinetic effects in a hot plasma; and ii) relative motion between the plasma and an inert plasma absorbing body like Rhea. As the wake is refilled with plasma in the downstream co-rotation flow [Roussos et al. 2008a], the plasma pressure gradient directed back toward Rhea results in diamagnetic current closure across the wake and perpendicular to the co-rotation flow. The pressure gradient exerts a force directed towards Rhea and mimics a real exosphere by generating a field-aligned Alfvénic current system, which extracts momentum from the co-rotating plasma outside the wake and transfers it to the wake. The Alfvén wings from the wake [Khurana et al. 2017] produce flow-directed magnetic field perturbations north and south of Rhea's equatorial plane, detected by MAG at the locations of R2 and R3 and also during two distant (102 R_H and 54 R_H away from Rhea on June 3, 2010, and October 17, 2010) [Khurana et al. 2012] downstream flybys.

Finally, we highlight the acceleration of particles that can occur at the bow shock of Saturn. In the presence of an obstacle, shock waves in a neutral gas efficiently dissipate the supersonic flow to subsonic through the action of collisions. In space plasmas however, shocks cannot rely on collisions to adequately dissipate the flow since the collisional mean free path is many orders of magnitude larger than the shock's width. Here, electromagnetic forces play a role to compensate for the additional dissipation required. Their roles are well understood for modest Mach numbers (e.g., 2–10), however this becomes more problematic at larger Mach numbers since additional kinetic processes, namely ion reflection and reformation, come into play to complete the dissipation process. Fortunately, such high Mach number phenomena were explored using the Cassini magnetometer dataset. Sulaiman et al. [2015] showed evidence for the timescales of ions reflection at a shock undergoing reformation to be 0.3 times the upstream gyro period. This was in excellent agreement with what had been theorized.

Radiation belts

- **M_AO3:** Investigate wave-particle interactions and dynamics of the dayside magnetosphere and the magnetotail of Saturn and their interactions with the solar wind, the satellites, and the rings.
- **MC1b:** Observe Saturn's magnetosphere over a solar cycle, from one solar minimum to the next.
  - Investigate what controls the interplay between the Dungey and Vasyliunas cycles?
  - Study the solar cycle dependence of the magnetospheric dynamics.
  - Investigate magnetospheric structure: variations in force balance.
  - Investigate non-static and other variant radiation belt features.
- **MN1b:** Conduct in situ studies of Saturn's ionosphere and inner radiation belt.
  - Investigate the effects on aurora of solar wind and seasons.
  - Are there UV satellite footprints on Saturn? (like at Jupiter)
  - Is there a seasonal variation in auroral activity?
  - Investigate solar wind–ionosphere–magnetosphere coupling through the auroral regions.
  - Investigate whether there are UV satellite footprints on Saturn and whether there are Region 1 currents connecting the ionosphere and the magnetopause.
  - Investigate the composition of Saturn's ionosphere.
  - Study whether there is a significant polar outflow from Saturn's high latitude ionosphere and whether the outflow exhibits seasonal or solar cycle variation.
  - Determine whether there is a radiation belt between the D-ring inner edge and the atmosphere.

Cassini MAPS instruments, especially the MIMI instrument, have made measurements of Saturn's magnetosphere that provide the most comprehensive description of the radiation belts of a planet besides Earth. More than 200 orbits crossed into the radiation belts, allowing us to understand and quantify their average structure, but also to monitor time variations, despite the single point measurements. The most detailed description of the radiation belts is given by Kollmann et al. [2011] where the L-shell, local time, and pitch angle (latitudinal) structure of the belts is given for electrons and protons of different energies. Heavier ions and their charge states are studied by DiFabio et al. [2011]; Dialynas et al. [2009]; Carbary et al. [2010c]; Christon et al. [2014a, 2014b, 2013]. The latter three studies provide the most detailed characterization of trace energetic ions and their charge states at an outer planet, showing how their origin may be connected to the planet's rings, the activity of Enceladus and seasonal or solar cycle effects.

Allen et al. [2018] conducted a mission long overview of internal to external sources of energetic plasma at Saturn. They found that solar wind-originating He^{++} ions are able to penetrate into the inner magnetosphere, although the fractional abundance in the inner magnetosphere is only about 0.001%.

Detailed investigations of the proton radiation belts in the MeV range have been published by Roussos et al. [2018a, 2016a, 2011]; Kollmann et al. [2017, 2015, 2013]; Armstrong et al. [2009]; Paranicas et al. [2010, 2008]; Buratti et al. [2018]. All studies establish how the protons belts are segmented by the icy moons of Saturn (Pandora, Prometheus, Janus, Epimetheus, Mimas, Enceladus, and Tethys) and the planet's main rings. They highlight interaction features with minor rings or ring arcs, such as those from Methone, Pallene, the G-ring, and the ringlets of the D-ring, most of which were unknown prior to Cassini. All studies established that the proton radiation belts inward of Tethys are disconnected from the short-term and large-scale changes that occur in the rest of the magnetosphere, and develop only over long time-scales due to the combined influence from variable particle transport effects and the solar cycle, with the former being much more important. The origin of those belts is attributed to CRAND, rather than to extreme solar wind transients, a possibility that was considered before Cassini. Transient extensions of these belts, outside Tethys, have been linked with certainty to the occurrence of Interplanetary Coronal Mass Ejections (CMEs) in the vicinity of Saturn [Roussos et al. 2008b, 2018c], one of the first direct demonstrations of space weather at an outer planet with in situ data.

The electron radiation belts in the MeV range have been studied in a series of papers by Roussos et al. [2018b, 2016a, 2014, 2006]; Paranicas et al. [2014, 2012, 2010]; Mauk et al. [2010]; Buratti [2019]. They are much more variable and longitudinally asymmetric than the corresponding proton belts, but on average they tend to increase monotonically in intensity inward towards the main rings at which point electrons get instantly absorbed. They evolve in time scales of weeks (as opposed to years for the protons) and are controlled by numerous factors, including the solar wind and internal magnetospheric dynamics. Interaction features of MeV electrons with material (e.g., scattering and energy loss in collisions with material) and moons have help to constrain radial transport rates in the magnetosphere and discover previously unknown ring arcs. The source population of the MeV electron belts is now believed to reside in the ring current (middle magnetosphere).

Between energies of tens of keV and few hundred keV, both electrons and ions are on average diminished significantly inward of the orbit of Tethys, due to interactions of these particles with the neutral cloud of Enceladus, the dust of the E-ring, or due to absorption by the moons [Paranicas et al. 2007; Kollmann et al. 2011; Carbary et al. 2009b; Kurth et al. 2006; Ye et al. 2016a]. The region between 5 and 9 R_S has been found to be dominated by transient population of interchange injection events, which have been analyzed in single case studies and statistically [Paranicas et al. 2010, 2008, 2007; Müeller et al. 2010; Mauk et al. 2005; Rymer et al. 2009b, 2008, 2007]. The results have been used to constrain the plasma corotation speed in the inner magnetosphere, the inward radial transport velocities of plasma, and assess the importance of interchange for energetic particle transport and acceleration with respect to other processes like diffusion. The inner magnetosphere is also dominated by energetic electron microsignatures (gaps

in the electron fluxes caused by electron absorption by Saturn's moons), which have been used to define the convective flows in the inner magnetosphere (a noon-to-midnight electric field) and radial diffusion rates [Paranicas et al. 2005; Roussos et al. 2018b, 2013, 2008a, 2007; Andriopoulou et al. 2014, 2012; Thomsen et al. 2012]. Statistically significant results on the angular distributions and energy spectra of electrons have been described for the first time in Carbary et al. [2011a, 2011b] and Clark et al. [2014].

In April 2017, the proximal orbits began, also called the mission Grand Finale. This enabled a comprehensive study of the proton radiation belt trapped approximately between the F-ring and A-ring. MIMI also found a previously unknown partial, transient electron belt within the F-ring, partial because it is only observed outbound at local noon, transient because it is very variable. These results are compiled in Buratti et al. [2019].

The LEMMS instrument discovered a previously unknown radiation belt collocated with the D-ring and extending up to the dense atmosphere of Saturn. This belt was predicted earlier [Kollmann et al. 2015], but its properties were unknown. It was found that the belt is dominated by protons up to the GeV range, which is the first time that such high energies were directly observed at any of the giant planets. Their pitch angle distribution is very steep, likely due to a strong interaction with Saturn's atmosphere. The suggested source is CRAND. There is no evidence for the presence of energetic electrons or ions heavier than protons. These results are compiled in Roussos et al. [2018c].

During SOI, Cassini remotely detected protons at tens of keV from low (atmospheric) altitudes [Krimigis et al. 2005]. The proximal orbits revealed that this was a huge coincidence since similar observations were only found once during the proximal orbits [Roussos and Kollmann et al. 2018], suggesting this this ion population is transient. Since the ions derive from ENAs produced in the magnetosphere, their intensity likely depends on the conditions in the magnetosphere. Because these ions were not observed in situ, they must be located at altitudes below 3800 km.

Saturn Science

High-order magnetic moments of Saturn

- **M_AO1:** Determine the configuration of the nearly axially symmetric magnetic field and its relation to the modulation of SKR.
- **MN1c:** Investigate magnetospheric periodicities, their coupling to the ionosphere, and how the SKR periods are imposed from close to the planet (3–5 R_S) out to the deep tail.
  - Determine what controls the SKR periods and whether there is a solar cycle and/or seasonal variation.
  - Investigate the coupling mechanism between the SKR periods and the internal rotation rate.

- Study whether the ionosphere and/or thermosphere is differentially rotating.
- Determine which hemispherical SKR period dominates other periodicities in the magnetosphere and whether this varies with time.

Numerous planetary magnetic field models have been developed over the time of the Cassini orbital mission at Saturn beginning with SOI [Dougherty et al. 2005]. Burton [2009] derived a model of Saturn's internal planetary magnetic field based on data obtained from the first three years of the mission, from July 1, 2004–July 1, 2007. Due to the uncertainty in the rotation rate, the model was constrained to be axisymmetric. In that analysis, one-minute averages of the vector magnetic field data obtained by the fluxgate magnetometer from all orbits within 10 R_S (1 R_S = 60,268 km). Data from 45 orbits were used in that study. The contribution of the eastward flowing ring current is known to be significantly close to the planet. Its contribution was modeled using the analytical expression derived by Giampieri and Dougherty [2004] based on the simple axisymmetric equatorial current sheet centered on the planet's equator, first described by Connerney et al. [1981]. The ring current magnetic field was modeled separately for the inbound and outbound legs of each orbit because the current sheet structure and characteristics are known to vary with local time [Arridge et al. 2008b] and temporal variations in the solar wind and magnetosphere are likely to occur over time scales corresponding to that of a periapsis pass (several days). The ring current field was modeled and removed from the data and standard generalized inversion techniques were used to model the magnetic field presumed to originate in Saturn's interior.

The contribution of the eastward flowing ring current is known to be significantly close to the planet.

The internal field model derived in that study was found to be quite consistent with previous models. An axisymmetric octupolar (degree 3) model was found to fit the data adequately based on an examination of the root-mean-square misfit or residual for each orbit. The spherical harmonic coefficients derived were g10 = 21,162, g20 = 1,514, g30 = 2,283. (Units are nano-Teslas (nT) and are based on a planetary radius of 60,268 km.) Saturn's magnetic was found to be offset northward by 0.036 Saturn radii, consistent with earlier Pioneer-11 and Voyager models. Reanalysis and comparison with data obtained by Pioneer-11 and Voyager-1 and Voyager-2 showed little evidence for secular variation in the field in the almost thirty years since those data were obtained.

A subsequent study [Burton et al. 2010] used data from the entire Cassini prime mission (through July 2008) and a methodology that differed in significant ways from the earlier modeling approach [Burton et al. 2009]. Only data obtained at radial distances closer than the L-shell of Enceladus (dipole L-value of 3.8) were used to derive the model. Measurements obtained by all Cassini fields and particles instruments had demonstrated that the structure and dynamics of Saturn's inner magnetosphere are governed by plasma created at Enceladus [Kivelson 2006]. The observed field at radial distances outside the orbit of Enceladus is modified by processes in the inner magnetosphere and does not necessarily reflect the magnetic field generated in Saturn's interior.

The approach to modeling the external ring current field also differed from the earlier modeling approach. As time went on our understanding of Saturn's magnetodisc had evolved and a simple symmetric ring current centered on the equator was no longer thought to an accurately representation. Instead the current sheet was found to be displaced from Saturn's rotational equator and to assume the shape of a bowl or basin, referred to as a magnetodisc [Arridge et al. 2008a]. Instead of modeling the external field as an oversimplified axisymmetric ring current as in Burton [2009], the internal plus external field was modeled using the standard spherical harmonic formulation and a single set of spherical harmonic coefficients was obtained that describes the internal and external field in a least squares sense. Accordingly, the axisymmetric model coefficients differ somewhat from the previous model.

In Burton [2010] an attempt was made to determine the planetary rotation rate by deriving a number of non-axisymmetric magnetic field models for a plausible range of planetary rotation periods and assessing the power in the non-axisymmetric components of the field and the root-mean-square misfit between the model and the data. The methodology is as follows. A presumed planetary rotation period was varied in 1 second increments from 10 hours 28 minutes to 10 hours 40 minutes and a pseudo-longitude calculated for each measured data point. A degree 3, non-axisymmetric magnetic field model was derived and the power in the non-axial magnetic field and the misfit were calculated. The underlying premise is that the planetary rotation period could be determined based on a peak in the non-axial power and minimum in the misfit. Although no such peak was identified unambiguously, the analysis did provide an upper limit on the extent of the dipole tilt. Based on the distribution of the non-axial spherical harmonic model coefficients for the range of rotation rates, a mean value for the dipole tilt was determined to be 0.03 degrees. The upper limit of all tilt angles was found to be 0.1 degrees.

The magnetometer team have developed the state-of-the-art internal magnetic field model for Saturn using Cassini magnetometer measurements prior to the Grand Finale, which placed the most stringent constraint to date on the tilt and secular variation of Saturn's intrinsic magnetic field [Cao et al. 2011]. The tilt of Saturn's dipole must be smaller than 0.06 degrees from the spin-axis of Saturn, and the time variation of Saturn's intrinsic magnetic field must be an order of magnitude slower than that of the Earth's [Cao et al. 2011]. These results are very challenging for dynamo theory, as Cowling's theorem excludes the possibility of a purely axisymmetric magnetic field being maintained by dynamo action.

The magnetometer team have also derived degree 4 and degree 5 internal magnetic moments for Saturn, albeit with relatively large uncertainties, from re-analyzing the Cassini SOI magnetometer measurements [Cao et al. 2012]. Based on these observational findings, we worked out the implications on helium rain inside Saturn [Cao et al. 2012, 2011]. These also provided the framework for our current analysis of the magnetometer measurements from the Cassini Grand Finale.

The latest Cassini Grand Finale gravity measurements indicate that the ~100 m/s zonal flows observed at the cloud deck of Saturn extend almost ten thousand kilometers into the planetary interior. Given that the electrical conductivity at such depth are high enough for significant MHD

effects, zonal flow magnetic field interaction in the semi-conducting region of Saturn is now a central issue in understanding the interior dynamics. On the theoretical side, we have developed a mean-field model for zonal flow magnetic field interaction in the semi-conducting region of Saturn [Cao and Stevenson 2017]. In this work, we proposed that the interaction between zonal flow and magnetic field in the semi-conduction region of Saturn would generate small-scale axisymmetric magnetic field that are spatially correlated with zonal flows [Cao and Stevenson 2017]. The amplitude of the wind-induced magnetic perturbations would depend on the amplitude of the deep differential rotation as well as the amplitude of the small-scale deep convective flow. Thus, measuring/constraining wind-induced magnetic perturbations along the Cassini Grand Finale orbits would place important constraints on the properties (profile and amplitude) of deep differential rotation and convective flow in the semi-conducting region of Saturn.

With magnetic field measurements at unprecedented proximity to Saturn by Cassini Grand Finale [Dougherty et al. 2018], we are working on deriving: i) non-axisymmetric internal magnetic moments of Saturn from Cassini Grand Finale magnetometer measurements, which can tell us about the deep interior rotation rate of Saturn and/or helium rainout and stable stratification inside Saturn; ii) small-scale axisymmetric magnetic features (e.g., high-degree axisymmetric internal magnetic moments) which can be used to constrain deep differential rotation inside Saturn; and iii) time variations in the internal magnetic fields, which would reveal characteristic time scale in Saturn's internal magnetic field and deep interior dynamics. These expected results would constitute the observational facts about the internal magnetic fields of Saturn for many years to come, which would further serve as tests for theories about giant planet interiors and have profound implications about giant planets outside the solar system.

Time varying modulation of SKR and associated PPO signals

- **M_AO1:** Determine the configuration of the nearly axially symmetric magnetic field and its relation to the modulation of SKR.
- **MN1c:** Investigate magnetospheric periodicities, their coupling to the ionosphere, and how the SKR periods are imposed from close to the planet (3–5 R_S) out to the deep tail.
  - Determine what controls the SKR periods and whether there is a solar cycle and/or seasonal variation.
  - Investigate the coupling mechanism between the SKR periods and the internal rotation rate.
  - Study whether the ionosphere and/or thermosphere is differentially rotating.
  - Determine which hemispherical SKR period dominates other periodicities in the magnetosphere and whether this varies with time.

Saturn's radio emissions started to be observed by Cassini/RPWS over the 10–1000 kHz range from distances of a few astronomical units. From late 2002 to early 2003, they were embedded in Jovian radio emissions and solar radio bursts. Their signal-to-noise ratio increasing with decreasing distance to Saturn, they became the dominant emission for the mid-2003 to mid-2004 preceding Saturn's orbit insertion. The most important and the most intense radio component is the SKR produced in the auroral regions. Several reviews of SKR properties have accompanied the Cassini mission [Kurth et al. 2009; Badman et al. 2015], the most recent one summarizing our current knowledge before Cassini Grand Finale [Lamy 2017].

The most important and the most intense radio component is the SKR produced in the auroral regions.

There are two important features of the SKR signal that we highlight here: 1) the SKR spectrum appears to be most intense when observed from the dawn-side at mid-latitude [Lamy et al. 2008; Kimura et al. 2013]. Southern SKR was predominant up to 2010-mid 2011 (slightly after the equinox of 2009), while the northern SKR was predominant after, consistent with a seasonal control of field-aligned currents driving auroral emissions by solar illumination of Saturn's ionosphere; and 2) the important feature of the SKR is that at the timescales of 11 hours (Saturn's rotation period), the emission is strongly rotationally modulated [Kurth et al. 2016, 2005; Clarke et al. 2005; Crary et al. 2005; Jackman et al. 2010, 2009a, 2005; Badman et al. 2016, 2008; Nichols et al. 2009; Lamy et al. 2013; Reed et al. 2018].

The remaining comments in this section concentrate on the modulation of the SKR.

Until the cruise phase of Cassini, the modulation of the SKR signal was taken to mark the rotation rate of the core of Saturn. Similar radio signals at Jupiter are clearly indicative of the rotation of the magnetic core of planet and therefore a similar interpretation was made for Saturn. Such magnetic rotation should theoretically be stable for planets as large as Jupiter and Saturn on a timescale not measurable by Cassini. However, the first SKR periodicity measured by RPWS witnessed a value differing by 1% to the SKR period identified from Voyager/PRA observations 25 years earlier [Gurnett et al. 2005]. Such a large variation implies that the SKR period does not probe the internal rotation rate. The measured SKR period was then found to display weak variations associated with those of solar wind speed [Cecconi and Zarka 2005; Zarka et al. 2007].

The major discovery brought by RPWS was the identification of two SKR periods [Kurth et al. 2008] corresponding to the two Kronian hemispheres, differing by ~1%. These periods were found to both vary with time in anti-correlation over yearly timescales and crossed closely after equinox, a trend which was interpreted as a seasonal driving of solar illumination [Gurnett et al. 2011a, 2010b, 2009; Lamy 2011], for example see Figure MAPS-32. These dual periods were later noticed in NB emissions and auroral hiss as well [Gurnett et al. 2010b; Ye et al. 2017, 2010] and more generally observed in numerous magnetospheric observables including magnetic oscillations, ENA emissions, aurorae [Mitchell et al. 2009b; Carbary et al. 2011a, 2010a; Nichols et al. 2010; Andrews et al. 2011, 2010a; Provan et al. 2011; Badman et al. 2012a, 2012b]. It is now accepted that these

dual rotational modulations all originate from two rotating hemispheric systems of field-aligned currents, whose origin may be atmospheric vortices [Jia et al. 2012].

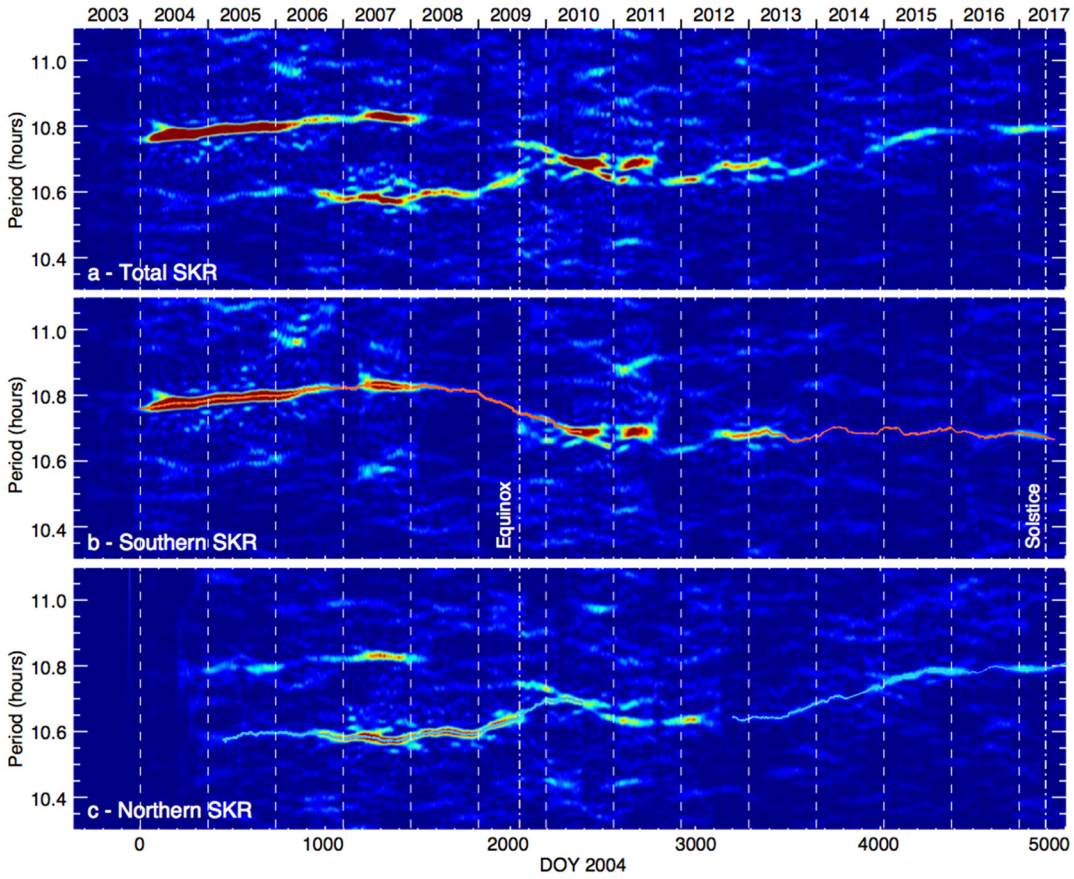

Figure MAPS-32. Lomb-Scargle periodograms of *Panel a*: total, *Panel b*: southern and *Panel c*: northern SKR flux density integrated over 100–500 kHz as a function of period and time from 2003-001 to 2017-258, extending of Lamy [2011] Figure 1. Southern and northern SKR were originally identified as LH and RH (X-mode) emission, excluding scarce intervals displaying ambiguous polarization measurements. The latter intervals were noticed to be more frequent at close distances and high latitudes which prevailed in the past two years. To improve the signal-to-noise ratio of *Panel b* and *Panel c*, southern and northern SKR were therefore identified as the total SKR signal observed beyond 10° latitude after days 2016-001 and 2016-180, respectively. Solid red and blue lines plot the southern and northern SKR periods derived by [Lamy 2011] from day 2004-001 to 2010-193, [Provan et al. 2016] from day 2012-278 to 2015-365 and tracked here from day 2016-001 to 2017-258. The latter will serve to build southern and northern SKR phases covering most of the Cassini mission.

This dual periodicity is not always detected, however, which may be a consequence of the observer location and/or its actual disappearance [Carbary 2016, 2014]. Single and dual periodicities were also observed in ENA fluxes detected by INCA [Carbary et al. 2014, 2008a; Carbary and Mitchell 2017]. INCA's global view of these periodicities revealed a local time dependence, namely, that one period might be detected at one local time but absent at another [Carbary et al. 2014]. Finally, the energetic electrons apparently have the same period (~10.8 h)

during the summer season when either the north or the South Pole tilts with respect to the direction to the Sun [Carbary et al. 2017]. This discovery, made possible by Cassini's solstice-to-solstice extension, has strong implications for the solar driving of these planetary periodicities. A complete review of Saturn's magnetospheric periodicities, as of 2013, appeared in Reviews of Geophysics [Carbary and Mitchell 2013], and should be consulted for the overall context within which particle periodicities can be placed.

The post-equinox period displayed a confused situation with poorly determined radio and magnetospheric periods. Over 2010–2012, they remained close to each other at locked phases, suggesting retro-interaction between both currents systems [Garnier et al. 2014], while sudden jumps of periods were tentatively attributed to Saturn's great white spot activity [Fischer et al. 2014] or to variable solar wind conditions [Provan et al. 2015]. Both periods eventually merged between mid-2013 and mid-2014 before crossing and diverging from each other after mid-2014 up to September 2017 [Provan et al. 2016; Ye et al. 2017, 2016b; Lamy 2017].

With the discovery that the SKR periodicity was not constant, the search for understanding began by all the MAPS instruments. Cassini observations have demonstrated the near ubiquity of oscillations near the planetary rotation period in essentially all magnetospheric plasma, field, and wave data despite the close axisymmetry of the internal planetary magnetic field. Due to the ubiquitous presence of these oscillations over most of the magnetosphere they were given the terminology PPO. Studying the PPO, with the goal to understand by the SKR period variation and the influence of PPO's on the magnetosphere has been a significant part of the Cassini mission.

Initial work on the magnetic PPOs established their basic properties, first confirming the rotational nature of the oscillations via the Doppler effect of the azimuthal spacecraft motion [Cowley et al. 2006], and second showing that while the perturbation fields in the equatorial region are quasi-uniform in nature [Andrews et al. 2010a], rotating in the equatorial plane as indicated by the earlier flyby studies, the fields at high latitudes are instead quasi-dipolar in form [Provan et al. 2009], associated with a rotating transverse dipole. The dipole moment is not internally generated by the planet, however, but by an external current system coupling the ionosphere and magnetosphere (see the section entitled Magnetospheric structure and convection). The PPOs are thus associated with a second large-scale current system, and, due to their ubiquitous nature, have proved to be a major aspect of the Cassini Magnetic Field Investigation throughout the mission. In addition, their imprint is seen more widely in the entire Cassini magnetosphere data set. It was shown that the radial distance of the dayside magnetopause and bow shock are also significantly modulated by this phenomenon [Clarke et al. 2010a, 2010b, 2006].

In the plasma data, the periodicities are clearest in the plasma sheet region. The density varies by more than an order of magnitude, depending on the SLS3 longitude [Arridge et al. 2008c]. This variability is likely due to periodic up-and-down motion of the plasma sheet. The temporal and spatial variations in plasma and field parameters are well organized by the flapping of the plasma disk about a periodically varying position [Arridge et al. 2008a; Szego et al. 2013, 2012, 2011; Nemeth et al. 2016]. Asymmetries in Cassini's periodic plasma sheet crossings [Thomsen et al. 2017b] are consistent with predictions of plasma sheet rocking and thickness variation made both

by the global MHD models that incorporate the effects of hypothesized atmospheric vortices [Jia and Kivelson 2012] and by the closely-related dual rotating current systems inferred from magnetic field observations, for example, Cowley et al. [2017] and references therein.

In the inner to middle magnetosphere, evidence was found for a plasma cam, in which the plasma density varies roughly sinusoidally with SLS3 [Burch et al. 2009; Goldstein et al. 2016] (see Figure MAPS-33). Theoretical arguments suggest that an asymmetric ring-current pressure coupled to Saturn's ionosphere can initiate a rotating two-cell interchange potential that is long-lived and stable [Goldstein et al. 2014]. Outflow from the dense sector was suggested as the driver of recurrent tail reconnection and plasmoid production (see sections entitled Plasma Loss Into The Magnetotail, and Magnetotail Configuration and Dynamics) inferred from periodic magnetic field variations in the tail [Burch et al. 2009], but subsequent authors argued that the field variations were more consistent with simple wave-like motion or periodic rocking of the plasma sheet rather than plasmoid formation [Jackman et al. 2009b]. In the more recent forward-modeling dataset of

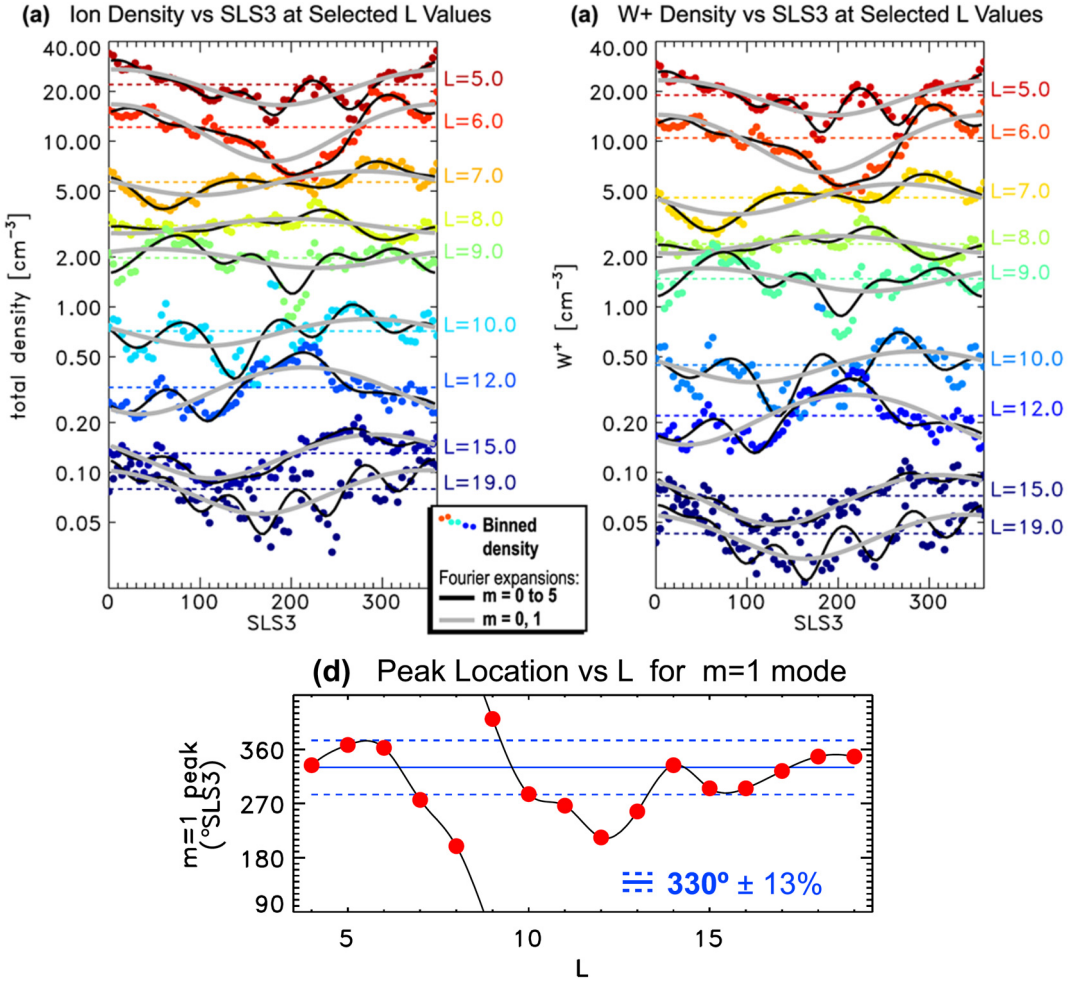

Figure MAPS-33. Evidence for the existence of a plasma cam, in which the density is generally highest in a particular SLS3 longitude sector. Figure from Goldstein et al. [2016].

ion densities [Wilson et al. 2017], the cam is not seen, so there remain questions about its existence and its consequences.

With the further realization, initially from SKR data, that two such oscillations are generally present with slightly different periods, one associated with the northern polar region and the other with the southern, it was shown that the phase jitter in the equatorial magnetic oscillations previously observed is due to the vector superposition of the two systems [Provan et al. 2011], while the polar oscillations were found to be pure northern and southern on the central polar field lines in the two hemispheres [Andrews et al. 2012]. Cassini data from the deeper tail passes in 2006 correspondingly showed that while the two tail lobes are modulated at their separate polar periods, mixed signals are again present within the plasma sheet that are associated with both north-south oscillations of the current layer together with significant modulations in its thickness [Provan et al. 2012; Szego et al. 2013; Nemeth et al. 2016, 2015]. A model of these PPO-related variations has been derived which provides a simple explanation of the sawtooth plasma sheet field variations observed during equinoctial conditions of near-equal northern and southern PPO amplitudes [Cowley et al. 2017; Thomsen et al. 2017a]. The model has further been successfully applied to the more northern-dominated conditions prevailing during northern spring [Cowley and Provan 2017].

With the additional realization that the two PPO periods slowly change with Saturn's seasons by ~ ±1% about ~ 10.7 h (i.e., ~ ±6 min), a long-term program of precise (~ ±10 s) measurement of the magnetic oscillation rotation period and phase has been carried out over the whole Cassini mission [Andrews et al. 2012, 2010b, 2008; Provan et al. 2018, 2016, 2014, 2013]. The results have subsequently been employed by many Cassini and HST teams as a framework to organize their data. The two PPO periods were found to be well-separated in late southern summer conditions at the beginning of the Cassini mission, ~10.6 h for the northern system and ~10.8 h for the dominant southern system, but then slowly converged with near-equal amplitudes to a near-common value ~10.7 h over a ~2 (Earth)-year interval centered near vernal equinox (August 2009) [Andrews et al. 2012]. There followed a ~3-year interval in early northern spring when the relative amplitudes changed abruptly at ~100–200-day intervals between southern and northern dominance and near-equal amplitudes [Provan et al. 2013], the southern period ~10.69 h remaining slightly longer than the northern ~10.65 h, before the periods of the two systems coalesced at ~10.70 h in antiphase during the first half of 2014 [Provan et al. 2016]. In mid-2014 the period of the then-dominant northern system began to increase towards ~10.8 h, similar to the southern system in southern summer, while the southern period remained near-fixed at ~10.7 h, thus leading to the first enduring reversal in PPO periods, northern longer than southern, during the Cassini era. The periods remained close to these values across northern summer solstice in May 2017 to the end of mission [Provan et al. 2018]. Possible physical origins of the post-equinox interval of abrupt changes have been discussed in terms of both atmospheric effects [Cowley and Provan 2013] and solar wind influences during the rising phase of the solar cycle [Provan et al. 2015], though clear causality remains to be demonstrated. An additional important theme of these studies has been the comparison of the magnetic field phases and periods with the related data derived independently by others from analysis of SKR modulations. Although some areas of contention

have been debated [Yates et al. 2015a, 2015b; Cowley and Provan 2016, 2015], the overall picture is one of good agreement [Andrews et al. 2012, 2011, 2010b, 2008; Provan et al. 2016, 2014].

The final proximal orbits have provided access to previously unexplored field lines crossing and inside Saturn's ring system. The behavior of the PPO oscillations on these field lines is presently under intense investigation.

Theoretical work [Southwood and Kivelson 2007] describes how a system of rotating field-aligned currents (cam currents) located on a magnetic shell in the range L = 12–15 would account for the periodicity observed in the magnetic field perturbations near the equator. Later it was shown that the interaction of the rotating cam currents would interact with the global magnetic structure of the magnetosphere to produce periodic variations of current intensity and account for the modulation of the power of SKR [Southwood and Kivelson 2009].

A series of papers elucidated how appropriately placed vertical flows in a rotating ionosphere drive field-aligned currents consistent with the cam current previously proposed. These rotating currents were shown to provide a quantitatively consistent description of all of the periodic dynamics reported in the system [Jia et al. 2012; Jia and Kivelson 2016; Kivelson and Jia 2014]. Theoretical work continues to best understand the origin of the two rotations rates [Southwood 2015, 2014, 2011; Southwood and Cowley 2014; Southwood and Chané 2016].

One important aspect of the PPO signal is to consider how reconnection fits into the bigger picture of global magnetospheric dynamics. Jackman et al. [2016] reported that, like so many other phenomena, tail reconnection at Saturn is organized by northern and southern magnetic phase. Events are specifically linked to current sheet thinning and outward displacement of field and plasma. Little evidence was found for visibility effects associated with the north-south motion of the plasma sheet.

One important aspect of the PPO signal is to consider how reconnection fits into the bigger picture of global magnetospheric dynamics.

Initial studies detected numerous reconnection-related events during the main Cassini tail exploration interval in 2006, namely planetward-travelling dipolarizations and tailward-travelling plasmoid structures, which were found to be related in timing to both the pulsing of the SKR emissions and the magnetic PPO phase [Jackman et al. 2016, 2009a]. Specifically, the events were found to be preferentially initiated during intervals when the PPO perturbations stretch the field lines radially outward from the planet and thin the plasma sheet leading to instability, especially when the two PPO systems act in this manner in concert, i.e., when they are near antiphase. Ongoing work is presently investigating dipolarization events and auroral storms during the sequence of proximal orbits observed just prior to end of mission.

The question of whether reconnection is linked to internal or external drivers is an important one, and one approach to exploring this is to examine the radio data which accompany the

magnetometer observations. Jackman et al. [2005b] explored concurrent IMF and SKR data from Cassini during SOI. They showed that the SKR intensified and extended to lower frequencies coincident with the arrival of a solar wind compression, while many other authors have also explored this strong link between the radio power (and frequency) and the nature of the solar wind.

Jackman et al. [2009a] explored the SKR in more detail, focusing on several case studies where reconnection had been observed in Saturn's magnetotail. In general, they found a good correlation between the timing of reconnection events and enhancements in the SKR emissions. A physical mechanism was put forward whereby reconnection increases the precipitation of energetic particles into the auroral zones, leads to the formation of a potential drop, and thus stimulates the motion of the SKR source region to higher altitudes along the field line (and hence lower frequencies of radio emission). These LFEs of the SKR were seen as strong proxies for dynamic solar wind compression and/or tail reconnection events.

Reed et al. [2018] attempted to automate the search for these LFEs in the SKR data and correlated 282 LFEs found during 2006 with a larger catalogue of reconnection events. LFEs were grouped into two categories, with short events of duration < 20 hours separated by a median waiting time of ~10 hours, and strongly correlated with the northern and southern SKR phases. Sixty percent of short LFEs have a reconnection event within the preceding six hours. The second category, long events, had duration > 20 hours, often lasting multiple planetary rotations and associated with increases in solar wind dynamic pressure.

Aurora and satellite footprints

- **MN1b:** Conduct in situ studies of Saturn's ionosphere and inner radiation belt.
  - Investigate the effects on aurora of solar wind and seasons.
  - Are there UV satellite footprints on Saturn? (like at Jupiter)
  - Is there a seasonal variation in auroral activity?
  - Investigate solar wind–ionosphere–magnetosphere coupling through the auroral regions.
  - Investigate whether there are UV satellite footprints on Saturn and whether there are Region 1 currents connecting the ionosphere and the magnetopause.
  - Investigate the composition of Saturn's ionosphere.
  - Study whether there is a significant polar outflow from Saturn's high latitude ionosphere and whether the outflow exhibits seasonal or solar cycle variation.
  - Determine whether there is a radiation belt between the D-ring inner edge and the atmosphere.

Cassini instruments have provided the first ever in situ measurements of the currents and particle populations that result in the Aurora and satellite footprints at Saturn. In addition to in situ measurements made by MAPS instruments, remote sensing images have been made by a range or Cassini instruments. This amazing set of Cassini data, together with a significant data from Earth-based observing platforms has resulted in a much more complete picture of the Kronian auroral processes. Fine structures of the aurora and nightside emissions have been revealed for the first time thanks to the observations acquired by the UVIS spectrograph on board Cassini. Spatial and dynamical characteristics of the complex pattern of auroral emissions at Saturn have been thoroughly described during the Cassini mission.

Previously observed with HST [Gérard et al. 2004; Grodent et al. 2005], the principal auroral component, so-called main emission, appeared through UVIS eyes as multiple substructures of various sizes. The dawn side of the main emission usually consists in a continuous narrow arc, rotating with the planet at approximately 70% of rigid corotation [Grodent et al. 2005]. This arc can get particularly bright during several hours while the emission rotates from midnight to noon, for example, Mitchell et al. [2009b]; Meredith et al. [2014]; Radioti et al. [2016]. Thanks to the combination between Cassini in situ measurements and auroral data, such a brightening has been associated with important magnetotail reconnection activity either induced by solar wind compression and closing magnetic flux [Cowley et al. 2005] or internally driven by stretching of the field lines in the nightside magnetosphere [Mitchell et al. 2009b; Radioti et al. 2016]. In both cases, the auroral intensification is produced by intense field-aligned currents on flux tubes moving from tail reconnection site to the dayside. Occasionally, these flux tubes could experience a blockage in the equatorial plane around noon local time, leading to the stagnation of the main emission dawn arc close to noon, as reported by Radioti et al. [2017a]. Furthermore, Yao et al. [2017c] surveyed Cassini-UVIS dataset, and revealed that transient auroral intensification near the noon local time is a systematic phenomenon, and proposed two potential mechanisms in driving such auroral phenomenon by analyzing simultaneous measurements from Cassini's magnetic field, plasma and auroral instruments.

In addition to the dawn arc, the main emission can exhibit isolated features of a few hundred kilometers wide which could be observed during the low-altitude orbits of Cassini. These individual spots have been tentatively interpreted as signatures of K-H vortices at the magnetopause [Grodent et al. 2011]. Alternatively, Meredith et al. [2013] argued that these spots might be produced by field-aligned currents of second harmonic ultra-low frequency (ULF) FLR waves propagating in Saturn's equatorial outer magnetosphere.

Furthermore, the main emission sometimes exhibits a localized brightening on the dayside which gradually gives birth to an extended arc-like structure rotating to the nightside with one extremity attached to the main emission while the other is moving towards the pole [Radioti et al. 2011; Badman et al. 2013]. These so-called bifurcations, together with an increase of the region threaded by open field lines (i.e., the polar cap), suggest that they are the signatures of dayside reconnection at the magnetopause, whereas the existence of magnetopause reconnection at Saturn was still subject of debate. Consecutive bifurcations and quasi-periodic brightening of an

individual bifurcation even suggest that such a dayside reconnection process can be pulsed [Radioti et al. 2013b, 2011; Mitchell et al. 2016].

Fixed in local time around noon, an auroral spot poleward of the main emission has been attributed to the auroral footprint of the cusp [Gérard et al. 2005, 2004; Palmaerts et al. 2016a; Kinrade et al. 2017] for which theoretical considerations connect it to high-latitude lobe reconnection [Bunce et al. 2005]. Thanks to extended UVIS observation time of Saturn's aurora, it has been shown that this polar cusp aurora can exhibit brightening with a periodicity of around one hour, indicative of a pulsed reconnection process [Palmaerts et al. 2016a]. In addition, Radioti et al. [2014] discovered a rare nightside auroral arc extending from the nightside main emission towards dayside, across the polar cap region. This polar arc is likely a tongue of closed flux tubes in the open field line region which appears during a period of enhanced tail reconnection combined with an absence of dayside reconnection.

Using the low-altitude UVIS observations during the Grand Finale phase of the Cassini mission, Radioti et al. [2017b] identified some auroral arcs which are azimuthally spread from high to low altitudes in the nightside sector. These arcs could be produced by plasma flows propagating from the outer tail magnetosphere toward the planet, akin to the terrestrial auroral streamers. Such plasma flows result from ballooning instability in the plasma sheet which has been shown to occur in Saturn's magnetosphere [Yao et al. 2017d].

Equatorward to the main auroral emission, two types of auroral structures can be encountered. The presence of a quasi-permanent partial ring of faint emissions mainly on the nightside sector has been established by Grodent et al. [2010]. These outer emissions are thought to be generated by an upward current layer carried by warm electrons detected by Cassini [Schippers et al. 2012]. Additionally, isolated transient auroral patches are occasionally observed along the equatorward edge of the dayside main emission. The combination of HST, in situ and remote Cassini observations, and simulations provided evidence that these spots behave as UV auroral signatures of energetic particle injections [Radioti et al. 2013a, 2009]. Furthermore, large-scale injections with strong corotation velocity gradients can give rise to spiral-shaped auroral features propagating from predawn to noon, as revealed by Radioti et al. [2015].

The combination of HST, in situ and remote Cassini observations, and simulations provided evidence that these spots behave as UV auroral signatures of energetic particle injections … .

During a coordinated auroral observing campaign on April 21–22, 2013, instruments onboard Cassini and the Hubble Space Telescope observed Saturn's northern and southern aurora while Cassini traversed Saturn's high latitude auroral field lines [Badman et al. 2016]. Signatures of upward and downward field-aligned currents were detected in the nightside magnetosphere, with the location of the upward current corresponded to the bright ultraviolet auroral arc seen in the auroral images, and the downward current region located poleward of the upward current in an

aurorally dark region. In the area poleward of the auroral oval, magnetic field and plasma fluctuations were identified with periods of ~20 and ~60 min. During April 11, the northern and southern auroral ovals were observed to rock in latitude in phase with the respective northern and southern planetary period oscillations. A solar wind compression impacted Saturn's magnetosphere at the start of April 22, 2013, identified by the intensification and extension to lower frequencies of the SKR. At this time a bulge appeared along the pre-dawn auroral oval, which appeared to have moved sunward when this region was next observed. The midnight sector aurora remained a narrow arc at this time. Subsequently, the post-midnight aurora broadened in latitude and contracted towards the pole. The motion in this sector was in the opposite direction to that expected from the planetary period oscillation. There was also an intensification of the auroral field-aligned currents. These observations are interpreted as the response to tail reconnection events instigated by solar wind compression, initially involving Vasyliunas-type reconnection of closed mass-loaded magnetotail field lines, and then proceeding onto open lobe field lines, causing the contraction of the polar cap region on the post-midnight sector.

During the same auroral campaign, Kurth et al. [2016] reports on the SKR measurements obtained during a Saturn auroral campaign carried out in the spring of 2013 which used multiple Earth-based observations, remote-sensing observations from Cassini, and in situ-observations from Cassini. Saturn kilometric radiation was remotely monitored nearly continuously providing a measure of the auroral activity and a means of understanding the temporal relationships between the sometimes widely spaced remote sensing observations of the auroral activity. While beaming characteristics of the radio emissions are known to prevent single spacecraft observations of this emission from being a perfect auroral activity indicator, a good correlation between the radio emission intensity and the level of UV auroral activity was observed, when both measurements are available, similar to what the previous studies had shown. Given the known influence of solar wind dynamics on both SKR intensity and auroral activity as discussed above, the SKR integrated power is also a proxy for solar wind activity. This study found that there is a good correlation between the 10 h averages of SKR power flux and the power estimated input to the aurora on the basis of the UV brightness, justifying the SKR as a simple proxy for auroral activity through the campaign. The SKR emissions also give evidence for a recurrent pattern of solar wind interaction with Saturn's magnetosphere, suggesting a two-sector structure and associated corotating interaction regions influencing the level of auroral activity on Saturn. But there are other SKR intensifications that may be due to internal processes.

Bunce et al. [2014] presented an unusual case in January 2009, where UVIS observes the entire northern UV auroral oval during a 2 h interval while Cassini traverses the magnetic flux tubes connecting to the auroral regions near 21 LT, sampling the related magnetic field, particle, and radio and plasma wave signatures. The motion of the auroral oval evident from the UVIS images was found to be consistent with the appropriate phase of the magnetosphere oscillations in the northern hemisphere, whereas previous interpretations have assumed a static current system. Concurrent observations of the auroral hiss (typically generated in regions of downward directed field-aligned current) support this revised interpretation of an oscillating current system.

Field-aligned current systems are at the heart of all aurora observed in the solar system. Large-scale field-aligned current systems which couple the magnetosphere to the planet's upper atmosphere, ultimately produce the auroral displays seen in, for example, UV images. As in other magnetized environments, field-aligned currents in Saturn's magnetosphere play a fundamental role in the transfer of momentum along field lines between the ionosphere, the magnetosphere, and (potentially) the solar wind. At their ends such currents close cross-field in association with j × B forces on the corresponding plasmas. Field-aligned currents further relate to the generation of bright discrete auroral forms at ionospheric heights, if current densities directed away from the planet exceed that which can be carried by the ambient precipitating magnetospheric electrons, at which point the latter are accelerated downward into the ionosphere by field-aligned voltages where they deposit their charge and energy. Initial theoretical expectations for Saturn related to meridional magnetosphere-ionosphere currents associated with the transfer of angular momentum from the planet's ionosphere to the net radially-outward transported equatorial plasma principally of Enceladus origin, i.e., the sub-corotation currents [Cowley et al. 2004], together with dawn–dusk asymmetries associated with the solar wind interaction [Jackman and Cowley 2006].

Observationally, field-aligned currents are detected and quantified via variations in the azimuthal magnetic field on high-latitude and relatively low-altitude passes across the planet's polar regions. The first such data were acquired by Cassini in 2006/2007, with simultaneous HST UV imagery on one pass confirming that Saturn's auroral oval indeed maps into a region of upward current requiring downward acceleration of the observed magnetospheric electrons [Bunce et al. 2008; Cowley et al. 2008]. An overall survey of these data showed that while their basic properties are consistent with theoretical expectations for subcorotation currents, with ~6 MA flowing down into the central polar ionosphere and the same return current flowing upward at lower latitudes in the auroral region, the currents are also modulated by the PPOs [Talboys et al. 2009a]. A much larger data set was then acquired in 2008 which allowed statistical studies to be undertaken [Talboys et al. 2011, 2009b]. It further allowed detailed exploration of the PPO dependence by comparing currents observed under conditions of differing PPO phase [Hunt et al. 2018b, 2015, 2014].

The principal PPO currents in a given hemisphere are found to be directed upward and downward on opposite sides of the planet's polar ionosphere and rotate around the pole at the PPO period of the corresponding hemisphere. They are also approximately co-located with the upward current region of the sub-corotation system, and of comparable strength, such that where the PPO current flows down, the total field-aligned current is reduced near to zero, while where it flows up the current is doubled, thus suggesting a dynamical connection. It is also found that the auroral region oscillates in latitude with amplitude ~1° in concert with these rotating modulations [Nichols et al. 2008; Provan et al. 2009; Hunt et al. 2014; Bunce et al. 2014]. A complementary multi-instrument study also established the typical locations of the boundary of open field lines in the two hemispheres at ~13° co-latitude in the north and ~16° in the south [Jinks et al. 2014], showing that the main PPO field-aligned currents flow just equatorward of this boundary on closed field lines. Correspondingly, inter-hemispheric coupling along closed magnetospheric field lines also occurs between the two PPO systems [Hunt et al. 2015; Provan et al. 2018]. Overall, the form of the PPO currents is consistent with driving by rotating twin-vortex flows in the two polar thermosphere/ionosphere [Hunt et al. 2014; Southwood and Cowley 2014].

Comparison between the 2008 data, obtained in the midnight sector, with the dawn-dayside data from 2006/2007 showed little difference, confounding expectations of observing long-term current asymmetries associated with the solar wind interaction [Hunt et al. 2016]. Highly unusual current distributions are observed in a small subset of passes, however, some of which have been associated with Saturn auroral storm solar wind compression events [Bunce et al. 2010]. Significant solar wind-related currents thus do flow in Saturn's magnetosphere at least intermittently. Indirect evidence of less dramatic solar wind effects have been obtained from HST studies of the dayside auroras (though not directly in field data), using Cassini as an upstream monitor of the IMF. Morphological auroral differences are found depending on the sense of the north-south component of the IMF, suggestive of dayside reconnection and related driving of flows and currents when the IMF points north [Meredith et al. 2014]. More generally, collaboration with colleagues at Moscow State University has resulted in the development of Saturn magnetospheric field models validated with Cassini data which incorporate ring/tail and magnetopause currents, and are also parameterized by the strength and direction of the IMF [Alexeev et al. 2006; Belenkaya et al. 2016, 2014, 2011, 2010, 2007, 2006]. These models have been used during intervals when Cassini was located in the solar wind measuring the impinging IMF to map auroral features observed by the HST along field lines into their magnetospheric source regions, namely the middle and outer ring current region typically at dawn, and to the vicinity of the open-closed field boundary for high-latitude emissions near noon.

While the 2006/2007 and 2008 high-latitude data sets both correspond to Saturn's late southern summer, a third interval of high-latitude data was obtained in 2012/2013 during northern spring [Bradley et al. 2018]. The PPO currents were found to be of similar form but somewhat weaker than in 2008, while the sub-corotation currents exhibited strong opposite seasonal asymmetries in the north and south Polar Regions, indicative of weak polar ionospheric conductivity in the winter polar cap. Investigation of the current signatures observed on the F-ring and proximal orbits spanning northern summer solstice at the end of the Cassini mission are currently ongoing [Hunt et al. 2018a].

Although Voyager radio data had previously demonstrated that SKR emissions are strongly positively correlated with solar wind dynamic pressure, the nature of the related magnetospheric dynamics remained unknown. This was partially revealed in early 2004 during Cassini approach to Saturn when an intensive HST campaign imaging Saturn's UV auroras was undertaken, with Cassini acting as upstream solar wind/IMF monitor. As expected during the declining phase of the solar cycle, the recurrent solar wind structure consisted of two corotating interaction regions (CIRs) per ~25-day solar rotation, exhibiting two few-day compression events of enhanced dynamic pressure, one major and one minor [Jackman et al. 2004]. The HST caught the impingement of the major compression region on Saturn's magnetosphere towards the end of the campaign, and observed a major increase in UV and SKR emissions with bright auroral forms extending throughout the dawn sector up to the planetary pole itself [Clarke et al. 2005; Bunce et al. 2006]. It was suggested that such auroral storms are caused by major bursts of compression-induced reconnection in Saturn's nightside tail, that inject hot plasma towards Saturn, which subsequently flows around the planet via dawn under the action of magnetosphere-ionosphere coupling [Cowley et al. 2005]. Estimates of the reconnection rate yielded associated voltages of at least several

hundred kV [Badman et al. 2005]. Monitoring of the interplanetary field prior to SOI showed that the same compression region would likely impinge on the system during the SOI fly-through of the magnetosphere [Jackman et al. 2005a, 2005b], and indeed did, with a corresponding magnetic dipolarization event, plasma energization, and enhanced SKR emissions being observed in the nightside magnetosphere on the outbound pass [Bunce et al. 2005]. Analysis of a larger number of compression events observed by Cassini acting as upstream IMF monitor during the approach phase, as well as outbound after SOI in late 2004, also showed characteristic enhancements in SKR, but with the regular pulsing at the PPO period generally being undisturbed in phase [Badman et al. 2008].

The passage of a moon through the magnetospheric plasmas of Jupiter, Saturn or the other giant planets is well known to create the potential for an auroral display at the footprint of the magnetic flux tube connecting the satellite and the planet's ionosphere. However, prior to Cassini all evidence of this process and of satellite footprints has been obtained at Jupiter. With the arrival of Cassini, the capability to perform coordinate in situ measurements yielded several new studies with the goal of observing the any such footprint if they existed. An initial study using a series of UV images of Saturn's aurora taken by the HST January 2004 and between February 2005 and January 2007 could not detect the faint auroral emission that would have been a signature of the Enceladus footprint [Wannawichian et al. 2008]. However, a follow-on study was able to report the detection of magnetic-field-aligned ion and electron beams (offset several moon radii downstream from Enceladus) with sufficient power to stimulate detectable aurora, and the subsequent discovery of Enceladus-associated aurora in a few per cent of the scans of the moon's footprint. The footprint varies in emission magnitude more than can plausibly be explained by changes in magnetospheric parameters, and as such is probably indicative of variable plume activity [Pryor et al. 2011].

Finally, using the spectra acquired by UVIS from 56 to 191 nm, it was possible to retrieve the characteristics of the energetic particles generating Saturn's aurora [Gustin et al. 2017, 2010, 2009]. Gustin et al. [2017] examined about 2000 FUV UVIS spectra to derive the mean energy of precipitating electrons for the different components of the aurora, using two different methods. The first one uses the absorption of the auroral emissions by hydrocarbons while the second one is based on the brightness ratio between the Lyman-α line and the total H_2 UV emission. Both methods give similar results with an average energy of the primary electrons ranging between 1 and 17 keV depending on the aurora component.

Composition of ionosphere and thermosphere

- **MN1b:** Conduct in situ studies of Saturn's ionosphere and inner radiation belt.
  - Investigate the effects on aurora of solar wind and seasons.
  - Are there UV satellite footprints on Saturn? (like at Jupiter)
  - Is there a seasonal variation in auroral activity?
  - Investigate solar wind–ionosphere–magnetosphere coupling through the auroral regions.

  - Investigate whether there are UV satellite footprints on Saturn and whether there are Region 1 currents connecting the ionosphere and the magnetopause.
  - Investigate the composition of Saturn's ionosphere.
  - Study whether there is a significant polar outflow from Saturn's high latitude ionosphere and whether the outflow exhibits seasonal or solar cycle variation.
  - Determine whether there is a radiation belt between the D-ring inner edge and the atmosphere.
- **MN2a:** Determine the coupling between Saturn's rings and ionosphere.
  - Study how field aligned currents are coupled to the rings and satellites.
  - Explore the dust dynamics in the proximity region.
  - Investigate the mid-plane of Saturn's D-ring.
  - Determine the grain composition in the proximity region.
  - Investigate the possible interaction of lightning with the inner magnetosphere and the rings.
  - Investigate Coupling Between E-ring and the Enceladus neutral and plasma tori.

Cassini was able to make unprecedented measurements of Saturn's topside atmosphere, neutral thermosphere and ionosphere. Some of these measurements were made possible by the Grand Finale orbits which dipped to the top of the atmosphere and allowed the first ever in situ measurements of Saturn's atmosphere and ionosphere.

Saturn Upper Atmosphere Major Findings (Neutral Thermosphere):

- INMS made first in situ measurements of Saturn's atmosphere, discovering the unexpected presence of several species of high mass neutrals, e.g., CH_4, CO, CO_2.
- The INMS made the first in situ characterization of the thermal structure in the upper atmosphere of Saturn, indirectly through its measurements of the H_2 densities.
- Helium has been measured for the first time in Saturn's upper atmosphere, providing constraints on possible deep-atmosphere mixing ratios of Helium and whether or not Saturn has a solar-like composition or something else.

During the Cassini Grand Finale, the INMS made an unprecedented series of measurements of Saturn's upper atmosphere during the proximal orbit phase, sampling from ~3500–1370 km altitude above the 1-bar pressure level. Prior to these orbits, it was anticipated that Saturn's upper atmosphere consisted primarily of H, H_2, with trace amounts of H_2O, and He. However, the INMS measurements revealed an atmosphere with an unexpectedly rich composition, containing significant amounts of organics spanning the entire mass range sampled by INMS, as seen in Figure MAPS-34. These results were completely unanticipated and they have effectively turned our understanding of the high-altitude thermosphere-ionosphere chemistry on its head.

In particular, INMS has identified methane, CH_4, as a significant component of the upper atmosphere of Saturn above 1370 km. As seen in Figure MAPS-35, INMS has found significant amounts of methane that reach up to ~10% of the composition near 3500-km altitude above the

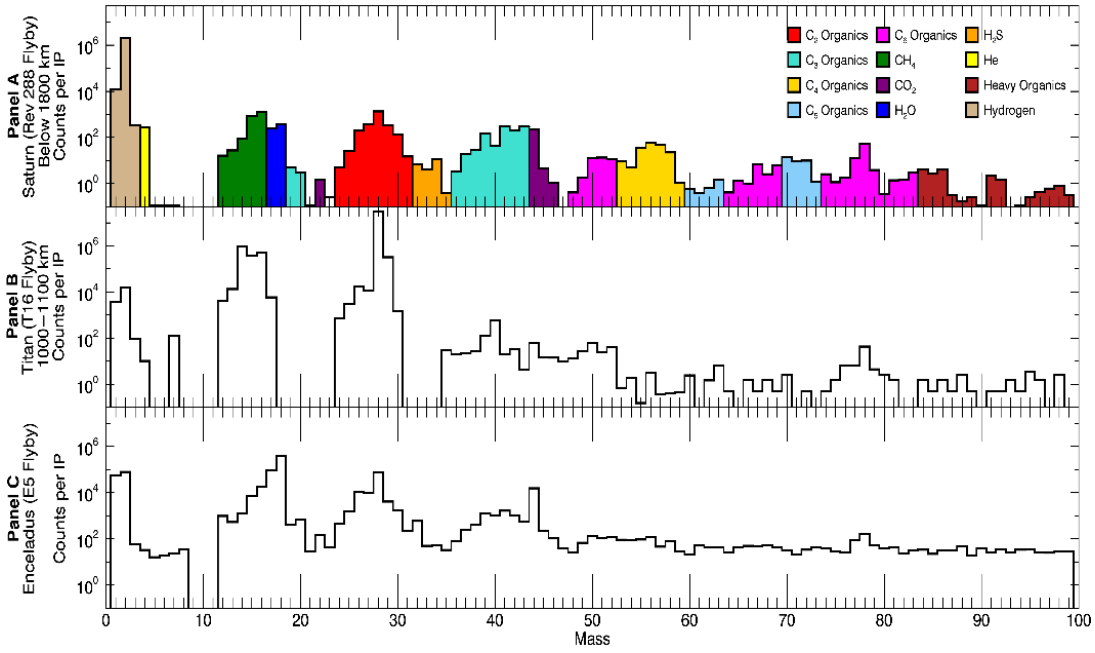

Figure MAPS-34. INMS Mass spectra from the Grand Finale orbits at Saturn (*Panel A*), compared with those of Titan (*Panel B*), and Enceladus (*Panel C*). Horizontal axis is in units of mass per charge.

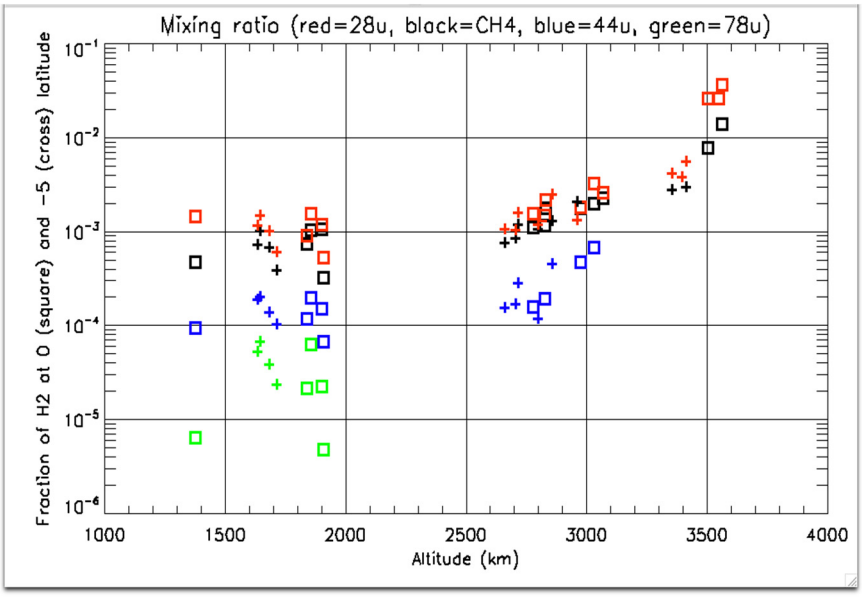

Figure MAPS-35. Volume mixing ratios (vertical axis) of the heavy species identified by INMS in the Saturnian upper atmosphere as a function of altitude above the 1 bar pressure level (horizontal axis).

1-bar pressure level. Additional heavy species (masses 28 u, 44 u, and 78 u) have also been identified. All of these species can potentially play major photochemical roles in the atmosphere of Saturn [cf. Moses and Bass 2000; Kim et al. 2014].

Using a combination of National Institute of Standards and Technology (NIST) data and calibration data collected using the refurbished engineering unit, preliminary fits to spectra at altitudes between 1700 and 1800 km for three representative orbits were made to identify contributing species. In general, the spectrum below ~70 u can be fit by a combination of species that is dominated by hydrocarbons. Ammonia (NH_3) is detected at 17 u. Other N-bearing species are neither excluded nor required by the spectra. The same is true for O-bearing organics. Inclusion of S species, especially H_2S, improves the fit of the spectrum. However, of the non-H_2, non-He material, less than 1 mol.% is contributed by S-bearing species. We estimate that between 30 and 50 mol.% of the non-H_2, non-He material measured by INMS is comprised of organics other than methane, which may constitute an additional 20 to 35 mol.%. C_4 species, including butane (C_4H_{10}) at 58 u, are particularly abundant compared to other hydrocarbons. Above 70 u, the spectra are consistent with contributions from heavier aromatic species, including species such as naphthalene ($C_{10}H_8$, 128 amu) with primary peaks that are beyond the range of INMS.

Other Cassini instruments, including the CHEMS from the MIMI, reported detections of heavy (8,000 to 40,000 amu) particles during the Grand Finale orbits [Mitchell et al. 2018, submitted]. To understand the relationship of these particles to INMS data, we compared the total amount of material detected by INMS to the particle sizes observed by MIMI. The results suggest that INMS may have mainly sampled smaller particles that were dominated by volatile and organic material with very little contribution from refractory mineral phases. The altitude-density profiles of these particles indicate very low densities, likely on the order of 0.1 g/cm^3 or less. These densities may be consistent with the densities of interplanetary dust particles from small bodies [Rietmeijer 1993]. Some masses, including 15 u (mainly from CH_4), 28 u (possibly N_2 or CO), and 17 u (mainly NH_3), have altitude-density profiles that are consistent with molecular radii. Other masses, including 58 u (possibly butane, C_4H_{10}) and 78 u (possibly benzene, C_6H_6), have profiles that suggest larger radii, on the order of nanometers or tens of nanometers.

In addition to the heavy species in the upper atmosphere of Saturn, INMS has also made the first in situ measurements of H_2, He, and H-D in the atmosphere of Saturn. Molecular hydrogen (H_2) is the dominant species in the thermosphere, and its density scale height reveals the expected background temperature of Saturn's upper atmosphere. Thus, measurements of H_2 reveal information about the thermal state of Saturn's upper atmosphere. Prior to the INMS measurements, only remote sensing observations were possible [cf. Koskinen et al. 2015; Vervack and Moses 2015], which provide temperatures through inversion techniques. The measurements in SIA3, however, provide the first-ever direct sampling of the Saturn atmosphere, allowing us to infer thermal structure from these measurements using models of the atmosphere, such as Müeller-Wodarg et al. [2012, 2006b].

Finally, there has been considerable uncertainty about the amount of Helium in the Saturnian atmosphere [Ben-Jaffel and Abbes 2015]. Helium abundances are key to determining the most

likely formation scenarios for Saturn's atmosphere. Currently, it has been suggested that Saturn would be depleted in Helium relative to Jupiter (~13.5% volume mixing ratio) or the protosolar value (~15.6%), due to Helium raining out in the lower atmosphere. The measurements provided by INMS, combined with diffusive modeling, can lead to constraints on the Helium content in the lower atmosphere, providing a missing component in our understanding of planetary evolution.

Saturn Upper Atmosphere Major Findings (Charged Ionosphere):

- INMS made repeated in situ measurements of Saturn's ionosphere, allowing the first determination of ion mixing ratios and number densities as well as their temporal variabilities.
- INMS measurements of the minor ion, H_2^+, represent a strong constraint on local ion production rates, providing a check on outer planet projections of solar irradiances.
- Combined with RWPS and MIMI measurements, INMS in situ data paint a clear picture of Saturn's equatorial ionosphere being dominated by heavy molecular ions that result from ring-derived material.

Prior to the Cassini Grand Finale, observations of Saturn's ionosphere were limited to altitude profiles of electron density (the presumed sum of the ion densities) at dawn or dusk, periods of rapid change in an ionosphere. Trace emissions from an expected major ion, H_3^+, were also detected, but column-integrated densities could only be derived at auroral latitudes. Therefore, ion densities throughout the majority of Saturn's ionosphere were based solely on model comparisons with radio occultation measurements, for example, Moses and Bass [2000]; Moore et al. [2010, 2006]. In situ measurements by INMS provided key constraints on the expected major ion species, H^+ and H_3^+, finally providing closure on a decades-long debate regarding the dominant chemical losses of H^+, for example, Connerney and Waite [1984].

In addition, INMS was able to measure the expected minor ion species H_2^+ and He^+. The chemistry of these ions is relatively straightforward, and the extremely short chemical lifetime of H_2^+ makes it an ideal marker for the in situ ion production rate. Therefore, H_2^+ densities from INMS measurements can be used to gauge the accuracy of commonly used projections of solar irradiances at Saturn. These projections rely on Earth-based data, and the assumption of a relatively stable solar irradiance over a period of days. Comparisons between measured H_2^+ with modeled H_2^+ based on projected solar irradiances find a ~50% discrepancy, implying that future outer planet modeling will require better estimates of the solar irradiance.

Finally, Cassini's high speed near periapse during the Grand Finale (~32 km s^{-1}), meant that INMS could only sample ions with mass up to 7 u. The sums of the light ions measured by INMS were found to be an excellent match with the electron density from RPWS at high altitudes (> ~2200 km), implying that Saturn's high-altitude ionosphere was charge-neutral and dominated by H^+ with minor contributions from H_3^+, as expected (Figures MAPS-36 and MAPS-37). However, at low altitudes the total ion densities from INMS differed significantly from the electron density.

This massive discrepancy could be interpreted as a signature of an ionosphere dominated by heavy (> 7 u) ions, which would be entirely consistent with the expected ion chemistry to follow from the ring-derived influx of complex neutrals measured by INMS.

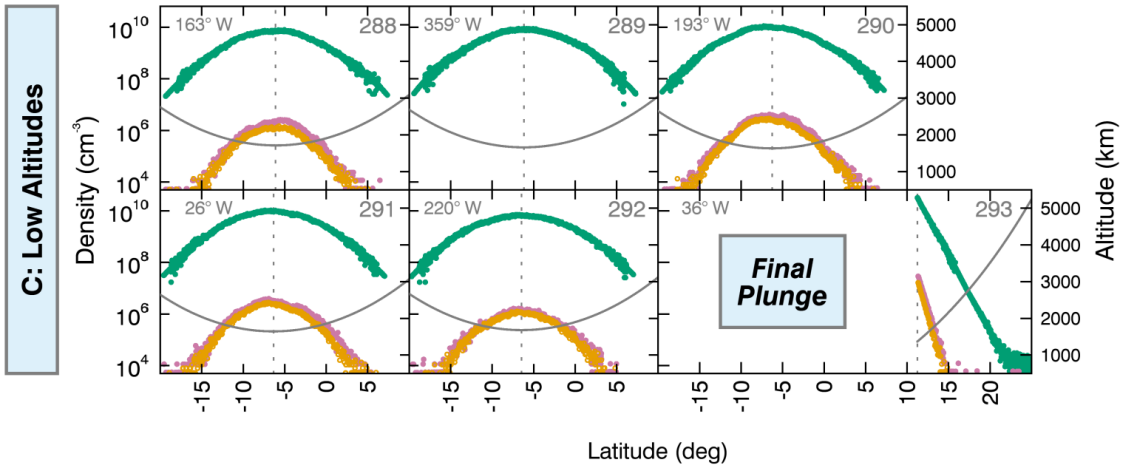

Figure MAPS-36. INMS measurements of H_2 (green), He (red), and Mass 3u (orange) as a function of altitude (right-hand axis) and latitude (horizontal axis).

Open Questions for Saturn System Science

Internal rotation rate and internal magnetic field of Saturn

- What is the rotation period of Saturn? How do the multiple, variable magnetospheric periods observed in radio, magnetic fields, energetic particles, plasma, aurora, and other phenomena tied to the internally-generated magnetic field at Saturn?
- How are the observed periodicities related to the actual rotation of Saturn, and does it matter? Most investigators agree that the observed periods of Saturn, which are generally magnetospheric in nature, do reflect the true rotation of the planet, and that such periods are probably slower than the real rotation period, which may be intimated from the planet's oblateness, see Helled et al. [2015] and references therein. If Saturn is a differential rotator, such as the Sun, then, indeed, the period may be ephemeral and not meaningful, for example, Dessler [1985].
- What are the implications of the extremely axisymmetric planetary magnetic field for the internal structure of Saturn? What is the dynamo process generating this planetary field?

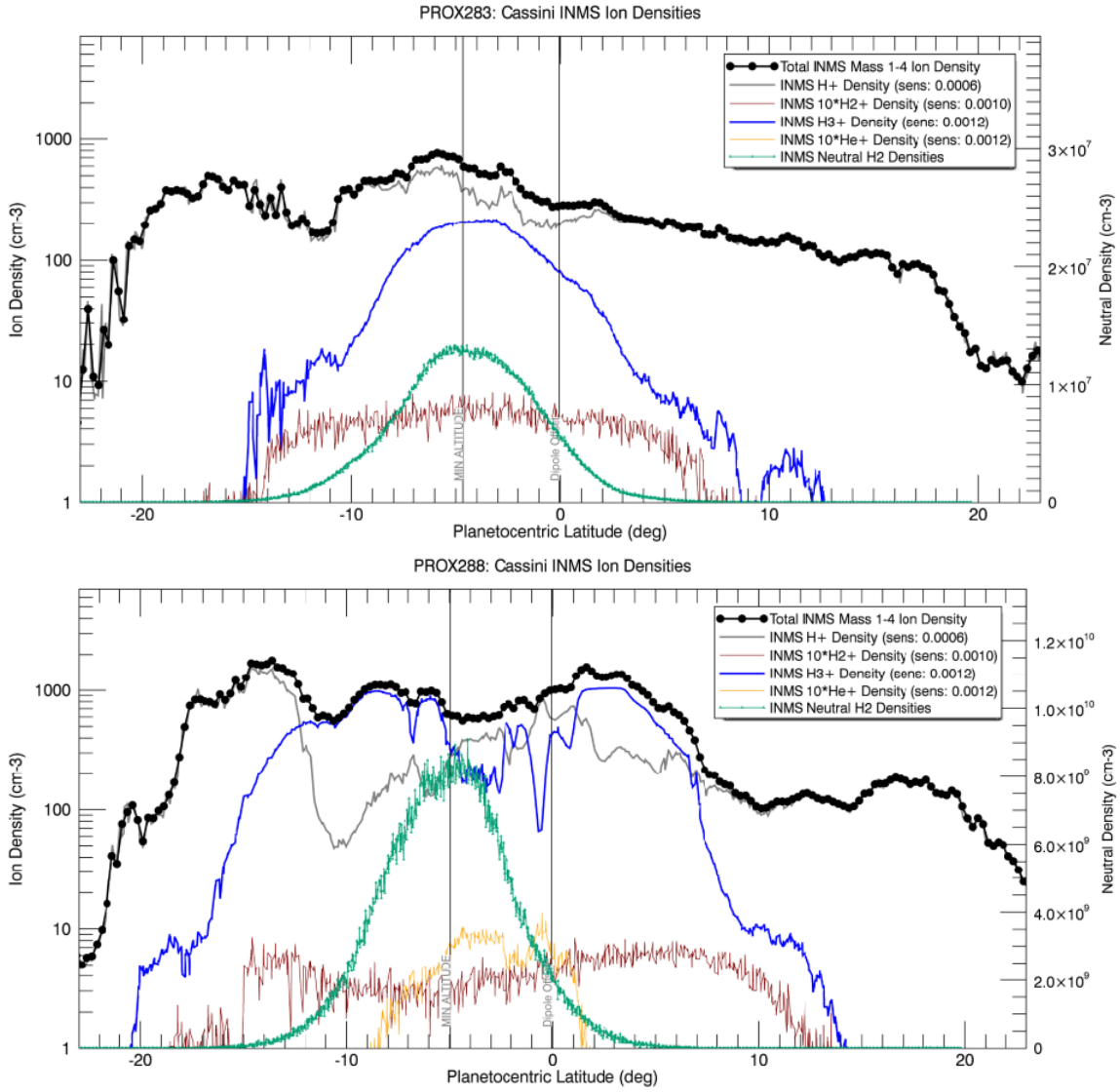

Figure MAPS-37. INMS measurements of H_2 (green), H^+ (gray), H_2^+ (red, multiplied by 10), H_3^+ (blue), He^+ (gold, multiplied by 10), and total light ion density (1–4 u, black) as a function of planetocentric latitude (horizontal axis). Ion measurements were taken for four proximal orbits, 283, 287, 288, and 292, though only one representative high altitude (283, *Top panel*) and low altitude (288, *Bottom panel*) orbit is presented here.

Rotational modulation in axisymmetric configuration

- Given the extraordinarily axisymmetric magnetic field, why are there such prominent rotational PPO modulations in Saturn's magnetosphere?
- What is the underlying cause of Saturn's periodicities? The current thinking is that the periodicities are related to disturbances, possibly vortices, in the upper polar atmosphere or lower ionosphere. The periodicities are not thought to arise in the

magnetosphere, although the magnetosphere probably provides a linkage, via field-aligned currents, between periods in the north and the south.

- How are the PPOs driven in the atmosphere, thermosphere and ionosphere of Saturn?

How are mass and magnetic flux transported in the middle and outer magnetosphere?

- Where and how does the magnetosphere unload its cold, dense plasma?
- How is plasma transported outward, and magnetic flux returned, in the region between 12 and 20 to 25 R_S?
- What is the connection between large-scale and small-scale injections at Saturn? How much material do injections transport relative to radial diffusion? What drives radial diffusion?
- What is the relationship between large-scale, tail-reconnection-driven injections and small-scale interchange injections?
- What determines the scale size and inflow speed of interchange injections? What determines the apparently variable rate and depth of such injections?
- Are the growth of the K-H instability and magnetic reconnection coupled?
- Where in the Saturnian system does Vasyliunas-type reconnection take place, and where does Dungey-type reconnection take place? Is there a region in Saturn's magnetosphere where one or the other dominates?

Solar wind control of the Saturnian magnetosphere

- What is the dominant mode of solar wind interaction with the magnetosphere, the viscous interaction or the large-scale reconnection interaction?
- How does the solar wind drive magnetospheric dynamics at Saturn? Is solar wind dynamic pressure the primary influence?

Neutral particle dominated Saturnian magnetosphere related to difference if compared to Jupiter?

- How does the abundant neutral population in Saturn's magnetosphere make it different from fully or mostly ionized magnetospheres?

Very limited plasma measurements in auroral acceleration and source region of related SKR

- What is the predominant form of the electron distribution function at the source of SKR?

Understanding the Enceladus plume-magnetosphere interaction

- What are the various populations of charged dust and molecules that balance charges in dusty media such as in the plumes of Enceladus and in Saturn's topside equatorial ionosphere?
- In the Enceladus plumes, the 28 u species measured during CSN operations is a fragment of a larger molecule. The identity of the larger molecule and of the 28 u fragment would help constrain the chemistry in the subsurface oceans of Enceladus. Similarly, the highly abundant 28 u neutral measured in Saturn's inner magnetosphere could be CO, N_2, or a fragment of a heavier molecule, and none of these is consistent with CAPS observations or with the Enceladus plume composition.
- How are heavy negative ions formed in the plume at Enceladus, and what is their contribution to nano-grain formation?

Composition of the negative ions at Titan and > 100 amu positive ions

- What are the detailed process that create the large ions and the negatively charge ions in Titan's upper atmosphere and ionosphere?

MAPS DWG Non-Saturn Science Results

Cruise-specific Science

Solar wind from Earth to Saturn

- **C_AO1:** Extend the sensitivity of composition measurements of interstellar ions by approximately three orders of magnitude.

The Cassini spacecraft obtained gravity-assists at Earth (August 1999) and Jupiter (December 2000–January 2001) arriving at Saturn July 2004. This extensive time spent in the solar wind allowed Cassini to make measurements that could be used, together with Galileo and Ulysses measurements, to better understand the evolution of the solar wind outward in the solar system.

During the cruise to Saturn the MIMI suite was able to make unique measurements of heliospheric suprathermal particles in the 2–60 keV/nuc range. There has never been an

investigation with species separation of this important class of particles, which ties the solar wind plasma to the energetic particles, beyond Jupiter. Hill et al. [2009] made CHEMS measurements that revealed that the radial intensity profiles of He^{+} and He^{++} are very different from both analytical and numerical theory, with the observations showing an increasing intensity with distance from the Sun, while the theory predicts the intensity should fall. This observation remains unexplained.

During same time period, the CAPS investigation made the first in situ observation of interstellar pick-up ions beyond the orbit of Jupiter. This was the first direct detection of mass-resolved interstellar pick-up ions, and confirmed the existence of helium focusing at these distances. Focusing of helium atoms at these distances is caused by the solar gravitational field (Figure MAPS-38). CAPS also made the first direct, in situ, measurements of a large shadow in the interstellar hydrogen population downstream from the Sun caused by motion through the interstellar medium [McComas et al. 2004]. The shape of the measured distribution function of the observed He+ as a function of energy was characteristic of a pick-up distribution with a flat top and cut off at about four times of the solar wind energy.

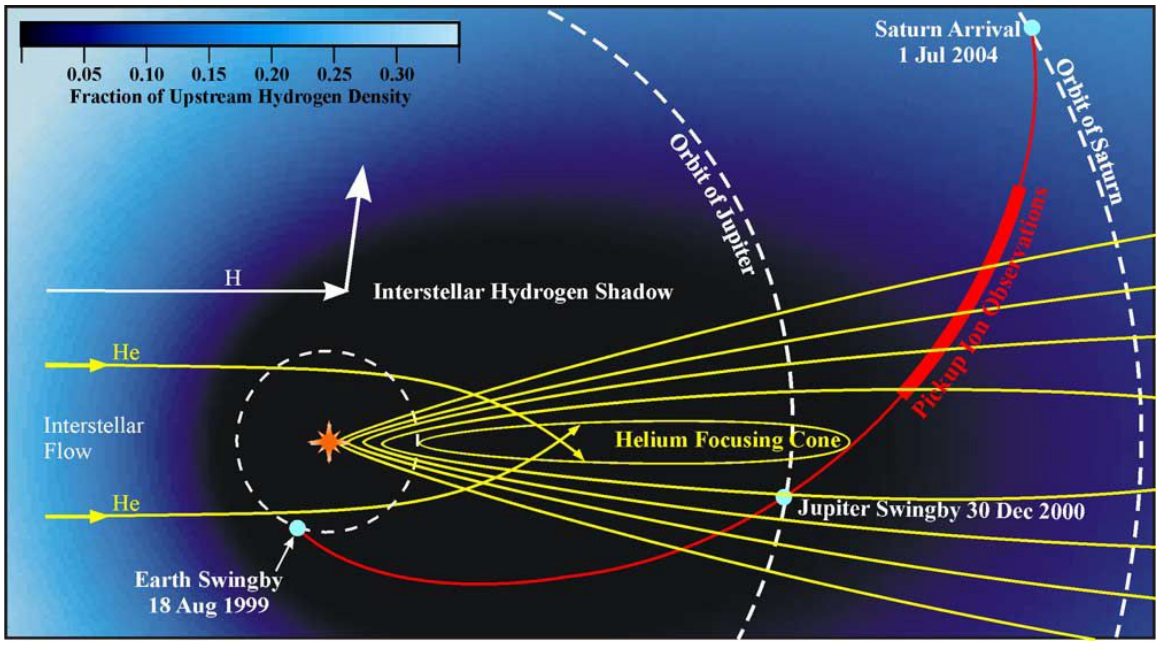

Figure MAPS-38. Schematic diagram of Cassini's trajectory between Earth swing-by and arrival at Saturn. Pick-up ion measurements were made between 6.4 and 8.2 AU (heavy line) as Cassini emerged from the down-stream direction. Simulation results show: i) the gravitational focusing of interstellar He in contours of 5/3, 2, 7/3, 8/3, and 3 times the upstream He density; and ii) the color-coded H density as a fraction of the interstellar value. The dark region downstream from the Sun is the interstellar hydrogen shadow. Figure from McComas et al. [2004].

CHEMS measurements of pick-up ions were used to determine solar wind speeds, which enabled a study [Hill and Hamilton 2010] of the spectral index of suprathermal particles. The slopes of the spectra were reported and widely put into and used to create context by the community, but Hill and Hamilton [2010] showed that the expected velocity v dependence was approximately v^{-5}

as reported by Fisk and Gloeckler [2008]. The solar wind speeds themselves are of inherent value for investigating the heliosphere and, near Saturn, as an input to magnetospheric studies. In 2014, data from 2001 to 2004, inclusive, at a 12-hour cadence, were published on the Cassini project's MAPSview website: [http://mapskp.cesr.fr/index.php].

The energetic particle population was further studied by Lario et al. [2004] using LEMMS observations. They found that intensity enhancements up to ~1 MeV were due to the passage of interplanetary shocks while at the highest energy (> 25 MeV), the prompt component of solar energetic particle events was responsible. For all but the largest SEP events the presence of magnetic field structures between the Sun and the spacecraft significantly modulates the intensity enhancements.

In addition to the measurements Cassini MAPS instruments made of solar system plasmas and neutrals, the RPWS instrument was able to make measurements of nanograin dust. During the flyby of Jupiter, Meyer-Vernet et al. [2009] reported wave measurements that corresponded to observations of nanograin dust streams moving at the solar wind speed made by the Cassini dust sensor. The result is the first wave detection simultaneous with a conventional detection by a dust analyzer attributed to nanoparticles. Following this detection, RPWS data from the cruise phase (between 1–5 AU) was analyzed in more detail. Schippers et al. [2015, 2014] analyze the low frequency bursty noise identified in the Cassini radio and plasma wave data during the spacecraft cruise phase and find the magnitude, spectral shape, and waveform of this broadband noise are consistent with the signatures of the nanoparticles that traveled at solar wind speed and impinged on the spacecraft surface. Nanoparticles were observed whenever the radio instrument was turned on and able to detect them at different heliocentric distances between Earth and Jupiter, suggesting their ubiquitous presence in the heliosphere. Analysis of the radial dependence of the nanodust flux with heliospheric distance and found that it is consistent with the dynamics of nanodust originating from the inner heliosphere and picked-up by the solar wind. The contribution of the nanodust produced in the asteroid belt appears to be negligible compared to the trapping region in the inner heliosphere. In contrast, further out, nanodust is mainly produced by the volcanism of active moons such as Io and Enceladus.

Due to a fortuitous alignment of the Earth and Jupiter during the Cassini Jupiter flyby Hanlon et al. [2004] were able to study the evolution of an interplanetary mass ejection during solar maximum. The pre-Jupiter data set reveals clear and numerous transient perturbations to the Parker Spiral solar wind structure typical of solar maximum. The limited plasma data is available at Cassini due to instrument pointing restrictions and this renders the identification of the nature of such structures ambiguous. However, the alignment of Jupiter and Earth during this encounter allowed the tracing of these structures back to those observed by the Wind spacecraft near the Earth. Of the phenomena that are satisfactorily able to

Due to a fortuitous alignment of the Earth and Jupiter during the Cassini Jupiter flyby Hanlon et al. [2004] were able to study the evolution of an interplanetary mass ejection during solar maximum.

trace back to their manifestation at 1 AU, two are identified as being due to interplanetary coronal mass ejections. One event at Cassini is shown to be a merged interaction region, which is formed from the compression of a magnetic cloud by two anomalously fast solar wind streams. The flux-rope structure associated with this magnetic cloud is not as apparent at Cassini and has most likely been compressed and deformed.

Other Non-Saturn System Science

Interstellar neutrals and the Heliotail

- **C_AO1:** Extend the sensitivity of composition measurements of interstellar ions by approximately three orders of magnitude.
- **J_AO4:** Obtain the first high-resolution images of the Io torus.

The Sun's atmosphere is not static but expands in the form of a magnetized fluid called the solar wind [Parker 1958], reaching to distances of potentially hundreds of Astronomical Units (1 AU = 1.5 × 10^8 km), shaping our local bubble, called the heliosphere, through its interaction with the Local Interstellar Medium (LISM). Voyager 1 and Voyager 2 (hereafter, V1 and V2) crossed the termination shock, where the supersonic solar wind presumably terminates at the shock front, at respective distances of ~94 and ~84 AU in 2004 and 2007 at +35° and −26° ecliptic latitudes [Decker et al. 2008, 2005], pinpointing both the—previously unanticipated—size of the local heliosphere and the scale of the heliospheric asymmetry.

After the discovery of the reservoir of ions and electrons that constitute the heliosheath (a region past the termination shock), V1 passed through an unexpected depletion region, where a decrease in ions of solar origin (by a factor of ~10^3) and a simultaneous increase of high energy cosmic rays (~9.3%) occurred, that forms part of the interface between the solar plasma and the galaxy, namely the heliopause [Krimigis et al. 2013], at a distance of ~122 AU. Since August 2012, V1 has continued its journey to the galaxy, measuring the distant and unexplored LISM (V1 is currently located at a distance of ~19 AU past the heliopause), while V2 is still surveying the heliosheath (expected to cross the heliopause in the next few years). Due to the powerful synergy between in situ ions from V1/LECP (Low Energy Charged Particle) instrument and ENAs from INCA (in overlapping energy bands), MIMI, beginning in about 2009, has made key discoveries that altered our past notions on the formation and interactions of the heliosphere, leading to a number of surprises concerning the physics that governs this enormous system, and providing insights on the plasma processes at ~100 AU that were substantially at variance with previous theories and models.

In 2009, an important paper by the MIMI team [Krimigis et al. 2009] showed, for the first time, images of the global heliosphere using > 5.2 keV ENA measurements obtained with INCA over the 2003–2009 time period, and identified two striking, previously unexpected, heliospheric signatures: i) the Belt, a broad band of emission in the sky, identified as a high intensity, relatively wide ENA region that wraps around the celestial sphere in ecliptic coordinates, passing through the nose the anti-nose (tail) and the north and south heliosphere poles; and (ii) the basins,

identified as two extended heliosphere lobes where the ENA minima occur. Interestingly, the ENA measurements are moderately well organized in galactic coordinates, with the Belt presenting a prominent tilt of ~30° with respect to the galactic equator, whereas the Basins were found to roughly coincide with the galactic north and south poles, although their boundaries were also tilted ~30° to the galactic equator. The same science issue hosted yet another significant publication (with contribution from the then-MIMI PI, Stamatios M. Krimigis), from the Interstellar Boundary Explorer team [McComas et al. 2009], showing, for the first time, images of the heliosphere in < 6 keV ENAs. A narrow bright ENA stripe known as the ribbon forms an incomplete circle around the heliospheric nose, most prominent at ~1.1 keV, surrounded by a broad ENA emission that became known as Globally Distributed Flux (GDF).

In a later publication, Dialynas et al. [2013] found that the deviation of the ENA emissions from the equator is effectively minimized in a rotated frame (interpreted interstellar magnetic field frame (ISMF)) where its north pole points toward 190° ecliptic longitude and 15° ecliptic latitude. The ENA spectra showed a power-law form in energy, presenting higher spectral slopes in the belt region and lower outside ($3.4 < \gamma < 4.4$), which are almost indistinguishable between the tail and the nose regions, i.e., no noticeable asymmetry was observed. Notably, the morphology of the belt (peak, width, and structure) is nearly energy independent of energy from 5.2 keV to 30 keV. The authors speculated that Interstellar Boundary Explorer (IBEX)-GDF evolves with increasing ENA energy to form the belt at high GDF energies, explaining that the GDF and the ribbon are distinct features that originate from different source plasma populations (heliosheath and outside the heliopause, respectively). This was recently confirmed by the IBEX team [McComas et al. 2017].

Taking into account the local partial pressure over the $\sim 5 < E < 4000$ keV energy range from V1, V2 and INCA (~ 0.1 pPa), an assumed thickness of the heliosheath (~50 AU) and the simulated pick-up ions (PUI) distribution [Giacalone and Decker 2010] that was used to estimate the $E < 6$ keV contribution (~0.12 pPa), Krimigis et al. [2010] concluded that there is a need for a substantially stronger magnetic field upstream of the heliopause than assumed before, in order to balance the non-thermal PUI pressure against the stagnation pressure of the interstellar plasma and the local ISMF at the heliospheric nose. The interstellar magnetic field was estimated to be ~0.5 nT and have an upper bound of ~0.64 nT. This calculation was confirmed a few years later after V1 crossed the heliopause and measured a strong interstellar magnetic field of ~0.5 nT [Burlaga et al. 2013] that exhibited a jump right outside the heliopause of ~0.6 nT. V1 is currently located at ~19 AU past the heliopause and still measures a magnetic field of ~0.5 nT, Burlaga and Ness [2016], and a relatively dense plasma of > 0.09/cm^3 that reached densities of ~0.12/cm^3 [Gurnett et al. 2015, 2013].

A different study, Dialynas et al. [2015] analyzed separately INCA images of the heliosphere and found that the very low (basin) and high (tail) ENA emissions in the heliosheath are separated with a relatively smooth boundary (called transition region), with a spatial width of ~30° in ecliptic longitude, which no theory had predicted to date. The ENA intensity gradient in this transition region was found to be almost invariant as a function of both ecliptic latitude and energy, with an average value of ~2.4% per degree and translates to a corresponding partial pressure gradient that occurs in the transition region, enabling a discussion on the Parker field towards the tail. Bearing in mind

that the plasma-β inside the heliosheath showed large fluctuations about an average of ~5–10, i.e., much larger than unity [Decker et al. 2015], this pressure gradient is possibly not consistent with a tail magnetic field configuration that is similar to the measured magnetic fields by the Voyagers in the nose hemisphere. Notably, the pick-up ion populations in the keV range play a dominant role in maintaining the pressure balance in the heliosheath.

In the pre-INCA imaging era, the size of the heliosphere had been estimated using several different models, where the heliosheath varied between 70 and 160 AU. By combining Voyager in situ ion measurements and remotely sensed INCA ENAs in overlapping energy bands, Krimigis et al. [2010, 2009], calculated that the heliosheath thickness should be ~54 (+30, −15) AU. A more detailed analysis performed by the MIMI team, included also the possible contributions from the Compton-Getting effect due to the radial velocity of the heliosheath plasma and concluded that the heliosheath appears to be twice as thick along the V2 line-of-sight (LOS) as it is along the LOS to V1: L_{V1} = 31(+31, −18) AU and L_{V2} = 71(+30, −15) AU [Roelof et al. 2012]. A breakthrough on this came in 2011, when the MIMI and Voyager teams published a brief report [Krimigis et al. 2011] showing that the radial component of the bulk plasma velocity had been decreasing almost linearly for three years, from 70 km/s to 0 km/s, and then it stabilized around this value for ~8 months. This study concluded that the ENA and ion spectra could be brought into agreement at V2 with a heliosheath thickness of L_{V2} ~54(+30, −15) AU, whereas the same normalization procedure applied to Voyager 1 results in L_{V1} ~27(+26, −11) AU. Surprisingly, the V1 crossing from the heliopause occurred ~1 month later than anticipated by Krimigis et al. [2011], in August 2012 [Krimigis et al. 2013], showing that the heliosheath thickness towards the nose (at V1 direction) is ~29 AU, i.e., much smaller and more compressed than expected in past models.

Admittedly, one of the milestones in the heliosphere research concerns the shape of this enormous system, because it strongly relates to the interpretation of several phenomena that were either theorized in the literature and/or resulted from measurements performed by modern detectors. For more than five decades, the shape and interactions of the heliosphere with the local interstellar medium have been discussed in the context of either a magnetosphere-like heliotail or a more symmetric bubble shape, posited in 1961 [Parker 1961]. Although past models broadly assumed the magnetosphere-like concept, the accurate heliospheric configuration remained largely undetermined due to lack of measurements.

Building upon previous analyses made by Krimigis et al. [2009] and Dialynas et al. [2013], and employing both Voyager in situ and INCA remote measurements, a recent MIMI publication, Dialynas et al. [2017a] used > 5.2 keV ENA measurements, obtained with MIMI/INCA over the 2003–2014 time period and provided a new paradigm on the heliosphere interaction with the LISM: the belt corresponds to a reservoir of particles that exist within the heliosheath, constantly replenished by new particles from the solar wind, while the ENAs that INCA detects are most likely associated with a region of enhanced particle pressure that is formed inside the heliopause and contributes to balancing the pressure of the ISMF (see Figures MAPS-39). The authors showed that the heliosheath ions are the source of > 5.2 keV ENA and that the heliosphere responds

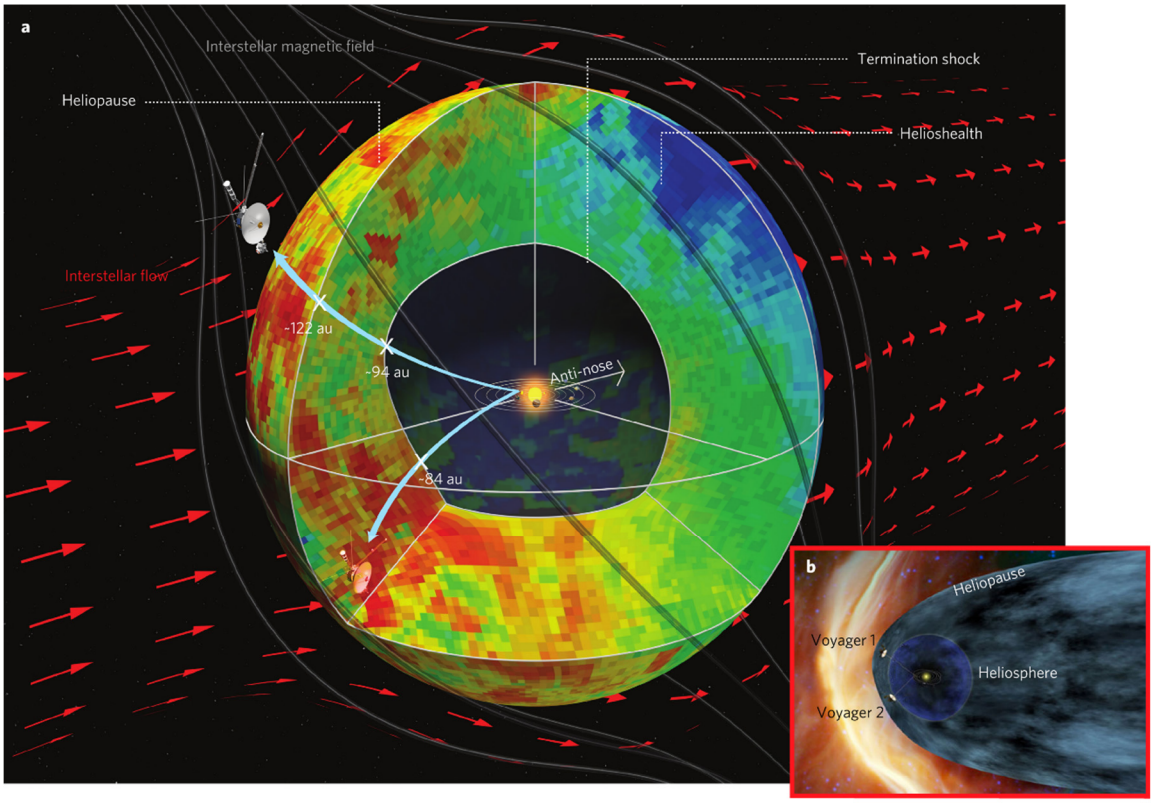

Figure MAPS-39. Adapted from Dialynas et al. [2017a] showing a conceptual model of the global heliosphere: (a) The gross shape and basic properties of the global heliosphere in three dimensions, summarizing our current understanding, based on both remote ENA and in situ ion measurements from Cassini/INCA and LECP/V1&V2, respectively. It shows a belt of varying ENA intensities surrounding the termination shock and extending to the outer boundary of the Heliosphere, called the heliopause, as identified by V1; it is anticipated that the heliopause south of the ecliptic will be crossed by V2 within the next few years. The red arrows represent the interstellar plasma flow deflected around the heliosphere bubble. The termination shock and heliopause are marked at the distances (in AU) observed by the Voyagers from 2004 through 2012 in their traversal of the heliosheath. The cutout illustrates the possible distribution of hot ion plasma in the heliosheath discerned by line-of-sight ENA images (E > 5.2 keV); relative scale ranging from 1 *(blue)* to 12 *(red)*. As the ENA emissions detected by INCA are LOS integrated, the 3rd dimension in this composite, conceptual representation of the global heliosheath (presenting the possible ENA distribution confined between the termination shock and the heliopause) is based on the knowledge of the variation of ion intensities measured at the Voyagers towards the nose hemisphere. These ion intensities are representative of the average ENA intensities along any LOS inside the heliosheath. Note that this concept of the heliosphere does not imply a closed system that cannot change its shape towards the tail to release the solar wind energy input. Inside the termination shock the ion intensities are lower by at least ×100. The orbits of the outer planets are drawn to scale around the Sun. Concept *(a)* is compared with *(b)*, a magnetosphere-like configuration (http://voyager.jpl.nasa.gov/mission/) widely adopted as one of two possibilities put forward by Parker [1961]. The termination shock is ~10 AU further out in the V1 direction, but the HS is possibly ~30–50% thicker towards the V2 direction (as detailed in the text), inconsistent with a compressed heliosheath in the southern hemisphere. That will be determined when V2 crosses the HP, expected in the next few years.

promptly, within ~2–3 years, to outward propagating solar wind changes (controlled by solar sunspot numbers and solar wind energy input) in both the upstream (nose) and downstream (tail) directions. These observations, taken together with the V1 measurement of a ~0.5 nT interstellar magnetic field, plasma density of > 0.09/cm^3 and the enhanced ratio between particle pressure and magnetic pressure in the heliosheath, strongly suggest a diamagnetic bubble-like heliosphere with few substantial tail-like features. A follow-up MIMI publication [Dialynas et al. 2017b] discussed the details of these results, and by calculating the recovery times of ENAs in the heliosphere, they found that the rough width of the heliosheath can be ~80–120 AU (or more) towards the tail, due to the ~2–3 year delay after solar minimum.

Dialynas et al. [2017a] also included two important implications concerning the heliosphere interaction with the LISM: 1) A perfectly symmetric and stable heliosphere in time would not be possible and/or physically correct, i.e., as the heliosphere cannot be a closed system, the heliosphere bubble can (and must) inflate with time in either the anti-nose direction (tail models) or along the direction of the interstellar magnetic field (Note: the polar jets [Opher et al. 2015; Drake et al. 2015], provide one of the possible mechanisms through which the solar wind input is evacuated from the system); and 2) due to the strong interstellar magnetic field, the Mach number of the local interstellar medium can be significantly decreased and the flow can become submagnetosonic, leading to the inability of forming a bow shock, as previously explained by Fahr et al. [1986] and simulated from Kivelson and Jia [2013] using the mini magnetosphere of Ganymede as a rough analogy to the heliosphere.

Jupiter

Jupiter's magnetotail

- **J_AO3:** Explore the dusk side of Jupiter's magnetosphere and intermediate regions of the magnetotail unvisited by previous spacecraft

Cassini flew by Jupiter on December 30, 2000, on its way to Saturn. Arriving from the pre-noon sector, closest approach occurred in the afternoon sector at 138 Jovian radii (~107 km) from the planet and was followed by an exploration of the dusk flank of the Jovian magnetosphere. During the Cassini flyby, the Galileo probe was still active (Figure MAPS-40).

In spite of the large distance of the flyby, several Cassini-MAPS instruments recorded high-quality data for about six months around closest approach. These observations benefited from the simultaneous presence of Galileo in orbit around Jupiter, enabling two-point measurements, and were complemented by remote observations by HST, Chandra, and ground-based radio. This resulted in a very rich data set that was the basis of many publications and will be further exploited in the coming years.

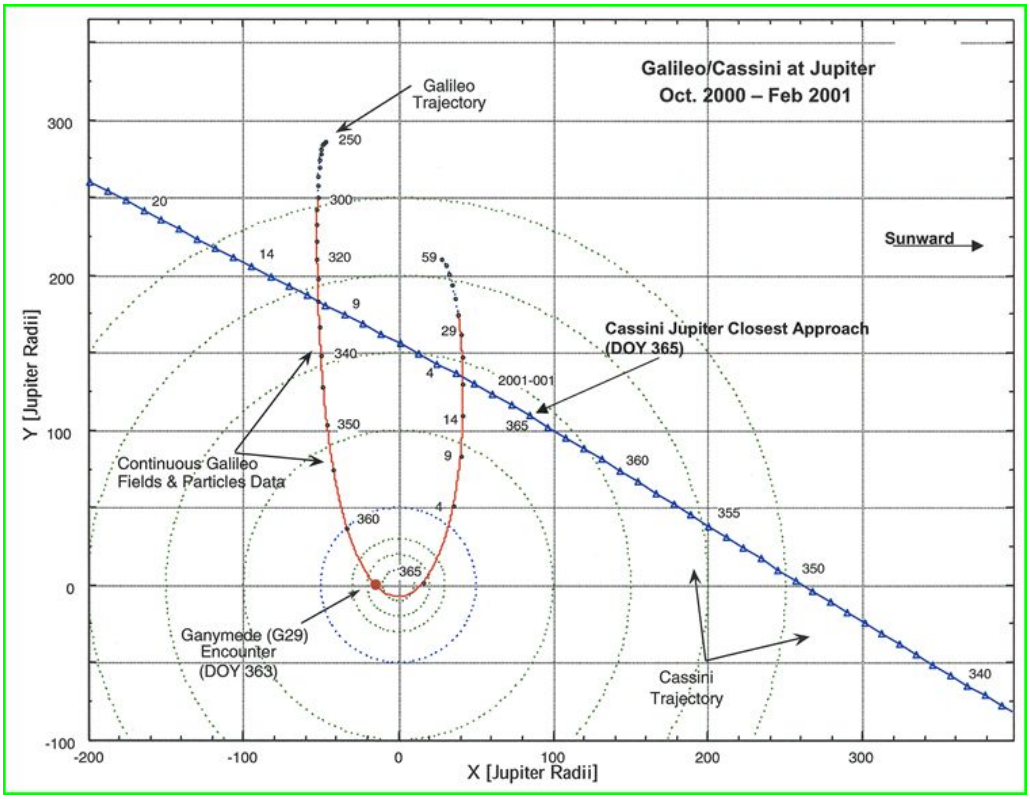

Figure MAPS-40. The orbits of Galileo and Cassini at Jupiter.

The dual Cassini/MAPS and Galileo measurements provided a chance to study the dynamic effects of the solar wind perturbations on the global configuration of the Jovian magnetosphere. These measurements showed clearly that magnetospheric particles leak directly into the interplanetary medium from the closed magnetosphere and are the source for the upstream particle events [Krupp 2002].

During its passage along Jupiter's dusk flank, Cassini made at least five bow shock crossings, one at ~1929 LT and four more between 2100 and 2130 LT on DOY 21. During the flyby, shock activity was high and variable, making a moving target for Cassini instruments. Cassini found that the shock is enormous, extending at least 700 R_J down the flank.

All three CAPS sensors were used to identify shock conditions and the times at which Cassini crossed into and out of it. See Szego et al. [2003] for a full description of shock studies based on all Cassini observations. By combining RPWS identification of Langmuir waves and IBS energy spectra, the upstream density could be measured at 0.5 to 1 cm^{-3} while at the same time ELS provided a measure of electron temperature at 2.6 eV. The data allowed the team to solve the Rankine-Hugoniot relations for transitions between the upstream and downstream conditions, deriving plasma density ratios of 2.74, and a downstream ion bulk energy of ~360 eV. The calculated downstream electron bulk temperature prediction was ~44 eV whereas ELS data gave ~11 eV and IMS ~24 eV, in fairly good agreement with the total energy jump predicted by theory.

IBS energy-time spectrograms were used to identify shock crossings far down the flank of the magnetosphere (Figure MAPS-41 is one example). Four examples that were observed using IBS data took place at 576, 618, 744, and 770 R_J were studied in detail by Szego et al. [2003].

Using CAPS, MAG, and RPWS, Cassini was able to investigate features of the downstream Jovian shock and magnetosheath out to ~700 R_R; a region not previously visited by any other spacecraft. As might be expected, the shock transition layer was broad and turbulent at that distance, but the transits were always easily observed using IBS data.

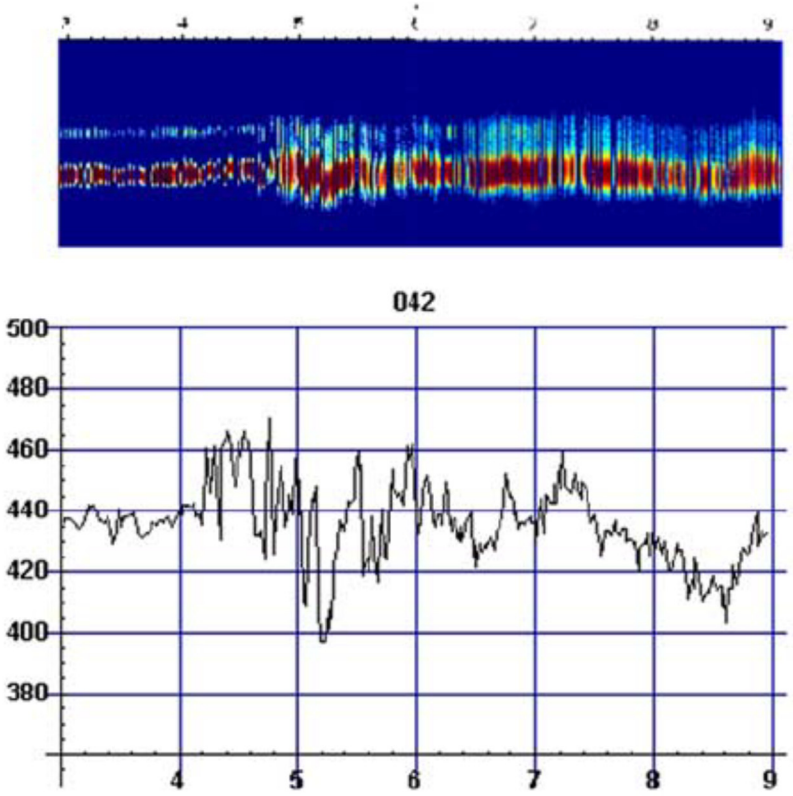

Figure MAPS-41. IBS data taken on DOY 042, 2000, 0300 to 0900 UT along the flanks of the Jovian magnetosphere. The velocity jump across the shock shows up as a jump in the velocity measured by IBS beginning at approximately 0420 UT. The most apparent feature is at ~4:40 UT when Cassini is inside the sheath and density and temperature both increase.

An important result of the coordinated measurements of Cassini and Galileo was good evidence of a change in magnetospheric shape in response to local solar wind magnetic field changes in the north-south component. There is increased flaring when the field is northward, opposite as to what happens at Earth. As the Jovian dipole is oppositely oriented, this is consistent with reconnection being important to magnetospheric configuration at Jupiter despite the high planetary rotation [Kivelson and Southwood 2005, 2003].

Not only did the passage of Cassini allow two-point measurements, but the MIMI/LEMMS and RPWS instruments on Cassini were very similar to instruments flown on Galileo. This allowed direct comparison of energetic particle and wave phenomena both inside and outside the magnetosphere of Jupiter. The comparison of energetic particle measurements made by both spacecraft is summarized in Krupp et al. [2004, 2002]. Figure MAPS-42 shows the differential fluxes and the pitch angle distributions of ions and electrons measured with LEMMS onboard Galileo and Cassini in the vicinity of the Jovian magnetopause.

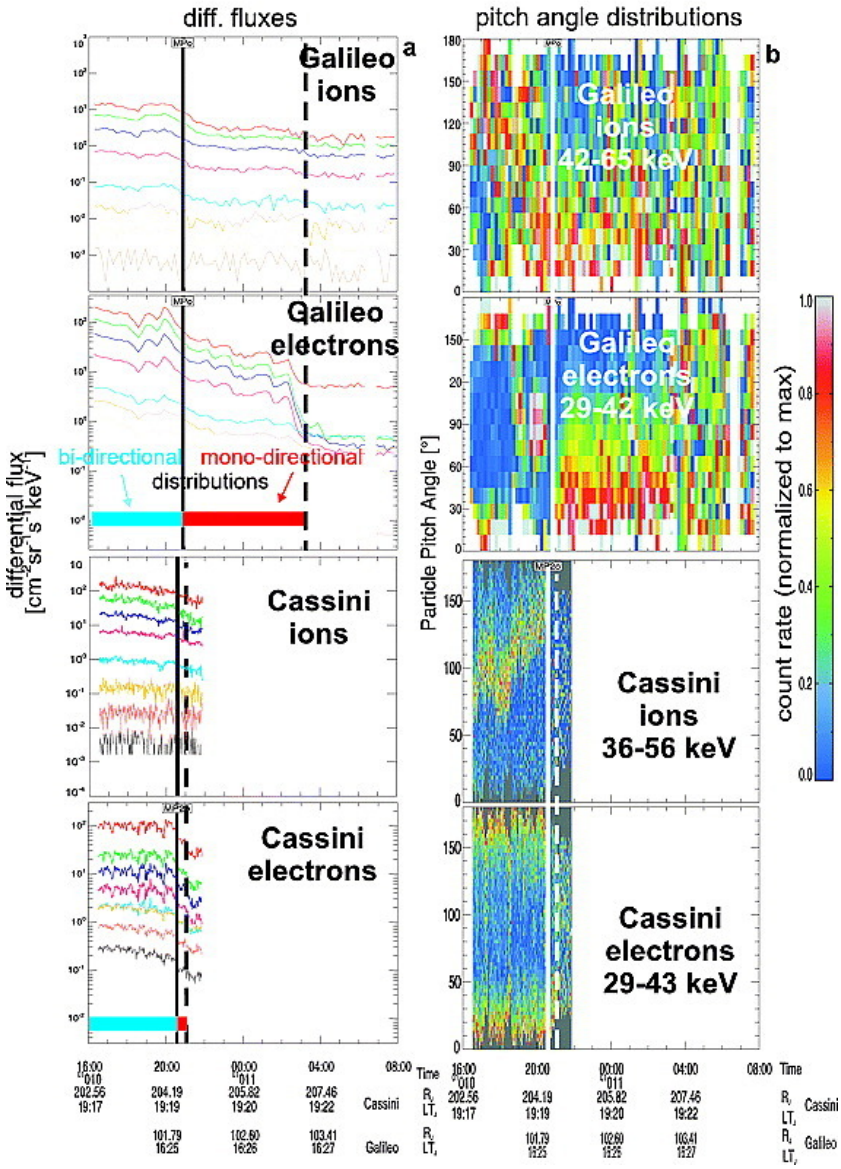

Figure MAPS-42. Differential fluxes and pitch angle distributions of ions and electrons measured with the LEMMS sensors onboard Galileo and Cassini in the vicinity of the magnetopause of Jupiter. Figure from Krupp et al. [2002].

Significant results from the coordinated measurements of the energetic particles include:

- Passage of closed to open planetary field lines with distributions from bi-directional to mono-directional, with respect to the magnetic field near the magnetopause.
- Periodic variations of electron fluxes on both spacecraft with 40 min periods near Cassini and about 60 min at Galileo's location.
- Leakage of magnetospheric particles into the interplanetary space.
- Sporadic electron beams outside the magnetosphere (Cassini at 300–900 R_J and Galileo at 130 R_J).

In addition, during the Jupiter flyby, INCA observed large fluxes of ENAs, primarily H and O, from the planet [Mitchell et al. 2004]. INCA discovered an ENA torus associated with and located just outside the orbit of Europa [Mauk et al. 2003]. The neutral densities in this torus were comparable to those found in the Io-associated cloud, and suggested that Europa is a strong source of neutrals. Figure MAPS-43 shows the discovery ENA image of the Europa torus.

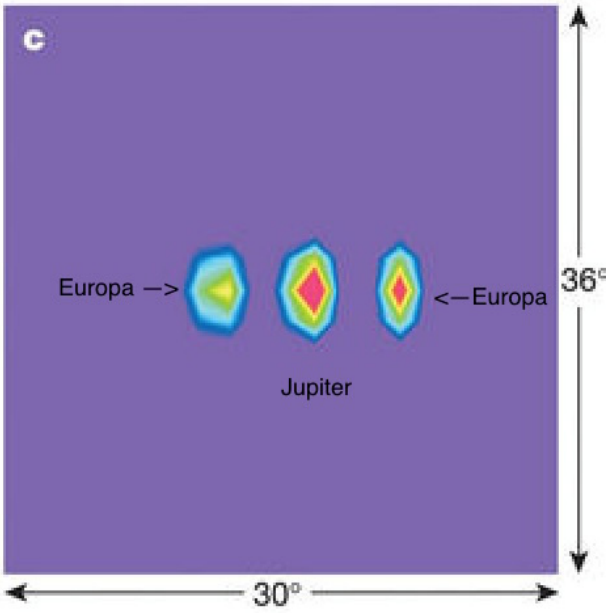

Figure MAPS-43. ENA image of the Europa torus, seen from the side, during the Cassini flyby of Jupiter in early 2001. The Europa torus appears on either side of Jupiter. The image was deconvolved for point sources and corrected for background. The intensity scale is linear.

Jupiter's radio emissions

The distant observations that Cassin made along the dusk flank of Jupiter's magnetosphere were well adapted to the study of the complex zoo of Jupiter's magnetospheric radio emissions, nicely covered by the Kronos receiver of RPWS, an example of which is given in Figure MAPS-44. An early overview is given in [Lecacheux 2001]. The intensity spectrum of all Jovian radio components was

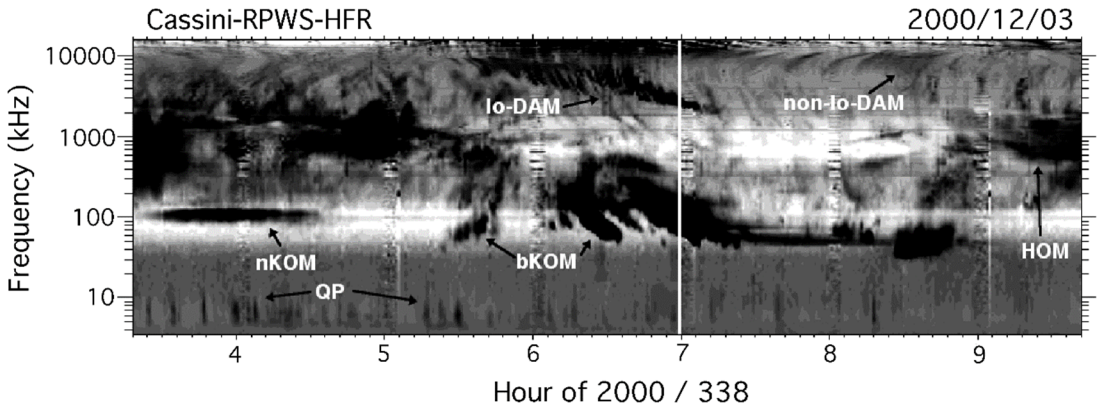

Figure MAPS-44. Jovian low-frequency radio emissions detected on December 3, 2000, by the RPWS experiment onboard Cassini approaching Jupiter. Frequency range is 3.5 kHz to 16.1 MHz. The Io-induced decameter emission (Io-DAM) appears here down to about 2 MHz, while weaker Io-independent (non-Io-DAM) arcs merge with the hectometer component (HOM) detected down to ~400 kHz. The auroral broadband kilometer component (bKOM) is detected down to ~40 kHz. The narrowband emission (nKOM) about 100 kHz is generated at or near the plasma frequency f_{pe} in Io's torus. The quasi-periodic (QP) bursts, spaced by 5 to > 15 min, are detected in the ~5 to 20 kHz range. Distance to Jupiter was 383 R_J (2.7×10^7 km) at the time of this observation.

accurately measured [Zarka et al. 2004] through calibration on the galactic background and Nançay observations, demonstrating in particular the absence of peak at 10 MHz in the decameter spectrum. The beaming of the decametric (DAM) and hectometric (HOM) components (a widely opened hollow cone of a few degrees thickness) were measured via two-point Cassini-Wind measurements [Kaiser et al. 2000] as well as frequency-longitude statistics and modelling [Imai et al. 2011a, 2011b, 2008]. The HOM low-frequency cutoff measured by Ulysses and Cassini provided constraints of its source location, in the outer regions of the Io plasma torus [Zarka et al. 2001].

The 6-month series of continuous homogeneous measurements provided unique measurements of time variations of the radio emission. Burst of auroral (non-Io) DAM emission were found to reoccur at a period slightly longer than the system III rotation period [Panchenko et al. 2013, 2010; Panchenko and Rucker 2011]. Gurnett et al. [2002] found from Cassini and Galileo observations that Jupiter's auroral radio and UV emissions were triggered by interplanetary shocks inducing magnetospheric compressions, in disagreement with theoretical predictions [Southwood and Kivelson 2001]. Hess et al. [2014] reconciled these views by a finer analysis of dawn and dusk radio emissions seen by Cassini, Galileo and Nançay, only dusk emissions being driven by both compressions and dilatations of the magnetosphere. They also used radio observations to deduce the subcorotation velocity of the magnetospheric plasma. Clarke et al. [2009] compared the effect of solar wind compressions on radio and UV aurora at Jupiter and Saturn, and found a weaker effect at Jupiter. Radio (non-Io-DAM, HOM and bKOM) and UV comparisons are used quite systematically in the study of Jupiter's aurora [Clarke et al. 2005, 2004; Pryor et al. 2005]. Comparison of Galileo/Jupiter and Cassini/Saturn observations also revealed similar energetic events where auroral radio intensifications are related to centrifugal plasma ejections, from the Io torus at Jupiter and from the equatorial plasma sheet at Saturn [Louarn et al. 2007].

Cassini, Galileo and Voyager radio observations were used to try to demonstrate the influence of satellites other than Io on DAM emissions. Marginal results were obtained statistically [Hospodarsky et al. 2001a], whereas clear evidence was obtained for Europa and Ganymede by comparison of observations with modelled dynamic spectra [Louis et al. 2017].

Fast recording modes of RPWS (spectral and waveform) allowed us to characterize the fine structure of Jovian radio emissions in the kilometer (bKOM) to decameter range [Kurth et al. 2001a; Lecacheux et al. 2001], including zebra-like patterns in the bKOM emission. Those were tentatively interpreted by bubble-like plasma inhomogeneities [Farrell et al. 2004] or the double plasma resonance mechanism involving ion cyclotron waves [Zlotnik et al. 2016]. Similar patterns have been observed at decameter wavelengths [Panchenko et al. 2018a, 2018b].

At the very low-frequency end of the radio spectrum (below a few 10 s of kHz), Cassini together with Ulysses and Galileo characterized the Jovian quasi-periodic bursts [Kaiser et al. 2004, 2001]. Stereoscopic observations demonstrated their strobe-like behavior and wide beaming [Hospodarsky et al. 2004], and direction-finding techniques localized their sources at high latitude regions of the magnetopause, implying complex propagation [Hospodarsky et al. 2004; Kimura et al. 2012]. Quasi-periodic (QP) bursts were tentatively related to the so-called Jovian anomalous continuum radiation [Ye et al. 2012]. Propagation of radio waves near the edges of the Io plasma torus were shown to generate the HOM attenuation lane, an intensity gap oscillating between ~1 and ~3 MHz, described by Boudjada et al. [2011] and modeled by Menietti et al. [2003] and Imai et al. [2015]. Occultations of Jovian radio emissions were used to probe the Io plasma torus [Boudjada et al. 2014].

Analysis of local low-frequency plasma waves recorded by RPWS was used to study the Jovian dust flank magnetopause and bow shock [Kurth et al. 2002; Szego et al. 2003], magnetosheath [Bebesi et al. 2011, 2010] and pre-shock [Szego et al. 2006]. The magnetopause was found to be in the process of being compressed by a solar wind pressure increase at the time of the Cassini flyby [Kurth et al. 2002]. Langmuir waves were detected upstream of the bow shock, and their level compared with that at other planets: the ratio of the energy density of the waves electric field to the plasma was found to increase with distance from the Sun [Hospodarsky et al. 2006].

Observations of Jupiter radio emissions were used to calibrate the Direction-Finding (actually Gonio-Polarimetric) capability of RPWS/Kronos [Vogl et al. 2004, 2001], which proved extremely successful at Saturn. Early use of this directional capability permitted to check the origin of lightning-like signals observed in Cassini's inbound leg to Saturn, which proved to be Jovian radio bursts [Fischer et al. 2006].

Overall, the radio observations made by the Cassini RPWS experiment were very successful at Jupiter. The obtained results were reported in several review papers about comparisons of radio waves [Zarka 2004, 2000; Zarka and Kurth 2005; de Pater and Kurth 2007; Rucker et al. 2014] and plasma waves [Hospodarsky et al. 2012] at the magnetized planets, as well as in reviews about auroras [Badman et al. 2015], magnetospheric processes [Blanc et al. 2002; Seki et al. 2015], or dust detection [Meyer-Vernet et al. 2017]. They greatly helped to prepare the magnetospheric measurements of the Juno mission in Jovian polar orbit [Bagenal et al. 2017].

Venus

Cassini made two very close gravity-assist flybys of Venus in route to Saturn. The first of the two flybys occurred on April 26, 1998, and the second occurred 14 months later on June 24. 1999. During the Venus flybys, the RPWS instrument conducted a search for high-frequency (0.125 to 16 MHz) radio impulses from Venus lightning. Despite the excellent sensitivity of the high-frequency RPWS receiver (down to the cosmic background), no impulses were detected [Gurnett et al. 2001]. During a subsequent close gravity-assist flyby of Earth on August 18, 1999, radio signals from lightning were observed essentially continuously at all radial distances inside of about 14 Earth radii, with maximum occurrence rates up to about 30 pulses per minute. These radio measurements made at Earth by Cassini are characteristic of terrestrial lightning and are commonly observed. The clear detection at Earth and the non-detection at Venus indicate that if lightning exists in the atmosphere of Venus, it is either extremely rare or is much weaker and at much lower frequencies than terrestrial lightning.

Earth

Cassini executed a flyby of Earth only 54 days after the second Venus encounter on August 18, 1999 in order to gain sufficient energy to continue its planned trajectory to Saturn. Although the principle purpose for the flyby was related to orbital mechanics, the flyby also offered an important opportunity for the Cassini MAPS instruments to operate in a well characterized magnetosphere. Operating the instruments in the Earth's magnetosphere allowed the MAPS teams to test planned operation modes and capabilities and to further characterize instrument performance in a planetary magnetosphere nearly five years prior to arrival at Saturn. Although the principle purpose of operating the MAPS instrument during the swift flyby of Earth was for calibration and other operational purposes, measurements made during flyby of Earth provided interesting scientific results [Burton et al. 2001; Kurth et al. 2001b; Lagg et al. 2001; Rymer et al. 2001; Southwood et al. 2001].

Figure MAPS-45, from Burton et al. [2001], shows the trajectory of the Cassini spacecraft during its encounter with Earth. The trajectory brings Cassini into the magnetosphere just past noon local time and carries it down the magnetotail in the post-midnight sector. Closest approach to Earth was just under 1200 km and was at a high rate of speed (~9 Earth radii per hour). The quick passage of the spacecraft through the magnetosphere provided a snapshot of the Earth's magnetosphere on a uniquely short timescale. In addition, Cassini's unique trajectory allowed near-continuous observations covering a range of distances down the magnetotail for the first time. Previous mission to the magnetotail (IMP 6, ISEE 1, ISEE 3, and Geotail), effectively made observations in the lobe at a single downtail distance due to their bound orbits. As Cassini flew by Earth, MAPS instruments were able to identify each of the typical magnetospheric boundaries and regions including the bow shock, magnetosheath, magnetopause, radiation belts, plasmasphere, plasma sheet, lobes, and crossings of the tail magnetopause [Burton et al. 2001; Kurth et al. 2001b; Lagg et al. 2001; Rymer et al. 2001; Southwood et al. 2001].

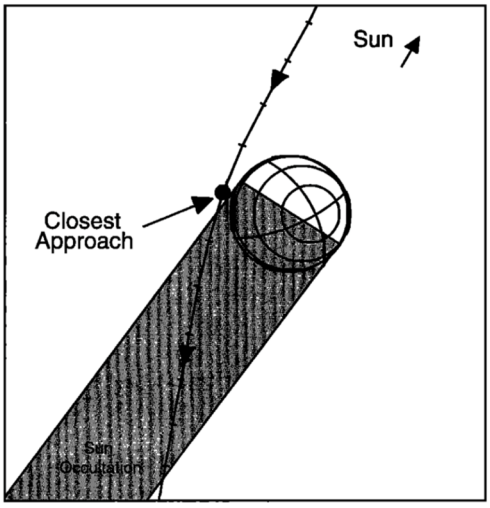

Figure MAPS-45. Trajectory of the Cassini spacecraft during it flyby of Earth on August 18, 1999. Reproduced from Burton et al. [2001] Figure 4.

During the Earth flyby the CAPS ELS sensor collected almost 9-hours of data in the Earth's magnetosphere and almost 10-hours of solar wind data upstream of the Earth. As noted above, CAPS, along with other MAPS instruments, sampled many plasma regions of the magnetosphere including electrons in the solar wind, bow shock, magnetosheath, magnetopause, radiation belts, plasmasphere, plasma sheet, lobes, and during crossings of the tail magnetopause. CAPS measurements were consistent with previous observations with a few exceptions and allowed the CAPS sensor to prepare for future operations at Saturn [Rymer et al. 2001]. In addition to anticipated results, CAPS found evidence of a low-energy field-aligned beam in the plasma sheet [Abel et al. 2001]. Bidirectional electrons were measured in the northern magnetotail lobe and were consistent with previous studies. However, measurements showed that was believed to be the first observations of a returning electron population in the magnetosheath. Bidirectional electrons were observed up to 0.02 keV, while at higher energies only unidirectional electrons were observed. The low energy of the returning electrons arises as a result of the electron populations' passage through the magnetopause twice and losses due to precipitation [Abel et al. 2001]. CAPS also found evidence of asymmetry on the dayside and nightside plasmapause position.

During the Earth flyby, the magnetometer performed important test and was able to make fairly original observations. One of the most important results of the Earth flyby for the magnetometer team was the testing of the helium magnetometer operating in the scalar mode and measuring the magnetic field magnitude with extremely high accuracy. Similar scalar mode measurements would be very important at Saturn for determining Saturn's intrinsic field, the near-Earth flyby provided a unique opportunity to test the magnetometer before arrival at Saturn [Smith et al. 2001]. In addition, the magnetometer observed what appeared to be interchange motions on the nightside outbound pass. Inbound, high resolution measurements of the whistler waves in the electron foreshock were reported [Southwood et al. 2001; Tsurutani et al. 2001].

Another important result of the Earth flyby was the large, international campaign of data gathering that was carried out on behalf of the magnetometer team by the Radio and Space Plasma Physics Group of the University of Leicester, United Kingdom [Khan et al. 2001]. Data obtained from various sources, together with the Cassini data, showed that during Cassini's outbound passage through the geomagnetic tail the magnetosphere underwent two complete classic substorm cycles and the data obtained by the fields and particles instruments on board Cassini confirmed that the flyby took place when the Earth's magnetosphere was generally in a disturbed state [Khan et al. 2001]. During the tail passage, RPWS observed a marked increase in the integrated auroral kilometric radiation power while at the same time CAPS and MIMI also saw evidence of these two substorm events in their data [Kurth et al. 2001b; Lagg et al. 2001; Rymer et al. 2001].

Finally, the RPWS instrument was able to make several different investigations to study Earth's magnetosphere and to test its capabilities in different modes. Figure MAPS-46 shows an overview of the RPWS observations during the Earth flyby. As one would expect, the RPWS observed broadband electrostatic waves at the bow shock, electron cyclotron harmonics and whistler mode chorus in the outer radiation belts and emissions between the plasma frequency and upper hybrid frequency in the ionosphere. Evidence for electron phase space holes was found in the near-Earth plasma sheet. At higher frequencies auroral kilometric radiation was observed on

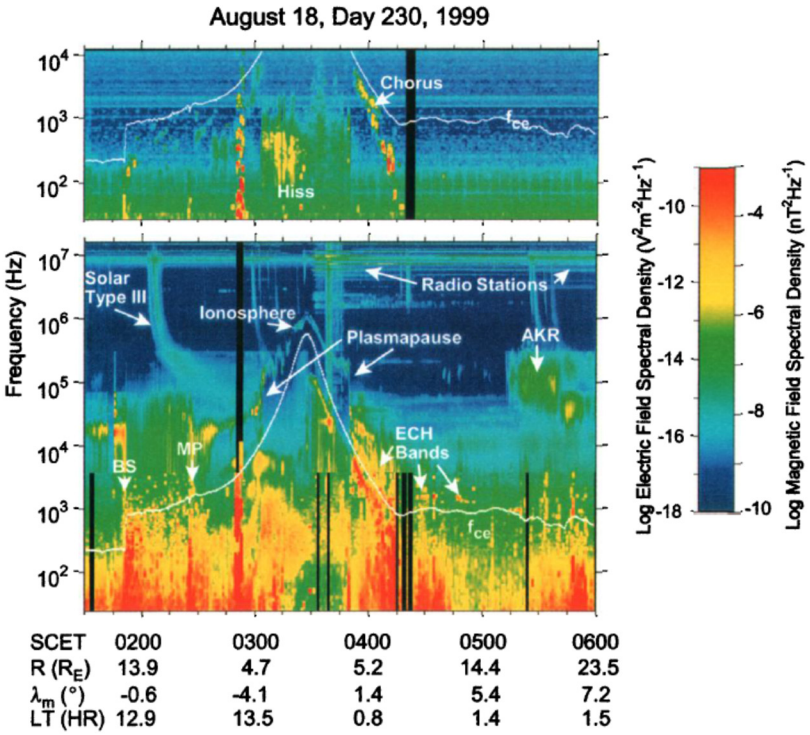

Figure MAPS-46. An overview of RPWS observations of the Earth flyby with magnetic fields shown in the top panel and electric fields below. The white trace is the electron cyclotron frequency f_{ce} derived from |B|. BS refers to the bow shock, MP refers to the magnetopause, ECH refers to electron cyclotron harmonics, and AKR refers to auroral kilometric radiation.

the night side indicating a series of auroral substorms and fixed frequency narrowband lines from man-made terrestrial radio stations were observed. Even Jovian hectometric radiation was observed from a position far downstream from Earth.

The RPWS instruments used a number of techniques to determine the plasma density from different wave excitations. The electron plasma frequency and upper hybrid resonance frequency are characteristic frequencies of the plasma dependent on the electron density. RPWS also includes a Langmuir probe that can determine the electron density and temperature. Finally, a relaxation sounder was used to stimulate the plasma frequency.

Another feature of the RPWS instrument that was tested during the Earth flyby was the capability of determining the wave normal angle of whistler mode waves using 5-channel waveform (WFR) measurements of three magnetic and two electric sensors. Hospodarsky et al. [2001b] used the WFR measurements to examine the propagation characteristics of a lightning whistler, chorus, and electromagnetic emissions in the magnetosheath, presumably lion roars.

Hospodarsky et al. [2001b] determined that the whistler analyzed was also detected at Palmer Station in Antarctica. The chorus waves were observed near the magnetic equator and appeared to reverse their direction of propagation at the equator, consistently propagating away from the equator where it is assumed the chorus source is located. The lion roars were found to consistently propagate nearly along the magnetic field but varied from burst to burst with some propagating near parallel and others near antiparallel to the field, suggesting multiple sources.

Cassini detected intense, fixed frequency emissions at close range to Earth in the frequency range above about 1 MHz that are attributed to man-made radio transmissions. Fischer and Rucker [2006] studied the occurrence of these in detail and demonstrated that most of the emissions could be identified with shortwave radio bands. A few brief detections of scientific transmitters include the High-frequency Active Auroral Research Program (HAARP) and the Russian SURA station, see also Tokarev et al. [2006]. Fischer and Rucker [2006] point out an interesting quiet period when Cassini was near closest approach over the Pacific Ocean where a combination of the rarity of transmitters in this location and ionospheric propagation characteristics effectively shielded Cassini from the radio transmission for a period of about 20 minutes.

ACRONYMS

Note: For a complete list of Acronyms, refer to Cassini Acronyms – Attachment A.

amu	atomic mass unit
AO	Announcement of Opportunity
AU	astronomical unit
bKOM	broadband kilometer
CA	closest approach
CAPS	Cassini Plasma Spectrometer
CHEMS	Charge-Energy-Mass Spectrometer
CRAND	Cosmic Ray Albedo Neutron Decay
DAM	decametric
DOY	day of year
DSMC	Direct Simulation Monte Carlo
DWG	Discipline Working Group
ELS	electron spectrometer
ENA	energetic neutral atom
EUV	extreme ultraviolet
FUV	far ultraviolet
GCR	Galactic Cosmic Ray
GDF	Globally Distributed Flux
HAARP	High-frequency Active Auroral Research Program
HCN	hydrogen cyanide
HOM	hectometric
HST	Hubble Space Telescope
IBEX	Interstellar Boundary Explorer
IBS	Ion Beam Spectrometer
IDS	Interdisciplinary Scientist
IMF	interplanetary magnetic field
IMS	Ion Mass Spectrometer
INCA	Ion and Neutral Camera
INMS	Ion and Neutral Mass Spectrometer
ISMF	interstellar magnetic field frame
ISS	Imaging Science Subsystem
K-H	Kelvin-Helmholtz
LECP	Low Energy Charged Particle
LEMMS	Low Energy Magnetospheric Measurement System
LFE	low frequency extension
LISM	Local Interstellar Medium
LLBL	low-latitude boundary layer

LOS	line-of-sight
LP	Langmuir Probe
LT	local time
MAG	Magnetometer
MAPS	Magnetospheres and Plasma Science
MHD	magnetohydrodynamic
MIMI	Magnetospheric Imaging Instrument
NB	narrowband
NIST	National Institute of Standards and Technology
OSI	open source ion
PLS	plasma spectrometer
PPO	planetary period oscillation
PRA	Planetary Radio Astronomy
PUI	pick-up ions
QP	quasi-periodic
RCM	Rice Convection Model
RPC	ring plasma cavity
RPWS	Radio and Plasma Wave Science
RS	Saturn radii
SCET	spacecraft event time
SED	Saturn electrostatic discharges
SEP	solar energetic particle
SKR	Saturn's kilometric radiation
SOI	Saturn Orbit Insertion
TOF	time-of-flight
ULF	ultra-low frequency
UT	universal time
UV	ultraviolet
UVIS	Ultraviolet Imaging Spectrograph
VIMS	Visual and Infrared Imaging Spectrometer
VLF	very low frequency
WFR	waveform

REFERENCES

Disclaimer: The partial list of references below correspond with in-text references indicated in this report. For all other Cassini references, refer to Attachment B – References & Bibliographies; Attachment C – Cassini Science Bibliographies; the sections entitled References contributed by individual Cassini instrument and discipline teams located in Volume 1 Sections 3.1 and 3.2 Science Results; and other resources outside of the Cassini Final Mission Report.

Abel, G., A. Coates, A. Rymer, D. Linder, M. Thomsen, D. Young, M. Dougherty, (2001), Cassini plasma spectrometer observations of bidirectional lobe electrons during the Earth flyby, August 18, 1999, Journal of Geophysical Research: Space Physics, 106, no. A12, pp. 30199-30208.

Achilleos, N., C. S. Arridge, C. Bertucci, P. Guio, N. Romanelli, N. Sergis, (2014), A combined model of pressure variations in Titan's plasma environment, Geophysical Research Letters 41 (24), 8730-8735, doi: 10.1002/2014GL061747.

Achilleos, N., P. Guio, C. S. Arridge, (2010a), A model of force balance in Saturn's magnetodisc, Monthly Notices of the Royal Astronomical Society, 401(4):2349–2371, doi: 10.1111/j.1365-2966.2009.15865.x.

Achilleos, N., P. Guio, C. S. Arridge, N. Sergis, R. J. Wilson, M. F. Thomsen, A. J. Coates, (2010b), Influence of hot plasma pressure on the global structure of Saturn's magnetodisk, Geophysical Research Letters, 37, L20201, doi: 10.1029/2010GL045159.

Achilleos, N., C. S. Arridge, C. Bertucci, C. M. Jackman, M. K. Dougherty, K. K. Khurana, C. T. Russell, (2008) Large-scale dynamics of Saturn's magnetopause: Observations by Cassini, Journal of Geophysical Research-Space Physics, 113 (A11), A11209, doi: 10.1029/2008ja013265.

Achilleos, N., C. Bertucci, C. T. Russell, G. B. Hospodarsky, A. M. Rymer, C. S. Arridge, M. E. Burton, M. K. Dougherty, S. Hendricks, E. J. Smith, B. T. Tsurutani, (2006), Orientation, location, and velocity of Saturn's bow shock: Initial results from the Cassini spacecraft, Journal of Geophysical Research, 111(A03201), doi: 10.1029/2005JA011297.

Ågren, K., N. J. T. Edberg, J. -E. Wahlund, (2012), Detection of negative ions in the deep ionosphere of Titan during the Cassini T70 flyby, Geophysical Research Letters, 39, L10201, doi: 10.1029/2012GL051714.

Ågren, K., D. J. Andrews, S. C. Buchert, A. J. Coates, S. W. H. Cowley, M. K. Dougherty, N. J. T. Edberg, P. Garnier, G. R. Lewis, R. Modolo, H. Opgenoorth, G. Provan, L. Rosenqvist, D. L. Talboys, J. E. Wahlund, A. Wellbrock, (2011), Detection of currents and associated electric fields in Titan's ionosphere from Cassini data, Journal of Geophysical Research-Space Physics 116, A04313, doi: 10.1029/2010ja016100.

Ågren, K., J. E. Wahlund, P. Garnier, R. Modolo, J. Cui, M. Galand, I. Müeller-Wodarg, (2009), On the ionospheric structure of Titan, Planetary and Space Science 57 (14-15), 1821-1827, doi: 10.1016/j.pss.2009.04.012.

Ågren, K., J. E. Wahlund, R. Modolo, D. Lummerzheim, M. Galand, I. Müeller-Wodarg, P. Canu, W. S. Kurth, T. E. Cravens, R. V. Yelle, J. H. Waite, A. J. Coates, G. R. Lewis, D. T. Young, C. Bertucci, M. K. Dougherty, (2007), On magnetospheric electron impact ionisation and dynamics in Titan's ram-side and polar ionosphere - a Cassini case study, Annales Geophysicae 25 (11), 2359-2369.

Alexeev, I. I., V. V. Kalegaev, E. S. Belenkaya, S. Y. Bobrovnikov, E. J. Bunce, S. W. H. Cowley, J. D. Nichols, (2006), A global magnetic model of Saturn's magnetosphere and a comparison with Cassini SOI data, Geophysical Research Letters 33 (8), L08101. doi: 10.1029/2006GL025896.

Allen, R. C., D. G. Mitchell, C. P. Paranicas, D. C. Hamilton, G. Clark, A. M. Rymer, S. K. Vines, E. C. Roelof, S. M. Krimigis, J. Vandegriff, (2018), Internal versus external sources of plasma at Saturn: Overview from magnetospheric imaging investigation/charge-energy-mass spectrometer data, Journal of Geophysical Research: Space Physics, submitted, doi: 10.1029/2018JA025262.

Amsif, A., J. Dandouras, E. C. Roelof, (1997), Modeling the production and the imaging of energetic neutral atoms from Titan's exosphere, Journal of Geophysical Research: Space Physics 102 (A10), 22169-22181, doi: 10.1029/97JA01597.

Andre, N., A. M. Persoon, J. Goldstein, J. L. Burch, P. Louarn, G. R. Lewis, A. M. Rymer, A. J. Coates, W. S. Kurth, E. C. Sittler, Jr., M. F. Thomsen, F. J. Crary, M. K. Dougherty, D. A. Gurnett, D. T. Young, (2007), Magnetic signatures of plasma-depleted flux tubes in the Saturnian inner magnetosphere, Geophysical Research Letters 34 (14), 14108, doi: 10.1029/2007GL030374.

Andre, N., M. K. Dougherty, C. T. Russell, J. S. Leisner, K. K. Khurana, (2005), Dynamics of the Saturnian inner magnetosphere: First inferences from the Cassini magnetometers about small-scale plasma transport in the magnetosphere, Geophysical Research Letters 32 (14), 14-06, doi: 10.1029/2005GL022643.

Andrews, D. J., S. W. H. Cowley, M. K. Dougherty, L. Lamy, G. Provan, D. J. Southwood, (2012), Planetary period oscillations in Saturn's magnetosphere: Evolution of magnetic oscillation properties from southern summer to post-equinox, Journal of Geophysical Research: Space Physics 117, A04224, doi: 10.1029/2011JA017444.

Andrews, D. J., B. Cecconi, S. W. H. Cowley, M. K. Dougherty, L. Lamy, G. Provan, P. Zarka, (2011), Planetary period oscillations in Saturn's magnetosphere: Evidence in magnetic field phase data for rotational modulation of Saturn kilometric radiation emissions, Journal of Geophysical Research: Space Physics 116, A09206, doi: 10.1029/2011ja016636.

Andrews, D. J., A. J. Coates, S. W. H. Cowley, M. K. Dougherty, L. Lamy, G. Provan, P. Zarka, (2010a), Magnetospheric period oscillations at Saturn: Comparison of equatorial and high-latitude magnetic field periods with north and south Saturn kilometric radiation periods, Journal of Geophysical Research: Space Physics, 115: 21 pp., doi: 10.1029/2010JA015666.

Andrews, D. J., S. W. H. Cowley, M. K. Dougherty, G. Provan, (2010b), Magnetic field oscillations near the planetary period in Saturn's equatorial magnetosphere: Variation of amplitude and

phase with radial distance and local time, Journal of Geophysical Research: Space Physics, 115: 28 pp., doi: 10.1029/2009JA014729.

Andrews, D. J., E. J. Bunce, S. W. H. Cowley, M. K. Dougherty, G. Provan, D. J. Southwood, (2008), Planetary period oscillations in Saturn's magnetosphere: Phase relation of equatorial magnetic field oscillations and Saturn kilometric radiation modulation, Journal of Geophysical Research: Space Physics 113 (A9), A09205, doi: 10.1029/2007ja012937.

Andriopoulou, M., E. Roussos, N. Krupp, C. Paranicas, M. Thomsen, S. Krimigis, M. K. Dougherty, K. H. Glassmeier, (2014), Spatial and temporal dependence of the convective electric field in Saturn's inner magnetosphere, Icarus 229, 57-70, doi: 10.1016/j.icarus.2013.10.028.

Andriopoulou, M., E. Roussos, N. Krupp, C. Paranicas, M. Thomsen, S. Krimigis, M. K. Dougherty, K. H. Glassmeier, (2012), A noon-to-midnight electric field and nightside dynamics in Saturn's inner magnetosphere, using microsignature observations, Icarus 220 (2), 503-513, doi: 10.1016/j.icarus.2012.05.010.

Anicich, V. G. and M. J. McEwan, (1997), Ion-molecule chemistry in Titan's ionosphere, Planetary and Space Science, 45 (8), 897-921.

Armstrong, T. P., S. Taherion, J. Manweiler, S. Krimigis, C. Paranicas, D. Mitchell, N. Krupp, (2009), Energetic ions trapped in Saturn's inner magnetosphere, Planetary and Space Science 57 (14-15),1723-1731, doi: 10.1016/j.pss.2009.03.008.

Arridge, C. S., J. M. Jasinski, N. Achilleos, Y. V. Bogdanova, E. J. Bunce, S. W. H. Cowley, A. N. Fazakerley, K. K. Khurana, L. Lamy, J. S. Leisner, E. Roussos, C. T. Russell, P. Zarka, A. J. Coates, M. K. Dougherty, G. H. Jones, S. M. Krimigis, N. Krupp, (2016a), Cassini observations of Saturn's southern polar cusp, Journal of Geophysical Research: Space Physics 121 (4), 3006-3030, doi: 10.1002/2015ja021957.

Arridge, C. S., J. P. Eastwood, C. M. Jackman, G. K. Poh, J. A. Slavin, M. F. Thomsen, N. Andre, X. Jia, A. Kidder, L. Lamy, A. Radioti, D. B. Reisenfeld, N. Sergis, M. Volwerk, A. P. Walsh, P. Zarka, A. J. Coates, M. K. Dougherty, (2016b), Cassini in situ observations of long-duration magnetic reconnection in Saturn's magnetotail, Nature Physics 12 (3), 268-271, doi: 10.1038/nphys3565.

Arridge, C. S., M. Kane, N. Sergis, K. K. Khurana, C. M. Jackman, (2015), Sources of local time asymmetries in magnetodiscs, Space Science Reviews 187 (1-4), 301-333, doi: 10.1007/s11214-015-0145-z.

Arridge, C. S., N. Andre, K. K. Khurana, C. T. Russell, S. W. H. Cowley, G. Provan, D. T. Young, (2011a), Periodic motion of Saturn's nightside plasma sheet, Journal of Geophysical Research: Space Physics, 116:22 pp., doi: 10.1029/2011JA016827.

Arridge, C. S., N. Achilleos, P. Guio, (2011b), Electric field variability and classifications of Titan's magnetoplasma environment, AnGeo Communicates, 29:1253–1258, doi: 10.5194/angeo-29-1253-2011.

Arridge, C. S., K. K. Khurana, C. T. Russell, D. J. Southwood, N. Achilleos, M. K. Dougherty, H. K. Leinweber, (2008a), Warping of Saturn's magnetospheric and magnetotail current

sheets, Journal of Geophysical Research: Space Physics, 113(A8), doi: 10.1029/2007JA012963.

Arridge, C. S., C. T. Russell, K. K. Khurana, N. Achilleos, S. W. H. Cowley, M. K. Dougherty, E. J. Bunce, (2008b), Saturn's magnetodisc current sheet, Journal of Geophysical Research: Space Physics, 113(A4):9 pp., doi: 10.1029/2007JA012540.

Arridge, C. S., N. Andre, N. Achilleos, K. K. Khurana, C. L. Bertucci, L. K. Gilbert, M. K. Dougherty, (2008c), Thermal electron periodicities at 20R_S in Saturn's magnetosphere, Geophysical Research Letters, 35(15):5 pp., doi: 10.1029/2008GL034132.

Arridge, C. S., C. T. Russell, K. K. Khurana, N. Achilleos, N. Andre, A. M. Rymer, M. K. Dougherty, A. J. Coates, (2007), Mass of Saturn's magnetodisc: Cassini observations, Geophysical Research Letters 34 (9), L09108.

Arridge, C. S., N. Achilleos, M. K. Dougherty, K. K., Khurana, C. T. Russell, (2006), Modeling the size and shape of Saturn's magnetopause with variable dynamic pressure, Journal of Geophysical Research: Space Physics, 111(A11):13 pp., doi: 10.1029/2005JA011574.

Backes, H., F. M. Neubauer, M. K. Dougherty, N. Achilleos, N. Andre, C. S. Arridge, C. Bertucci, G. H. Jones, K. K. Khurana, C. T. Russell, A. Wennmacher, (2005), Titan's magnetic field signature during the first Cassini encounter, Science 308 (5724), 992-995, doi: 10.1126/science.1109763.

Badman, S. V., G. Provan, E. J. Bunce, D. G. Mitchell, H. Melin, S. W. H. Cowley, A. Radioti, W. S. Kurth, W. R. Pryor, J. D. Nichols, S. L. Jinks, T. S. Stallard, R. H. Brown, K. H. Baines, M. K. Dougherty, (2016), Saturn's auroral morphology and field-aligned currents during a solar wind compression, Icarus 263, 83-93, doi: 10.1016/j.icarus.2014.11.014.

Badman, S.V., G. Branduardi-Raymont, M. Galand, S. L. Hess, N. Krupp, L. Lamy, H. Melin, C. Tao, (2015), Auroral processes at the giant planets: Energy deposition, emission mechanisms, morphology and spectra, Space Science Reviews, 187(1–4):99–179.

Badman, S. V., A. Masters, H. Hasegawa, M. Fujimoto, A. Radioti, D. Grodent, N. Sergis, M. K. Dougherty, A. J. Coates, (2013), Bursty magnetic reconnection at Saturn's magnetopause, Geophysical Research Letters 40 (6), 1027-1031, doi: 10.1002/grl.50199.

Badman, S. V., N. Achilleos, C. S. Arridge, K. H. Baines, R. H. Brown, E. J. Bunce, A. J. Coates, S. W. H. Cowley, M. K. Dougherty, M. Fujimoto, G. Hospodarsky, S. Kasahara, T. Kimura, H. Melin, D. G. Mitchell, T. Stallard, C. Tao, (2012a), Cassini observations of ion and electron beams at Saturn and their relationship to infrared auroral arcs, Journal of Geophysical Research: Space Physics 117, A01211, doi: 10.1029/2011JA017222.

Badman, S. V., D. J. Andrews, S. W. H. Cowley, L. Lamy, G. Provan, C. Tao, S. Kasahara, T. Kimura, M. Fujimoto, H. Melin, T. Stallard, R. H. Brown, K. H. Baines, (2012b), Rotational modulation and local time dependence of Saturn's infrared H_3^+ auroral intensity, Journal of Geophysical Research: Space Physics 117, doi: 10.1029/2012ja017990.

Badman, S. V., S. W. H. Cowley, B. Cecconi, L. Lamy, and P. Zarka, (2008), Relationship between solar wind corotating interaction regions and the phasing and intensity of Saturn kilometric radiation bursts, Annales Geophysicae, 26:3641–3651.

Badman, S. V., E. J. Bunce, J. T. Clarke, S. W. H. Cowley, J-C. Gérard, D. Grodent, S. E. Milan, (2005), Open flux estimates in Saturn's magnetosphere during the January 2004 Cassini-HST campaign, and implications for reconnection rates, Journal of Geophysical Research, 110(A11216), doi: 10.1029/2005JA011240.

Bagenal, F., A. Adriani, F. Allegrini, S. J. Bolton, B. Bonfond, E. J. Bunce, J. E. P. Connerney, S. W. H. Cowley, R. W. Ebert, G. R. Gladstone, C. J. Hansen, W. S. Kurth, S. M. Levin, B. H. Mauk, D. J. McComas, C. P. Paranicas, D. Santos-Costas, R. M. Thorne, P. Valek, J. H. Waite, P. Zarka, (2017), Magnetospheric science objectives of the Juno Mission, Space Science Reviews, 213, 219–287, doi: 10.1007/s11214-014-0036-8.

Bebesi, Z., K. Szego, A. Balogh, N. Krupp, G. Erdos, A. M. Rymer, G. R. Lewis, W. S. Kurth, D. T. Young, and M. K. Dougherty, (2011), Response to Comment on Slow-mode shock candidate in the Jovian magnetosheath, Planetary and Space Science 59 (5-6), 445-446, doi: 10.1016/j.pss.2010.10.007.

Bebesi, Z., K. Szego, A. Balogh, N. Krupp, G. Erdos, A. M. Rymer, G. R. Lewis, W. S. Kurth, D. T. Young, M. K. Dougherty, (2010), Slow-mode shock candidate in the Jovian magnetosheath, Planetary and Space Science 58 (5), 807-813. doi: 10.1016/j.pss.2009.12.008.

Belenkaya, E. S., V. V. Kalegaev, S. W. H. Cowley, G. Provan, M. S. Blokhina, O. G. Barinov, A. A. Kirillov, M. S. Grigoryan, (2016), Optimization of Saturn paraboloid magnetospheric field model parameters using Cassini equatorial magnetic field data, Annales Geophysicae 34 (7), 641-656, doi: 10.5194/angeo-34-641-2016.

Belenkaya, E. S., S. W. H. Cowley, C. J. Meredith, J. D. Nichols, V. V. Kalegaev, I. I. Alexeev, O. G. Barinov, W. O. Barinova, M. S. Blokhina, (2014), Magnetospheric magnetic field modelling for the 2011 and 2012 HST Saturn aurora campaigns – implications for auroral source regions, Annales Geophysicae, 32:689–704, doi: 10.5914/angeo-32-689-2014.

Belenkaya, E. S., S. W. H. Cowley, J. D. Nichols, M. S. Blokhina, V. V. Kalegaev, (2011), Magnetospheric mapping of the dayside UV auroral oval at Saturn using simultaneous HST images, Cassini IMF data, and a global magnetic field model, Annales Geophysicae 29 (7), 1233-1246, doi: 10.5194/angeo-29-1233-2011.

Belenkaya, E. S., I. I. Alexeev, M. S. Blokhina, E. J. Bunce, S. W. H. Cowley, J. D. Nichols, V. V. Kalegaev, V. G. Petrov, G. Provan, (2010), IMF dependence of Saturn's auroras: Modelling study of HST and Cassini data from 12-15 February 2008, Annales Geophysicae 28 (8), 1559-1570, doi: 10.5194/angeo-28-1559-2010.

Belenkaya, E. S., I. I. Alexeev, M. S. Blokhina, S. W. H. Cowley, S. V. Badman, V. V. Kalegaev, M. S. Grigoryan, (2007), IMF dependence of the open-closed field line boundary in Saturn's ionosphere, and its relation to the UV auroral oval observed by the Hubble Space Telescope, Annales Geophysicae 25 (5), 1215-1226.

Belenkaya, E. S., S. W. H. Cowley, I. I. Alexeev, (2006), Saturn's aurora in the January 2004 events, Annales Geophysicae 24 (6), 1649-1663.

Bell, J. M., H. Waite, J. Westlake, B. Magee, (2009), Simulating the 3-D structure of Titan's upper atmosphere, American Geophysical Union (AGU) Spring Meeting, abstract.

Ben-Jaffel, L. and I. Abbes, (2015), Helium abundance in giant planets and the local interstellar medium, In Journal of Physics: Conference Series, vol. 577, no. 1, p. 012003, Institute Of Physics Publishing, Bristol, United Kingdom.

Bertucci, C., D. C. Hamilton, W. S. Kurth, G. Hospodarsky, D. Mitchell, N. Sergis, N. J. T. Edberg, M. K. Dougherty, (2015), Titan's interaction with the supersonic solar wind, Geophysical Research Letters 42 (2), 193-200.

Bertucci, C., F. Duru, N. Edberg, M. Fraenz, C. Martinecz, K. Szego, O. Vaisberg, (2011), The induced magnetospheres of Mars, Venus, and Titan, Space Science Reviews 162 (1-4), 113-171, doi: 10.1007/s11214-011-9845-1.

Bertucci, C., N. Achilleos, M. K. Dougherty, R. Modolo, A. J. Coates, K. Szego, A. Masters, Y. Ma, F. M. Neubauer, P. Garnier, J. E. Wahlund, D. T. Young, (2008), The magnetic memory of Titan's ionized atmosphere, Science 321 (5895), 1475-1478. doi: 10.1126/science.1159780.

Bertucci, C., F. M. Neubauer, K. Szego, J. -E. Wahlund, A. J. Coates, M. K. Dougherty, D. T. Young, W. S. Kurth, (2007), Structure of Titan's mid-range magnetic tail: Cassini magnetometer observations during the T9 flyby, Geophysical Research Letters, 34(24):4 pp., doi: 10.1029/2007GL030865.

Bird, M. K., R. Dutta-Roy, S. W. Asmar, T. A. Rebold, (1997), Detection of Titan's ionosphere from Voyager 1 radio occultation observations, Icarus 130 (2), 426-436. doi: 10.1006/icar.1997.5831.

Blanc, M., S. Bolton, J. Bradley, M. Burton, T. E. Cravens, I. Dandouras, M. K. Dougherty, M. C. Festou, J. Feynman, R. E. Johnson, T. G. Gombosi, W. S. Kurth, P. C. Liewer, B. H. Mauk, S. Maurice, D. Mitchell, F. M. Neubauer, J. D. Richardson, D. E. Shemansky, E. C. Sittler, B. T. Tsurutani, P. H. Zarka, L. W. Esposito, E. Grun, D. A. Gurnett, A. J. Kliore, S. M. Krimigis, D. Southwood, J. H. Waite, D. T. Young, (2002), Magnetospheric and plasma science with Cassini-Huygens, Space Science Reviews 104 (1), 253-346. doi: 10.1023/A:1023605110711.

Boudjada, M. Y., P. H. M. Galopeau, S. Sawas, H. Lammer, (2014), Remote sensing of the Io torus plasma ribbon using natural radio occultation of the Jovian radio emission, Annales Geophysicae, 32, 1119–1128, doi: 10.5194/angeo-32-1119-2014.Boudjada, M. Y., P. H. M. Galopeau, H. O. Rucker, A. Lecacheux, N. Mebarki, W. Macher, and W. Voller, (2011), Morphological aspects of the attenuation bands associated with Jovian hectometric radiation, Journal of Geophysical Research-Space Physics 116, A11208, doi: 10.1029/2010JA016354.

Bouhram, M., R. E. Johnson, J.-J. Berthelier, J.-M. Illiano, R. L. Tokar, D. T. Young, F. J. Crary, (2006), A test-particle model of the atmosphere/ionosphere system of Saturn's main rings, Geophysical Research Letters, 33, L05106, doi: 10.1029/2005GL025011.

Bradley, T. J., S. W. H. Cowley, G. Provan, G. J. Hunt, E. J. Bunce, S. J. Wharton, I. I. Alexeev, E. S. Belenkaya, V. V. Kalegaev, M. K. Dougherty, (2018), Field-aligned currents in Saturn's nightside magnetosphere: Subcorotation and planetary period oscillation components

during northern spring, Journal of Geophysical Research: Space Physics, 123(5):3602–3636, doi: 10.1029/2017JA024885.

Brandt, P. C., K. Dialynas, I. Dandouras, D. G. Mitchell, P. Garnier, S. M. Krimigis, (2012), The distribution of Titan's high-altitude (out to 50,000 km) exosphere from energetic neutral atom (ENA) measurements by Cassini/INCA, Planetary and Space Science 60 (1), 107-114. doi: 10.1016/j.pss.2011.04.014.

Brown, W. L., W. M. Augustyniak, E. Simmons, K. J. Marcantonio, L. J. Lanzerotti, R. E. Johnson, J. W. Boring, C. T. Reimann, G. Foti, V. Pirronello, (1982), Erosion and molecule formation in condensed gas films by electronic energy loss of fast ions, Nuclear Instruments and Methods in Physics Research 198 (1), 1-8. doi: 10.1016/0167-5087(82)90043-6.

Bunce, E. J., D. C. Grodent, S. L. Jinks, D. J. Andrews, S. V. Badman, A. J. Coates, S. W. H. Cowley, M. K. Dougherty, W. S. Kurth, D. G. Mitchell, G. Provan, (2014), Cassini nightside observations of the oscillatory motion of Saturn's northern auroral oval, Journal of Geophysical Research-Space Physics 119 (5), 3528-3543. doi: 10.1002/2013ja019527.

Bunce, E. J., S. W. H. Cowley, D. L. Talboys, M. K. Dougherty, L. Lamy, W. S. Kurth, P. Schippers, B. Cecconi, P. Zarka, C. S. Arridge, A. J. Coates, (2010), Extraordinary field-aligned current signatures in Saturn's high-latitude magnetosphere: Analysis of Cassini data during Revolution 89, Journal of Geophysical Research-Space Physics 115, A10238. doi: 10.1029/2010ja015612.

Bunce, E. J., C. S. Arridge, S. W. H. Cowley, M. K. Dougherty, (2008), Magnetic field structure of Saturn's dayside magnetosphere and its mapping to the ionosphere: Results from ring current modeling, Journal of Geophysical Research-Space Physics 113 (A2), A02207.

Bunce, E. J., S. W. H. Cowley, I. I. Alexeev, C. S. Arridge, M. K. Dougherty, J. D. Nichols, C. T. Russell, (2007), Cassini observations of the variation of Saturn's ring current parameters with system size, Journal of Geophysical Research-Space Physics 112 (A10).

Bunce, E. J., S. W. H. Cowley, C. M. Jackman, J. T. Clarke, F. J. Crary, M. K. Dougherty, (2006), Cassini observations of the Interplanetary Medium Upstream of Saturn and their relation to the Hubble Space Telescope aurora data, Advances in Space Research, mercury, mars and saturn, 38(4):806–814, doi: 10.1016/j.asr.2005.08.005.

Bunce, E. J., S. W. H. Cowley, S. E. Milan, (2005), Interplanetary magnetic field control of Saturn's polar cusp aurora, Annales Geophysicae 23, 1405, doi: 10.5194/angeo-23-1405.

Buratti, B. J., P. C. Thomas, E. Roussos, C. Howett, M. Seiß, A. R. Hendrix, P. Helfenstein, R. H. Brown, R. N. Clark, T. Denk, (2019), Close Cassini flybys of Saturn's ring moons Pan, Daphnis, Atlas, Pandora, and Epimetheus, Science, 364(6445):eaat2349.

Burch, J. L., A. D. Dejong, J. Goldstein, D. T. Young, (2009), Periodicity in Saturn's magnetosphere: Plasma cam, Geophysical Research Letters, doi: 10.1029/2009GL039043.

Burch, J. L., J. Goldstein, T. W. Hill, D. T. Young, F. J. Crary, A. J. Coates, N. Andre, W. S. Kurth, E. C. Sittler Jr., (2005), Properties of local plasma injections in Saturn's magnetosphere, Geophysical Research Letters 32 (14), 14-02. doi: 10.1029/2005GL022611.

Burlaga, L. F. and N. F. Ness, (2016), Observations of the interstellar magnetic field in the outer heliosheath: Voyager 1, The Astrophysical Journal 829 (2), 134.

Burlaga, L. F., N. F. Ness, E. C. Stone, (2013), Magnetic field observations as Voyager 1 entered the heliosheath depletion region, Science 341 (6142), 147-150.

Burton, M. E., M. K. Dougherty, C. T. Russell, (2010), Saturn's internal planetary magnetic field, Geophysical Research Letters 37, L24105, doi: 10.1029/2010gl045148.

Burton, M. E., M. K. Dougherty, C. T. Russell, (2009), Model of Saturn's internal planetary magnetic field based on Cassini observations, Planetary and Space Science 57 (14-15), 1706-1713, doi: 10.1016/j.pss.2009.04.008.

Burton, M. E., B. Buratti, D. L. Matson, J. -P. Lebreton, (2001), The Cassini/Huygens Venus and Earth flybys: An overview of operations and results, Journal of Geophysical Research, 106(A12):30099–30107, doi: 10.1029/2001JA900088.

Cao, H. and D. J. Stevenson, (2017), Gravity and zonal flows of giant planets: From the Euler equation to the thermal wind equation, Journal of Geophysical Research-Planets 122 (4), 686-700, doi: 10.1002/2017je005272.

Cao, H., C. T. Russell, J. Wicht, U. R. Christensen, M. K. Dougherty, (2012), Saturn's high degree magnetic moments: Evidence for a unique planetary dynamo, Icarus, 221(1):388–394, doi: 10.1016/j.Icarus.2012.08.007.

Cao, H., C. T. Russell, U. R. Christensen, M. K. Dougherty, M. E. Burton, (2011), Saturn's very axisymmetric magnetic field: No detectable secular variation or tilt, Earth and Planetary Science Letters 304 (1-2), 22-28. doi: 10.1016/j.epsl.2011.02.035.

Carbary, J. F., D. G. Mitchell, P. Kollmann, N. Krupp, E. Roussos, (2017), Energetic electron periodicities during the Cassini Grand Finale, Journal of Geophysical Research-Space Physics 122 (12), 12229-12235, doi: 10.1002/2017ja024836.

Carbary, J. F. and D. G. Mitchell, (2017), Midnight flash model of ENA periodicities at Saturn, Journal of Geophysical Research: Space Physics, doi: 10.1002/2017JA024296.

Carbary, J. F., D. G. Mitchell, P. Kollmann, N. Krupp, E. Roussos, (2017), Energetic electron periodicities during the Cassini grand finale, Journal of Geophysical Research: Space Physics, 122, doi: 10.1002/2017JA024836.

Carbary, J. F., W. S. Kurth, D. G. Mitchell, (2016), Short periodicities in low-frequency plasma waves at Saturn, Journal of Geophysical Research: Space Physics, 121:6562–6572.

Carbary, J. F., N. Sergis, D. G. Mitchell, N. Krupp, (2015), Saturn's hinge parameter from Cassini magnetotail passes in 2013–2014, Journal of Geophysical Research: Space Physics, 120:4438.

Carbary, J. F., M. Kane, B. H. Mauk, S. M. Krimigis, (2014a), Using the kappa function to investigate hot plasmas in the magnetospheres of the giant planets, Journal of Geophysical Research, 119, doi: 10.1002/2014JA020324.

Carbary, J. F., D. G. Mitchell, P. C. Brandt, (2014b), Local time dependences of oxygen ENA periodicities at Saturn, Journal of Geophysical Research, 119, 2014JA020214.

Carbary, J. F., (2013), Wavy magnetodisk in Saturn's outer magnetosphere, Geophysical Research Letters, 40:5024.

Carbary, J. F., E. C. Roelof, D. G. Mitchell, D. C. Hamilton, (2013), Solar periodicity in energetic ions at Saturn, Journal of Geophysical Research, 118, doi: 10.1002/jgra.50282.

Carbary, J. F., N. Achilleos, C. S. Arridge, (2012), Statistical ring current of Saturn, Journal of Geophysical Research, 117(A06223).

Carbary, J. F., D. G. Mitchell, S. M. Krimigis, N. Krupp, (2011a), Post-equinox periodicities in Saturn's energetic electrons, Geophysical Research Letters, 28(L24104), 2011GL050259.

Carbary, J. F., C. Paranicas, D. G. Mitchell, S. M. Krimigis, N. Krupp, (2011b), Energetic electron spectra in Saturn's plasma sheet, Journal of Geophysical Research, 116(A07210).

Carbary, J. F., D. G. Mitchell, S. M. Krimigis, D. A. Gurnett, W. S. Kurth, (2010a), Phase relations between energetic neutral atom intensities and kilometric radio emissions at Saturn, Journal of Geophysical Research, 115(A01203).

Carbary, J. F., N. Achilleos, C. S. Arridge, K. K. Khurana, M. K. Dougherty, (2010b), Global configuration of Saturn's magnetic field derived from observations, Geophysical Research Letters, 37(L21806), doi: 10.1029/2010GL044622.

Carbary, J. F., D. C. Hamilton, S. P. Christon, D. G. Mitchell, S. M. Krimigis, (2010c), Longitude dependencies of energetic H+ and O+ at Saturn, Journal of Geophysical Research, 115(A07226), doi: 10.1029/2009JA015133.

Carbary, J. F., E. C. Roelof, D. G. Mitchell, S. M. Krimigis, N. Krupp, (2009a), Solar wind periodicity in energetic electrons at Saturn, Geophysical Research Letters, 36(L22104), doi: 10.1029/2009GL041086.

Carbary, J. F., D. G. Mitchell, N. Krupp, S. M. Krimigis, (2009b), L shell distribution of energetic electrons at Saturn, Journal of Geophysical Research, 114(A09210), doi: 10.1029/2009JA014341.

Carbary, J. F., D. G. Mitchell, P. Brandt, E. C. Reolof, S. M. Krimigis, (2008a), Track analysis of energetic neutral atom blobs at Saturn, Journal of Geophysical Research, 113(A01209), doi: 10.1029/2007JA012708.

Carbary, J. F., D. G. Mitchell, C. Paranicas, E. C. Roelof, S. M. Krimigis, (2008b), Direct observation of warping in the plasma sheet of Saturn, Geophysical Research Letters, 35(L24201), doi: 10.1029/2008GL035970.

Cassidy, T. A. and R. E. Johnson, (2010), Collisional spreading of Enceladus' neutral cloud, Icarus 209 (2), 696-703, doi: 10.1016/j.icarus.2010.04.010.

Caudal, G., (1986), A self-consistent model of Jupiter's magnetodisc including the effects of centrifugal force and pressure, Journal of Geophysical Research: Space Physics 91, no. A4, 4201-4221.

Cecconi, B. and P. Zarka, (2005), Model of a variable radio period for Saturn, Journal of Geophysical Research, 110, A12203, doi: 10.1029/2005JA011085.

Chen, Y., T. W. Hill, A. M. Rymer, R. J. Wilson, (2010), Rate of radial transport of plasma in Saturn's inner magnetosphere, Journal of Geophysical Research, 115(A10211), doi: 10.1029/2010JA015412.

Chen, Y. and T. W. Hill, (2008), Statistical analysis of injection dispersion events in Saturn's inner magnetosphere, Journal of Geophysical Research-Space Physics 113 (A7), A07215.

Christon, S. P., D. C. Hamilton, D. G. Mitchell, R. B. DiFabio, S. M. Krimigis (2014a), Suprathermal magnetospheric minor ions heavier than water at Saturn: Discovery of 28M+ seasonal variations, J. Geophys. Res., 119, 2014JA020010.

Christon, S.P., D. C. Hamilton, D. G. Mitchell, J. M. C. Plane, R. D. DiFabio, S. M. Krimigis, S. R. Nylund, A. Lui, (2014b), December. Discovery of suprathermal Fe+ in the magnetospheres of Earth and Saturn, American Geophysical Union (AGU) Fall Meeting, abstract.

Christon, S. P., D. C. Hamilton, R. D. DiFabio, D. G. Mitchell, S. M. Krimigis, D. S. Jontof-Hutter, (2013), Saturn suprathermal O-2(+) and mass-28(+) molecular ions: Long-term seasonal and solar variation, Journal of Geophysical Research-Space Physics 118 (6), 3446-3462. doi: 10.1002/jgra.50383.

Clark, G., C. Paranicas, D. Santos-Costa, S. Livi, N. Krupp, D. G. Mitchell, E. Roussos, W. L. Tseng, (2014), Evolution of electron pitch angle distributions across Saturn's middle magnetospheric region from MIMI/LEMMS, Planetary and Space Science, 104:18–28, doi: 10.1016/pss.2014.07.004.

Clarke, J. T., J. Nichols, J. C. Gerard, D. Grodent, K. C. Hansen, W. Kurth, G. R. Gladstone, J. Duval, S. Wannawichian, E. Bunce, S. W. H. Cowley, F. Crary, M. Dougherty, L. Lamy, D. Mitchell, W. Pryor, K. Retherford, T. Stallard, B. Zieger, (2009), Response of Jupiter's and Saturn's auroral activity to the solar wind, Journal of Geophysical Research Space Physics 114 (A5), A05210, doi: 10.1029/2008ja013694.

Clarke, J. T., J. C. Gerard, D. Grodent, S. Wannawichian, J. Gustin, J. Connerney, F. Crary, M. Dougherty, W. Kurth, S. W. H. Cowley, E. J. Bunce, T. Hill, J. Kim, (2005), Morphological differences between Saturn's ultraviolet aurorae and those of Earth and Jupiter, Nature 433 (7027), 717-719, doi: 10.1038/nature03331.

Clarke, J. T., D. Grodent, S. W. H. Cowley, E. J. Bunce, P. Zarka, J. E. P. Connerney, T. Satoh, (2004), Jupiter's aurora, In Jupiter: the Planet, Satellites, and Magnetosphere, (eds.) F. Bagenal, W. McKinnon, T. Dowling, Cambridge University Press, Cambridge.

Clarke, K. E., D. J. Andrews, A. J. Coates, S. W. H. Cowley, A. Masters, (2010a), Magnetospheric period oscillations of Saturn's bow shock, Journal of Geophysical Research-Space Physics 115, A05202, doi: 10.1029/2009ja015164.

Clarke, K. E., D. J. Andrews, C. S. Arridge, A. J. Coates, S. W. H. Cowley, (2010b), Magnetopause oscillations near the planetary period at Saturn: Occurrence, phase, and amplitude, Journal of Geophysical Research, 115(A08209), doi: 10.1029/2009JA014745.

Clarke, K. E., N. Andre, D. J. Andrews, A. J. Coates, S. W. H. Cowley, M. K. Dougherty, D. M. Wright, (2006), Cassini observations of planetary-period oscillations of Saturn's magnetopause, Geophysical Research Letters, 33(23), doi: 10.1029/2006GL027821.

Coates, A. J., A. Wellbrock, J. H. Waite, G. H. Jones, (2015), A new upper limit to the field-aligned potential near Titan, Geophysical Research Letters 42 (12), 4676–4684, doi: 10.1002/2015GL064474.

Coates, A. J., A. Wellbrock, G. R. Lewis, C. S. Arridge, F. J. Crary, D. T. Young, M. F. Thomsen, D. B. Reisenfeld, E. C. Sittler Jr., R. E. Johnson, K. Szego, Z. Bebesi, G. H. Jones, (2012), Cassini in Titan's tail: CAPS observations of plasma escape, Journal of Geophysical Research, 117(A5), doi:10.1029/2012JA017595.

Coates, A. J., J. -E. Wahlund, K. Ågren, N. J. T. Edberg, J. Cui, A. Wellbrock, K. Szego, (2011), Recent results from Titan's ionosphere, Space Science Review, 162:85–211, doi: 10.1007/s11214-011-9826-4.

Coates, A. J., A. Wellbrock, G. R. Lewis, G. H.Jones, D. T. Young, F. J. Crary, J. H. Waite, R. E. Johnson, T. W. Hill, E. C. Sittler Jr., (2010), Negative ions at Titan and Enceladus: recent results, Faraday Discussion, 147(1):293–305, doi: 10.1039/C004700G.

Coates, A. J., A. Wellbrock, G. R. Lewis, G. H. Jones, D. T. Young, F. J. Crary, J. H. Waite Jr., (2009), Heavy negative ions in Titan's ionosphere: altitude and latitude dependence, Planetary and Space Science, 57(14–15):1866–1871, doi: 10.1016/j.pss.2009.05.009.

Coates, A.J ., F. J. Crary, G. R. Lewis, D. T. Young, J. H. Waite Jr., E. C. Sittler Jr., (2007), Discovery of heavy negative ions in Titan's ionosphere, Geophysical Research Letters, 34, L22103, doi: 10.1029/2007GL030978.

Connerney, J. E. P. and J. H. Waite, (1984), New model of Saturn's ionosphere with an influx of water from the rings, Nature 312 (5990), 136.

Connerney, J. E. P., (1981), The magnetic field of Jupiter: A generalized inverse approach, Journal of Geophysical Research: Space Physics, 86(A9):7679–7693, doi: 10.1029/JA086iA09p07679.

Cooper, N. J., C. D. Murray, S. Renner, (2017), F-ring objects, Cassini End of Mission, Project Science Group (PSG), September 16, 2017, Pasadena, California.

Cowley, S. W. H. and G. Provan, (2017), Planetary period modulations of Saturn's magnetotail current sheet during northern spring: Observations and modeling, Journal of Geophysical Research, 122:6049–6077, doi: 10.1002/2017JA023993.

Cowley, S. W. H., G. Provan, G. J. Hunt, C. M. Jackman, (2017), Planetary period modulations of Saturn's magnetotail current sheet: A simple illustrative mathematical model, Journal of Geophysical Research, 122:258–279, doi: 10.1002/2016JA023367.

Cowley, S. W. H. and G. Provan, (2016), Planetary period oscillations in Saturn's magnetosphere: Further comments on the relationship between post-equinox properties deduced from magnetic field and Saturn kilometric radiation measurements, Icarus, 272:258–276, doi: 10.1016/j.Icarus.2016.02.051.

Cowley, S. W. H. and G. Provan, (2015), Planetary period oscillations in Saturn's magnetosphere: Comments on the relation between post-equinox periods determined from magnetic field and SKR emission data, Annales Geophysicae, 33:901–912.

Cowley, S. W. H., J. D. Nichols, C. M. Jackman, (2015), Down-tail mass loss by plasmoids in Jupiter's and Saturn's magnetospheres, Journal of Geophysical Research-Space Physics 120 (8), 6347-6356, doi: 10.1002/2015ja021500.

Cowley, S. W. H. and G. Provan, (2013), Saturn's magnetospheric planetary period oscillations, neutral atmosphere circulation, and thunderstorm activity: Implications, or otherwise, for physical links, Journal of Geophysical Research, 118:7246–7261, doi: 10.1002/2013JA019200.

Cowley, S. W. H., C. S. Arridge, E. J. Bunce, J. T. Clarke, A. J. Coates, M. K. Dougherty, J. C. Gerard, D. Grodent, J. D. Nichols, D. L. Talboys, (2008), Auroral current systems in Saturn's magnetosphere: Comparison of theoretical models with Cassini and HST observations, Annales Geophysicae 26 (9), 2613-2630.

Cowley, S. W. H., D. M. Wright, E. J. Bunce, A. C. Carter, M. K. Dougherty, G. Giampieri, T. R. Robinson, (2006), Cassini observations of planetary-period magnetic field oscillations in Saturn's magnetosphere: Doppler shifts and phase motion, Geophysical Research Letters, 33(7):4 pp., doi: 10.1029/2005GL025522.

Cowley, S. W. H., S. V. Badman, E. J. Bunce, J. T. Clarke, J. C. Gérard, D. Grodent, C. M. Jackman, S. E. Milan, T. K. Yeoman, (2005), Reconnection in a rotation-dominated magnetosphere and its relation to Saturn's auroral dynamics, Journal of Geophysical Research, 110(A02201), doi: 10.1029/2004JA010796.

Cowley, S. W. H., E. J. Bunce, J. M. O'Rourke, (2004), A simple quantitative model of plasma flows and currents in Saturn's polar ionosphere, Journal of Geophysical Research Space Physics 109 (A5).

Crary, F. J., B. A. Magee, K. Mandt, J. H. Waite Jr., J. Westlake, D. T. Young, (2009), Heavy ions, temperatures and winds in Titan's ionosphere: Combined Cassini CAPS and INMS observations, Planetary and Space Science 57 (14-15), 1847-1856. doi: 10.1016/j.pss.2009.09.006.

Crary, F. J., J. T. Clarke, M. K. Dougherty, P. G. Hanton, K. C. Hansen, J. T. Steinberg, B. L. Barraclough, A. J. Coates, J. C. Gerard, D. Grodent, W. S. Kurth, D. G. Mitchell, A. M. Rymer, D. T. Young, (2005), Solar wind dynamic pressure and electric field as the main factors controlling Saturn's aurorae, Nature Volume 433 (no. 7027), 720-722. doi: 10.1038/nature03333.

Cravens, T. E., I. P. Robertson, J. H. Waite, R. V. Yelle, V. Vuitton, A. J. Coates, J.-E. Wahlund, K. Ågren, M. S. Richard, V. de La Haye, A. Wellbrock, F. M. Neubauer, (2009a), Model-data comparisons for Titan's nightside ionosphere, Icarus, 199:174–188, doi: 10.1016/j.icarus.2008.09.005.

Cravens, T. E., R. V. Yelle, J.-E. Wahlund, D. E. Shemansky, A. F. Nagy, (2009b), Composition and structure of the ionosphere and thermosphere, in Titan from Cassini-Huygens, (eds.) R. H. Brown, J.-P. Lebreton, J. H. Waite, Springer, Dordrecht, doi: 10.1007/978-1-420-9215-2_11, pp. 259-295.

Cravens, T. E., I. P. Robertson, S. A. Ledvina, D. Mitchell, S. M. Krimigis, J. H. Waite Jr., et al., (2008a), Energetic ion precipitation at Titan, Geophysical Research Letters, 35(3), doi: 10.1029/2007GL032451.

Cravens, T. E., I. P. Robertson, J. H. Waite Jr., R. V. Yelle, V. Vuitton, A. J. Coates, J. -E. Wahlund, K. Ågren, M. S. Richard, V. De La Haye, A. Wellbrock, F. N. Neubauer, (2008b),

Model-data comparisons for Titan's nightside ionosphere, Icarus, doi: 10.1016/j.icarus.2008.09.005.

Cravens, T. E., I. P. Robertson, J. H. Waite, W. T. Kasprzak, R. V. Yelle, V. Vuitton, J. Clark, J. G. Luhmann, S. A. Ledvina, R. L. McNutt, W. Ip, I. Müeller-Wodarg, J. Wahlund, A. J. Coates, (2006), Solar radiation and magnetospheric electron sources of the ionosphere of Titan: Model comparisons with Cassini data, American Geophysical Union (AGU) Fall Meeting, San Francisco, California, 11-15 Dec. 2006.

Cui, J., R. V. Yelle, V. Vuitton, J. H. Waite, W. T. Kasprzak, D. A. Gell, H. B. Niemann, I. C. F. Müller-Wodarg, N. Borggren, G. G. Fletcher, E. L. Patrick, E. Raaen, B. A. Magee, (2009), Analysis of Titan's neutral upper atmosphere from Cassini ion neutral mass spectrometer measurements, Icarus, 200:581–615, doi: 10.1016/j.icarus.2008.12.005.

Cui, J., R. V. Yelle, K. Volk, (2008), Distribution and escape of molecular hydrogen in Titan's thermosphere and exosphere, Journal of Geophysical Research, 113, E10004, doi: 10.1029/2007JE003032.

Dandouras, I., P. Garnier, D. G. Mitchell, E. C. Roelof, P. C. Brandt, N. Krupp, S. M. Krimigis, (2008), Titan's exosphere and its interaction with Saturn's magnetosphere, Philosophical Transactions of the Royal Society A: Mathematical, Physical and Engineering Sciences, 367(1889):743-752.

Dandouras, J. and A. Amsif, (1999), Production and imaging of energetic neutral atoms from Titan's exosphere: A 3-D model, Planetary and Space Science 47 (10), 1355-1369, doi: 10.1016/S0032-0633(99)00057-4.

De La Haye, V., J. H. Waite, E. Cravens, A. F. Nagy, R. E. Johnson, S. Lebonnois, I. P. Robertson, (2007a), Titan's corona: The contribution of exothermic chemistry, Icarus 191 (1), 236-250, doi: 10.1016/j.icarus.2007.04.031.

De La Haye, V., J. H. Waite, R. E. Johnson, R. V. Yelle, T. E. Cravens, J. G. Luhmann, W. T. Kasprzak, D. A. Gell, B. Magee, F. Leblanc, M. Michael, S. Jurac, I. P. Robertson, (2007b), Cassini ion and neutral mass spectrometer data in Titan's upper atmosphere and exosphere: Observation of a suprathermal corona, Journal of Geophysical Research-Space Physics 112 (A7), A07309, doi: 10.1029/2006JA012222.

de Pater, I, and W. S. Kurth, (2007), The solar system at radio wavelengths, In Encyclopedia of the Solar System, (eds.), L.-A. Adams McFadden, P. R. Weissman, T. V. Johnson, 695-718, San Diego, California, Academic Press/Elsevier.

Decker, R. B., S. M. Krimigis, E. C. Roelof, M. E. Hill, (2015), Recent particle measurements from Voyagers 1 and 2, Journal of Physics: Conference Series, vol. 577, doi: 10.1088/1742-6596/577/1/012006.

Decker, R. B., S. M. Krimigis, E. C. Roelof, M. E. Hill, T. P. Armstrong, G. Gloeckler, D. C. Hamilton, L. J. Lanzerotti, (2008), Mediation of the solar wind termination shock by non-thermal ions, Nature, 454, 67-70.

Decker, R. B., S. M. Krimigis, E. C. Roelof, M. E. Hill, T. P. Armstrong, G. Gloeckler, D. C. Hamilton, L. J. Lanzerotti, (2005), Voyager 1 in the foreshock, termination shock, and heliosheath, Science 309 (5743), 2020-2024.

- - - - - - - - - - - - - -

DeJong, A. D., J. L. Burch, J. Goldstein, A. J. Coates, D. T. Young, (2010), Low-energy electrons in Saturn's inner magnetosphere and their role in interchange injections, Journal of Geophysical Research-Space Physics 115, A10229, doi: 10.1029/2010ja015510.

Delamere, P. A., A. Otto, X. Ma, F. Bagenal, R. J. Wilson, (2015), Magnetic flux circulation in the rotationally driven giant magnetospheres, Journal of Geophysical Research: Space Physics 120, no. 6, 4229-4245, doi: 10.1002/2015JA021036

Delamere, P. A., R. J. Wilson, S. Eriksson, F. Bagenal, (2013), Magnetic signatures of Kelvin-Helmholtz vortices on Saturn's magnetopause: Global survey, Journal of Geophysical Research: Space Physics, 118, 393–404, doi: 10.1029/2012JA018197.

Desai, R. T., S. A. Taylor, L. H. Regoli, A. J. Coates, T. A. Nordheim, M. A. Cordiner, B. D. Teolis, M. F. Thomsen, R. E. Johnson, G. H. Jones, M. M. Cowee, J. H. Waite, (2018), Cassini CAPS identification of pickup ion compositions at Rhea, Geophysical Research Letters 45 (4), 1704-1712, doi: 10.1002/2017GL076588.

Desai, R. T., A. J. Coates, A. Wellbrock, V. Vuitton, F. J. Crary, D. Gonzalez-Caniulef, O. Shebanits, G. H. Jones, G. R. Lewis, J. H. Waite, M. Cordiner, S. A. Taylor, D. O. Kataria, J. E. Wahlund, N. J. T. Edberg, E. C. Sittler, (2017), Carbon chain anions and the growth of complex organic molecules in Titan's ionosphere, Astrophysical Journal Letters 844 (2), doi: 10.3847/2041-8213/aa7851.

Desch, M. D., G. Fischer, M. L. Kaiser, W. M. Farrell, W. S. Kurth, D. A. Gurnet, P. Zarka, A. Lecacheax, C. C. Porco, A. P. Ingersoll, U. Dyudina, (2006), Cassini RPWS and imaging observations of Saturn lightning, Planetary Radio Emissions VI: 6th International Workshop on Planetary and Solar Radio Emissions, 2005, Graz, Austria.

Dessler, A. J., (1985), Differential rotation of the magnetic fields of gaseous planets, Geophysical Research Letters 12 (5), 299-302.

Dialynas, K., E. Roussos, L. Regoli, C. P. Paranicas, S. M. Krimigis, M. Kane, D. G. Mitchell, D. C. Hamilton, N. Krupp, J. F. Carbary, (2018), Energetic ion moments and polytropic index in Saturn's magnetosphere using Cassini/MIMI measurements: A simple model based on *K*-Distribution functions, Journal of Geophysical Research: Space Physics 123, no. 10, 8066-8086.

Dialynas, K., S. M. Krimigis, D. G. Mitchell, R. B. Decker, E. C. Roelof, (2017a), The bubble-like shape of the heliosphere observed by Voyager and Cassini, Nature Astronomy, 1, 115.

Dialynas, K., S. M. Krimigis, D. G. Mitchell, R. B. Decker, E. C. Roelof, (2017b), Response times of Cassini/INCA > 5.2 keV ENAs and Voyager ions in the heliosheath over the solar cycle, Journal of Physics: Conference Series, 900(1).

Dialynas, K., S. M. Krimigis, D. G. Mitchell, E. C. Roelof, (2015), Energetic neutral atom (ENA) intensity gradients in the heliotail during year 2003, using Cassini/INCA measurements, Journal of Physics: Conference Series 577 (1), 12007-12016, doi: 10.1088/1742-6596/577/1/012007.

Dialynas, K., S. M. Krimigis, D. G. Mitchell, E. C. Roelof, R. B. Decker, (2013), A three-coordinate system (Ecliptic, Galactic, ISMF) spectral analysis of heliospheric ENA emissions using

Cassini/INCA measurements, Astrophysical Journal 778 (1), 40, doi: 10.1088/0004-637X/778/1/40.

Dialynas, K., S. M. Krimigis, D. G. Mitchell, D. C. Hamilton, N. Krupp, P. C. Brandt, (2009), Energetic ion spectral characteristics in the Saturnian magnetosphere using Cassini/MIMI measurements, Journal of Geophysical Research-Space Physics 114, A01212, doi: 10.1029/2008ja013761.

DiFabio, R. D., D. C. Hamilton, S. M. Krimigis, D. G. Mitchell, (2011), Long term time variations of the suprathermal ions in Saturn's magnetosphere, Geophysical Research Letters 38 (18), L18103, doi: 10.1029/2011GL048841.

Dong, Y., T. W. Hill, S. Y. Ye, (2015), Characteristics of ice grains in the Enceladus plume from Cassini observations, Journal of Geophysical Research-Space Physics 120 (2), 915-937, doi: 10.1002/2014ja020288.

Dougherty, M. K., H. Cao, K. K. Khurana, G. J. Hunt, G. Provan, S. Kellock, M. E. Burton, T. A. Burk, E. J. Bunce, S. W. H. Cowley, M. G. Kivelson, C. T. Russell, D. J. Southwood, (2018), Saturn's magnetic field revealed by the Cassini Grand Finale, Science 362 (6410), doi: 10.1126/science.aat5434.

Dougherty, M. K., K. K. Khurana, F. M. Neubauer, C. T. Russell, J. Saur, J. S. Leisner, M. E. Burton, (2006), Identification of a dynamic atmosphere at Enceladus with the Cassini magnetometer, Science 311 (5766), 1406-1409. doi: 10.1126/science.1120985.

Dougherty, M. K., N. Achilleos, N. Andre, C. S. Arridge, A. Balogh, C. Bertucci, B. T. Tsurutani, (2005), Cassini magnetometer observations during Saturn orbit insertion, Science, 307(5713):1266–1270, doi: 10.1126/science.1106098.

Drake, J. F., M. Swisdak, M. Opher, (2015), A model of the heliosphere with jets, The Astrophysical Journal Letters 808 (2), L44.

Dungey, J. W., (1965), The length of the magnetospheric tail, Journal of Geophysical Research 70 (7), 1753-1753, doi: 10.1029/JZ070i007p01753.

Dyudina, U. A., A. P. Ingersoll, S. P. Ewald, C. C. Porco, G. Fischer, W. S. Kurth, R. A. West, (2010), Detection of visible lightning on Saturn, Geophysical Research Letters 37, L09205. doi: 10.1029/2010gl043188.

Edberg, N. J. T., D. J. Andrews, O. Shebanits, K. Ågren, J.-E. Wahlund, H. J. Opgenoorth, T. E. Cravens, Z. Girazian, (2013a), Solar cycle modulation of Titan's ionosphere, Journal of Geophysical Research, 118, 5255–5264, doi: 10.1002/jgra.50463.

Edberg, N. J. T., D. J. Andrews, O. Shebanits, K. Ögren, J.-E. Wahlund, H. J. Opgenoorth, E. Roussos, P. Garnier, T. E. Cravens, S. V. Badman, R. Modolo, C. Bertucci, M. K. Dougherty, (2013b), Extreme densities in Titan's ionosphere during the T85 magnetosheath encounter, Geophysical Research Letters, 40, 2879–2883, doi: 10.1002/grl.50579.

Edberg, N. J. T., K. Ågren, J. E. Wahlund, M. W. Morooka, D. J. Andrews, S. W. H. Cowley, A. Wellbrock, A. J. Coates, C. Bertucci, M. K. Dougherty, (2011), Structured ionospheric outflow during the Cassini T55-T59 Titan flybys, Planetary and Space Science 59 (8), 788-797, doi: 10.1016/j.pss.2011.03.007.

Edberg, N. J. T., J. E. Wahlund, K. Ågren, M. W. Morooka, R. Modolo, C. Bertucci, M. K. Dougherty, (2010), Electron density and temperature measurements in the cold plasma environment of Titan: Implications for atmospheric escape, Geophysical Research Letters 37 (20), L20105, doi: 10.1029/2010GL044544.

Elrod, M. K., W. L. Tseng, A. K. Woodson, R. E. Johnson, (2014), Seasonal and radial trends in Saturn's thermal plasma between the main rings and Enceladus, Icarus 242:130-137, doi: 10.1016/j.icarus.2014.07.020.

Elrod, M. K., W. L. Tseng, R. J. Wilson, R. E. Johnson, (2012), Seasonal variations in Saturn's plasma between the main rings and Enceladus, Journal of Geophysical Research-Space Physics 117, A03207, doi: 10.1029/2011JA017332.

Fahr, H. J., (1986), Is the heliospheric interface submagnetosonic? Consequences for the LISM presence in the heliosphere, Advances in Space Research 6 (2), 13-25.

Farrell, W. M., W. S. Kurth, D. A. Gurnett, A. M. Persoon, R. J. MacDowall, (2017), Saturn's rings and associated ring plasma cavity: Evidence for slow ring erosion, Icarus, 292, 48–52, doi: 10.1016/j.icarus.2017.03.022.

Farrell, W. M., W. S. Kurth, D. A. Gurnett, R. E. Johnson, M. L. Kaiser, J. E. Wahlund, J. H. Waite Jr., (2009), Electron density dropout near Enceladus in the context of water-vapor and water-ice, Geophysical Research Letters 36, L10203, doi: 10.1029/2008gl037108.

Farrell, W. M., M. L. Kaiser, W. S. Kurth, M. D. Desch, D. A. Gurnett, G. B. Hospodarsky, and R. J. MacDowall, (2004), Remote sensing of possible plasma density bubbles in the inner Jovian dayside magnetosphere, Journal of Geophysical Research-Space Physics 109 (A9), 14, doi: 10.1029/2003JA010130.

Felici, M., C. S. Arridge, A. J. Coates, S. V. Badman, M. K. Dougherty, C. M. Jackman, W. S. Kurth, H. Melin, D. G. Mitchell, D. B. Reisenfeld, N. Sergis, (2016), Cassini observations of ionospheric plasma in Saturn's magnetotail lobes, Journal of Geophysical Research-Space Physics 121 (1), 338-357, doi: 10.1002/2015ja021648.

Feyerabend, M., S. Simon, F. M. Neubauer, U. Motschmann, C. Bertucci, N. J. T. Edberg, G. B. Hospodarsky, W. S. Kurth, (2016), Hybrid simulation of Titan's interaction with the supersonic solar wind during Cassini's T96 flyby, Geophysical Research Letters 43 (1), 35-42.

Fischer, G., S.-Y. Ye, J. B. Groene, A. P. Ingersoll, K. Sayanagi, J. D. Menietti, W. S. Kurth, D. A. Gurnett, (2014), A possible influence of the Great White Spot on Saturn kilometric radiation periodicity, Annales Geophysicae, 32, 1463–1476, doi: 10.5194/angeo-32-1463-2014.

Fischer, G., W. S. Kurth, D. A. Gurnett, P. Zarka, U. A. Dyudina, A. P. Ingersoll, S. P. Ewald, C. C. Porco, A. Wesley, C. Go, M. Delcroix, (2011a), A giant thunderstorm on Saturn, Nature, 475, 75–77, doi: 10.1038/nature10205.

Fischer, G., U. A. Dyudina, W. S. Kurth, D. A. Gurnett, P. Zarka, T. Barry, M. Delcroix, C. Go, D. Peach, R. Vandebergh, A. Wesley, (2011b), Overview of Saturn lightning observations, in Planetary Radio Emissions VII, (eds.) H. O. Rucker, W. S. Kurth, P. Louarn, G. Fischer, Austrian Academy of Sciences, Vienna, Austria, pp. 135–144.

Fischer, G., D. A. Gurnett, Y. Yair, (2011c), Extraterrestrial lightning and its past and future investigation, lightning; properties, formation and types, (eds.) M. D. Wood, NOVA Science Publishers, Inc., New York.

Fischer, G., W. Macher, D. A. Gurnett, M. D. Desch, A. Lecacheux, P. Zarka, W. S. Kurth, M. L. Kaiser, (2006), The discrimination between Jovian radio emissions and Saturn electrostatic discharges, Geophysical Research Letters, 33, L21201, doi: 10.1029/2006GL026766.

Fischer, G. and H. O. Rucker, (2006), Man-made radio emissions recorded by Cassini/RPWS during Earth flyby, Planetary Radio Emissions VI, Proceedings from the 6th International Workshop on Planetary and Solar Radio Emissions, April 20-22, 2005, Graz, Austria.

Fisk, L. A. and G. Gloeckler, (2008), Acceleration of suprathermal tails in the solar wind, The Astrophysical Journal 686 (2), 1466.

Fleshman, B. L., P. A. Delamere, F. Bagenal, T. Cassidy, (2013), A 1-D model of physical chemistry in Saturn's inner magnetosphere, Journal of Geophysical Research-Planets 118 (8), 1567-1581, doi: 10.1002/jgre.20106.

Fox, J. L. and R. V. Yelle, (1997), Hydrocarbon ions in the ionosphere of Titan, Geophysical Research Letters 24 (17), 2179-2182.

Fuselier, S. A., R. Frahm, W. S. Lewis, A. Masters, J. Mukherjee, S. M. Petrinec, I. J. Sillanpää, (2014), The location of magnetic reconnection at Saturn's magnetopause: A comparison with Earth, Journal of Geophysical Research-Space Physics 119 (4), 2563-2578, doi: 10.1002/2013ja019684.

Galand, M., A. J. Coates, T. E. Cravens, J. -E. Wahlund, (2014), Titan's ionosphere, in Titan: Interior, Surface, Atmosphere, and Space Environment, Chapter 11, (eds.) I. Müller-Wodarg, C. A. Griffith, E. Lellouch, T. E. Cravens, Cambridge University Press, pp. 376–419.

Garnier, P., M. K. G. Holmberg, J. E. Wahlund, G. R. Lewis, P. Schippers, A. Coates, D. A. Gurnett, J. H. Waite, I. Dandouras, (2014), Deriving the characteristics of warm electrons (100-500 eV) in the magnetosphere of Saturn with the Cassini Langmuir probe, Planetary and Space Science 104 (Part B), 173-184. doi: 10.1016/j.pss.2014.09.008.

Garnier, P., J. E. Wahlund, L. Rosenqvist, R. Modolo, K. Ågren, N. Sergis, P. Canu, M. Andre, D. A. Gurnett, W. S. Kurth, S. M. Krimigis, A. Coates, M. Dougherty, J. H. Waite, (2009), Titan's ionosphere in the magnetosheath: Cassini RPWS results during the T32 flyby, Annales Geophysicae 27 (11), 4257-4272, doi: 10.5194/angeo-27-4257-2009.

Gérard, J.-C., E. J. Bunce, D. Grodent, S. W. H. Cowley, J. T. Clarke, S. V. Badman, (2005), Signature of Saturn's auroral cusp: Simultaneous Hubble Space Telescope FUV observations and upstream solar wind monitoring, Journal of Geophysical Research Space Physics 110, A11201, doi: 10.1029/2005JA011094.

Gérard, J.-C., D. Grodent, J. Gustin, A. Saglam, J. T. Clarke, J. T. Trauger, (2004), Characteristics of Saturn's FUV aurora observed with the Space Telescope Imaging Spectrograph, Journal of Geophysical Research Space Physics 109, A09207, doi: 10.1029/2004JA010513.

Giacalone, J. and R. Decker, (2010), The origin of low-energy anomalous cosmic rays at the solar-wind termination shock, The Astrophysical Journal 710 (1), 91.

Giampieri, G. and M. K. Dougherty, (2004), Modelling of the ring current in Saturn's magnetosphere, Annales Geophysicae, 22(2):653–659, doi: 10.5194/angeo-22-653-2004.

Goldstein, J., J. H. Waite, J. L. Burch, R. Livi, (2016), Evidence of m=1 density mode (plasma cam) in Saturn's rotating magnetosphere, Journal of Geophysical Research-Space Physics 121 (3), 2335-2348, doi: 10.1002/2015ja022131.

Goldstein, J., T. W. Hill, J. H. Waite, J. L. Burch, (2014), Analytical model of rotating two-cell convection at Saturn, Journal of Geophysical Research-Space Physics 119 (3), 1980-1993. doi: 10.1002/2013ja019615.

Grodent, D., (2015), A brief review of ultraviolet auroral emissions on giant planets, Space Science Reviews 187, (1-4), 23-50, doi: 10.1007/s11214-014-0052-8.

Grodent, D., J. Gustin, J. C. Gerard, A. Radioti, B. Bonfond, W. R. Pryor, (2011), Small-scale structures in Saturn's ultraviolet aurora, Journal of Geophysical Research Space Physics 116, A09225, doi: 10.1029/2011JA016818.

Grodent, D., A. Radioti, B. Bonfond, J.-C. Gérard, (2010), On the origin of Saturn's outer auroral emission, Journal of Geophysical Research Space Physics 115, A08219, doi: 10.1029/2009JA014901.

Grodent, D., J.-C. Gérard, S. W. H. Cowley, E. J. Bunce, J. T. Clarke, (2005), Variable morphology of Saturn's southern ultraviolet aurora, Journal of Geophysical Research Space Physics 110, 16, A07215, doi: 10.1029/2004JA010983.

Guo, R. L., Z. H. Yao, Y. Wei, L. C. Ray, I. J. Rae, C. S. Arridge, A. J. Coates, P. A. Delamere, N. Sergis, P. Kollmann, (2018), Rotationally driven magnetic reconnection in Saturn's dayside, Nature Astronomy 2, no. 8, 640, doi: 10.1038/s41550-018-0461-9.

Gurnett, D. A., W. S. Kurth, E. C. Stone, A. C. Cummings, S. M. Krimigis, R. B. Decker, N. F. Ness, L. F. Burlaga, (2015), Precursors to interstellar shocks of solar origin, The Astrophysical Journal 809 (2), 121.

Gurnett, D. A., W. S. Kurth, L. F. Burlaga, N. F. Ness, (2013), In situ observations of interstellar plasma with Voyager 1, Science 341, 1489-1492.

Gurnett, D. A. and W. R. Pryor, (2012), Auroral processes associated with Saturn's moon Enceladus, In Auroral Phenomenology and Magnetospheric Processes: Earth and Other Planets, (eds.), A. Keiling, E. Donovan, F. Bagenal, T. Karlsson, Geographical Monograph Series, vol. 197, pp. 305-313, Washington, DC, American Geophysical Union, doi:10.1029/2011GM001174.

Gurnett, D. A., J. B. Groene, T. F. Averkamp, W. S. Kurth, S.-Y. Ye, G. Fischer, (2011a), A SLS4 longitude system based on a tracking filter analysis of the rotational modulation of Saturn kilometric radiation, in Planetary Radio Emissions VII, (eds.) H. O. Rucker, W. S. Kurth, P. Louarn, G. Fischer, Austrian Academy of Sciences, Vienna, Austria, pp. 51–63.

Gurnett, D. A., T. F. Averkamp, P. Schippers, A. M. Persoon, G. B. Hospodarsky, J. S. Leisner, W. S. Kurth, G. H. Jones, A. J. Coates, F. J. Crary, M. K. Dougherty, (2011b), Auroral hiss,

electron beams and standing Alfven wave currents near Saturn's moon Enceladus, Geophysical Research Letters, 38, L06102, doi: 10.1029/2011GL046854.

Gurnett, D. A., J. B. Groene, A. M. Persoon, J. D. Menietti, S.-Y. Ye, W. S. Kurth, R. J. MacDowall, A. Lecacheux, (2010a), The reversal of the rotational modulation rates of the north and south components of Saturn kilometric radiation near equinox, Geophysical Research Letters, 37, L24101, doi: 10.1029/2010GL045796.

Gurnett, D. A., A. M. Persoon, A. J. Kopf, W. S. Kurth, M. W. Morooka, J.-E. Wahlund, K. K. Khurana, M. K. Dougherty, D. G. Mitchell, S. M. Krimigis, N. Krupp, (2010b), A plasmapause-like density boundary at high latitudes in Saturn's magnetosphere, Geophysical Research Letters, 37, L16806, doi: 10.1029/2010GL044466.

Gurnett, D. A., A. Lecacheux, W. S. Kurth, A. M. Persoon, J. B. Groene, L. Lamy, P. Zarka, J. F. Carbary, (2009), Discovery of a north-south asymmetry in Saturn's radio rotation period, Geophysical Research Letters, 36, L16102, doi: 10.1029/2009GL039621.

Gurnett, D. A., A. M. Persoon, W. S. Kurth, J. B. Groene, T. F. Averkamp, M. K. Dougherty, D. J. Southwood, (2007), The variable rotation period of the inner region of Saturn's plasma disk, Science, 316(5823):442–445, doi: 10.1126/science.1138562.

Gurnett, D. A., W. S. Kurth, G. B. Hospodarsky, A. M. Persoon, T. F. Averkamp, B. Cecconi, A. Lecacheux, P. Zarka, P. Canu, N. Cornilleau-Wehrlin, P. Galopeau, A. Roux, C. Harvey, P. Louarn, R. Bostrom, G. Gustafsson, J. -E. Wahlund, M. D. Desch, W. M. Farrell, M. L. Kaiser, K. Goetz, P. J. Kellogg, G. Fischer, H.-P. Ladreiter, H. Rucker, H. Alleyne, A. Pedersen, (2005), Radio and plasma wave observations at Saturn from Cassini's approach and first orbit, Science, 307, 1255–1259, doi: 10.1126/science.1105356.

Gurnett, D. A., W. S. Kurth, G. B. Hospodarsky, A. M. Persoon, P. Zarka, A. Lecacheux, S. J. Bolton, M. D. Desch, W. M. Farrell, M. L. Kalser, H. P. Ladreiter, H. O. Rucker, P. Galopeau, P. Louarn, D. T. Young, W. R. Pryor, M. K. Dougherty, (2002), Control of Jupiter’s radio emission and aurorae by the solar wind, Nature 415 (6875), 985-987, doi: 10.1038/415985a.

Gurnett, D. A., P. Zarka, R. Manning, W. S. Kurth, G. B. Hospodarsky, T. F. Averkamp, M. L. Kaiser, W. M. Farrell, (2001), Non-detection at Venus of high-frequency radio signals characteristic of terrestrial lightning, Nature 409 (6818), 313-315. doi: 10.1038/35053009.

Gustin, J., D. Grodent, A. Radioti, W. Pryor, L. Lamy, J. Ajello, (2017), Statistical study of Saturn’s auroral electron properties with Cassini/UVIS FUV spectral images, Icarus 284, 264-283 doi: 10.1016/j.icarus.2016.11.017.

Gustin, J., I. Stewart, J.-C. Gérard, L. Esposito, (2010), Characteristics of Saturn’s FUV airglow from limb-viewing spectra obtained with Cassini-UVIS, Icarus 210 (1), 270-283. doi: 10.1016/j.icarus.2010.06.031.

Gustin, J., J.-C. Gérard, W. Pryor, P. D. Feldman, D. Grodent, G. Holsclaw, (2009), Characteristics of Saturn’s polar atmosphere and auroral electrons derived from HST/STIS, FUSE and Cassini/UVIS spectra, Icarus 200 (1), 176-187, doi: 10.1016/j.icarus.2008.11.013.

Hanlon, P. G., M. K. Dougherty, R. J. Forsyth, M. J. Owens, K. C. Hansen, G. Toth, D. T. Young, (2004), On the evolution of the solar wind between 1 and 5 AU at the time of the Cassini Jupiter flyby: Multispacecraft observations of interplanetary coronal mass ejections including the formation of a merged interaction region, Journal of Geophysical Research: Space Physics, 109(A9):10 pp., doi: 10.1029/2003JA010112.

Hartle, R. E., M. Sarantos, E. C. Sittler Jr., (2011), Pickup ion distributions from three-dimensional neutral exospheres, Journal of Geophysical Research-Space Physics 116, A10101. doi: 10.1029/2011JA016859.

Hartle, R. E., E. C. Sittler Jr., A. Lipatov, (2008), Ion Escape from the Ionosphere of Titan, European Geosciences Union Annual Meeting, Vienna Austria, 14–18 April 2008.

Hartle, R. E. and E. C. Sittler Jr., (2007), Pickup ion phase space distributions: effects of atmospheric spatial gradients, Journal of Geophysical Research-Part A-Space Physics 112:A07104, doi: 10.1029/2006JA012157.

Hartle, R. E., E. C. Sittler Jr., F. M. Neubauer, R. E. Johnson, H. T. Smith, F. Crary, D. J. McComas, D. T. Young, A. J. Coates, D. Simpson, S. Bolton, D. Reisenfeld, K. Szego, J. J. Berthelier, A. Rymer, J. Vilppola, J. T. Steinberg, N. Andre, (2006a), Preliminary interpretation of Titan plasma interaction as observed by the Cassini plasma spectrometer: Comparisons with Voyager 1, Geophysical Research Letters, 33, L08201, doi: 10.1029/2005GL024817.

Hartle, R. E., E. C. Sittler Jr., F. M. Neubauer, R. E. Johnson, H. T. Smith, F. Crary, D. J. McComas, D. T. Young, A. J. Coates, D. Simpson, S. Bolton, D. Reisenfeld, K. Szego, J. J. Berthelier, A. Rymer, J. Vilppola, J. T. Steinberg, N. Andre, (2006b), Initial interpretation of Titan plasma interaction as observed by the Cassini plasma spectrometer: Comparisons with Voyager 1, Planetary and Space Science, 54, 1211.

Hartle, R. E. and R. Killen, (2006), Measuring pickup ions to characterize the surfaces and exospheres of planetary bodies: Applications to the Moon, Geophysical Research Letters 33 (5), doi: 10.1029/2005GL024520.

Hartle, R., E. C. Sittler Jr., F. M. Neubauer, R. E. Johnson, H. T. Smith, F. Crary, D. J. McComas, D. T. Young, A. J. Coates, D. Simpson, S. Boltan, D. Reisenfeld, K. Szego, J. J. Berthelier, A. Rymer, J. Vilppola, J. T. Steinberg, N. Andre, (2006), Preliminary interpretation of Titan plasma interaction as observed by the Cassini plasma spectrometer: Comparisons with Voyager 1, Geophysical Research Letters, vol. 33(8), L08201, doi: 10.1029/2005GL024817.

Hedman, M. M., C. M. Gosmeyer, P. D. Nicholson, C. Sotin, Robert H. Brown, R. N. Clark, K. H. Baines, B. J. Buratti, M. R. Showalter, (2013), An observed correlation between plume activity and tidal stresses on Enceladus, Nature, 500, 182–184, doi: 10.1038/nature12371.

Helled, R., E. Galanti, Y. Kaspi, (2015), Saturn's fast spin determined from its gravitational field and oblateness, Nature 520 (7546):202-204, doi: 10.1038/nature14278.

Hess, S. L. G., E. Echer, P. Zarka, L. Lamy, P. A. Delamere, (2014), Multi-instrument study of the Jovian radio emissions triggered by solar wind shocks and inferred magnetospheric subcorotation rates, Planetary and Space Science 99, 136-148, doi: 10.1016/j.pss.2014.05.015.

Hill, M. E. and D. C. Hamilton, (2010), Interim report on the power law index of interplanetary suprathermal ion spectra, In AIP Conference Proceedings, vol. 1302, no. 1, pp. 58-63, American Institute of Physics, doi: 10.1063/1.3529991.

Hill, M. E., N. A. Schwadron, D. C. Hamilton, R. D. DiFabio, R. K. Squier, (2009), Interplanetary suprathermal He+ and He++ observations during quiet periods from 1 to 9 AU and implications for particle acceleration, Astrophysical Journal Letters 699 (1), L26-L30, doi: 10.1088/0004-637x/699/1/l26.

Hill, T. W., A. Jaggi, S. Sazykin, R. A. Wolf, (2018), Plasma circulation time scale of Saturn's magnetosphere.

Hill, T. W., (2017), Magnetosphere-Ionosphere coupling at Jupiter and Saturn, in Magnetosphere-Ionosphere Coupling in the Solar System, Part VI: Chapter 24, (eds.) C. R. Chappell, R. W. Schunk, P. M. Banks, J. L. Burch, R. M. Thorne, pp. 307–318, doi: 10.1002/9781119066880.ch24.

Hill, T. W., (2016), Penetration of external plasma into a rotation-driven magnetosphere, Journal of Geophysical Research: Space Physics, 121, doi: 10.1002/ 2016JA023430.

Hill, T. W., M. F. Thomsen, R. L. Tokar, A. J. Coates, G. R. Lewis, D. T. Young, F. J. Crary, et al., (2012), Charged nanograins in the Enceladus plume, Journal of Geophysical Research: Space Physics, 117(A5).

Hill, T. W., M. F. Thomsen, M. G. Henderson, R. L. Tokar, A. J. Coates, H. J. McAndrews, G. R. Lewis, D. G. Mitchell, C. M. Jackman, C. T. Russell, M. K. Dougherty, F. J. Crary, D. T. Young, (2008), Plasmoids in Saturn's magnetotail, Journal of Geophysical Research, 113, A01214, doi: 10.1029/2007JA012626.

Hill, T. W., A. M. Rymer, J. L. Burch, F. J. Crary, D. T. Young, M. F. Thomsen, D. Delapp, N. Andre, A. J. Coates, G. R. Lewis, (2005), Evidence for rotationally driven plasma transport in Saturn's magnetosphere, Geophysical Research Letters 32 (14), 14-10, doi: 10.1029/2005GL022620.

Hörst, S. M., V. Vuitton, R. V. Yelle, (2008), Origin of oxygen species in Titan's atmosphere, Journal of Geophysical Research-Planets 113 (E10), E10006. doi: 10.1029/2008je003135.

Hospodarsky, G. B., J. S. Leisner, K. Sigsbee, J. D. Menietti, W. S. Kurth, D. A. Gurnett, C. A. Kletzing, O. Santolik, (2012), Plasma wave observations at Earth, Jupiter, and Saturn in dynamics of Earth's radiation belts and inner magnetosphere, vol. 199, American Geophysical Union, Washington, DC.

Hospodarsky, G. B., J. E. Nelson, W. S. Kurth, D. A. Gurnett, P. Zarka, P. Canu, M. K. Dougherty, A. J. Coates, D. T. Young, A. M. Rymer, (2006), Solar wind electron densities upstream of Saturn determined from Langmuir Wave observations by the Cassini RPWS instrument, American Geophysical Union (AGU) Fall Meeting, San Francisco, California, 11-15 Dec. 2006.

Hospodarsky, G. B., W. S. Kurth, B. Cecconi, D. A. Gumett, M. L. Kaiser, M. D. Desch, P. Zarka, (2004), Simultaneous observations of Jovian quasi-periodic radio emissions by the Galileo and Cassini spacecraft, Journal of Geophysical Research-Space Physics 109 (A9), A09S07, doi: 10.1029/2003JA010263.

Hospodarsky, G. B., I. W. Christopher, J. D. Menietti, W. S. Kurth, D. A. Gurnett, T. F. Averkamp, J. B. Groene, P. Zarka, (2001a), Control of Jovian radio emissions by the Galilean moons as observed by Cassini and Galileo, in Planetary Radio Emissions V, (eds.) H. O. Rucker, M. L. Kaiser, Y. Leblanc, Austrian Academy of Sciences Press, Vienna, Austria, pp. 155–164.

Hospodarsky, G. B., T. F. Averkamp, W. S. Kurth, D. A. Gurnett, M. Dougherty, U. Inan, T. Wood, (2001b), Wave normal and poynting vector calculations using the Cassini Radio and Plasma Wave instrument, Journal of Geophysical Research, 106, 30253–30269, doi: 10.1029/10.1029/2001JA900114.

Hsu, H. W., J. Schmidt, S. Kempf, F. Postberg, G. Moragas-Klostermeyer, M. Seiss, H. Hoffmann, M. Burton, S. Y. Ye, W. S. Kurth, M. Horanyi, N. Khawaja, F. Spahn, D. Schirdewahn, J. O'Donoghue, L. Moore, J. Cuzzi, G. H. Jones, R. Srama, (2018), Cosmic dust analyser onboard Cassini collects material from Saturn's main rings, Science 362, 49.

Hunt, G. J., G. Provan, E. J. Bunce, S. W. H. Cowley, M. K. Dougherty, D. J. Southwood, (2018a), Field-aligned currents in Saturn's magnetosphere: Observations from the F-ring orbits, Journal of Geophysical Research, 123(5):3806–3821, doi: 10.1029/2017JA025067.

Hunt, G. J., S. W. H. Cowley, J. D. Nichols, (2018b), Ionospheric currents due to ionosphere-magnetosphere coupling at Jupiter and Saturn, in Electric Currents in Geospace and Beyond, (eds.) A. Keiling, O. Marghitu, M. Wheatland, John Wiley & Sons, Inc., p. 459.

Hunt, G. J., S. W. H. Cowley, G. Provan, E. J. Bunce, I. I. Alexeev, E. S. Belenkaya, V. V. Kalegaev, M. K. Dougherty, A. J. Coates, (2016), Field-aligned currents in Saturn's magnetosphere: Local time dependence of southern summer currents in the dawn sector between midnight and noon, Journal of Geophysical Research: Space Physics 121, no. 8, 7785-7804, doi: 10.1002/2016ja022712.

Hunt, G. J., S. W. H. Cowley, G. Provan, E. J. Bunce, I. I. Alexeev, E. S. Belenkaya, V. V. Kalegaev, M. K. Dougherty, A. J. Coates, (2015), Field-aligned currents in Saturn's northern nightside magnetosphere: Evidence for interhemispheric current flow associated with planetary period oscillations, Journal of Geophysical Research-Space Physics 120 (9), 7552-7584, doi: 10.1002/2015ja021454.

Hunt, G. J., S. W. H. Cowley, G. Provan, E. J. Bunce, I. I. Alexeev, E. S. Belenkaya, V. V. Kalegaev, M. K. Dougherty, A. J. Coates, (2014), Field-aligned currents in Saturn's southern nightside magnetosphere: Subcorotation and planetary period oscillation components, Journal of Geophysical Research-Space Physics 119 (12), 9847-9899, doi: 10.1002/2014ja020506.

Hurley, D. M., M. E. Perry, J. H. Waite, (2015), Modeling insights into the locations of density enhancements from the Enceladus water vapor jets, Journal of Geophysical Research: Planets 120 (11), 1763-1773.

Imai, M., A. Lecacheux, M. Moncuquet, F. Bagenal, C. A. Higgins, K. Imai, J. R. Thieman, (2015), Modeling Jovian hectometric attenuation lanes during the Cassini flyby of Jupiter, Journal of Geophysical Research-Space Physics 120 (3), 1888-1907, doi: 10.1002/2014ja020815.

Imai, M., A. Lecacheux, K. Imai, C. A. Higgins, J. R. Thieman, (2011a), Jupiter's decametric and hectomectric radio emissions observed by Voyager PRA and Cassini RPWS, in Planetary Radio Emissions VII, (eds.) H. O. Rucker, W. S. Kurth, P. Louarn, G. Fischer, Austrian Academy of Sciences, Vienna, Austria, pp. 167–176.

Imai, M., K. Imai, C. A. Higgins, J. R. Thieman, (2011b), Comparison between Cassini and Voyager observations of Jupiter's decametric and hectometric radio emissions, Journal of Geophysical Research, 116, A12233, doi: 10.1029/2011JA016456.

Imai, M., K. Imai, C. A. Higgins, J. R. Thieman, (2008), Angular beaming model of Jupiter's decametric radio emissions based on Cassini RPWS data analysis, Geophysical Research Letters 35 (17), L17103, doi: 10.1029/2008gl034987.

Jackman, C. M., G. Provan, S. W. H. Cowley, (2016), Reconnection events in Saturn's magnetotail: Dependence of plasmoid occurrence on planetary period oscillation phase, Journal of Geophysical Research-Space Physics 121 (4), 2922-2934. doi: 10.1002/2015ja021985.

Jackman, C. M., M. F. Thomsen, D. G. Mitchell, N. Sergis, C. S. Arridge, M. Felici, S. V. Badman, C. Paranicas, X. Jia, G. B. Hospodarksy, (2015), Field dipolarization in Saturn's magnetotail with planetward ion flows and energetic particle flow bursts: Evidence of quasi-steady reconnection, Journal of Geophysical Research Space Physics 120 (5), 3603-3617.

Jackman, C. M., J. A. Slavin, M. G. Kivelson, D. J. Southwood, N. Achilleos, M. F. Thomsen, G. A. DiBraccio, J. P. Eastwood, M. P. Freeman, M. K. Dougherty, M. F. Vogt, (2014), Saturn's dynamic magnetotail: A comprehensive magnetic field and plasma survey of plasmoids and traveling compression regions and their role in global magnetospheric dynamics, Journal of Geophysical Research-Space Physics 119 (7), 5465-5494, doi: 10.1002/2013ja019388.

Jackman, C. M., N. Achilleos, S. W. H. Cowley, E. J. Bunce, A. Radioti, D. Grodent, S. V. Badman, M. K. Dougherty, W. Pryor, (2013), Auroral counterpart of magnetic field dipolarizations in Saturn's tail, Planetary and Space Science 82-83, 34-42, doi: 10.1016/j.pss.2013.03.010.

Jackman, C. M., J. A. Slavin, S. W. H. Cowley, (2011), Cassini observations of plasmoid structure and dynamics: Implications for the role of magnetic reconnection in magnetospheric circulation at Saturn, Journal of Geophysical Research, 116, A10212, doi: 10.1029/2011JA016682.

Jackman, C. M. and C. S. Arridge, (2011a), Solar cycle effects on the dynamics of Jupiter's and Saturn's magnetospheres, Solar Physics, 274:481–502, doi 10.1007/s11207-011-9748-z.

Jackman, C. M. and C. S. Arridge, (2011b), Statistical properties of the magnetic field in the Kronian magnetotail lobes and current sheet, Journal of Geophysical Research, 116(A05224), doi: 10.1029/2010JA015973.

Jackman, C. M., C. S. Arridge, J. A. Slavin, S. E. Milan, L. Lamy, M. K. Dougherty, A. J. Coates, (2010), In situ observations of the effect of a solar wind compression on Saturn's magnetotail, Journal of Geophysical Research-Space Physics 115:A10240. doi: 10.1029/2010ja015312.

Jackman, C. M., L. Lamy, M. P. Freeman, P. Zarka, B. Cecconi, W. S. Kurth, M. K. Dougherty, (2009a), On the character and distribution of lower-frequency radio emissions at Saturn and their relationship to substorm-like events, Journal of Geophysical Research: Space Physics, 114:13 pp., doi: 10.1029/2008JA013997.

Jackman, C. M., C. S. Arridge, H. J. McAndrews, M. G. Henderson, R. J. Wilson, (2009b), Northward field excursions in Saturn's magnetotail and their relationship to magnetospheric periodicities, Geophysical Research Letters, 36(L16101), doi: 10.1029/2009GL039149.

Jackman, C. M., C. S. Arridge, N. Krupp, E. J. Bunce, D. G. Mitchell, H. J. McAndrews, M. K. Dougherty, C. T. Russell, N. Achilleos, G. H. Jones, A. J. Coates, (2008), A multi-instrument view of tail reconnection at Saturn, Journal of Geophysical Research-Space Physics 113 (A11), A11213, doi: 10.1029/2008ja013592.

Jackman, C. M., C. T. Russell, D. J. Southwood, C. S. Arridge, N. Achilleos, M. K. Dougherty, (2007), Strong rapid dipolarizations in Saturn's magnetotail: In situ evidence of reconnection, Geophysical Research Letters 34 (11), L11203.

Jackman, C. M. and S. W. H. Cowley, (2006), A model of the plasma flow and current in Saturn's polar ionosphere under conditions of strong Dungey cycle driving, Annales Geophysicae 24(3), pp. 1029-1055, European Geosciences Union.

Jackman, C. M., N. Achilleos, E. J. Bunce, S. W. H. Cowley, S. E. Milan, (2005a), Structure of the interplanetary magnetic field during the interval spanning the first Cassini fly-through of Saturn's magnetosphere and its implications for Saturn's magnetospheric dynamics, Advances in Space Research, 36:2120–2126, doi: 10.1016/j.asr.2004.12.023.

Jackman, C. M., N. Achilleos, E. J. Bunce, B. Cecconi, J. T. Clarke, S. W. H. Cowley, W. S. Kurth, P. Zarka, (2005b), Interplanetary conditions and magnetospheric dynamics during the Cassini orbit insertion fly-through of Saturn's magnetosphere, Journal of Geophysical Research, 110(A10212), doi: 10.1029/2005JA011054.

Jackman, C. M., N. Achilleos, E. J. Bunce, S. W. H. Cowley, M. K. Dougherty, G. H. Jones, S. E. Milan, E. J. Smith, (2004), Interplanetary magnetic field at ~9 AU during the declining phase of the solar cycle and its implications for Saturn's magnetospheric dynamics, Journal of Geophysical Research-Space Physics 109 (A11), 19. doi: 10.1029/2004JA010614.

Jasinski, J. M., C. S. Arridge, A. J. Coates, G. H. Jones, N. Sergis, M. F. Thomsen, N. Krupp, (2017), Diamagnetic depression observations at Saturn's magnetospheric cusp by the Cassini spacecraft, Journal of Geophysical Research Space Physics 122 (6), 6283-6303, doi: 10.1002/2016ja023738.

Jasinski, J. M., C. S. Arridge, A. J. Coates, G. H. Jones, N. Sergis, M. F. Thomsen, D. B. Reisenfeld, N. Krupp, J. H. Waite, (2016), Cassini plasma observations of Saturn's magnetospheric cusp, Journal of Geophysical Research Space Physics 121 (12), 12047-12067, doi: 10.1002/2016ja023310.

Jasinski, J. M., C. S. Arridge, L. Lamy, J. S. Leisner, M. F. Thomsen, D. G. Mitchell, A. J. Coates, A. Radioti, G. H. Jones, E. Roussos, N. Krupp, D. Grodent, M. K. Dougherty, J. H. Waite, (2014), Cusp observation at Saturn's high latitude magnetosphere by the Cassini spacecraft, Geophysical Research Letters, 41, 1382–1388, doi: 10.1002/2014GL059319.

Jia, X. Z. and M. G. Kivelson, (2016), Dawn-dusk asymmetries in rotating magnetospheres: Lessons from modeling Saturn, Journal of Geophysical Research Space Physics 121 (2), 1413-1424, doi: 10.1002/2015ja021950.

Jia, X. and M. G. Kivelson, (2012), Driving Saturn's magnetospheric periodicities from the upper atmosphere/ionosphere: Magnetotail response to dual sources, Journal of Geophysical Research-Space Physics 117, A11219, doi: 10.1029/2012JA018183.

Jia, X., M. G. Kivelson, T. I. Gombosi, (2012), Driving Saturn's magnetospheric periodicities from the upper atmosphere/ionosphere, Journal of Geophysical Research, 117(A04215), doi: 10.1029/2011JA017367.

Jia, Y. D., C. T. Russell, K. K. Khurana, H. Y. Wei, Y. J. Ma, J. S. Leisner, A. M. Persoon, M. K. Dougherty, (2011), Cassini magnetometer observations over the Enceladus poles, Geophysical Research Letters 38 (19), L19109, doi: 10.1029/2011GL049013.

Jia, Y. -D., C. T. Russell, K. K. Khurana, J. S. Leisner, T. I. Gombosi, (2010a), The interaction of Saturn's magnetosphere and its moons 1: Interaction between co-rotating plasma and standard obstacles, Journal of Geophysical Research, 115(A04214), doi: 10.1029/2009JA014630.

Jia, Y. -D., C. T. Russell, K. K. Khurana, Y. J. Ma, D. Najib, T. I. Gombosi, (2010b), The interaction of Saturn's magnetosphere and its moons 2: Shape of the Enceladus plume, Journal of Geophysical Research, 115(A04215), doi: 10.1029/2009JA014873.

Jia, Y. -D., C. T. Russell, K. K. Khurana, J. S. Leisner, Y. J. Ma, M. K. Dougherty, (2010c), Time-varying magnetospheric environment near Enceladus as seen by the Cassini magnetometer, Geophysical Research Letters, 37:5 pp., doi: 10.1029/2010GL042948.

Jia, Y. -D., C. T. Russell, Y. J. Ma, K. K. Khurana, W. Kurth, T. I. Gombosi, (2010d), The interaction of Saturn's magnetosphere and its moons 3: Time Variation of the Enceladus Plume, Journal of Geophysical Research, 115(12):A12243, doi: 10.1029/2010JA015534.

Jinks, S. L., E. J. Bunce, S. W. H. Cowley, G. Provan, T. K. Yeoman, C. S. Arridge, M. K. Dougherty, D. A. Gurnett, N. Krupp, W. S. Kurth, D. G. Mitchell, M. Morooka, J. E. Wahlund, (2014), Cassini multi-instrument assessment of Saturn's polar cap boundary, Journal of Geophysical Research-Space Physics 119 (10), 8161-8177, doi: 10.1002/2014ja020367.

Johnson, R. E., W. L. Tseng, M. K. Elrod, A. M. Persoon, (2017), Nanograin density outside Saturn's A ring, Astrophysical Journal Letters 834 (1), doi: 10.3847/2041-8213/834/1/l6.

Johnson, R. E., O. J. Tucker, M. Michael, E. C. Sittler, H. T. Smith, D. T. Young, J. H. Waite, (2009), Mass loss processes in Titan's upper atmosphere, in Titan from Cassini-Huygens, R. H. Brown, J.-P. Lebreton, and J. H. White (eds.), pp. 373-391, Springer, Dordrecht.

Johnson, R. E., J. G.Luhmann, R. L. Tokar, M. Bouhram, J. J. Berthelier, E. C. Sittler, J. F. Cooper, T. W. Hill, H. T. Smith, M. Michael, M. Liu, F. J. Crary, D. T. Young, (2006), Production, ionization and redistribution of O2 Saturn's ring atmosphere, Icarus180, 393–402.

Johnson, R. E., M. Liu, E. C. Sittler Jr., (2005), Plasma-induced clearing and redistribution of material embedded in planetary magnetospheres, Geophysical Research Letters, 32, L24201, doi: 10.1029/2005GL024275.

Jones, G. H., C. S. Arridge, A. J. Coates, G. R. Lewis, S. Kanani, A. Wellbrock, D. T. Young, F. J. Crary, R. L. Tokar, R. J. Wilson, T. W. Hill, R. E. Johnson, D. G. Mitchell, J. Schmidt, S. Kempf, U. Beckmann, C. T. Russell, Y. D. Jia, M. K. Dougherty, J. H. Waite Jr., B. A. Magee, (2009), Fine jet structure of electrically charged grains in Enceladus' plume, Geophysical Research Letters 36, L16204, doi: 10.1029/2009gl038284.

Kaiser, M. L., W. M. Farrell, W. S. Kurth, G. B. Hospodarsky, D. A. Gurnett, (2004), New observations from Cassini and Ulysses of Jovian VLF radio emissions, Journal of Geophysical Research, 109, A09S08, doi: 10.1029/2003JA010233.

Kaiser, M. L., W. M. Farrell, M. D. Desch, G. B. Hospodarsky, W. S. Kurth, D. A. Gurnett, (2001), Ulysses and Cassini at Jupiter: Comparison of the quasi-periodic radio bursts, In Planetary Radio Emissions V, (eds.) H. O. Rucker, M. L. Kaiser, Y. Leblanc, Austrian Academy of Sciences Press, Vienna, Austria, pp. 41–48.

Kaiser, M. L., P. Zarka, W. S. Kurth, G. B. Hospodarsky, D. A. Gurnett, (2000), Cassini and wind stereoscopic observations of Jovian nonthermal radio emissions – Measurement of beam widths, Journal of Geophysical Research-Space Physics 105 (A7), 16, 053-16, 062.

Kallio, E., I. Sillanpää, R. Jarvinen, P. Janhunen, M. Dougherty, C. Bertucci, F. Neubauer, (2007), Morphology of the magnetic field near Titan: Hybrid model study of the Cassini T9 flyby, Geophysical Research Letters 34 (24), L24S09.

Kanani, S. J., C. S. Arridge, G. H. Jones, A. N. Fazakerley, H. J. McAndrews, N. Sergis, S. M. Krimigis, M. K. Dougherty, A. J. Coates, D. T. Young, K. C. Hansen, N. Krupp, (2010), A new form of Saturn's magnetopause using a dynamic pressure balance model, based on in situ, multi-instrument Cassini measurements, Journal of Geophysical Research-Space Physics 115, A06207, doi: 10.1029/2009ja014262.

Keller, C. N., V. G. Anicich, T. E. Cravens, (1998), Model of Titan's ionosphere with detailed hydrocarbon ion chemistry, Planetary and Space Science 46 (9), 1157-1174, doi: 10.1016/S0032-0633(98)00053-1.

Keller, C. N., T. E. Cravens, L. Gan, (1992), A model of the ionosphere of Titan, Journal of Geophysical Research Space Physics 97 (A8), 12117-12135.

Kellett, S., C. S. Arridge, E. J. Bunce, A. J. Coates, S. W. H. Cowley, M. K. Dougherty, A. M. Persoon, N. Sergis, R. J. Wilson, (2011), Saturn's ring current: Local time dependence and temporal variability, Journal of Geophysical Research Space Physics 116, A05220, doi: 10.1029/2010ja016216.

Kellett, S., C. S. Arridge, E. J. Bunce, A. J. Coates, S. W. H. Cowley, M. K. Dougherty, A. M. Persoon, N. Sergis, R. J. Wilson, (2010), Nature of the ring current in Saturn's dayside magnetosphere, Journal of Geophysical Research Space Physics 115, A08201. doi: 10.1029/2009ja015146.

Kellett, S., E. J. Bunce, A. J. Coates, S. W. H. Cowley, (2009), Thickness of Saturn's ring current determined from north-south Cassini passes through the current layer, Journal of Geophysical Research Space Physics 114, A04209, doi: 10.1029/2008ja013942.

Khan, H., S. W. H. Cowley, E. Kolesnikova, M. Lester, M. J. Brittnacher, T. J. Hughes, W. J. Hughes, W. S. Kurth, D. J. McComas, L. Newitt, C. J. Owen, G. D. Reeves, H. J. Singer, C. W. Smith, D. J. Southwood, J. F. Watermann, (2001), Observations of two complete substorm cycles during the Cassini Earth swing-by: Cassini magnetometer data in a global context, Journal of Geophysical Research Space Physics 106 (A12), 30141-75, doi: 10.1029/2001JA900049.

Khurana, K. K., S. Fatemi, J. Lindkvist, E. Roussos, N. Krupp, M. Holmstrom, C. T. Russell, M. K. Dougherty, (2017), The role of plasma slowdown in the generation of Rhea's Alfven wings, Journal of Geophysical Research Space Physics 122 (2), 1778-1788, doi: 10.1002/2016ja023595.

Khurana, K. K., N. Krupp, M. G. Kivelson, E. Roussos, C. T. Russell, M. K. Dougherty, (2012), Cassini's flyby through Rhea's distant Alfven wing, European Planetary Science Congress 2012.

Kim, Y. H., J. L. Fox, J. H. Black, J. I. Moses, (2014), Hydrocarbon ions in the lower ionosphere of Saturn, Journal of Geophysical Research Space Physics 119 (1), 384-395, doi: 10.1002/2013JA019022.

Kimura, T., L. Lamy, C. Tao, S. V. Badman, S. Kasahara, B. Cecconi, P. Zarka, A. Morioka, Y. Miyoshi, D. Maruno, Y. Kasaba, M. Fujimoto, (2013), Long-term modulations of Saturn's auroral radio emissions by the solar wind and seasonal variations controlled by the solar ultraviolet flux, Journal of Geophysical Research Space Physics 118 (11), 7019-7035, doi: 10.1002/2013JA018833.

Kimura, T., B. Cecconi, P. Zarka, Y. Kasaba, F. Tsuchiya, H. Misawa, A. Morioka, (2012), Polarization and direction of arrival of Jovian quasiperiodic bursts observed by Cassini, Journal of Geophysical Research Space Physics 117, A11209, doi: 10.1029/2012JA017506.

Kinrade, J., S. V. Badman, E. J. Bunce, C. Tao, G. Provan, S. W. H. Cowley, A. Grocott, R. L. Gray, D. Grodent, T. Kimura, J. D. Nichols, C. S. Arridge, A. Radioti, J. T. Clarke, F. J. Crary, W. R. Pryor, H. Melin, K. H. Baines, M. K. Dougherty, (2017), An isolated, bright cusp aurora at Saturn, Journal of Geophysical Research Space Physics 122 (6), 6121-6138, doi: 10.1002/2016ja023792.

Kivelson, M. G. and X. Z. Jia, (2014), Control of periodic variations in Saturn's magnetosphere by compressional waves, Journal of Geophysical Research Space Physics 119 (10), 8030-8045, doi: 10.1002/2014ja020258.

Kivelson, M. G. and X. Jia, (2013), An MHD model of Ganymede's mini-magnetosphere suggests that the heliosphere forms in a sub-Alfvénic flow, Journal of Geophysical Research Space Physics 118 (11), 6839-6846.

Kivelson, M. G., (2006), Does Enceladus govern magnetospheric dynamics at Saturn?, Science 311 (5766), 1391-2, doi: 10.1126/science.1124494.

Kivelson, M. G. and D. J. Southwood, (2005), Dynamical consequences of two modes of centrifugal instability in Jupiter's outer magnetosphere, Journal of Geophysical Research Space Physics 110 (A12).

Kivelson, M. G. and D. J. Southwood, (2003), First evidence of IMF control of Jovian magnetospheric boundary locations: Cassini and Galileo magnetic field measurements compared, Planetary and Space Science 51 (13), 891-8, doi: 10.1016/S0032-0633(03)00075-8.

Kollmann, P., E. Roussos, C. Paranicas, E. E. Woodfield, B. H. Mauk, G. Clark, D. C. Smith, J. Vandegriff, (2018), Electron acceleration to MeV energies at Jupiter and Saturn, Journal of Geophysical Physics 123 (11), 9110-9129.

Kollmann, P., E. Roussos, A. Kotova, C. Paranicas, N. Krupp, (2017), The evolution of Saturn's radiation belts modulated by changes in radial diffusion, Nature Astronomy 1 (12), 872-877, doi: 10.1038/s41550-017-0287-x.

Kollmann, P., E. Roussos, A. Kotova, J. F. Cooper, D. G. Mitchell, N. Krupp, C. Paranicas, (2015), MeV proton flux predictions near Saturn's D ring, Journal of Geophysical Research Space Physics 120 (10), 8586-8602, doi: 10.1002/2015ja021621.

Kollmann, P., E. Roussos, C. Paranicas, N. Krupp, D. K. Haggerty, (2013), Processes forming and sustaining Saturn's proton radiation belts, Icarus 222 (1), 323-341, doi: 10.1016/j.icarus.2012.10.033.

Kollmann, P., E. Roussos, C. Paranicas, N. Krupp, C. M. Jackman, E. Kirsch, K. H. Glassmeier, (2011), Energetic particle phase space densities at Saturn: Cassini observations and interpretations, Journal of Geophysical Research Space Physics 116, A05222, doi: 10.1029/2010ja016221.

Koskinen, T. T., B. R. Sandel, R. V. Yelle, D. F. Strobel, I. C. F. Müeller-Wodarg, J. T. Erwin, (2015), Saturn's variable thermosphere from Cassini/UVIS occultations, Icarus 260, 174-189, doi: 10.1016/j.icarus.2015.07.008.

Krasnopolsky, V. A., (2012), Titan's photochemical model: Further update, oxygen species, and comparison with Triton and Pluto, Planetary and Space Science 73 (1), 318-326, doi: 10.1016/j.pss.2012.08.013.

Kriegel, H., S. Simon, U. Motschmann, J. Saur, F. M. Neubauer, A. M. Persoon, M. K. Dougherty, D. A. Gurnett, (2011), Influence of negatively charged plume grains on the structure of Enceladus' Alfven wings: Hybrid simulations versus Cassini Magnetometer data, Journal of Geophysical Research Space Physics 116, A10223, doi: 10.1029/2011JA016842.

Krimigis, S. M., R. B. Decker, E. C. Roelof, M. E. Hill, T. P. Armstrong, G. Gloeckler, D. C. Hamilton, L. J. Lanzerotti, (2013), Search for the exit: Voyager 1 at heliosphere's border with the galaxy, Science 341 (6142), 144-147.

Krimigis, S. M., E. C. Roelof, R. B. Decker, M. E. Hill, (2011), Zero outward flow velocity for plasma in a heliosheath transition layer, Nature, 474, 359–361.

Krimigis, S. M., D. G. Mitchell, E. C. Roelof, R. B. Decker, (2010), ENA (E>5 keV) images from Cassini and Voyager "ground truth": Suprathermal pressure in the heliosheath, In AIP

Conference Proceedings, vol. 1302, no. 1, pp. 79-85, American Institute of Physics, doi: 10.1063/1.3529994.

Krimigis, S. M., D. G. Mitchell, E. C. Roelof, K. C. Hsieh, D. J. McComas, (2009), Imaging the interaction of the heliosphere with the interstellar medium from Saturn with Cassini, Science 326 (5955), 971-973, doi: 10.1126/science.1181079.

Krimigis, S. M., N. Sergis, D. G. Mitchell, N. Krupp, (2007), A dynamic, rotating ring current around Saturn, Nature, 450, 1050-1053.

Krimigis, S. M., Krimigis, S. M., D. G. Mitchell, D. C. Hamilton, N. Krupp, S. Livi, E. C. Roelof, J. Dandouras, et al., (2005), Dynamics of Saturn's magnetosphere from MIMI during Cassini's orbital insertion, Science, 307, 1270-1273.

Krupp, N., J. Woch, A. Lagg, S. Livi, D. G. Mitchell, S. M. Krimigis, M. K. Dougherty, P. G. Hanlon, T. P. Armstrong, S. A. Espinosa, (2004), Energetic particle observations in the vicinity of Jupiter: Cassini MIMI/LEMMS results, Journal of Geophysical Research Space Physics 109 (A9), 10, doi: 10.1029/2003JA0101.

Krupp, N., J. Woch, A. Lagg, S. A. Espinosa, S. Livi, S. M. Krimigis, D. G. Mitchell, D. J. Williams, A. F. Cheng, B. H. Mauk, R. W. McEntire, T. P. Armstrong, D. C. Hamilton, G. Gloeckler, J. Dandouras, L. J. Lanzerotti, (2002), Leakage of energetic particles from Jupiter's dusk magnetosphere: dual spacecraft observations, Geophysical Research Letters 29 (15), 26-1, doi: 10.1029/2001GL014290.

Krupp, N., J. Woch, A. Lagg, S. A. Espinosa, S. Livi, S. M. Krimigis, D. G. Mi, et al., (2002), Leakage of energetic particles from Jupiter's dusk magnetosphere: Dual spacecraft observations, Geophysical Research Letters, 29, doi: 10.1029/2001GL014290.

Kurth, W. S., G. B. Hospodarsky, D. A. Gurnett, L. Lamy, M. K. Dougherty, J. Nichols, E. J. Bunce, W. Pryor, K. Baines, T. Stallard, H. Melin, F. J. Crary, (2016), Saturn kilometric radiation intensities during the Saturn auroral campaign of 2013, Icarus 263, 2-9, doi: 10.1016/j.icarus.2015.01.003.

Kurth, W. S., E. J. Bunce, J. T. Clarke, F. J. Crary, D. C. Grodent, A. P. Ingersoll, U. A. Dyudina, L. Lamy, D. G. Mitchell, A. M. Persoon, W. R. Pryor, J. Saur, T. Stallard, (2009), Auroral Processes, In Saturn from Cassini-Huygens, (eds.), M. K. Dougherty, L. W. Esposito S. M. Krimigis, 333-374, Dordrecht, New York, Springer.

Kurth, W. S., T. F. Averkamp, D. A. Gurnett, J. B. Groene, A. Lecacheux, (2008), An update to a Saturnian longitude system based on kilometric radio emissions, Journal of Geophysical Research Space Physics 113 (A5), A05222.

Kurth, W. S., T. F. Averkamp, D. A. Gurnett, Z. Wang, (2006), Cassini RPWS observations of dust in Saturn's E ring, Planetary and Space Science, 54, 988–998, doi: 10.1016/j.pss.2006.05011.

Kurth, W. S., G. B. Hospodarsky, D. A. Gurnett, B. Cecconi, P. Louarn, A. Lecacheux, P. Zarka, H. O. Rucker, M. Boudjada, M. L. Kaiser, (2005), High spectral and temporal resolution observations of Saturn kilometric radiation, Geophysical Research Letters, 32, L20S07, doi: 10.1029/2005GL022648.

Kurth, W. S., D. A. Gurnett, G. B. Hospodarsky, W. M. Farrell, A. Roux, M. K. Dougherty, S. P. Joy, M. G. Kivelson, R. J. Walker, F. J. Crary, C. J. Alexander, (2002), The dusk flank of Jupiter's magnetosphere, Nature 415 (6875), 991-994.

Kurth, W. S., G. B. Hospodarsky, D. A. Gurnett, A. Lecacheux, P. Zarka, M. D. Desch, M. L. Kaiser, W. M. Farrell, (2001a), High-resolution observations of low-frequency Jovian radio emissions by Cassini, In Planetary Radio Emissions V, (eds.) H. O. Rucker, M. L. Kaiser, Y. Leblanc, Austrian Academy of Sciences Press, Vienna, Austria, pp. 15–28.

Kurth, W. S., G. B. Hospodarsky, D. A. Gurnett, M. L. Kaiser, J.-E. Wahlund, A. Roux, P. Canu, P. Zarka, Y. Tokarev, (2001b), An overview of observations by the Cassini radio and plasma wave investigation at Earth, Journal of Geophysical Research, 106, 30,239-30,252, doi: 10.1029/2001JA900033.

Lagg, A., N. Krupp, S. Livi, J. Woch, S. Krimigis, M. Dougherty, (2001), Energetic particle measurements during the Earth swing-by of the Cassini spacecraft in August 1999, Journal of Geophysical Research Space Physics 106 (A12), 30, 209-30, 222.

Lamy, L., (2017), The Saturnian kilometric radiation before the Cassini grand finale, arXiv preprint arXiv:1709.07693.

Lamy, L., R. Prange, W. Pryor, J. Gustin, S. V. Badman, H. Melin, T. Stallard, D. G. Mitchell, P. C. Brandt, (2013), Multispectral simultaneous diagnosis of Saturn's aurorae throughout a planetary rotation, Journal of Geophysical Research Space Physics 118 (8), 4817-4843, doi: 10.1002/jgra.50404.

Lamy, L., (2011), Variability of southern and northern periodicities of Saturn Kilometric Radiation, arXiv preprint arXiv:1102.3099.

Lamy, L., P. Zarka, B. Cecconi, R. Prangé, W. S. Kurth, D. A. Gurnett, (2008), Saturn kilometric radiation: Average and statistical properties, Journal of Geophysical Research: Space Physics, 113, no. A7.

Lario, D., S. Livi, E. C. Roelof, R. B. Decker, S. M. Krimigis, M. K. Dougherty, (2004), Heliospheric energetic particle observations by the Cassini spacecraft: Correlation with 1 AU observations, Journal of Geophysical Research: Space Physics, 109, no. A9.

Lavvas, P., R. V. Yelle, T. Koskinen, A. Bazin, V. Vuitton, E. Vigren, M. Galand, A. Wellbrock, A. J. Coates, J.-E. Wahlund, F. J. Crary, D. Snowden, (2013), Aerosol growth in Titan's ionosphere, Proceedings of the National Academy of Sciences of the United States of America 110 (8), 2729-2734, doi: 10.1073/pnas.1217059110.

Lecacheux, A., W. S. Kurth, R. Manning, (2001), Sub-second time scales in jovian radio emissions as measured by Cassini/RPWS: Comparison with ground-based observations, https://austriaca.at/pre5/lecacheux2.pdf.

Lecacheux, A., (2001), Radio observations during the Cassini flyby of Jupiter, http://austriaca.at/pre5/lecacheux1.pdf.

Lipatov, A. S., E. C. Sittler Jr., R. E. Hartle, J. F. Cooper, and D. G. Simpson, (2014), Titan's plasma environment: 3D hybrid kinetic modeling of the TA flyby and comparison with CAPS-ELS and RPWS LP observations, Planetary and Space Science 93-94, 119-128, doi: 10.1016/j.pss.2014.02.012.

Lipatov, A. S., E. C. Sittler Jr., R. E. Hartle, J. F. Cooper, D. G. Simpson, (2012), Saturn's magnetosphere interaction with Titan for T9 encounter: 3D hybrid modeling and comparison with CAPS observations, Planetary and Space Science 61 (1), 66-78, doi: 10.1016/j.pss.2011.08.017.

Lipatov, A. S., E. C. Sittler Jr., R. E. Hartle, J. F. Cooper, D. G. Simpson, (2011), Background and pickup ion velocity distribution dynamics in Titan's plasma environment: 3D hybrid simulation and comparison with CAPS T9 observations, Advances in Space Research 48 (6), 1114-1125, doi: 10.1016/j.asr.2011.05.026.

Liu, X. and T. W. Hill, (2012), Effects of finite plasma pressure on centrifugally driven convection in Saturn's inner magnetosphere, Journal of Geophysical Research Space Physics 117, A07216, doi: 10.1029/2012JA017827.

Liu, X., T. W. Hill, R. A. Wolf, S. Sazykin, R. W. Spiro, H. Wu, (2010), Numerical simulation of plasma transport in Saturn's inner magnetosphere using the Rice Convection Model, Journal of Geophysical Research Space Physics 115, A12254, doi: 10.1029/2010ja015859.

Livi, R., J. Goldstein, J. L. Burch, F. Crary, A. M. Rymer, D. G. Mitchell, A. M. Persoon, (2014), Multi-instrument analysis of plasma parameters in Saturn's equatorial, inner magnetosphere using corrections for corrections for spacecraft potential and penetrating background radiation, Journal of Geophysical Research: Space Physics, 119, no. 5, 3683—3707.

Louarn, P., W. S. Kurth, D. A. Gurnett, G. B. Hospodarsky, A. M. Persoon, B. Cecconi, A. Lecacheux, P. Zarka, P. Canu, A. Roux, H. O. Rucker, W. M. Farrell, M. L. Kaiser, N. Andre, C. Harvey, M. Blanc, (2007), Observation of similar radio signatures at Saturn and Jupiter: Implications for the magnetospheric dynamics, Geophysical Research Letters 34 (20), L20113.

Louis, C. K., L. Lamy, P. Zarka, B. Cecconi, S. L. G. Hess, (2017), Detection of Jupiter decametric emissions controlled by Europa and Ganymede with Voyager/PRA and Cassini/RPWS, Journal of Geophysical Research: Space Physics, 122, no. 9, 9228–9247.

Luhmann, J. G., R. E. Johnson, R. L. Tokar, S. A. Ledvina, T. E. Cravens, (2006), A model of the ionosphere of Saturn's rings and its implications, Icarus 181 (2), 465-74. doi: 10.1016/j.icarus.2005.11.022.

Ma, Y.-J., C. T. Russell, A. F. Nagy, G. Toth, C. Bertucci, M. K. Dougherty, F. M. Neubauer, A. Wellbrock, A. J. Coates, P. Garnier, J. E. Wahlund, T. E. Cravens, F. J. Crary, (2009), Time-dependent global MHD simulations of Cassini T32 flyby: From magnetosphere to magnetosheath, Journal of Geophysical Research-Space Physics 114, A03204, doi: 10.1029/2008ja013676.

Ma, Y.-J., A. F. Nagy, G. Toth, T. E. Cravens, C. T. Russell, T. I. Gombosi, J.-E. Wahlund, et al., (2007), 3D global multi-species Hall-MHD simulation of the Cassini T9 flyby, Geophysical Research Letters, 34, no. 24.

Madanian, H., T. E. Cravens, M. S. Richard, J. H. Waite, N. J. T. Edberg, J. H. Westlake, J. E. Wahlund, (2016), Solar cycle variations in ion composition in the dayside ionosphere of Titan, Journal of Geophysical Research Space Physics 121 (8), 8013-8037, doi: 10.1002/2015ja022274.

Magee, B. A., et al., (2018), in preparation.

Magee, B. A., J. H. Waite, K. E. Mandt, J. Westlake, J. Bell, D. A. Gell, (2009), INMS-derived composition of Titan's upper atmosphere: Analysis methods and model comparison, Planetary and Space Science 57 (14-15), 1895-1916, doi: 10.1016/j.pss.2009.06.016.

Mandt, K. E., D. A. Gell, M. Perry, J. H.r Waite, F. A. Crary, D. Young, B. A. Magee, et al., (2012), Ion densities and composition of Titan's upper atmosphere derived from the Cassini Ion Neutral Mass Spectrometer: Analysis methods and comparison of measured ion densities to photochemical model simulations, Journal of Geophysical Research: Planets 117, no. E10.

MAPSview, (2019), MAPS Key Parameter Database, Regents of the University of Michigan & IRAP Toulouse, France, http://mapskp.cesr.fr/index.php.

Martens, H. R., D. B. Reisenfeld, J. D. Williams, R. E. Johnson, H. T. Smith, (2008), Observations of molecular oxygen ions in Saturn's inner magnetosphere, Geophysical Research Letters 35 (20), 20103, doi: 10.1029/2008GL035433.

Martin, C. J. and C. S. Arridge, (2017), Cassini observations of aperiodic waves on Saturn's magnetodisc, Journal of Geophysical Research: Space Physics, 122, no. 8, 8063–8077.

Masters, A., A. H. Sulaiman, L. Stawarz, B. Reville, N. Sergis, M. Fujimoto, D. Burgess, A. J. Coates, M. K. Dougherty, (2017), An in situ comparison of electron acceleration at collisionless shocks under differing upstream magnetic field orientations, Astrophysical Journal 843 (2), doi: 10.3847/1538-4357/aa76ea.

Masters, A., A. H. Sulaiman, N. Sergis, L. Stawarz, M. Fujimoto, A. J. Coates, M. K. Dougherty, (2016), Suprathermal electrons at Saturn's bow shock, Astrophysical Journal 826 (1), doi: 10.3847/0004-637x/826/1/48.

Masters, A., (2015), The dayside reconnection voltage applied to Saturn's magnetosphere, Geophysical Research Letters 42 (8), 2577-2585, doi: 10.1002/2015GL063361.

Masters, A., M. Fujimoto, H. Hasegawa, C. T. Russell, A. J. Coates, M. K. Dougherty, (2014), Can magnetopause reconnection drive Saturn's magnetosphere?, Geophysical Research Letters 41 (6), 1862-1868, doi: 10.1002/2014GL059288.

Masters, A., J. A. Slavin, G. A. DiBraccio, T. Sundberg, R. M. Winslow, C. L. Johnson, B. J. Anderson, H. Korth, (2013a), A comparison of magnetic overshoots at the bow shocks of Mercury and Saturn, Journal of Geophysical Research: Space Physics, 118, no. 7, 4381–4390.

Masters, A., L. Stawarz, M. Fujimoto, S. J. Schwartz, N. Sergis, M. F. Thomsen, A. Retino, et al., (2013b), Electron acceleration to relativistic energies at a strong quasi-parallel shock wave, Nature Physics, 9, no. 3, 164.

Masters, A., J. P. Eastwood, M. Swisdak, M. F. Thomsen, C. T. Russell, N. Sergis, F. J. Crary, M. K. Dougherty, A. J. Coates, S. M. Krimigis, (2012a), The importance of plasma β conditions for magnetic reconnection at Saturn's magnetopause, Geophysical Research Letters, 39, no. 8.

Masters, A., N. Achilleos, J. C. Cutler, A. J. Coates, M. K. Dougherty, G. H. Jones, (2012b), Surface waves on Saturn's magnetopause, Planetary and Space Science, 65, no. 1, 109-121.

Masters, A., S. J. Schwartz, E. M. Henley, M. F. Thomsen, B. Zieger, A. J. Coates, N. Achilleos, J. Mitchell, K. C. Hansen, M. K. Dougherty, (2011a), Electron heating at Saturn's bow shock, Journal of Geophysical Research Space Physics 116, A10107, doi: 10.1029/2011JA016941.

Masters, A., D. G. Mitchell, A. J. Coates, M. K. Dougherty, (2011b), Saturn's low-latitude boundary layer: 1. Properties and variability, Journal of Geophysical Research: Space Physics, 116, no. A6.

Masters, A., A. P. Walsh, A. N. Fazakerley, A. J. Coates, M. K. Dougherty, (2011c), Saturn's low-latitude boundary layer: 2. Electron structure, Journal of Geophysical Research: Space Physics, 116, no. A6.

Masters, A., N. Achilleos, M. G. Kivelson, N. Sergis, M. K. Dougherty, M. F. Thomsen, C. S. Arridge, S. M. Krimigis, H. J. McAndrews, S. J. Kanani, N. Krupp, A. J. Coates, (2010), Cassini observations of a Kelvin-Helmholtz vortex in Saturn's outer magnetosphere, Journal of Geophysical Research Space Physics 115, A07225, doi: 10.1029/2010ja015351.

Masters, A., H. J. McAndrews, J. T. Steinberg, M. F. Thomsen, C. S. Arridge, M. K. Dougherty, L. Billingham, S. J. Schwartz, N. Sergis, G. B. Hospodarsky, A. J. Coates, (2009), Hot flow anomalies at Saturn's bow shock, Journal of Geophysical Research Space Physics 114, A08217, doi: 10.1029/2009ja014112.

Masters, A., N. Achilleos, M. K. Dougherty, J. A. Slavin, G. B. Hospodarsky, C. S. Arridge, A. J. Coates, (2008), An empirical model of Saturn's bow shock: Cassini observations of shock location and shape, Journal of Geophysical Research: Space Physics, 113, no. A10.

Mauk, B. H. and N. J. Fox, (2010), Electron radiation belts of the solar system, Journal of Geophysical Research Space Physics 115 (A12), doi: 10.1029/2010JA015660.

Mauk, B. H., J. Saur, D. G. Mitchell, E. C. Roelof, P. C. Brandt, T. P. Armstrong, D. C. Hamilton, S. M. Krimigis, N. Krupp, S. A. Livi, J. W. Manweiler, C. P. Paranicas, (2005), Energetic particle injections in Saturn's magnetosphere, Geophysical Research Letters 32 (14), 14-05, doi: 10.1029/2005GL022485.

Mauk, B. H., D. G. Mitchell, S. M. Krimigis, E. C. Roelof, C. P. Paranicas, (2003), Energetic neutral atoms from a trans-Europa gas torus at Jupiter, Nature 421, no. 6926, 920.

Mauk, B. H., S. M. Krimigis, D. G. Mitchell, E. C. Roelof, E. P. Keath, J. Dandouras, (1998), Imaging Saturns dust rings using energetic neutral atoms, Planetary and Space Science, 46, no. 9–10, 1349–1362.

McAndrews, H. J., M. F. Thomsen, C. S. Arridge, C. M. Jackman, R. J. Wilson, M. G. Henderson, R. L. Tokar, K. K. Khurana, E. C. Sittler, A. J. Coates, M. K. Dougherty, (2009), Plasma in Saturn's nightside magnetosphere and the implications for global circulation, Planetary and Space Science 57 (14-15), 1714-1722, doi: 10.1016/j.pss.2009.03.003.

McAndrews, H. J., C. J. Owen, M. F. Thomsen, B. Lavraud, A. J. Coates, M. K. Dougherty, D. T. Young, (2008), Evidence for reconnection at Saturn's magnetopause, Journal of Geophysical Research Space Physics 113 (A4), A04210.

McComas, D. J., E. J. Zirnstein, M. Bzowski, M. A. Dayeh, H. O. Funsten, S. A. Fuselier, P. H. Janzen, M. A. Kubiak, H. Kucharek, E. Möbius, (2017), Seven years of imaging the global heliosphere with IBEX, The Astrophysical Journal Supplement Series 229 (2), 41.

McComas, D. J., F. Allegrini, P. Bochsler, M. Bzowski, E. R. Christian, G. B. Crew, R. DeMajistre, H. Fahr, H. Fichtner, P. C. Frisch, (2009), Global observations of the interstellar interaction from the Interstellar Boundary Explorer (IBEX), Science.

McComas, D. J., N. A. Schwadron, F. J. Crary, H. A. Elliott, D. T. Young, J. T. Gosling, M. F. Thomsen, E. Sittler, J. J. Berthelier, K. Szego, A. J. Coates, (2004), The interstellar hydrogen shadow: observations of interstellar pickup ions beyond Jupiter, Journal of Geophysical Research Space Physics 109 (A2), 6. doi: 10.1029/2003JA010217.

Meier, P., U. Motschmann, J. Schmidt, F. Spahn, T. W. Hill, Y. Dong, G. H. Jones, H. Kriegel, (2015), Modeling the total dust production of Enceladus from stochastic charge equilibrium and simulations, Planetary and Space Science, 119, 208–221.

Meier, P., H. Kriegel, U. Motschmann, J. Schmidt, F. Spahn, T. W. Hill, Y. Dong, G. H. Jones, (2014), A model of the spatial and size distribution of Enceladus' dust plume, Planetary and Space Science 104 (Part B), 216-233, doi: 10.1016/j.pss.2014.09.016.

Menietti, J. D., O. Santolik, A. M. Rymer, G. B. Hospodarsky, D. A. Gurnett, A. J. Coates, (2008), Analysis of plasma waves observed in the inner Saturn magnetosphere, Annales Geophysicae 26 (9), 2631-2644.

Menietti, J. D., D. A. Gurnett, G. B. Hospodarsky, C. A. Higgions, W. S. Kurth, P. Zarka, (2003), Modeling radio emission attenuation lanes observed by the Galileo and Cassini spacecraft, Planetary and Space Science 51 (9), 533-40, doi: 10.1016/S0032-0633(03)00078-3.

Meredith, C. J., S. W. H. Cowley, J. D. Nichols, (2014), Survey of Saturn auroral storms observed by the Hubble Space Telescope: Implications for storm time scales, Journal of Geophysical Research Space Physics 119 (12), 9624-9642, doi: 10.1002/2014JA020601.

Meredith, C. J., S. W. H. Cowley, K. C. Hansen, J. D. Nichols, T. K. Yeoman, (2013), Simultaneous conjugate observations of small-scale structures in Saturn's dayside ultraviolet auroras: Implications for physical origins, Journal of Geophysical Research Space Physics 118 (5), 2244-2266, doi: 10.1002/jgra.50270.

Meyer-Vernet, N., M. Moncuquet, K. Issautier, P. Schippers, (2017), Frequency range of dust detection in space with radio and plasma wave receivers: Theory and application to interplanetary nanodust impacts on Cassini, Journal of Geophysical Research Space Physics 122 (1), 8-22, doi: 10.1002/2016ja023081.

Meyer-Vernet, N., A. Lecacheux, M. L. Kaiser, D. A. Gurnett, (2009), Detecting nanoparticles at radio frequencies: Jovian dust stream impacts on Cassini/RPWS, Geophysical Research Letters 36, L03103, doi: 10.1029/2008gl036752.

Michael, M., S. N. Tripathi, P. Arya, A. Coates, A. Wellbrock, D. T. Young, (2011), High-altitude charged aerosols in the atmosphere of Titan, Planetary and Space Science 59 (9), 880-885. doi: 10.1016/j.pss.2011.03.010.

Milan, S. E., E. J. Bunce, S. W. H. Cowley, C. M. Jackman, (2005), Implications of rapid planetary rotation for the Dungey magnetotail of Saturn, Journal of Geophysical Research Space Physics 110 (A3), 10, doi: 10.1029/2004JA010716.

Mitchell, D. G., et al., (2018), submitted.

Mitchell, D. G., M. E. Perry, D. C. Hamilton, J. H. Westlake, P. Kollmann, H. T. Smith, J. F. Carbary, Jr. J. H. Waite, R. Perryman, H.-W. Hsu, J.-E. Wahlund, M. W. Morooka, L. Z. Hadid, A. M. Persoon, W. S. Kurth, (2018), Dust grains fall from Saturn's D-ring into its equatorial upper atmosphere, Science 362, no. 6410, eaat2236.

Mitchell, D. G., J. F. Carbary, E. J. Bunce, Aikaterini Radioti, S. V. Badman, W. R. Pryor, G. B. Hospodarsky, W. S. Kurth, (2016), Recurrent pulsations in Saturn's high latitude magnetosphere, Icarus, 263, 94-100.

Mitchell, D. G., P. C. Brandt, J. F. Carbary, W. S. Kurth, S. M. Krimigis, C. Paranicas, N. Krupp, D. C. Hamilton, B. H. Mauk, G. B. Hospodarsky, M. K. Dougherty, W. R. Pryor, (2015), Injection, interchange, and reconnection: Energetic particle observations in Saturn's magnetosphere, In Magnetotails in the Solar System, (eds.), A. Keiling, C. M. Jackman P. A. Delamere, 327-343, Hoboken, New Jersey, John Wiley & Sons, Inc.

Mitchell, D. G., W. S. Kurth, G. B. Hospodarsky, N. Krupp, J. Saur, B. H. Mauk, J. F. Carbary, S. M. Krimigis, M. K. Dougherty, D. C. Hamilton, (2009a), Ion conics and electron beams associated with auroral processes on Saturn, Journal of Geophysical Research: Space Physics, 114, no. A2.

Mitchell, D. G., S. M. Krimigis, C. Paranicas, P. C. Brandt, J. F. Carbary, E. C. Roelof, W. S. Kurth, et al., (2009b), Recurrent energization of plasma in the midnight-to-dawn quadrant of Saturn's magnetosphere, and its relationship to auroral UV and radio emissions, Planetary and Space Science, 57, no. 14–15, 1732–1742.

Mitchell, D. G., P. C. Brandt, E. C. Roelof, J. Dandouras, S. M. Krimigis, B. H. Mauk, C. P. Paranicas, et al., (2005), Energetic ion acceleration in Saturn's magnetotail: Substorms at Saturn?, Geophysical Research Letters, 32, no. 20.

Mitchell, D. G., C. P. Paranicas, B. H. Mauk, E. C. Roelof, S. M. Krimigis, (2004), Energetic neutral atoms from Jupiter measured with the Cassini magnetospheric imaging instrument: Time dependence and composition, Journal of Geophysical Research: Space Physics, 109, no. A9.

Modolo, R., M. Chanteur, J. E. Wahlund, P. Canu, W. S. Kurth, D. Gurnett, A. P. Matthews, C. Bertucci, (2007a), Plasma environment in the wake of Titan from hybrid simulation: A case study, Geophysical Research Letters 34 (24), L24S07.

Modolo, R., J. E. Wahlund, R. Bostrom, P. Canu, W. S. Kurth, D. Gurnett, G. R. Lewis, A. J. Coates, (2007b), Far plasma wake of Titan from the RPWS observations: A case study, Geophysical Research Letters 34 (24), L24S04.

Moore, L., I. Müeller-Wodarg, M. Galand, A. Kliore, M. Mendillo, (2010), Latitudinal variations in Saturn's ionosphere: Cassini measurements and model comparisons, Journal of Geophysical Research: Space Physics, 115, no. A11.

Moore, L., A. F. Nagy, A. J. Kliore, I. Müller-Wodarg, J. D. Richardson, M. Mendillo, (2006), Cassini radio occultations of Saturn's ionosphere: Model comparisons using a constant water flux, Geophysical Research Letters, 33, no. 22.

Morooka, M. W., J. E. Wahlund, A. I. Eriksson, W. M. Farrell, D. A. Gurnett, W. S. Kurth, A. M. Persoon, M. Shafiq, M. Andre, M. K. G. Holmberg, (2011), Dusty plasma in the vicinity of Enceladus, Journal of Geophysical Research Space Physics 116, A12221, doi: 10.1029/2011JA017038.

Moses, J. I. and S. F. Bass, (2000), The effects of external material on the chemistry and structure of Saturn's ionosphere, Journal of Geophysical Research Planets 105 (E3), 7013-7052, doi: 10.1029/1999JE001172.

Müeller, A. L., J. Saur, N. Krupp, E. Roussos, B. H. Mauk, A. M. Rymer, D. G. Mitchell, S. M. Krimigis, (2010), Azimuthal plasma flow in the Kronian magnetosphere, Journal of Geophysical Research Space Physics 115, A08203, doi: 10.1029/2009ja015122.

Müeller-Wodarg, I. C. F., L. Moore, M. Galand, S. Miller, M. Mendillo, (2012), Magnetosphere-atmosphere coupling at Saturn: 1-Response of thermosphere and ionosphere to steady state polar forcing, Icarus 221(2), 481-494, doi: 10.1016/j.icarus.2012.08.034.

Müeller-Wodarg, I. C. F., R. V. Yelle, J. Cui, J. H. Waite, (2008), Horizontal structures and dynamics of Titan's thermosphere, Journal of Geophysical Research: Planets, 113, no. E10.

Müeller-Wodarg, I. C. F., R. V. Yelle, N. Borggren, J. H. Waite, (2006a), Waves and horizontal structures in Titan's thermosphere, Journal of Geophysical Research Space Physics 111 (A12), A12315.

Müeller-Wodarg, I. C. F., M. Mendillo, R. V. Yelle, A. D. Aylward, (2006b), A global circulation model of Saturn's thermosphere, Icarus, 180, no. 1, 147–160.

Müeller-Wodarg, I. C. F., R. V. Yelle, M. J. Mendillo, A. D. Aylward, (2003), On the global distribution of neutral gases in Titan's upper atmosphere and its effect on the thermal structure, Journal of Geophysical Research: Space Physics, 108, no. A12.

Müeller-Wodarg, I. C. F. and R. V. Yelle, (2002), The effect of dynamics on the composition of Titan's upper atmosphere, Geophysical Research Letters, 29, no. 23, 54-1–54-4.

Müeller-Wodarg, I. C. F., R. V. Yelle, M. Mendillo, L. A. Young, A. D. Aylward, (2002), The thermosphere of Titan simulated by a global three-dimensional time-dependent model, Journal of Geophysical Research: Space Physics, 105, no. A9, 20833–20856.

Nagy, A. and T. Cravens, (1998), Titan's ionosphere: A review, Planetary and Space Science 46, no. 9-10, 1149-1155, doi: 10.1016/S0032-0633(98)00049-X.

Nemeth, Z., K. Szego, L. Foldy, S. W. H. Cowley, G. Provan, M. Thomsen, (2016), Periodic motion of the magnetodisk as a cause of quasi-periodic variations in the Kronian magnetosphere, Planetary and Space Science 130, 54-59.

Nemeth, Z., K. Szego, L. Foldy, M. G. Kivelson, X. Jia, K. M. Ramer, S. W. H. Cowley, G. Provan, M. Thomsen, (2015), The latitudinal structure of the nightside outer magnetosphere of Saturn as revealed by velocity moments of thermal ions, Annales Geophysicae 33 (9), 1195-1202, doi: 10.5194/angeo-33-1195-2015.

Nemeth, Z., K. Szego, Z. Bebesi, G. Erdos, L. Foldy, A. Rymer, E. C. Sittler, A. J. Coates, A. Wellbrock, (2011), Ion distributions of different Kronian plasma regions, Journal of Geophysical Research Space Physics 116, A09212, doi: 10.1029/2011JA016585.

Neubauer, F. M., H. Backes, M. K. Dougherty, A. Wennmacher, C. T. Russell, A. Coates, D. Young, et al, (2006), Titan's near magnetotail from magnetic field and electron plasma observations and modeling: Cassini flybys TA, TB, and T3, Journal of Geophysical Research: Space Physics, 111, no. A10.Neubauer, F. M., D. A. Gurnett, J. D. Scudder, and R. E. Hartle, (1984), Titan’s magnetospheric interaction, Saturn 1, 760-787.

Nichols, J. D., B. Cecconi, J. T. Clarke, S. W. H. Cowley, J. C. Gerard, A. Grocott, D. Grodent, L. Lamy, P. Zarka, (2010), Variation of Saturn’s UV aurora with SKR phase, Geophysical Research Letters 37, L15102, doi: 10.1029/2010gl044057.

Nichols, J. D., S. V. Badman, E. J. Bunce, J. T. Clarke, S. W. H. Cowley, F. J. Crary, M. K. Dougherty, J. C. Gerard, D. Grodent, K. C. Hansen, W. S. Kurth, D. G. Mitchell, W. R. Pryor, T. S. Stallard, D. L. Talboys, S. Wannawichian, (2009), Saturn’s equinoctial auroras, Geophysical Research Letters 36, doi: 10.1029/2009gl041491.

Nichols, J. D., J. T. Clarke, S. W. H. Cowley, J. Duval, A. J. Farmer, J.-C. Gérard, D. Grodent, S. Wannawichian, (2008), Oscillation of Saturn's southern auroral oval, Journal of Geophysical Research: Space Physics, 113, no. A11.

Omidi, N., A. H. Sulaiman, W. Kurth, H. Madanian, T. Cravens, N. Sergis, M. K. Dougherty, N. J. T. Edberg, (2017), A single deformed bow shock for Titan-Saturn system, Journal of Geophysical Research Space Physics 122 (11), 11058-11075, doi: 10.1002/2017ja024672.

Opher, M., J. F. Drake, B. Zieger, T. I. Gombosi, (2015), Magnetized jets driven by the Sun: The structure of the heliosphere revisited, The Astrophysical Journal Letters 800 (2), L28, doi: 10.1088/2041-8205/800/2/L28.

Palmaerts, B., A. Radioti, E. Roussos, D. Grodent, J.-C. Gérard, N. Krupp, D. G. Mitchell., (2016a), Pulsations of the polar cusp aurora at Saturn, Journal of Geophysical Research: Space Physics, 121, no. 12, 11–952.

Palmaerts, B., E. Roussos, N. Krupp, W. S. Kurth, D. G. Mitchell, J. N. Yates, (2016b), Statistical analysis and multi-instrument overview of the quasi-periodic 1-hour pulsations in Saturn’s outer magnetosphere, Icarus, 271, 1–18.

Panchenko, M., S. Rošker, H. O. Rucker, A. Brazhenko, P. Zarka, G. Litvinenko, V. E. Shaposhnikov, A. A. Konovalenko, V. Melnik, A. V. Franzuzenko, (2018a), Zebra pattern in decametric radio emission of Jupiter, Astronomy & Astrophysics 610, A69.

Panchenko, M., S. Rosker, H. O. Rucker, A. Brazhenko, A. A. Konovalenko, G. Litvinenko, P. Zarka, V. Melnik, V. E. Shaposhnikov, A. V. Frantsuzenko, (2018b), Zebra-like fine spectral structures in Jovian decametric radio emission, 103–116.

Panchenko, M., H. O. Rucker, W. M. Farrell, (2013), Periodic bursts of Jovian non-Io decametric radio emission, Planetary and Space Science 77 (SI), 3-11. doi: 10.1016/j.pss.2012.08.015.

Panchenko, M. and H. O. Rucker, (2011), New type of periodic bursts of non-Io Jovian decametric radio emission, Planetary, Solar and Heliospheric Radio Emissions, Planetary Radio Emissions VII, Proceedings of the 7th International Workshop held at Graz, Austria, September 15-17, 2010, (eds.), H. O. Rucker, W. S. Kurth, P. Louarn, G. Fischer. Austrian Academy of Sciences Press, Vienna, p. 157-166.

Panchenko, M., H. O. Rucker, M. L. Kaiser, O. C. St Cyr, J. L. Bougeret, K. Goetz, S. D. Bale, (2010), New periodicity in Jovian decametric radio emission, Geophysical Research Letters 37, L05106, doi: 10.1029/2010gl042488.

Paranicas, C., M. F. Thomsen, N. Achilleos, M. Andriopoulou, S. V. Badman, G. Hospodarsky, C. M. Jackman, X. Jia, T. Kennelly, K. Khurana, P. Kollmann, N. Krupp, P. Louarn, E. Roussos, N. Sergis, (2016), Effects of radial motion on interchange injections at Saturn, Icarus 264, 342-351, doi: 10.1016/j.icarus.2015.10.002.

Paranicas, C., E. Roussos, R. B. Decker, R. E. Johnson, A. R. Hendrix, P. Schenk, T. A. Cassidy, J. B. Dalton, III, C. J. A. Howett, P. Kollmann, W. Patterson, K. P. Hand, T. A. Nordheim, N. Krupp, D. G. Mitchell, (2014), The lens feature on the inner saturnian satellites, Icarus 234, 155-161, doi: 10.1016/j.icarus.2014.02.026.

Paranicas, C., E. Roussos, N. Krupp, P. Kollmann, A. R. Hendrix, T. Cassidy, R. E. Johnson, P. Schenk, G. Jones, J. Carbary, D. G. Mitchell, K. Dialynas, (2012), Energetic charged particle weathering of Saturn's inner satellites, Planetary and Space Science 61 (1), 60-65, doi: 10.1016/j.pss.2011.02.012.

Paranicas, C., D. G. Mitchell, E. Roussos, P. Kollmann, N. Krupp, A. L. Müeller, S. M. Krimigis, F. S. Turner, P. C. Brandt, A. M. Rymer, R. E. Johnson, (2010), Transport of energetic electrons into Saturn's inner magnetosphere, Journal of Geophysical Research Space Physics 115, A09214, doi: 10.1029/2010ja015853.

Paranicas, C., D. G. Mitchell, S. M. Krimigis, D. C. Hamilton, E. Roussos, N. Krupp, G. H. Jones, R. E. Johnson, J. F. Cooper, T. P. Armstrong, (2008), Sources and losses of energetic protons in Saturn's magnetosphere, Icarus 197 (2), 519-525, doi: 10.1016/j.icarus.2008.05.011.

Paranicas, C., D. G. Mitchell, E. C. Roelof, B. H. Mauk, S. M. Krimigis, P. C. Brandt, M. Kusterer, F. S. Turner, J. Vandegriff, N. Krupp, (2007), Energetic electrons injected into Saturn's neutral gas cloud, Geophysical Research Letters 34 (2), L02109.

Paranicas, C., D. G. Mitchell, S. Livi, S. M. Krimigis, E. Roussos, N. Krupp, J. Woch, A. Lagg, J. Saur, F. S. Turner, (2005), Evidence of Enceladus and Tethys microsignatures, Geophysical Research Letters, 32, no. 20.

Parker, E. N., (1961), The stellar-wind regions, The Astrophysical Journal 134, 20-27.

Parker, E. N., (1958), Dynamics of the interplanetary gas and magnetic fields, The Astrophysical Journal, 128, 664.

Perry, M. E., B. D. Teolis, D. M. Hurley, B. A. Magee, J. H. Waite, T. G. Brockwell, R. S. Perryman, R. L. McNutt, (2015), Cassini INMS measurements of Enceladus plume density, Icarus 257, 139-162, doi: 10.1016/j.icarus.2015.04.037.

Persoon, A. M., D. A. Gurnett, W. S. Kurth, J. B. Groene, J. B. Faden, (2015), Evidence for a seasonally dependent ring plasma in the region between Saturn's A ring and Enceladus' orbit, Journal of Geophysical Research Space Physics 120 (8), 6276-6285, doi: 10.1002/2015ja021180.

Persoon, A. M., D. A. Gurnett, J. S. Leisner, W. S. Kurth, J. B. Groene, J. B. Faden, (2013), The plasma density distribution in the inner region of Saturn's magnetosphere, Journal of Geophysical Research Space Physics 118 (6), 2970-2974, doi: 10.1002/jgra.50182.

Persoon, A. M., D. A. Gurnett, O. Santolik, W. S. Kurth, J. B. Faden, J. B. Groene, G. R. Lewis, A. J. Coates, R. J. Wilson, R. L. Tokar, J. E. Wahlund, M. Moncuquet, (2009), A diffusive equilibrium model for the plasma density in Saturn's magnetosphere, Journal of Geophysical Research Space Physics 114, A04211, doi: 10.1029/2008ja013912.

Pilkington, N. M., N. Achilleos, C. S. Arridge, P. Guio, A. Masters, L. C. Ray, N. Sergis, M. F. Thomsen, A. J. Coates, M. K. Dougherty, (2015), Internally driven large-scale changes in the size of Saturn's magnetosphere, Journal of Geophysical Research Space Physics 120 (9), 7289-7306, doi: 10.1002/2015ja021290.

Pontius Jr., D. H. and T. W. Hill, (2009), Plasma mass loading from the extended neutral gas torus of Enceladus as inferred from the observed plasma corotation lag, Geophysical Research Letters 36, L23103, doi: 10.1029/2009gl041030.

Porco, C., D. DiNino, F. Nimmo, (2014), How the geysers, tidal stresses, and thermal emission across the south polar terrain of Enceladus are related, Astronomical Journal 148 (3), 45-69, doi: 10.1088/0004-6256/148/3/45.

Provan, G., S. W. H. Cowley, T. J. Bradley, E. J. Bunce, G. J. Hunt, M. K. Dougherty, (2018), Planetary period oscillations in Saturn's magnetosphere: Cassini magnetic field observations over the northern summer solstice interval, Journal of Geophysical Research: Space Physics, 123, no. 5, 3859–3899.

Provan, G., S. W. H. Cowley, L. Lamy, E. J. Bunce, G. J. Hunt, P. Zarka, M. K. Dougherty, (2016), Planetary period oscillations in Saturn's magnetosphere: Coalescence and reversal of northern and southern periods in late northern spring, Journal of Geophysical Research: Space Physics, 121, no. 10, 9829–9862.

Provan, G., C. Tao, S. W. H. Cowley, M. K. Dougherty, A. J. Coates, (2015), Planetary period oscillations in Saturn's magnetosphere: Examining the relationship between abrupt changes in behavior and solar wind-induced magnetospheric compressions and expansions, Journal of Geophysical Research: Space Physics, 120, no. 11, 9524–9544.

Provan, G., L. Lamy, S. W. H. Cowley, M. K. Dougherty, (2014), Planetary period oscillations in Saturn's magnetosphere: Comparison of magnetic oscillations and SKR modulations in the postequinox interval, Journal of Geophysical Research Space Physics 119 (9), 7380–7401, doi: 10.1002/2014ja020011.

Provan, G., S. W. H. Cowley, J. Sandhu, D. J. Andrews, M. K. Dougherty, (2013), Planetary period magnetic field oscillations in Saturn's magnetosphere: Postequinox abrupt nonmonotonic transitions to northern system dominance, Journal of Geophysical Research Space Physics 118 (6), 3243-3264, doi: 10.1002/jgra.50186.

Provan, G., D. J. Andrews, C. S. Arridge, A. J. Coates, S. W. H Cowley, G. Cox, M. K. Dougherty, C. M. Jackman, (2012), Dual periodicities in planetary-period magnetic field oscillations in Saturn's tail, Journal of Geophysical Research Space Physics 117 (A01), A01209, doi: 10.1029/2011JA017104.

Provan, G., D. J. Andrews, B. Cecconi, S. W. H. Cowley, M. K. Dougherty, L. Lamy, P. M. Zarka, (2011), Magnetospheric period magnetic field oscillations at Saturn: Equatorial phase "jitter" produced by superposition of southern and northern period oscillations, Journal of Geophysical Research Space Physics 116, A04225, doi: 10.1029/2010ja016213.

Provan, G., D. J. Andrews, C. S. Arridge, A. J. Coates, S. W. H. Cowley, S. E. Milan, M. K. Dougherty, D. M. Wright, (2009), Polarization and phase of planetary-period magnetic field oscillations on high-latitude field lines in Saturn's magnetosphere, Journal of Geophysical Research: Space Physics, 114, no. A2.

Pryor, W. R., A. M. Rymer, D. G. Mitchell, T. W. Hill, D. T. Young, J. Saur, G. H. Jones, S. Jacobsen, S. W. H. Cowley, B. H. Mauk, A. J. Coates, J. Gustin, D. Grodent, J.-C. Gerard, L. Lamy, J. D. Nichols, S. M. Krimigis, L. W. Esposito, M. K. Dougherty, A. J. Jouchoux, A. I. F. Stewart, W. E. McClintock, G. M. Holsclaw, J. M. Ajello, J. E. Colwell, A. R. Hendrix, F. J. Crary, J. T. Clarke, X. Zhou, (2011), The auroral footprint of Enceladus on Saturn, Nature 472 (7343), 331-333, doi: 10.1038/nature09928.

Pryor, W. R., A. I. F. Stewart, L. W. Esposito, W. E. McClintock, J. E. Colwell, A. J. Jouchoux, A. J. Steffl, D. E. Shemansky, J. M. Ajello, R. A. West, C. J. Hansen, B. T. Tsurutani, W. S. Kurth, G. B. Hospodarsky, D. A. Gurnett, K. C. Hansen, J. H. Waite, Jr., F. J. Crary, D. T. Young, N. Krupp, J. T. Clarke, D. Grodent, M. K. Dougherty, (2005), Cassini UVIS observations of Jupiter's auroral variability, Icarus 178 (2), 312-26, doi: 10.1016/j.icarus.2005.05.021.

Radioti, A., D. Grodent, J.-C. Gérard, D. J. Southwood, E. Chané, B. Bonfond, W. Pryor, (2017a), Stagnation of Saturn's auroral emission at noon, Journal of Geophysical Research: Space Physics, 122, no. 6, 6078–6087.

Radioti, A., D. Grodent, Z. H. Yao, J.-C. Gérard, S. V. Badman, W. Pryor, B. Bonfond, (2017b), Dawn auroral breakup at Saturn initiated by auroral arcs: UVIS/Cassini beginning of Grand Finale Phase, Journal of Geophysical Research: Space Physics, 122, 12, doi: 10.1002/2017JA024653.

Radioti, A., D. Grodent, X. Jia, J. C. Gerard, B. Bonfond, W. Pryor, J. Gustin, D. G. Mitchell, C. M. Jackman, (2016), A multi-scale magnetotail reconnection event at Saturn and associated flows: Cassini/UVIS observations, Icarus 263, 75-82, doi: 10.1016/j.icarus.2014.12.016.

Radioti, A., D. Grodent, J. C. Gerard, E. Roussos, D. Mitchell, B. Bonfond, W. Pryor, (2015), Auroral spirals at Saturn, Journal of Geophysical Research Space Physics 120 (10), 8633-8643, doi: 10.1002/2015ja021442.

Radioti, A., D. Grodent, J.-C. Gérard, S. E. Milan, R. C. Fear, C. M. Jackman, B. Bonfond, W. Pryor, (2014), Saturn's elusive nightside polar arc, Geophysical Research Letters 41, 6321, doi: 10.1002/2014GL061081.

Radioti, A., E. Roussos, D. Grodent, J.-C. Gérard, N. Krupp, D. G. Mitchell, J. Gustin, B. Bonfond, W. Pryor, (2013a), Signatures of magnetospheric injections in Saturn's aurora, Journal of Geophysical Research Space Physics 118, 1922, doi: 10.1002/jgra.50161.

Radioti, A., D. Grodent, J.-C. Gérard, B. Bonfond, J. Gustin, W. Pryor, J. M. Jasinski, C. S. Arridge, (2013b), Auroral signatures of multiple magnetopause reconnection at Saturn, Geophysical Research Letters 40, 4498, doi: 10.1002/grl.50889.

Radioti, A., D. Grodent, J. C. Gerard, S. E. Milan, B. Bonfond, J. Gustin, W. Pryor, (2011), Bifurcations of the main auroral ring at Saturn: ionospheric signatures of consecutive reconnection events at the magnetopause, Journal of Geophysical Research Space Physics 116, A11209, doi: 10.1029/2011JA016661.

Radioti, A., D. Grodent, J. C. Gerard, E. Roussos, C. Paranicas, B. Bonfond, D. G. Mitchell, N. Krupp, S. Krimigis, J. T. Clarke, (2009), Transient auroral features at Saturn: Signatures of energetic particle injections in the magnetosphere, Journal of Geophysical Research Space Physics 114, A03210, doi: 10.1029/2008ja013632.

Ramer, K. M., M. G. Kivelson, N. Sergis, K. K. Khurana, X. Jia, (2017), Spinning, breathing, and flapping: Periodicities in Saturn's middle magnetosphere, Journal of Geophysical Research: Space Physics 122 (1), 393-416.

Reed, J. J., C. M. Jackman, L. Lamy, W. S. Kurth, D. K. Whiter, (2018), Low-frequency extensions of the Saturn kilometric radiation as a proxy for magnetospheric dynamics, Journal of Geophysical Research Space Physics 123 (1), 443-463, doi: 10.1002/2017ja024499.

Regoli, L. H., A. J. Coates, M. F. Thomsen, G. H. Jones, E. Roussos, J. H. Waite, N. Krupp, G. Cox, (2016), Survey of pickup ion signatures in the vicinity of Titan using CAPS/IMS, Journal of Geophysical Research Space Physics 121 (9), 8317-8328, doi: 10.1002/2016ja022617.

Richard, M. S., T. E. Cravens, C. Wylie, D. Webb, Q. Chediak, K. Mandt, J. H. Waite, A. Rymer, C. Bertucci, A. Wellbrock, A. Windsor, A. J. Coates, (2015a), An empirical approach to modeling ion production rates in Titan's ionosphere II: Ion production rates on the nightside, Journal of Geophysical Research Space Physics 120 (2), 1281-1298, doi: 10.1002/2014ja020343.

Richard, M. S., T. E. Cravens, C. Wylie, D. Webb, Q. Chediak, R. Perryman, K. Mandt, J. Westlake, J. H. Waite, I. Robertson, B. A. Magee, N. J. T. Edberg, (2015b), An empirical approach to modeling ion production rates in Titan's ionosphere I: Ion production rates on the dayside and globally, Journal of Geophysical Research Space Physics 120 (2), 1264-1280, doi: 10.1002/2013ja019706.

Rietmeijer, F. J. M., (1993), Size distributions in two porous chondritic micrometeorites, Earth and Planetary Science Letters 117 (3-4), 609-617.

Robertson, I. P., T. E. Cravens, J. H. Waite Jr., R. V. Yelle, V. Vuitton, A. J. Coates, J. E. Wahlund, K. Ågren, K. Mandt, B. Magee, M. S. Richard, E. Fattig, (2009), Structure of Titan's ionosphere: Model comparisons with Cassini data, Planetary and Space Science 57 (14-15), 1834-1846, doi: 10.1016/j.pss.2009.07.011.

Roelof, E. C., S. M. Krimigis, D. G. Mitchell, R. B. Decker, K. Dialynas, (2012), Cassini ENA images of the heliosheath and Voyager "ground truth": Thickness of the heliosheath, In AIP Conference Proceedings, vol. 1436, no. 1, pp. 239-244, American Institute of Physics, doi: 10.1063/1.4723614.

Rosenqvist, L., J. E. Wahlund, K. Ågren, R. Modolo, H. J. Opgenoorth, D. Strobel, I. Müeller-Wodarg, P. Garnier, C. Bertucci, (2009), Titan ionospheric conductivities from Cassini measurements, Planetary and Space Science 57 (14-15), 1828-1833, doi: 10.1016/j.pss.2009.01.007.

Roussos, E., P. Kollmann, N. Krupp, A. Kotova, L. Regoli, C. Paranicas, D. G. Mitchell, et al., (2018a), A radiation belt of energetic protons located between Saturn and its rings, Science, 362, no. 6410, eaat1962.

Roussos, E., P. Kollmann, N. Krupp, C. Paranicas, K. Dialynas, N. Sergis, D. G. Mitchell, D. C. Hamilton, S. M. Krimigis, (2018b), Drift-resonant, relativistic electron acceleration at the outer planets: Insights from the response of Saturn's radiation belts to magnetospheric storms, Icarus, 305, 160–173.

Roussos, E., C. M. Jackman, M. F. Thomsen, W. S. Kurth, S. V. Badman, C. Paranicas, P. Kollmann, et al., (2018c), Solar Energetic Particles (SEP) and Galactic Cosmic Rays (GCR) as tracers of solar wind conditions near Saturn: Event lists and applications, Icarus, 300, 47–71.

Roussos, E., N. Krupp, P. Kollmann, C. Paranicas, D. G. Mitchell, S. M. Krimigis, M. Andriopoulou, (2016a), Evidence for dust-driven, radial plasma transport in Saturn's inner radiation belts, Icarus, 274, 272–283.

Roussos, E., N. Krupp, D. G. Mitchell, C. Paranicas, S. M. Krimigis, M. Andriopoulou, B. Palmaerts, et al., (2016b), Quasi-periodic injections of relativistic electrons in Saturn's outer magnetosphere, Icarus, 263, 101–116.

Roussos, E., N. Krupp, C. Paranicas, J. F. Carbary, P. Kollmann, S. M. Krimigis, D. G. Mitchell, (2014), The variable extension of Saturn's electron radiation belts, Planetary and Space Science 104, 3-17, doi: 10.1016/j.pss.2014.03.021.

Roussos, E., M. Andriopoulou, N. Krupp, A. Kotova, C. Paranicas, S. M. Krimigis, D. G. Mitchell, (2013), Numerical simulation of energetic electron microsignature drifts at Saturn: Methods and applications, Icarus 226 (2), 1595-1611, doi: 10.1016/j.icarus.2013.08.023.

Roussos, E., N. Krupp, C. P. Paranicas, P. Kollmann, D. G. Mitchell, S. M. Krimigis, T. P. Armstrong, D. R. Went, M. K. Dougherty, G. H. Jones, (2011), Long- and short-term variability of Saturn's ionic radiation belts, Journal of Geophysical Research Space Physics 116, A02217, doi: 10.1029/2010ja015954.

Roussos, E., J. Wuller, S. Simon, (2008a), Plasma and fields in the wake of Rhea: 3-D hybrid simulation and comparison with Cassini data, In Annales geophysicae: atmospheres, hydrospheres and space sciences, vol. 26, no. 3, p. 619.

Roussos, E., N. Krupp, T. P. Armstrong, C. Paranicas, D. G. Mitchell, S. M. Krimigis, G. H. Jones, K. Dialynas, N. Sergis, D. C. Hamilton, Discovery of a transient radiation belt at Saturn, Geophysical Research Letters, 35, no. 22.

Roussos, E., G. H. Jones, N. Krupp, C. Paranicas, D. G. Mitchell, A. Lagg, J. Woch, U. Motschmann, S. M. Krimigis, M. K. Dougherty, (2007), Electron microdiffusion in the Saturnian radiation belts: Cassini MIMI/LEMMS observations of energetic electron absorption by the icy moons, Journal of Geophysical Research Space Physics 112 (A6), doi: 10.1029/2006ja012027.

Roussos, E., N. Krupp, G. H. Jones, C. Paranicas, D. G. Mitchell, S. M. Krimigis, U. Motschmann, M. K. Dougherty, A. Lagg, J. Woch, (2006), Icy Moon Absorption Signatures: Probes of Saturnian Magnetospheric Dynamics and Moon Activity, American Geophysical Union (AGU) Fall Meeting, abstract.

Rucker, H. O., M. Panchenko, C. Weber, (2014), Planetary radio astronomy: Earth, giant planets, and beyond, Advances in Radio Science 12, 211-220, doi: 10.5194/ars-12-211-2014.

Russell, C. T., H. Y. Wei, M. M. Cowee, F. M. Neubauer, M. K. Dougherty, (2016), Ion cyclotron waves at Titan, Journal of Geophysical Research Space Physics 121 (3), 2095-2103, doi: 10.1002/2015ja022293.

Rymer, A. M., (2010), Electron-ion thermal equilibration at Saturn: Electron signatures of ion pick-up?, In AIP Conference Proceedings, American Institute of Physics, vol. 1302, no. 1, pp. 250-255, doi: 10.1063/1.3529979.

Rymer, A. M., H. T. Smith, A. Wellbrock, A. J. Coates, D. T. Young, (2009a), Discrete classification and electron energy spectra of Titan's varied magnetospheric environment, Geophysical Research Letters, 36, no. 15.

Rymer, A. M., B. H. Mauk, T. W. Hill, N. Andre, D. G. Mitchell, C. Paranicas, D. T. Young, H. T. Smith, A. M. Persoon, J. D. Menietti, G. B. Hospodarsky, A. J. Coates, M. K. Dougherty, (2009b), Cassini evidence for rapid interchange transport at Saturn, Planetary and Space Science 57 (14-15), 1779-1784, doi: 10.1016/j.pss.2009.04.010.

Rymer, A. M., B. H. Mauk, T. W. Hill, C. Paranicas, D. G. Mitchell, A. J. Coates, D. T. Young, (2008), Electron circulation in Saturn’s magnetosphere, Journal of Geophysical Research Space Physics 113 (A1).

Rymer, A. M., B. H. Mauk, T. W. Hill, C. Paranicas, N. Andre, E. C. Sittler, D. G. Mitchell, H. T. Smith, R. E. Johnson, A. J. Coates, D. T. Young, S. J. Bolton, M. F. Thomsen, M. K. Dougherty, (2007), Electron sources in Saturn’s magnetosphere, Journal of Geophysical Research Space Physics 112 (A2), A02201.

Rymer, A., A. Coates, K. Svenes, G. Abel, D. Linder, B. Narheim, M. Thomsen, T. Young, (2001), Cassini plasma spectrometer electron spectrometer measurements during the Earth swing-by on August 18, 1999, Journal of Geophysical Research Space Physics 106 (A12), 30, 177-30, 198.

Sagnieres, L. B. M., M. Galand, J. Cui, P. P. Lavvas, E. Vigren, V. Vuitton, R. V. Yelle, A. Wellbrock, A. J. Coates, (2015), Influence of local ionization on ionospheric densities in Titan's upper atmosphere, Journal of Geophysical Research Space Physics 120 (7), 5899-5921, doi: 10.1002/2014ja020890.

Saur, J, N. Schilling, F. M. Neubauer, D. F. Strobel, S. Simon, M. K. Dougherty, C. T. Russell, R. T. Pappalardo, (2008), Evidence for temporal variability of Enceladus' gas jets: Modeling of Cassini observations, Geophysical Research Letters, 35, no. 20.

Saur, J., F. M. Neubauer, N. Schilling, (2007), Hemisphere coupling in Enceladus' asymmetric plasma interaction, Journal of Geophysical Research Space Physics 112 (A11), A11209.

Schippers, P., N. Meyer-Vernet, A. Lecacheux, S. Belheouane, M. Moncuquet, W. S. Kurth, I. Mann, D. G. Mitchell, N. Andre, (2015), Nanodust detection between 1 and 5AU using Cassini wave measurements, Astrophysical Journal 806 (1), 77, doi: 10.1088/0004-637x/806/1/77.

Schippers, P., N. Meyer-Vernet, A. Lecacheux, W. S. Kurth, D. G. Mitchell, N. Andre, (2014), Nanodust detection near 1AU from spectral analysis of Cassini/radio and plasma wave science data, Geophysical Research Letters 41 (15), 5382-5388, doi: 10.1002/2014GL060566.

Schippers, P., N. André, D. A. Gurnett, G. R. Lewis, A. M. Persoon, A. J. Coates, (2012), Identification of electron field-aligned current systems in Saturn's magnetosphere, Journal of Geophysical Research Space Physics 117 (A5).

Schippers, P., M. Blanc, N. Andre, I. Dandouras, G. R. Lewis, L. K. Gilbert, A. M. Persoon, N. Krupp, D. A. Gurnett, A. J. Coates, S. M. Krimigis, D. T. Young, M. K. Dougherty, (2008), Multi-instrument analysis of electron populations in Saturn's magnetosphere, Journal of Geophysical Research Space Physics 113 (A7), A07208, doi: 10.1029/2008ja013098.

Seki, K., A. Nagy, C. M. Jackman, F. Crary, D. Fontaine, P. Zarka, P. Wurz, et al., (2015), A review of general physical and chemical processes related to plasma sources and losses for Solar System magnetospheres, Space Science Reviews, 192, no. 1–4, 27–89.

Sergis, N., E. J. Bunce, J. F. Carbary, S. W. H. Cowley, X. Jia, D. C. Hamilton, S. M. Krimigis, D. G. Mitchell, M. K. Dougherty, (2018), The ring current of Saturn, In Electric Currents in Geospace and Beyond, (eds.) A. Keiling, O. Marghitu, and M. Wheatland, vol. 235, pp. 139-154, Hoboken, New Jersey, American Geophysical Union and John Wiley & Sons.

Sergis, N., C. M. Jackman, M. F. Thomsen, S. M. Krimigis, D. G. Mitchell, D. C. Hamilton, M. K. Dougherty, N. Krupp, R. J. Wilson, (2017), Radial and local time structure of the Saturnian ring current, revealed by Cassini, Journal of Geophysical Research Space Physics 122 (2), 1803-1815, doi: 10.1002/2016ja023742.

Sergis, N., C. M. Jackman, A. Masters, S. M. Krimigis, M. F. Thomsen, D. C. Hamilton, D. G. Mitchell, M. K. Dougherty, A. J. Coates, (2013), Particle and magnetic field properties of the Saturnian magnetosheath: Presence and upstream escape of hot magnetospheric plasma, Journal of Geophysical Research Space Physics 118 (4), 1620-1634, doi: 10.1002/jgra.50164.

Sergis, N., C. S. Arridge, S. M. Krimigis, D. G. Mitchell, A. M. Rymer, D. C. Hamilton, N. Krupp, M. K. Dougherty, A. J. Coates, (2011), Dynamics and seasonal variations in Saturn's magnetospheric plasma sheet, as measured by Cassini, Journal of Geophysical Research Space Physics 116, A04203, doi: 10.1029/2010ja016180.

Sergis, N., S. M. Krimigis, E. C. Roelof, C. S. Arridge, A. M. Rymer, D. G. Mitchell, D. C. Hamilton, N. Krupp, M. F. Thomsen, M. K. Dougherty, A. J. Coates, D. T. Young, (2010), Particle pressure, inertial force, and ring current density profiles in the magnetosphere of Saturn, based on Cassini measurements, Geophysical Research Letters 37, L02102, doi: 10.1029/2009gl041920.

Sergis, N., S. M. Krimigis, D. G. Mitchell, D. C. Hamilton, N. Krupp, B. H. Mauk, E. C. Roelof, M. K. Dougherty, (2009), Energetic particle pressure in Saturn's magnetosphere measured with the magnetospheric imaging instrument on Cassini, Journal of Geophysical Research Space Physics 114, A02214, doi: 10.1029/2008ja013774.

Sergis, N., S. M. Krimigis, D. G. Mitchell, D. C. Hamilton, N. Krupp, B. M. Mauk, E. C. Roelof, M. Dougherty, (2007), Ring current at Saturn: Energetic particle pressure in Saturn's equatorial magnetosphere measured with Cassini/MIMI, Geophysical Research Letters 34 (9), L09102.

Shafiq, Muhammad, J. E. Wahlund, M. W. Morooka, W. S. Kurth, W. M. Farrell, (2011), Characteristics of the dust-plasma interaction near Enceladus' South Pole, Planetary and Space Science 59 (1), 17-25, doi: h10.1016/j.pss.2010.10.006.

Shebanits, O., E. Vigren, J. E. Wahlund, M. Holmberg, M. Morooka, N. Edberg, K. Mandt, J. Waite, (2017), Titan's ionosphere: A survey of solar EUV influences, Journal of Geophysical Research Space Physics 122, no. 7, 7491-7503, doi: 10.1002/2017JA023987.

Shebanits, O., J. E. Wahlund, N. J. T. Edberg, F. J. Crary, A. Wellbrock, D. J. Andrews, E. Vigren, R. T. Desai, A. J. Coates, K. E. Mandt, J. H. Waite, (2016), Ion and aerosol precursor densities in Titan's ionosphere: A multi-instrument case study, Journal of Geophysical Research Space Physics 121 (10), 10075-10090, doi: 10.1002/2016ja022980.

Shebanits, O., J. E. Wahlund, K. Mandt, K. Ågren, N. J. T. Edberg, J. H. Waite Jr., (2013), Negative ion densities in the ionosphere of Titan-Cassini RPWS/LP results, Planetary and Space Science 84, 153-162, doi: 10.1016/j.pss.2013.05.021.

Sillanpää, I., E. Kallio, P. Janhunen, W. Schmidt, K. Mursula, J. Vilppola, P. Tanskanen, (2006), Hybrid simulation study of ion escape at Titan for different orbital positions, Advances in Space Research 38 (4), 799-805.

Simon, S., F. M. Neubauer, A. Wennmacher, M. K. Dougherty, (2014), Variability of Titan's induced magnetotail: Cassini magnetometer observations, Journal of Geophysical Research Space Physics 119 (3), 2024-2037, doi: 10.1002/2013ja019608.

Simon, S., S. C. van Treeck, A. Wennmacher, J. Saur, F. M. Neubauer, C. L. Bertucci, M. K. Dougherty, (2013), Structure of Titan's induced magnetosphere under varying background magnetic field conditions: Survey of Cassini magnetometer data from flybys TA–T85, Journal of Geophysical Research: Space Physics, 118, no. 4, 1679–1699.

Simon, S., J. Saur, H. Kriegel, F. M. Neubauer, U. Motschmann, M. K. Dougherty, (2011), Influence of negatively charged plume grains and hemisphere coupling currents on the

structure of Enceladus' Alfvén wings: Analytical modeling of Cassini magnetometer observations, Journal of Geophysical Research: Space Physics, 116, no. A4.

Sittler Jr., E. C., R. E. Hartle, R. E. Johnson, J. F. Cooper, A. S. Lipatov, C. Bertucci, A. J. Coates, et al., (2010), Saturn's magnetospheric interaction with Titan as defined by Cassini encounters T9 and T18: New results, Planetary and Space Science, 58, no. 3, 327–350.

Sittler, E. C., R. E. Hartle, C. Bertucci, A. Coates, T. Cravens, I. Dandouras, D. Shemansky, (2009a), Energy deposition processes in Titan's upper atmosphere and its induced magnetosphere, In Titan from Cassini-Huygens, (eds.) R. H. Brown, J.-P. Lebreton, J. H. Waite, Jr., 393-453, Dordrecht, New York, Springer.

Sittler Jr., E. C., A. Ali, J. F. Cooper, R. E. Hartle, R. E. Johnson, A. J. Coates, D. T. Young, (2009b), Heavy ion formation in Titan's ionosphere: Magnetospheric introduction of free oxygen and a source of Titan's aerosols?, Planetary and Space Science, 57, no. 13, 1547–1557.

Sittler Jr., E. C., N. Andre, M. Blanc, M. Burger, R. E. Johnson, A. Coates, A. Rymer, et al, (2008), Ion and neutral sources and sinks within Saturn's inner magnetosphere: Cassini results, Planetary and Space Science, 56, no. 1, 3–18.

Sittler, E. C., M. Blanc, J. D. Richardson, A. Rymer, N. Andre, M. Thomsen, J. F. Cooper, et al., (2006a), Cassini Observations of Saturn's Dawn-Magnetotail Region and their Relation to Models of Saturn's Aurora: Preliminary results, American Geophysical Union (AGU) Fall Meeting, abstract.

Sittler Jr., E. C., R. E. Johnson, H. T. Smith, J. D. Richardson, S. Jurac, M. Moore, J. F. Cooper, et al., (2006b), Energetic nitrogen ions within the inner magnetosphere of Saturn, Journal of Geophysical Research: Space Physics, 111, no. A9.

Sittler Jr., E. C., M. Thomsen, D. Chornay, M. D. Shappirio, D. Simpson, R. E. Johnson, H. T. Smith, A. J. Coates, A. M. Rymer, F. Crary, D. J. McComas, D. T. Young, D. Reisenfeld, M. Dougherty, N. Andre, (2005), Preliminary results on Saturn's inner plasmasphere as observed by Cassini: Comparison with Voyager, Geophysical Research Letters 32 (14), 5, doi: 10.1029/2005GL022653.

Smith, A. W., C. M. Jackman, M. F. Thomsen, L. Lamy, N. Sergis, (2018a), Multi-instrument investigation of the location of Saturn's magnetotail X-line, Journal of Geophysical Research: Space Physics, 123, no. 7, 5494–5505.

Smith, A. W., C. M. Jackman, M. F. Thomsen, N. Sergis, D. G. Mitchell, E. Roussos, (2018b), Dipolarization fronts with associated energized electrons in Saturn's magnetotail, Journal of Geophysical Research: Space Physics, 123, no. 4, 2714–2735.

Smith, A. W., C. M. Jackman, M. F. Thomsen, (2016), Magnetic reconnection in Saturn's magnetotail: A comprehensive magnetic field survey, Journal of Geophysical Research Space Physics 121 (4), 2984-3005, doi: 10.1002/2015ja022005.

Smith, E. J., M. K. Dougherty, C. T. Russell, D. J. Southwood, (2001), Scalar helium magnetometer observations at Cassini Earth swing-by, Journal of Geophysical Research Space Physics 106 (A12), 30129-39, doi: 10.1029/2001JA900115.

Smith, H. T., R. E. Johnson, M. E. Perry, D. G. Mitchell, R. L. McNutt, D. T. Young, (2010), Enceladus plume variability and the neutral gas densities in Saturn's magnetosphere, Journal of Geophysical Research Space Physics 115, A10252, doi: 10.1029/2009ja015184.

Smith, H. T., (2010), Neutral Clouds and Their Influence on Pick-up Ions in Saturn's Magnetosphere, In AIP Conference Proceedings, vol. 1302, no. 1, pp. 256–262.

Smith, H. T., D. G. Mitchell, R. E. Johnson, C. P. Paranicas, (2009), Investigation of energetic proton penetration in Titan's atmosphere using the Cassini INCA instrument, Planetary and Space Science 57, no. 13, 1538–1546.

Smith, H. T., M. Shappirio, R. E. Johnson, D. Reisenfeld, E. C. Sittler, F. J. Crary, D. J. McComas, D. T. Young, (2008), Enceladus: A potential source of ammonia products and molecular nitrogen for Saturn's magnetosphere, Journal of Geophysical Research: Space Physics 113, no. A11.

Smith, H. T., R. E. Johnson, E. C. Sittler, M. Shappirio, D. Reisenfeld, O. J. Tucker, M. Burger, F. J. Crary, D. J. McComas, D. T. Young, (2007), Enceladus: The likely dominant nitrogen source in Saturn's magnetosphere, Icarus 188, no. 2, 356–366.

Smith, H. T., M. Shappirio, E. C. Sittler, D. Reisenfeld, R. E. Johnson, R. A. Baragiola, F. J. Crary, D. J. McComas, D. T. Young, (2005), Discovery of nitrogen in Saturn's inner magnetosphere, Geophysical Research Letters 32 (14), 14-03, doi: 10.1029/2005GL022654.

Snowden, D. and R. V. Yelle, (2014a), The global precipitation of magnetospheric electrons into Titan's upper atmosphere, Icarus 243, 1-15. doi: 10.1016/j.icarus.2014.08.027.

Snowden, D. and R. V. Yelle, (2014b), The thermal structure of Titan's upper atmosphere, II: Energetics, Icarus 228, 64-77, doi: 10.1016/j.icarus.2013.08.027.

Snowden, D., R. V. Yelle, J. Cui, J.-E. Wahlund, N. J. T. Edberg, K. Ågren, (2013), The thermal structure of Titan's upper atmosphere, I: Temperature profiles from Cassini INMS observations, Icarus, 226, no. 1, 552–582.

Sorba, A. M., N. A. Achilleos, P. Guio, C. S. Arridge, N. M. Pilkington, A. Masters, N. Sergis, A. J. Coates, M. K. Dougherty, (2017), Modeling the compressibility of Saturn's magnetosphere in response to internal and external influences, Journal of Geophysical Research Space Physics 122 (2),1572-1589, doi: 10.1002/2016ja023544.

Southwood, D. J. and E. Chané, (2016), High-latitude circulation in giant planet magnetospheres, Journal of Geophysical Research: Space Physics, 121, no. 6, 5394–5403.

Southwood, D. J., (2015), Formation of magnetotails: Fast and slow rotators compared, In Magnetotails in the Solar System, (eds.) A. Keiling, C. M. Jackman, P. A. Delamere, pp. 199-215, Hoboken, New Jersey, John Wiley & Sons, Inc., doi: 10.1002/9781118842324.ch12.

Southwood, D. J. and S. W. H. Cowley, (2014), The origin of Saturn's magnetic periodicities: Northern and southern current systems, Journal of Geophysical Research Space Physics 119 (3), 1563-1571, doi: 10.1002/2013ja019632.

Southwood, D. J., (2014), Saturn's mysterious magnetism, Astronomy & Geophysics, vol. 55, Issue 1, pp. 1.13–1.18, doi: 10.1093/astrogeo/atu034.

Southwood, D., (2011), Direct evidence of differences in magnetic rotation rate between Saturn's northern and southern polar regions, Journal of Geophysical Research Space Physics 116, A01201, doi: 10.1029/2010ja016070.

Southwood, D. J. and M. G. Kivelson, (2009), The source of Saturn's periodic radio emission, Journal of Geophysical Research Space Physics 114, A09201, doi: 10.1029/2008ja013800.

Southwood, D. J. and M. G. Kivelson, (2007), Saturnian magnetospheric dynamics: Elucidation of a camshaft model, Journal of Geophysical Research Space Physics 112 (A12), A12222.

Southwood, D. J., M. K. Dougherty, A. Balogh, S. W. H. Cowley, E. J. Smith, B. T. Tsurutani, C. T. Russell, et al., (2001), Magnetometer measurements from the Cassini Earth swing-by, Journal of Geophysical Research: Space Physics, 106, no. A12, 30109–30128.

Southwood, D. J. and M. G. Kivelson, (2001), A new perspective concerning the influence of the solar wind on the Jovian magnetosphere, Journal of Geophysical Research Space Physics 106 (A4), 6123-6130.

Sromovsky, L. A., K. H. Baines, P. M. Fry, (2013), Saturn's Great Storm of 2010-2011: Evidence for ammonia and water ices from analysis of VIMS spectra, Icarus 226 (1), 402-418, doi: 10.1016/j.icarus.2013.05.043.

Strobel, D. F., (2008), Titan's hydrodynamically escaping atmosphere, Icarus 193 (2), 588-594.

Sulaiman, A. H., W. S. Kurth, G. B. Hospodarsky, T. F. Averkamp, A. M. Persoon, J. D. Menietti, S.-Y. Ye, et al., (2018), Auroral hiss emissions during Cassini's Grand Finale: Diverse electrodynamic interactions between Saturn and its rings, Geophysical Research Letters, 45, no. 14, 6782–6789.

Sulaiman, A. H., D. A. Gurnett, J. S. Halekas, J. N. Yates, W. S. Kurth, M. K. Dougherty, (2017), Whistler mode waves upstream of Saturn, Journal of Geophysical Research: Space Physics, 122, no. 1, 227–234.

Sulaiman, A. H., A. Masters, M. K. Dougherty, (2016), Characterization of Saturn's bow shock: Magnetic field observations of quasi-perpendicular shocks, Journal of Geophysical Research-Space Physics 121 (5), 4425-4434, doi: 10.1002/2016ja022449.

Sulaiman, A. H., A. Masters, M. K. Dougherty, D. Burgess, M. Fujimoto, G. B. Hospodarsky, (2015),Quasiperpendicular high Mach number shocks, Physical Review Letters 115 (12), 125001, doi: 10.1103/PhysRevLett.115.125001.

Sulaiman, A. H., A. Masters, M. K. Dougherty, X. Jia, (2014), The magnetic structure of Saturn's magnetosheath, Journal of Geophysical Research Space Physics 119 (7), 5651-5661, doi: 10.1002/2014ja020019.

Sundberg, T., D. Burgess, M. Scholer, A. Masters, A. Haidar, (2017), The dynamics of very high Alfvén Mach number shocks in space plasmas, The Astrophysical Journal Letters 836, no. 1, L4, doi: 10.3847/2041-8213/836/1/L4.

Szego, K., Z. Nemeth, L. Foldy, S. W. H. Cowley, G. Provan, (2013), Dual periodicities in the flapping of Saturn's magnetodisk, Journal of Geophysical Research Space Physics 118 (6), 2883-2887, doi: 10.1002/jgra.50316.

Szego, K., Z. Nemeth, G. Erdos, L. Foldy, Z. Bebesi, M. Thomsen, D. Delapp, (2012), Location of the magnetodisk in the nightside outer magnetosphere of Saturn near equinox based on ion densities, Journal of Geophysical Research Space Physics 117, A09225, doi: 10.1029/2012JA017817.

Szego, K., Z. Nemeth, G. Erdos, L. Foldy, M. Thomsen, D. Delapp, (2011), The plasma environment of Titan: The magnetodisk of Saturn near the encounters as derived from ion densities measured by the Cassini/CAPS plasma spectrometer, Journal of Geophysical Research Space Physics 116, A10219, doi: 10.1029/2011JA016629.

Szego, K., C. Bertucci, A. J. Coates, Z. Bebesi, G. Erdos, L. Foldy, D. T. Young, F. Crary, E. C. Sittler, R. Hartle, M. Thomsen, (2006), On the flowside plasma environment of Titan, American Geophysical Union (AGU) Fall Meeting, San Francisco, CA, 11-15 Dec. 2006.

Szego, K., D. T. Young, B. Barraclough, J. J. Berthelier, A. J. Coates, D. J. McComas, F. J. Crary, M. K. Dougherty, G. Erdos, D. A. Gurnett, W. S. Kurth, M. F. Thomsen, (2003), Cassini plasma spectrometer measurements of Jovian bow shock structure, Journal of Geophysical Research Space Physics 108 (A7), 11-1. doi: 10.1029/2002JA009517.

Talboys, D. L., E. J. Bunce, S. W. H. Cowley, C. S. Arridge, A. J. Coates, M. K. Dougherty, (2011), Statistical characteristics of field-aligned currents in Saturn's nightside magnetosphere, Journal of Geophysical Research Space Physics 116, A04213, doi: 10.1029/2010ja016102.

Talboys, D. L., C. S. Arridge, E. J. Bunce, A. J. Coates, S. W. H. Cowley, M. K. Dougherty, (2009a), Characterization of auroral current systems in Saturn's magnetosphere: High-latitude Cassini observations, Journal of Geophysical Research: Space Physics, 114, no. A6.

Talboys, D. L., C. S. Arridge, E. J. Bunce, A. J. Coates, S. W. H. Cowley, M. K. Dougherty, K. K. Khurana, (2009b), Signatures of field-aligned currents in Saturn's nightside magnetosphere, Geophysical Research Letters, 36, no. 19.

Teolis, B. D., M. E. Perry, C. J. Hansen, J. H. Waite, C. C. Porco, J. R. Spencer, C. J. A. Howett, (2017), Enceladus plume structure and time variability: comparison of Cassini observations, Astrobiology, 17, no. 9, 926–940.

Thomsen, M. F., S. V. Badman, C. M. Jackman, X. Jia, M. G. Kivelson, W. S. Kurth, (2017a), Energy-banded ions in Saturn's magnetosphere, Journal of Geophysical Research Space Physics 122 (5), 5181-5202, doi: 10.1002/2017ja024147.

Thomsen, M. F., C. M. Jackman, S. W. H. Cowley, X. Jia, M. G. Kivelson, G. Provan, (2017b), Evidence for periodic variations in the thickness of Saturn's nightside plasma sheet, Journal of Geophysical Research: Space Physics, 122, no. 1, 280–292.

Thomsen, M. F., A. J. Coates, E. Roussos, R. J. Wilson, K. C. Hansen, G. R. Lewis, (2016), Suprathermal electron penetration into the inner magnetosphere of Saturn, Journal of Geophysical Research: Space Physics, 121, no. 6, 5436–5448.

Thomsen, M. F., C. M. Jackman, D. G. Mitchell, G. Hospodarsky, W. S. Kurth, K. C. Hansen, (2015a), Sustained lobe reconnection in Saturn's magnetotail, Journal of Geophysical Research: Space Physics, 120, no. 12, 10257–10274.

Thomsen, M. F., D. G. Mitchell, X. Jia, C. M. Jackman, G. Hospodarsky, A. J. Coates, (2015b), Plasmapause formation at Saturn, Journal of Geophysical Research: Space Physics, 120, no. 4, 2571–2583.

Thomsen, M. F., C. M. Jackman, R. L. Tokar, R. J. Wilson, (2014a), Plasma flows in Saturn's nightside magnetosphere, Journal of Geophysical Research Space Physics 119 (6), 4521-4535, doi: 10.1002/2014ja019912.

Thomsen, M. F., D.B. Reisenfeld, R. J. Wilson, M. Andriopoulou, F. J. Crary, G. B. Hospodarsky, C. M. Jackman, et al, (2014b), Ion composition in interchange injection events in Saturn's magnetosphere, Journal of Geophysical Research: Space Physics, 119, no. 12, 9761–9772.

Thomsen, M. F., (2013), Saturn's magnetospheric dynamics, Geophysical Research Letters 40 (20), 5337-5344, doi: 10.1002/2013GL057967.

Thomsen, M. F., E. Roussos, M. Andriopoulou, P. Kollmann, C. S. Arridge, C. P. Paranicas, D. A. Gurnett, R. L. Powell, R. L. Tokar, D. T. Young, (2012), Saturn's inner magnetospheric convection pattern: Further evidence, Journal of Geophysical Research Space Physics 117, A09208, doi: 10.1029/2011JA017482.

Thomsen, M. F., D. B. Reisenfeld, D. M. Delapp, R. L. Tokar, D. T. Young, F. J. Crary, E. C. Sittler, M. A. McGraw, J. D. Williams, (2010), Survey of ion plasma parameters in Saturn's magnetosphere, Journal of Geophysical Research Space Physics 115, A10220, doi: 10.1029/2010ja015267.

Thomsen, M. F., J. P. DiLorenzo, D. J. McComas, D. T. Young, F. J. Crary, D. Delapp, D. B. Reisenfeld, N. Andre, (2007), Assessment of the magnetospheric contribution to the suprathermal ions in Saturn's foreshock region, Journal of Geophysical Research: Space Physics 112, no. A5.

Tobiska, W. K., (2004), SOLAR2000 irradiances for climate change research, aeronomy and space system engineering, Advances in Space Research 34 (8), 1736-1746.

Tokar, R. L., R. E. Johnson, M. F. Thomsen, E. C. Sittler, A. J. Coates, R. J. Wilson, F. J. Crary, D. T. Young, G. H. Jones, (2012), Detection of exospheric O2+ at Saturn's moon Dione, Geophysical Research Letters 39 (3), L03105, doi: 10.1029/2011GL050452.

Tokar, R. L., R. E. Johnson, M. F. Thomsen, R. J. Wilson, D. T. Young, F. J. Crary, A. J. Coates, G. H. Jones, C. S. Paty, (2009), Cassini detection of Enceladus' cold water-group plume ionosphere, Geophysical Research Letters 36 (13), doi: 10.1029/2009GL038923.

Tokar, R. L., R. J. Wilson, R. E. Johnson, M. G. Henderson, M. F. Thomsen, M. M. Cowee, E. C. Sittler, D. T. Young, F. J. Crary, H. J. McAndrews, H. T. Smith, (2008), Cassini detection of water-group pick-up ions in the Enceladus torus, Geophysical Research Letters 35 (14), L14202.

Tokar, R. L., R. E. Johnson, T. W. Hill, D. H. Pontius, W. S. Kurth, F. J. Crary, D. T. Young, M. F. Thomsen, D. B. Reisenfeld, A. J. Coates, G. R. Lewis, E. C. Sittler, D. A. Gurnett,

(2006), The interaction of the atmosphere of Enceladus with Saturn's plasma, Science 311 (5766), 1409-12, doi: 10.1126/science.1121061.

Tokar, R. L., R. E. Johnson, M. F. Thomsen, D. M. Delapp, R. A. Baragiola, M. F. Francis, D. B. Reisenfeld, B. A. Fish, D. T. Young, F. J. Crary, A. J. Coates, D. A. Gurnett, W. S. Kurth, (2005), Cassini observations of the thermal plasma in the vicinity of Saturn's main rings and the F and G rings, Geophysical Research Letters 32 (14), L14S04.

Tokarev, Y., J.-L. Bougeret, B. Cecconi, A. Lecacheux, M. L. Kaiser, W. S. Kurth, (2006), Sura-waves experiments: calibration of the Cassini/RPWS/HFR instrumentation, Verlag der Österreichischen Akademie der Wissenschaften, https://austriaca.at/0xc1aa5576_0x0015cbe6.pdf.

Tseng, W.-L., R. E. Johnson, M. K. Elrod, (2013a), Modeling the seasonal variability of the plasma environment in Saturn's magnetosphere between main rings and Mimas, Planetary and Space Science 77, 126-135, doi: 10.1016/j.pss.2012.05.001.

Tseng, W.-L., R. E. Johnson, W.-H. Ip, (2013b), The atomic hydrogen cloud in the saturnian system, Planetary and Space Science, 85, 164–174.

Tseng, W.-L., R. E. Johnson, M. F. Thomsen, T. A. Cassidy, M. K. Elrod, (2011), Neutral H_2 and H_2^+ ions in the Saturnian magnetosphere, (2011), Journal of Geophysical Research: Space Physics, 116, no. A3.

Tseng, W. L., W. H. Ip, R. E. Johnson, T. A. Cassidy, M. K. Elrod, (2010), The structure and time variability of the ring atmosphere and ionosphere, Icarus 206 (2), 382-389, doi: 10.1016/j.icarus.2009.05.019.

Tsurutani, B. T., E. J. Smith, M. E. Burton, J. K. Arballo, C. Galvan, Xiao-Yan Zhou, D. J. Southwood, M. K. Dougherty, K. H. Glassmeier, F. M. Neubauer, J. K. Chao, (2001), Oblique "1-Hz" whistler mode waves in an electron foreshock: The Cassini near-Earth encounter, Journal of Geophysical Research Space Physics 106 (A12), 30223-30238, doi: 10.1029/2001JA900108.

Tsyganenko, N. A. and V. A. Andreeva, (2014), On the "bowl-shaped" deformation of planetary equatorial current sheets, Geophysical Research Letters 41, no. 4, 1079-1084, doi: 10.1002/2014GL059295.

Tucker, O. J., W. Waalkes, V. M. Tenishev, R. E. Johnson, A. Bieler, M. R. Combi, A. F. Nagy, (2016), Examining the exobase approximation: DSMC models of Titan's upper atmosphere, Icarus 272:290-300, doi: 10.1016/j.icarus.2016.02.044.

Tucker, O. J., R. E. Johnson, J. I. Deighan, A. N. Volkov, (2013), Diffusion and thermal escape of H-2 from Titan's atmosphere: Monte Carlo simulations, Icarus 222 (1), 149-158, doi: 10.1016/j.icarus.2012.10.016.

Tucker, O. J. and R. E. Johnson, (2009), Thermally driven atmospheric escape: Monte Carlo simulations for Titan's atmosphere, Planetary and Space Science, 57, no. 14-15, 1889–1894.

Vervack, R. J. and J. I. Moses, (2015), Saturn's upper atmosphere during the Voyager era: Reanalysis and modeling of the UVS occultations, Icarus 258, 135-163, doi: 10.1016/j.icarus.2015.06.007.

Vigren, E., M. Galand, R. V. Yelle, A. Wellbrock, A. J. Coates, D. Snowden, J. Cui, P. Lavvas, N. J. T. Edberg, O. Shebanits, J. E. Wahlund, V. Vuitton, K. Mandt, (2015), Ionization balance in Titan's nightside ionosphere, Icarus 248, 539-546, doi: 10.1016/j.icarus.2014.11.012.

Vogl, D. F., B. Cecconi, W. Macher, P. Zarka, H. P. Ladreiter, P. Fedou, A. Lecacheux, T. Averkamp, G. Fischer, H. O. Rucker, D. A. Gurnett, W. S. Kurth, G. B. Hospodarsky, (2004), In-flight calibration of the Cassini-Radio and Plasma Wave Science (RPWS) antenna system for direction-finding and polarization measurements, Journal of Geophysical Research Space Physics 109 (A9), 15, doi: 10.1029/2003JA010261.

Vogl, D. F., H. P. Ladreiter, P. Zarka, H. O. Rucker, W. Macher, W. S. Kurth, D. A. Gurnett, G. Fischer, (2001), First results on the calibration of the Cassini RPWS antenna system: Verlag der Österreichischen Akademie der Wissenschaften.

Volkov, A. N., O. J. Tucker, J. T. Erwin, R. E. Johnson, (2011a), Kinetic simulations of thermal escape from a single component atmosphere, Physics of Fluids, 23, no. 6, 066601.

Volkov, A. N., R. E. Johnson, O. J. Tucker, J. T. Erwin, (2011b), Thermally driven atmospheric escape: Transition from hydrodynamic to Jeans escape, The Astrophysical Journal Letters, 729, no. 2, L24.

Vuitton, V., P. Lavvas, R. V. Yelle, M. Galand, A. Wellbrock, G. R. Lewis, A. J. Coates, J.-E. Wahlund, (2009), Negative ion chemistry in Titan's upper atmosphere, Planetary and Space Science 57, no. 13, 1558–1572.

Vuitton, V., R. V. Yelle, M. J. McEwan, (2007), Ion chemistry and N-containing molecules in Titan's upper atmosphere, Icarus 191, no. 2, 722–742.

Vuitton, V., R. V. Yelle, V. G. Anicich, (2006), The nitrogen chemistry of Titan's upper atmosphere revealed, The Astrophysical Journal Letters, 647, no. 2, L175.

Wahlund, J. E., M. W. Morooka, L. Z. Hadid, A. M. Persoon, W. M. Farrell, D. A. Gurnett, G. Hospodarsky, W. S. Kurth, S. Y. Ye, D. J. Andrews, N. J. T. Edberg, A. I. Eriksson, E. Vigren, (2018), In situ measurements of Saturn's ionosphere show that it is dynamic and interacts with the rings, Science 359 (6371), 66-68, doi: 10.1126/science.aao4134.

Wahlund, J.-E., M. Galand, I. Müeller-Wodarg, J. Cui, R. V. Yelle, F. J. Crary, K. Mandt, et al., (2009), On the amount of heavy molecular ions in Titan's ionosphere, Planetary and Space Science, 57, no. 14–15, 1857–1865.

Wahlund, J.-E., R. Boström, G. A. G. D. Gustafsson, D. A. Gurnett, W. S. Kurth, A. Pedersen, T. F. Averkamp, et al., (2005), Cassini measurements of cold plasma in the ionosphere of Titan, Science, 308, no. 5724, 986–989.

Waite, J. H., C. R. Glein, R. S. Perryman, B. D. Teolis, B. A. Magee, G. Miller, J. Grimes, M. E. Perry, K. E. Miller, A. Bouquet, J. I. Lunine, T. Brockwell, S. J. Bolton, (2017), Cassini finds molecular hydrogen in the Enceladus plume: Evidence for hydrothermal processes, Science 356 (6334), 155-159, doi: 10.1126/science.aai8703.

Waite, J. H., W. S. Lewis, B. A. Magee, J. I. Lunine, W. B. McKinnon, C. R. Glein, O. Mousis, D. T. Young, T. Brockwell, J. Westlake, M. J. Nguyen, B. D. Teolis, B. Niemann,

R. L. McNutt, M. Perry, W. H. Ip, (2009), Liquid water on Enceladus from observations of ammonia and ^{40}Ar in the plume, Nature 460 (7254), 487-490, doi: 10.1038/nature08153.

Waite, J. H., D. T. Young, T. E. Cravens, A. J. Coates, F. J. Crary, B. Magee, J. Westlake, (2007), The process of tholin formation in Titan's upper atmosphere, Science, 316, no. 5826, 870–875.

Waite, J. H., T. E. Cravens, W. H. Ip, W. T. Kasprzak, J. G. Luhmann, R. L. McNutt, H. B. Niemann, R. V. Yelle, I. Müeller-Wodarg, S. A. Ledvina, S. Scherer, (2005), Oxygen ions observed near Saturn's A ring, Science 307 (5713), 1260-1262, doi: 10.1126/science.1105734.

Walker, J. D., S. Chocron, J. H. Waite, T. Brockwell, (2015), The vaporization threshold: Hypervelocity impacts of ice grains into a titanium Cassini spacecraft instrument chamber, Procedia Engineering, 103, 628–635.

Wang, Z., D. A. Gurnett, T. F. Averkamp, A. M. Persoon, W. S. Kurth, (2006), Characteristics of dust particles detected near Saturn's ring plane with the Cassini Radio and Plasma Wave instrument, Planetary and Space Science, 54, no. 9–10, 957–966.

Wannawichian, S., J. T. Clarke, D. H. Pontius, (2008), Interaction evidence between Enceladus' atmosphere and Saturn's magnetosphere, Journal of Geophysical Research Space Physics 113, A07217, doi: 10.1029/2007JA012899.

Warwick, J. W., J. B. Pearce, D. R. Evans, T. D. Carr, J. J. Schauble, J. K. Alexander, M. L. Kaiser, M. D. Desch, M. Pedersen, A. Lecacheux, (1981), Planetary radio astronomy observations from Voyager 1 near Saturn, Science 212 (4491), 239-243.

Wei, H. Y., C. T. Russell, M. K. Dougherty, F. M. Neubauer, Y. J. Ma, (2010), Upper limits on Titan's magnetic moment and implications for its interior, Journal of Geophysical Research: Planets, 115, no. E10.

Wei, H. Y., C. T. Russell, J.-E. Wahlund, M. K. Dougherty, C. Bertucci, R. Modolo, Y. J. Ma, F. M. Neubauer, (2007), Cold ionospheric plasma in Titan's magnetotail, Geophysical Research Letters, 34, no. 24.

Wellbrock, A., A. J. Coates, G. H. Jones, V. Vuitton, P. Lavvas, R. T. Desai, J. H. Waite, (2019), Heavy negative ion growth in Titan's polar winter, Monthly Notices of the Royal Astronomical Society 490, no. 2, 2254–2261.

Wellbrock, A., A. J. Coates, G. H. Jones, G. R. Lewis, J. H. Waite, (2013), Cassini CAPS-ELS observations of negative ions in Titan's ionosphere: Trends of density with altitude, Geophysical Research Letters 40 (17), 4481-4485, doi: 10.1002/grl.50751.

Went, D. R., G. B. Hospodarsky, A. Masters, K. C. Hansen, M. K. Dougherty, (2011), A new semiempirical model of Saturn's bow shock based on propagated solar wind parameters, Journal of Geophysical Research: Space Physics, 116, no. A7.

Westlake, J. H., J. H. Waite, N. Carrasco, M. Richard, T. Cravens, (2014), The role of ion-molecule reactions in the growth of heavy ions in Titan's ionosphere,Journal of Geophysical Research: Space Physics, 119, no. 7, 5951–5963.

Westlake, J. H., J. M. Bell, J. H. Waite Jr., R. E. Johnson, J. G. Luhmann, K. E. Mandt, B. A. Magee, A. M. Rymer, (2011), Titan's thermospheric response to various plasma environments, Journal of Geophysical Research: Space Physics, 116, no. A3.

Wilson, A., (2004), Planetary probe atmospheric entry and descent trajectory analysis and science, Proceedings of the International Workshop Planetary Probe Atmospheric Entry and Descent Trajectory Analysis and Science, 6-9 October 2003, Lisbon, Portugal, (ed.), A. Wilson, ESA SP-544, Noordwijk, Netherlands: ESA Publications Division, pp. VI + 364.

Wilson, E. H. and S. K. Atreya, (2004), Current state of modeling the photochemistry of Titan’s mutually dependent atmosphere and ionosphere, Journal of Geophysical Research-Planets 109 (E6), E06002, doi: 10.1029/2003JE002181.

Wilson, G. R. and J. H. Waite Jr., (1989), Kinetic modeling of the Saturn ring-ionosphere plasma environment, Journal of Geophysical Research: Space Physics, 94, no. A12, 17287–17298.

Wilson, R. J., F. Bagenal, A. M. Persoon, (2017), Survey of thermal plasma ions in Saturn’s magnetosphere utilizing a forward model, Journal of Geophysical Research Space Physics 122 (7), 7256-7278, doi: 10.1002/2017ja024117.

Wilson, R. J., F. Bagenal, T. Cassidy, B. L. Fleshman, F. Crary, (2015), The relative proportions of water group ions in Saturn's inner magnetosphere: A preliminary study, Journal of Geophysical Research: Space Physics, 120, no. 8, 6624–6632.

Wilson, R. J., F. Bagenal, P. A. Delamere, M. Desroche, B. L. Fleshman, V. Dols, (2013), Evidence from radial velocity measurements of a global electric field in Saturn’s inner magnetosphere, Journal of Geophysical Research Space Physics 118 (5), 2122-2132, doi: 10.1002/jgra.50251.

Wilson, R. J., P. A. Delamere, F. Bagenal, Adam Masters, (2012), Kelvin-Helmholtz instability at Saturn's magnetopause: Cassini ion data analysis, Journal of Geophysical Research: Space Physics, 117, no. A3.

Wilson, R. J., R. L. Tokar, W. S. Kurth, A. M. Persoon, (2010), Properties of the thermal ion plasma near Rhea as measured by the Cassini plasma spectrometer, Journal of Geophysical Research Space Physics 115, A05201, doi: 10.1029/2009ja014679.

Wilson, R. J., R. L. Tokar, M. G. Henderson, (2009), Thermal ion flow in Saturn’s inner magnetosphere measured by the Cassini plasma spectrometer: A signature of the Enceladus torus?, Geophysical Research Letters 36, L23104, doi: 10.1029/2009gl040225.

Wilson, R. J., R. L. Tokar, M. G. Henderson, T. W. Hill, M. F. Thomsen, D. H. Pontius Jr., (2008), Cassini plasma spectrometer thermal ion measurements in Saturn’s inner magnetosphere, Journal of Geophysical Research Space Physics 113 (A12), A12218, doi: 10.1029/2008ja013486.

Xin, L., D. A. Gurnett, O. Santolik, W. S. Kurth, G. B. Hospodarsky, (2006), Whistler-mode auroral hiss emissions observed near Saturn’s B ring, Journal of Geophysical Research Space Physics 111 (A6), A06214.

Yao, Z. H., D. Grodent, L. C. Ray, I. J. Rae, A. J. Coates, Z. Y. Pu, A. T. Lui et al., (2017a), Two fundamentally different drivers of dipolarizations at Saturn, Journal of Geophysical Research: Space Physics, 122, no. 4, 4348–4356.

- - - - - - - - - - - - - -

Yao, Z. H., A. J. Coates, L. C. Ray, I. J. Rae, D. Grodent, G. H. Jones, M. K. Dougherty, C. J. Owen, R. L. Guo, W. R. Dunn, A. Radioti, Z. Y. Pu, G. R. Lewis, J. H. Waite, J.-C. Gérard, (2017b), Corotating magnetic reconnection site in Saturn's magnetosphere, The Astrophysical Journal 846, L25, doi: 10.3847/2041-8213/aa88af.

Yao, Z. H., A. Radioti, I. J. Rae, J. Liu, D. Grodent, L. C. Ray, S. V. Badman, A. J. Coates, J.-C. Gérard, J. H. Waite, J. N. Yates, Q. Q. Shi, Y. Wei, B. Bonfond, M. K. Dougherty, E. Roussos, N. Sergis, B. Palmaerts, (2017c), Mechanisms of Saturn's near-noon transient aurora: In situ evidence from Cassini measurements, Geophysical Research Letters 44, 11, doi: 10.1002/2017GL075108.

Yao, Z., Z. Y. Pu, I. J. Rae, A. Radioti, M. V. Kubyshkina, (2017d), Auroral streamer and its role in driving wave-like pre-onset aurora, Geoscience Letters 4, no. 1, 8.

Yates, J. N., D. J. Southwood, M. K. Dougherty, (2015a), Magnetic phase structure of Saturn's 10.7 h oscillations, Journal of Geophysical Research: Space Physics, 120, no. 4, 2631–2648.

Yates, J. N., D. J. Southwood, M. K. Dougherty, (2015b), Reply to the comment by Cowley et al. on Magnetic phase structure of Saturn's 10.7 h oscillations.

Ye, S.-Y., W. S. Kurth, G. B. Hospodarsky, A. M. Persoon, A. H. Sulaiman, D. A. Gurnett, M. Morooka et al., (2018), Dust Observations by the Radio and Plasma Wave Science Instrument During Cassini's Grand Finale, Geophysical Research Letters, 45, no. 19, 10–101.

Ye, S.-Y., G. Fischer, W. S. Kurth, J. D. Menietti, D. A. Gurnett, (2017), Rotational modulation of Saturn kilometric radiation, narrrowband emission and auroral hiss, 191-204, doi: 10.1553/PRE8s191.

Ye, S.-Y., D. A. Gurnett, W. S. Kurth, (2016a), In-situ measurements of Saturn's dusty rings based on dust impact signals detected by Cassini RPWS, Icarus, 279, 51–61.

Ye, S.-Y., G. Fischer, W. S. Kurth, J. D. Menietti, D. A. Gurnett, (2016b), Rotational modulation of Saturn's radio emissions after equinox, Journal of Geophysical Research: Space Physics, 121, no. 12, 11714–11728.

Ye, S.-Y., D. A. Gurnett, W. S. Kurth, T. F. Averkamp, S. Kempf, H.-W. Hsu, R. Srama, E. Grün, (2014a), Properties of dust particles near Saturn inferred from voltage pulses induced by dust impacts on Cassini spacecraft, Journal of Geophysical Research: Space Physics, 119, no. 8, 6294–6312.

Ye, S.-Y., D. A. Gurnett, W. S. Kurth, T. F. Averkamp, M. Morooka, S. Sakai, J.-E. Wahlund, (2014b), Electron density inside Enceladus plume inferred from plasma oscillations excited by dust impacts, Journal of Geophysical Research: Space Physics, 119, no. 5, 3373–3380.

Ye, S., H. Hsu, T. F. Averkamp, W. S. Kurth, D. A. Gurnett, S. Kempf, (2012), Cassini/RPWS Dust Measurements During Enceladus Flybys, American Geophysical Union (AGU) Fall Meeting, abstract.

Ye, S.-Y., D. A. Gurnett, J. B. Groene, Z. Wang, W. S. Kurth, (2010), Dual periodicities in the rotational modulation of Saturn narrowband emissions, Journal of Geophysical Research: Space Physics, 115, no. A12.

Yelle, R. V., J. Cui, I. C. F. Müeller-Wodarg, (2008), Methane escape from Titan's atmosphere, Journal of Geophysical Research Planets 113 (E10), E10003, doi: 10.1029/2007je003031.

Young, D. T., J. J. Berthelier, M. Blanc, J. L. Burch, S. Bolton, A. J. Coates, F. J. Crary, R. Goldstein, M. Grande, et al., (2005), Composition and dynamics of plasma in Saturn's magnetosphere, Science 307 (5713), 1262-1266, doi: 10.1126/science.1106151.

Zarka, P., L. Lamy, B. Cecconi, R. Prange, H. O. Rucker, (2007), Modulation of Saturn's radio clock by solar wind speed, Nature 450 (7167), 265-267, doi: 10.1038/nature06237.

Zarka, P. and W. S. Kurth, (2005), Radio wave emission from the outer planets before Cassini, Space Science Reviews 116 (1), 371-397, doi: 10.1007/s11214-005-1962-2.

Zarka, P., B. Cecconi, W. S. Kurth, (2004), Jupiter's low-frequency radio spectrum from Cassini/Radio and Plasma Wave Science (RPWS) absolute flux density measurements, Journal of Geophysical Research: Space Physics, 109, no. A9.

Zarka, P., (2004), Radio and plasma waves at the outer planets, Advances in Space Research, 33, no. 11, 2045–2060.

Zarka, P., J. Queinnec, F. J. Crary, (2001), Low-frequency limit of Jovian radio emissions and implications on source locations and Io plasma wake, Planetary and Space Science, 49, no. 10–11, 1137–1149.

Zarka, P., (2000), Radio emissions from the planets and their moons, Geophysical Monograph American Geophysical Union 119, 167-178.

Zlotnik, E. Y., V. E. Shaposhnikov, V. V. Zaitsev, (2016), Interpretation of the zebra pattern in the Jovian kilometric radiation, Journal of Geophysical Research, Space Physics 121 (6), 5307-5318.